THE OXIDATION STATE OF

FISSION FRAGMENT IODINE IN POTASSIUM CHLORIDE

by

CHRISTINE MARY WALLER, B.Sc. Hons.

A thesis submitted for the degree of
Doctor of Philosophy
of the University of London

Department of Chemical Engineering and
Chemical Technology,
Nuclear Technology Laboratory,
Imperial College of Science and Technology,
London, S.W.7.

September, 1976.

Acknowledgements

I am extremely grateful to my supervisor, Professor G.N. Walton, for his invaluable assistance throughout and especially during the difficult task of writing and correcting this work.

Sincere thanks are due to Mr. B. Bennett for his practical and computational assistance, and to Mr. E. Caesar and all the staff of the University of London Reactor Centre for the irradiation of samples. The financial support from the Science Research Council is gratefully appreciated.

Finally, I would like to thank my family for the many sacrifices they made during my studies.

Abstract

The oxidation states adopted by fission fragment iodine in a KCl tablet have been determined by using a chemical extraction procedure with water and CCl_4 as the two solvents. Preliminary experiments showed that only the oxidised condition (IO_3^-) and the reduced condition (I^-) could be clearly distinguished. The fractions of iodine found in an oxidised state were the same for the different isotopes investigated, except for ^{132}I, which showed higher oxidation. This effect was attributed to the length of time spent by this isotope as ^{132}Te, its precursor in the mass decay chain, and with the increased thermodynamical stability of K_2TeO_3 over KIO_3.

Experiments were carried out to find the effect of changing the manufacturing pH of the crystals and the pressing loads which were used to mould the tablets. These showed that there was no significant effect on the redox distribution at room temperature. However, experiments showed that the presence of water prior to analysis acts to increase the oxidised form of iodine. This effect was attributed to the water molecules forming a boundary around parts of the lattice, which could promote local interaction between the decomposed V_K centre and the iodine fragment, on dissolution of the tablet.

Isothermal annealing effects at 100°C, 150°C and 200°C are reported. The existence of oxidising and reducing entities, such as V_K centres, in the tablet of KCl is envisaged and a crude model is proposed. From this, coefficients were derived for the disappearance of oxidising entities during the annealing of KCl and for the interaction of these entities with the fission fragment iodine

atoms. Activation energies were found for the effect of annealing temperature on these processes.

An attempt was made to correlate the ratio of the oxidised to reduced form of fission product iodine with the chlorine potential in the KCl tablet. This correlation appeared to be consistent with thermodynamical predictions made in connection with the corrosive potentiality of fission products and other materials in the molten salt reactor. The passage of a fission fragment through KCl will raise a small fraction of the tablet above its melting point, and could be taken as simulating the conditions inside a molten salt reactor core.

CONTENTS

		Page No.
Acknowledgements		2
Abstract		3
Contents		5
List of figures		6
List of tables		8
Introduction		10
Chapter 1:	Fission and Fission Fragments	12
Chapter 2:	Reactor Technology	73
Chapter 3:	Literature Survey	102
Chapter 4:	Experimental	148
Chapter 5:	Results and Discussion	224
Chapter 6:	Conclusion	271
References		276
Appendix 1		286
Appendix 2		299

List of Figures

Chapter 1:

Fig. 1.1. Variation of Mass Yield with Energy for ^{133}I

Fig. 1.2. Variation of Neutron Yield with Fragment Mass

Fig. 1.3. Variation of Charge with Energy for Fission Fragment ^{133}I

Fig. 1.4. Diagrammatic Representation of Various Range Measurements

Fig. 1.5. Diagram for Calculating the Number of Fission Fragments Entering the Tablet of KCl

Fig. 1.6. Temperature Distribution in a Typical Thermal Spike at Various Times

Fig. 1.7. Variation of Mean Free Path in the Transfer of Energy T by a Fragment of Energy E

Fig. 1.8. Damage Created by Primary knock on

Fig. 1.9. Schematic Representation of the Fission Spike

Chapter 2:

Fig. 2.1. Simplified Flowsheet for Processing the MSBR

Fig. 2.2. Simplified Flow Diagram for a Molten-Salt Breeder-Reactor

Fig. 2.3. Chlorine Potential Diagram at 1000 ^{o}K

Fig. 2.4. Modified Pourbaix Diagram

Fig. 2.5. Part of a Transverse Cross Section of an Irradiated Mixed Oxide Fuel Pin

Fig. 2.6. Pu/U Segregation on DFR Mixed Oxide Fuel Pins

Chapter 3:

Fig. 3.1. Models of the Centres $V_K(A)$, H(B), $V_F(C)$, $V_t(D)$ in KCl

Fig. 3.2. Models of a $V_K(a)$ and $V_F(b)$ TYPE I_2^- Centre in Pb^{++} and I^- Doped KCl Lattice

Chapter 4:

Fig. 4.1. Alpha Spectrum

Fig. 4.2. Calibration of Alpha Counter

Fig. 4.3. Alpha Spectrum U_3O_8 Enriched 80% (1 x 10λ addn. of solution)

Fig. 4.4. Alpha Spectrum U_3O_8 Enriched 80% (6 x 10λ addn. of solution)

Fig. 4.5. Self Absorption of Alpha Particles in U_3O_8 Film

Fig. 4.6. Decay Curves
Fig. 4.7. Typical γ-ray Spectrum of Fission Product Iodine
Fig. 4.8. Variation of Efficiency with Distance
Fig. 4.9. Beer's Law Curve

Chapter 5:
Fig. 5.1. Isothermal Annealing Curves
Fig. 5.2. Annealing at 100 ^{o}C for ^{131}I, ^{132}I, ^{133}I
Fig. 5.3. Arrhenius Plot
Fig. 5.4. Ionisation Potential Diagram
Fig. 5.5. Self Diffusion of Cl^{-} ions in Crushed Crystal Specimens of KCl
Fig. 5.6. Moisture Effect

Appendices:
Fig. A1.1 Flow Diagram for CHRIS 1

List of Tables

Chapter 1:

1.1 Distribution of fission energy for ^{235}U

1.2 Frequency of occurrence of ^{133}I from fission, with different energy

1.3 Properties of fission fragments

1.4 Effect of thermal neutron capture in KCl

Chapter 2:

2.1 Equilibrium distributions (mole fractions)

2.2 Chlorine balance of the major stable fission products

Chapter 4:

4.1 Data for standard americium source

4.2 Data for α-spectrum observed in uranium sample

4.3 Pipetting results for equal portions of ^{60}Co solution

4.4 Self absorption of alpha particles in U_3O_8 film

4.5 Natural and enriched abundances of uranium isotopes

4.6 Record of samples used in experiments

4.7 Variation of iodate fraction with tablet pressing load

4.8 Exchange reactions for iodine ions in aqueous solutions

4.9 Distribution of ^{131}I activity in carrier solution (KI, KIO_3, I_2)

4.10 Carrier solutions that were used in the analysis

4.11 Samples counted as $CCl_4.I_2$ (solution) and AgI (solid)

4.12 Data for iodine isotopes which are suitable for analysis

4.13 Decay schemes for isotopes

4.14 Standard sources used for calibration

4.15 Characteristics of detectors used for experimental work

4.16 Displacement of samples in the horizontal plane

4.17 Effect of sealing the tablets

4.18 Moisture Results

4.19 Acid/alkali results

4.20 Calibration curve values for the spectrophotometer (Beer's Law Curve)

4.21 % transmission values for KCl tablets

Chapter 5:

5.1 Isothermal annealing results for ^{131}I

5.2 Annealing at 100°C for ^{131}I, ^{132}I, ^{133}I, ^{135}I

5.3 Determination of the error associated with choosing the "best span"

5.4 Effect of shaking the sample before the count

5.5 No form of iodine is being lost by the thermal annealing process

5.6 Thermodynamical values

5.7 Values used for "best fit" to experimental points

5.8 Distances between certain species in the KCl tablet

5.9 Moisture effect

Appendices:

A 1.1 Symbol listing for the programs

INTRODUCTION

A knowledge of the chemical state of fission products released through reactor operation is of importance if any accurate predictions about reactor conditions are to be made. Most information is obtained from experience in working reactors and, sometimes, unpredicted effects have been observed (1).

The introduction of the fast breeder reactor will require a quicker fuel recycling program in order to reduce the total fuel inventory and decrease the doubling time for breeding. This emphasises the desirability of quick, efficient fuel reprocessing, which will have to use an overall decontamination factor of 10^6 for ^{131}I in 50 days cooled fuel (2). At present, cooling times are not important, and so decontamination factors are much lower at 10^2 . A precise knowledge of fission product chemistry will help in this field.

Fission products are also responsible for corrosion and embrittlement of materials used in the reactor. Iodine, again, is one of the worst offenders, both in the fast breeders and thermal reactor systems. An understanding of the unusual chemistry could be applied to reducing a hazardous situation in the core, which could prove costly to rectify through shutdown and component replacement.

A reactor system that has not yet been developed commercially is the system that uses uranium dissolved in molten salts as a fuel. As discussed in section 2.2, this system has certain advantages of safety and simplicity over current systems. The experimental system for this thesis was chosen for its similarity with the molten salt reactor. The passage of fission products through potassium

chloride creates localised melting along the fission track. This environment can be compared with that inside a molten salt reactor, using an alkali halide as the molten salt.

Chapter 1. Fission and Fission Fragments.

Contents:

1.1	The Fissioning Process	14
1.1.1	The kinetic energy released in fission	15
1.1.2	The distribution in fragment mass	20
1.1.3	The distribution in fragment charge	22
1.1.4	Fission fragment decay	23
	(a) β-decay	
	(b) γ-decay	
1.2	Fission Damage - the fragment	28
1.2.1	Initial charge on the fission fragment	28
1.2.2	Passage of fission fragment through medium	29
1.2.3	Range of fission fragment	33
1.2.4	A calculation of the number and energy of fission fragments entering KCl	38
	(a) Theory	
	(i) The total number of fragments N_t emitted from a source of thickness s through an absorber of thickness d	
	(ii) The total energy E_t of fragments emitted from a source of thickness s through an absorber of thickness d	
	(b) Calculation	
1.3	Fission Damage - the host atoms	42
1.3.1	Displacement and replacement of atoms	42
	(a) Replacement energy	
	(b) Displacement threshold	
1.3.2	Displacement in KCl	43
1.3.3	Energy transferred in collisions	44
1.3.4	Number of displacements	45
1.3.5	Crystal lattice effects	47
	(a) Focussing	
	(b) Channelling	
1.3.6	Other sources of damage	50
	(a) Neutron irradiation damage	
	(b) Damage due to electromagnetic radiation	
	(c) Damage due to β-irradiation	

1.4	Fission Spikes	58
1.4.1	Thermal spikes	58
	(a) Calculations	
	(i) To find the volume of tablet made molten	
	(ii) To find the number of atoms raised above the melting point	
	(b) Diffusion of ions	
1.4.2	Plastic spikes	65
1.4.3	Displacement spikes	67

CHAPTER 1

FISSION AND FISSION FRAGMENTS

1.1. The Fissioning Process

The precise physics of fission is still a matter for controversy, 37 years after its discovery by Hahn and Strassman in 1939. Several models have been proposed for the structure of the nucleus. The features of the shell model and liquid drop model are combined in the collective model, which provides one of the better descriptions based on experimental observations.

The shell model proposes a nuclear structure for the nucleus, similar to the electronic structure in an atom. It successfully explains the occurence of exceptionally stable numbers of nucleons (magic numbers) as those needed to complete a nuclear shell. The occurence of nuclear isomerism can also be explained by the nucleons occuping states of higher energy than the lowest unfilled levels.

The liquid drop model correlates spontaneous radioactive decay with the evaporation of molecules from the surface of a liquid. Bohr and Wheeler (3) used this analogy to show that, just as the drop increasing in size becomes more unstable, so the addition of protons to the nucleus increases the repulsive forces. A point is reached where the nucleus spontaneously fissions. This occurs readily among very heavy nuclei, but for elements in the actinide region sufficient energy has to be added to overcome the fission barrier. Some spontaneous fission of these elements does occur but the half life is very low, e.g. ^{238}U, $t_{\frac{1}{2}} = 10^{16}$ y; ^{254}Cf, $t_{\frac{1}{2}} = 56$ d. Energy is usually added by the nucleus capturing a neutron. The excitation energy

introduced is equal to the difference between the mass of the capturing nucleus plus the mass of the neutron and the ground state mass of the compound nucleus. For thermal neutron capture by ^{235}U to form ^{236}U, the additional energy is sufficient to overcome the fission barrier potential and ^{236}U undergoes fission.

The fissioning process gives rise to a range of elements with different masses, charge, and kinetic energy. A discussion of these varying properties, for which no complete physical explanation has been given, follows.

1.1.1 The kinetic energy released in fission

The kinetic energy is found to depend on the mass and charge of the fissioning nucleus. If symmetric fission is considered, this can best be described as the Coulomb repulsion between two spheres in contact. The Coulomb energy can be shown to be proportional to $Z^2/A^{1/3}$ where Z and A are the charge and mass number of the compound nucleus undergoing fission. Although the deformation of the fragments at the moment of fission (scission) has not been considered, an empirical fit of

$$E_K = 0.1071(Z^2/A^{1/3}) + 22.2$$

has been reported for the most probable value of the total fission fragment kinetic energy. This gives 168.9 MeV for $^{236}_{92}U$, which is very similar to the value of 168.3 MeV reported by Viola (4) for the thermal neutron fission of ^{235}U. This last value was obtained before neutron emission, and such values are generally 1% - 2% higher than post-neutron kinetic energies. The r.m.s. deviation from the average total kinetic energy for a fixed mass ratio is 8 MeV. This reflects the distribution of nuclear elongation

at the scission point. The width of the total kinetic energy distribution curve increases with excitation energy and the $Z^2/A^{1/3}$ value of the fissioning nucleus.

The total kinetic energy of the fragments depends on the mass division. Asymmetric fission, where A = 132 for the heavy fragment, has maximum kinetic energy release. As the mass number of the fissioning nucleus increases, the heavy fragment with maximum kinetic energy remains at A = 132, but the mass number of the light one increases. This is another consequence of the strong shell effect. It seems that the heavy fragment alters the scission shape to produce higher Coulomb interaction energy. An increase in excitation energy helps to reduce the closed shell effect. The kinetic energy for symmetric fission is increased and the need to produce a fragment with $A \simeq 132$ is decreased. However, the excitation energy has little effect on the kinetic energy release. Early fission studies showed the similarity in ranges of fission products from 350 MeV proton-induced fission and thermal neutron-induced fission.

Of all the energy released in fission, the largest fraction goes into the kinetic energy of the fragments. Energy is also given to electrons, protons, neutrons and neutrinos emitted by the fragment at fission and later. Table 1.1 shows how the energy is distributed.

Table 1.1 (14)

Distribution of fission energy for ^{235}U

	MeV
Kinetic energy of fission fragments	165
β-decay energy of fission fragments	9
γ-decay energy of fission fragments	7.2
Neutrino energy	16
Energy of fission neutrons (prompt)	4.9
γ-ray energy (prompt)	7.9
Total	210

The total kinetic energy is distributed between the fission fragments in a manner similar to the mass distribution (next section). Momentum is conserved so that the lighter fragment has greater energy than the heavier fragment. An energy spectrum of ^{235}U fission fragments after thermal neutron bombardment reveals an asymmetric distribution with the maximum energy for the heavier fragment at 61.4 MeV and that for the lighter fragment at 93.1 MeV (5).

The relative frequency of occurrence of the fission modes for different energies and mass splittings is shown by a contour diagram in (6). From this figure, it is possible to estimate the kinetic energy of iodine fission fragments released in fission. The following table was compiled for ^{133}I. Data for this isotope was preferred to that for ^{131}I which required intermediate values to be interpolated from the diagram.

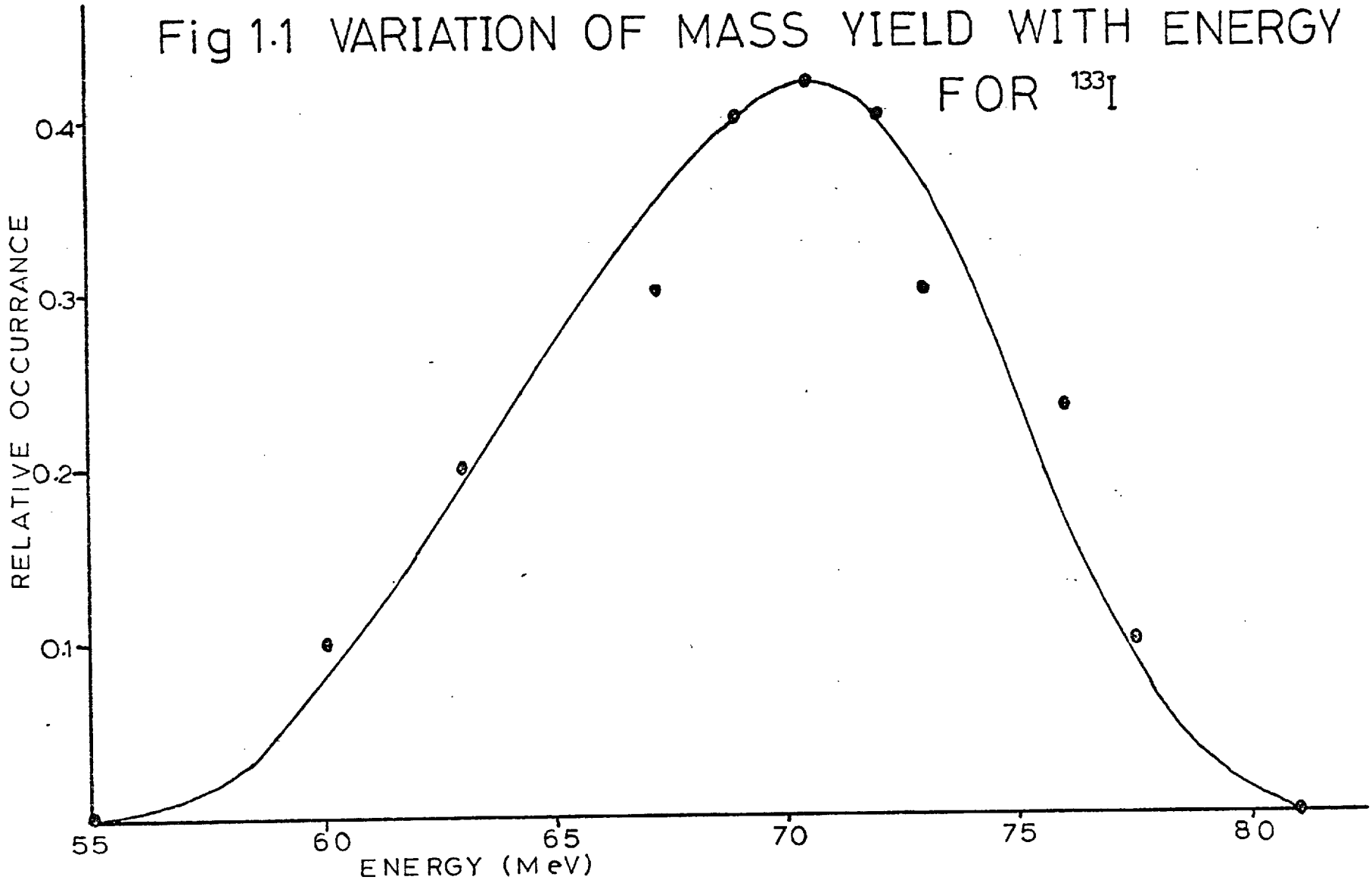
Table 1.2

Frequency of occurrence of ^{133}I from fission, with different energy

Relative occurrence of mass 133 α	Energy MeV E		αE	
0.1	60.0	77.5	6.0	7.75
0.2	63.0	76.0	12.6	15.2
0.3	66.0	73.0	19.8	21.3
0.4	69.0	72.0	27.6	28.8

A graph of the energy vs. yield is shown in figure 1.1. An average energy of 69.6 MeV was found for ^{133}I. The average energy was $\sim$74 MeV for ^{129}I, since little data was available. This suggests that the average energy for ^{131}I is $\sim$72 MeV.

Fig 1.1 VARIATION OF MASS YIELD WITH ENERGY FOR ^{133}I



1.1.2. The distribution in fragment mass

The overall energy balance in fission can be written as:

$$M_Z^A = M_{Z_1}^{A_1} + M_{Z_2}^{A_2} + \nu n + E_n + E_m + E_\gamma \quad (1.1)$$

M_Z^A = mass of original nucleus

$M_{Z_1}^{A_1}$, $M_{Z_2}^{A_2}$ = masses of fragments

ν = number of neutrons, rest mass n

E_n = kinetic energy of the neutrons

E_m = kinetic energy of the fragments

E_γ = energy of prompt γ-rays emitted during fission

From this, it can be seen that there are many possible combinations of mass and charge for fission fragments. These variations are enhanced by the considerable range in the kinetic energy of the fragments, which is dependent on the mass split. Experiments have shown that the mass distribution changes with excitation energy and depends on the mass number of the system undergoing fission. Most surprising of all is the strong preference for heavy elements, at low excitation energy, to fission into fragments of unequal mass. This is not predicted by the liquid drop model, from which a symmetrical mass division would be expected. At present, no theoretical model is rigorous enough or sufficiently free of parameter fitting to explain this phenomenon of asymmetric mass distribution. It is thought to depend in some way on the dynamics of the nuclear motion between the saddle point (compound nucleus) and the moment of scission (7).

The median mass number at half the maximum height for the heavy group is approximately constant at between 137 and 140. It is independent of the neutron energy and

mass of the fissile target. However, the mass number for the light group varies to account for the total mass of the fissioning system (8). The pronounced stability of the heavy peak is another illustration of the closed proton (Z = 50) and closed neutron (N = 82) shell structures in this region. The constancy in position of the light side of the heavy peak for various fissioning nuclei is also explained in this way. However, this can only be part of the explanation, as the yields of adjacent nuclei with incomplete nuclear shells, or with too many nucleons for closed shells, are not lowered correspondingly. Values of the mass distribution for thermal neutron-induced fission of ^{235}U are expressed as the median mass number at half-maximum height. These are 95 for the lighter group and 138.5 for the heavier group (8). Approximately 97% of all the fragments emitted have mass numbers between 72 and 162.

The symmetric mass yield, which is lowest for thermal neutron-induced fission of ^{235}U, increases with neutron energy. In changing from thermal neutrons to fission-spectrum neutrons, it is increased by a factor of 3. 14 MeV neutrons increase it by a factor of 100. Table 4.13 shows the mass yields of the iodine fission fragments formed in thermal fission.

Fine structure has been observed in the fission product mass distribution and has been correlated with structure observed in the energy release in fission. It is thought to occur because energy release is greater for even-even fragments than for odd mass fragments. The former have a lower ground state, due to nuclear pairing of the nucleons. There is also a preference for forming even-even primary fragments in the fission of an even-even compound nucleus such as ^{236}U. The structure has a period of 5 mass units (9).

This agrees with theory because the mass number of the most stable nuclei for a given Z changes by about 2.5 units for a unit change in Z (10). See figure 1.2 which was taken from reference 7.

1.1.3 The distribution in fragment charge

The division of charge between the two fragments can be determined from a knowledge of the independent yield of each isobar in the mass chains involved. However, these values are sometimes difficult or impossible to obtain by radiochemical determination. Fissioning nuclei have a lower charge-to-mass ratio than stable nuclei. The primary fission products are neutron rich and decay by β-decay to more stable nuclear masses. Often, the primary products are so neutron rich that their β-decay half lives are too short for radiochemical yields to be measured.

It is known that the charge distribution for any mass number is Gaussian. Also, the thermal neutron induced fission of ^{235}U gives a similar distribution width for all masses. This has led to the assumption of a universal charge distribution curve, from which the most probable charge for any mass chain can be obtained, if a single independent yield is known.

The independent yield is defined as the yield for an isobar, which does not result from the β-decay of the adjacent isobar. It is a fraction of the total yield of all the isobars of the same mass. Its dependence on charge is given by:

$$P(Z) = (C\,\pi)^{-1/2} \exp\left[-(Z - Z_p)^2/C\right] \qquad (1.2)$$

The normalising constant C has an average value of 0.82 ± 0.14, the largest deviation occurring near closed shells. It is included because the sum of the independent yields must

equal unity for each mass.

The most probable charge, Z_P, can be predicted on the basis of the equal charge displacement postulate (10). This assumes that the difference between the most probable charge Z_P and the charge of the most stable isobar of that mass chain, Z_A, will be equal for the light and heavy complementary fragments. This general trend has been confirmed by experiment (11).

If $$(Z_P - Z_A)_l = (Z_P - Z_A)_h$$

For thermal fission of uranium

$$Z_{Pl} = 92 - Z_{Ph}$$

$$\therefore \quad Z_{Ph} = 46 - (Z_{Al} - A_{Ah}) / 2 \qquad (1.3)$$

Also, $$A_l + A_h = 236 - \nu \qquad (1.4)$$

Using these equations, the most probable charge for mass A_h can be found as discussed in section 4.4.1. where the independent yield analysis is described, and calculations of the charge distribution and independent yield of the iodine isotopes are shown.

The number of prompt neutrons ν emitted after scission is strongly dependent on the fragment mass and the mass split. A strong saw toothed variation is found in the graph of neutron yield vs. fragment mass, see figure 1.2(7). Most neutrons are emitted near closed shell nuclear structures (12). An average value of 2.5 is used for the thermal neutron-induced fission of ^{235}U.

1.1.4. Fission Fragment Decay

The fragments emitted in fission often have lower charge to mass ratios than those observed in the stable isotopes of the same element. They reach stability through

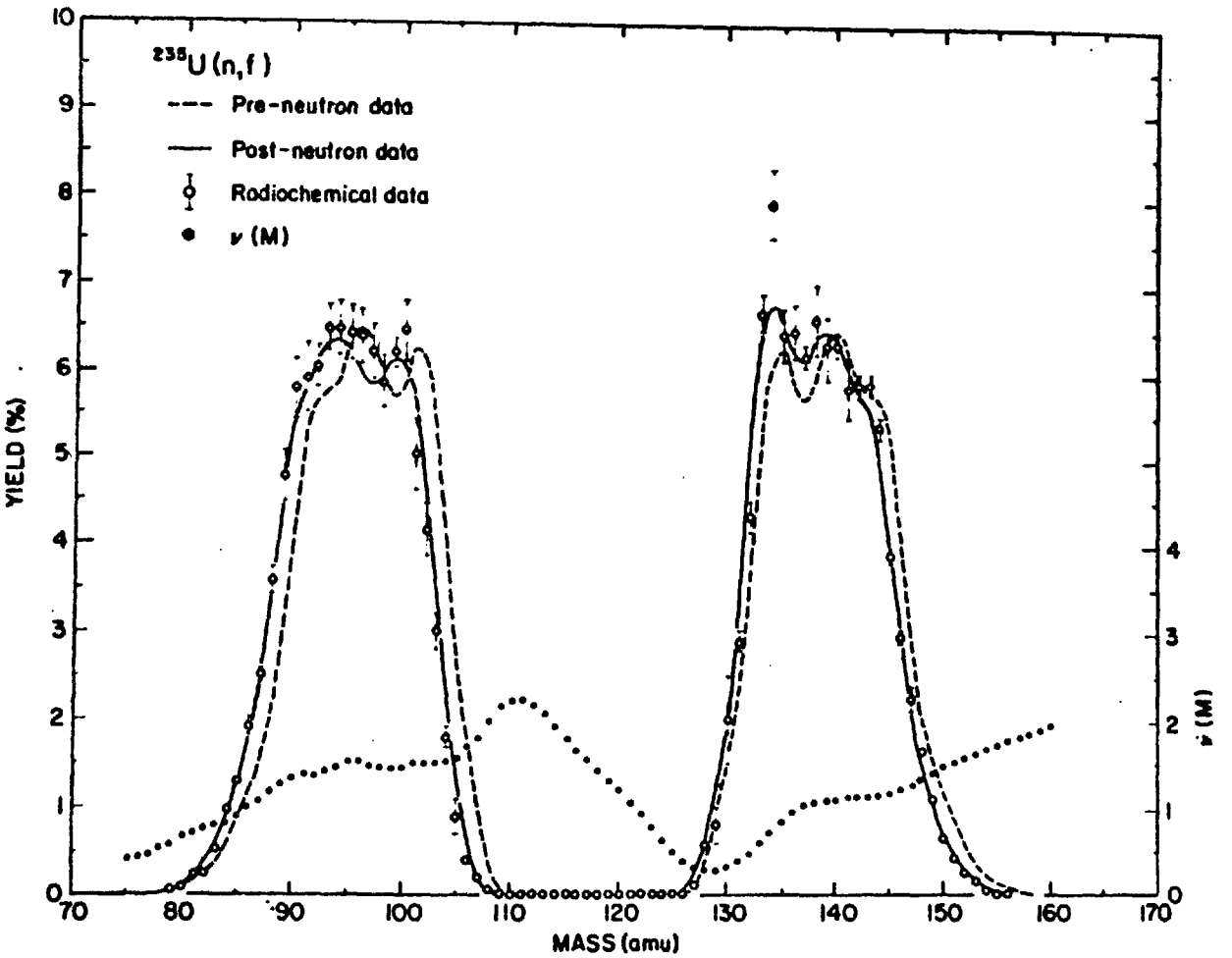


Fig 1.2 VARIATION OF NEUTRON YIELD WITH FRAGMENT MASS (curve •)

THE DATA IS USED TO CALCULATE THE POST NEUTRON EMISSION MASS DISTRIBUTIONS. THIS CURVE IS SHOWN TOGETHER WITH RESOLUTION CORRECTED PRENEUTRON EMISSION MASS DISTRIBUTIONS AND THE RADIOCHEMICAL FISSION PRODUCT MASS DISTRIBUTIONS.

β-and γ-decay in radioactive decay chains. On average, each fragment undergoes three β-decays before it reaches stability. Other radioactive decay processes such as positron emission, α-particle emission and electron capture processes are characteristic of proton rich nuclei, and so have a very small probability of occurrence in fission fragment decay. Several prompt neutrons are emitted within 10^{-12}s after scission. Later, delayed neutrons are emitted. Although these only amount to 0.0173 neutrons per fission of ^{235}U, they are very important in reactor control. They are emitted after β-decay has occurred in the decay chain, e.g. ^{87}Br, $t_{\frac{1}{2}} = 55s$; ^{137}I, $t_{\frac{1}{2}} = 22s$.

(a) β-decay

The stability of a nucleus to β-decay can be found from a consideration of the nuclear binding energy. A semi-empirical formula has been derived which relates the binding energy E_B(MeV) to its nuclear composition.

$$E_B = 14.0A - 13.1A^{2/3} - 0.585Z(Z-1)A^{-1/3} - 18.1(A-2Z)^2A^{-1} + \delta A^{-1}$$

The last term shows that E_B for a given mass number A depends on whether Z and N are even or odd. δ is called the pairing term and varies slightly with A. Above A = 80, an average value for N, Z even is +0.132 MeV amu^{-1}. If N, Z are odd, δ = -0.132 MeV amu^{-1}. If N is even or odd and Z is the opposite, δ = 0.

If the total atomic mass M of the element is considered

$$M = ZM_H + (A-Z)M_N - E_B \qquad (1.5)$$

M_H is the mass of a hydrogen atom (one proton and electron)
M_N is the mass of a neutron.
Substituting for E_B gives a quadratic in Z

$$M = aZ^2 + bZ + c - \delta A^{-1} \qquad (1.6)$$

The most stable nuclear charge, Z_A, for a given mass is the

nucleus with minimum mass or maximum E_B , and can be found by differentiating the above equation

$$Z_A = - b/2a$$

The error in Z_A values calculated this way is approximately 1 unit. The major discrepancies between these values and experiment occur near magic numbers and reflect the omission of the shell model in deriving the binding energy formula. Rearrangement of the above equation gives

$$M = a\left(Z + \frac{b}{2a}\right)^2 - \delta A^{-1} + \left(c - \frac{b^2}{4a}\right)$$

Substituting for Z_A

$$M = a(Z - Z_A)^2 - \delta A^{-1} + \left(c - \frac{b^2}{4a}\right) \qquad (1.7)$$

This is the form of the equation which is ued to plot the energy parabolas. For a given value of A, the last term is a constant and need not be evaluated. The ordinate is taken as $a(Z - Z_A)^2$ and the abscissa is Z. Thus the zero on the ordinate scale corresponds to Z_A. The term δ provides two parabolas if A is even and with them arises the possibility of several stable nuclei. In general, the width of the parabola determines the number of stable nuclei. It increases with increasing A (decreasing values of a). If A is odd, $\delta = 0$ and only one parabola is obtained. Such a plot provides approximate values for the available energy for β-decay between neighbouring isobars.

β-particles have a continuous energy distribution from zero to the maximum value of the energy lost by the nucleus through β-decay. A neutrino is emitted simultaneously with the β-particle and accounts for differences in energy and momentum between the parent and daughter nucleus not manifested in the β-particle properties. The neutrino has no mass and so it does not interact with matter. Only a fraction

of the β-decay energy is seen in sources as radiation effects and heat. Calorimetric experiments have shown this fraction to be a third of the total energy available.

(b) γ-decay

The daughter nucleus is often left in an excited state after β-decay. The nucleus looses this energy through the emission of γ-rays which are sometimes accompanied by internal conversion processes. In these decay modes, the excited nucleus transfers its energy to an electron which is ejected from the atom with an energy equal to the difference between the transition energy and the binding energy of the electron to the atom.

β- and γ-irradiation will occur due to decay of fission fragments in the host lattice. However, this source of radiation will be expected to cause less damage than that associated with fission fragment recoil. See section 1.3.6.

1.2. Fission Damage - The Fragment

1.2.1. Initial charge on the fission fragment

Contrary to expectation, the electrons orbiting around the uranium nucleus before fission are not found redistributed between the fission fragments in accordance with their nuclear charge. Only those electrons with average velocities in the uranium nucleus before fission which are greater than the initial linear velocity of the fragment after fission, are carried away, and many are left behind. The relationship between the effective atomic charge and the velocity of the fragment has been derived by Bohr (13). The velocity V of an electron in an atom of effective atomic charge Z_{eff} and in an orbit of effective quantum number n is given approximately by

$$V = Z_{eff}V_o/n \qquad (1.8)$$

where V_o is the velocity of an electron in the first Bohr orbit of the hydrogen atom, with energy 13.6 eV. The effective quantum number of outer electrons in partially stripped heavy atoms has a flat maximum over a large range, and is given by $n = Z^{1/3}$. Substitution of this into the above equation gives

$$Z_{eff} = Z^{1/3}V/V_o \qquad (1.9)$$

Using this formula, the effective atomic charge Z_{eff} for a fragment of iodine, mass 133 amu and energy 69.6 MeV (see section 1.1.1.) was calculated as follows.

It is known that electrons with orbital velocities less than the linear velocity of the fragment will be left behind. Using the kinetic energy relationship $E = \frac{1}{2}mv^2$, the velocity of the fragment was found to be 1.005×10^6 $m.s^{-1}$. (An electron with similar velocity would have energy 287 eV).

From the same relationship the velocity of an electron in the first Bohr atom is $2.186 \times 10^{5}\ ms^{-1}$. Since $Z = 53$ for iodine, $Z_{eff} = 17.25$.

Figure 1.3 shows the relationship between the effective atomic charge and the fragment energy. Of course, this neglects the effect of the medium as the fragment slows down, and only describes the initial relationship. It is interesting to note that when $Z_{eff} = 1$, the velocity of the fragment is $5.8 \times 10^{4} ms^{-1}$ and the energy is 0.234 MeV. This is much smaller than the energies expected from the fission fragments entering KCl, but is still large enough to damage the medium.

Z_{eff} was also found for the average heavy and light fragments resulting from thermal neutron induced fission of ^{235}U, described in section 1.1. Table 1.3. is a tabulation of the properties of heavy and light fragments.

Table 1.3

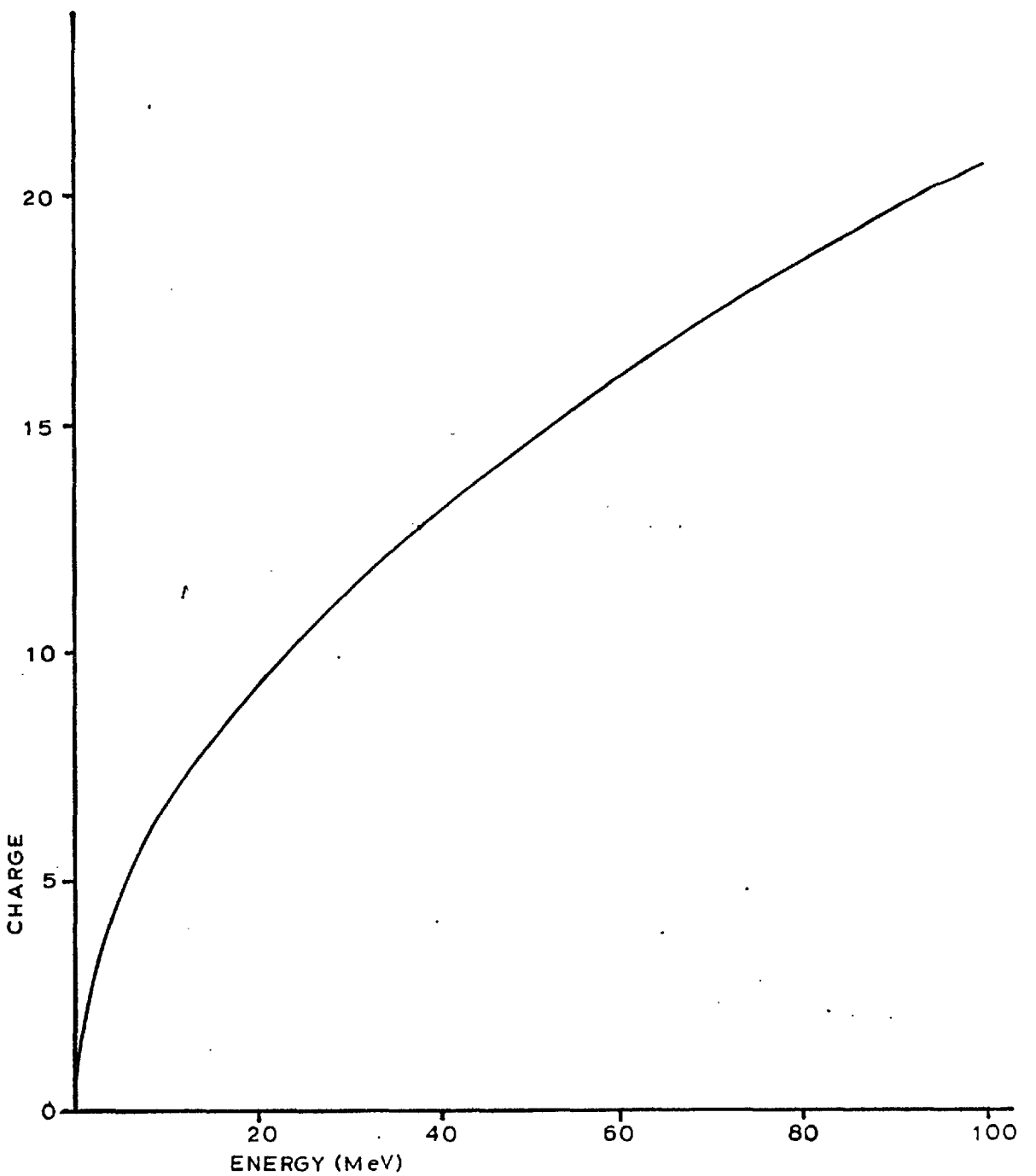
Properties of fission fragments

	Average Heavy	Average Light
Mass (amu)	138.5	95
Energy (MeV)	61.4	93.1
Velocity (ms^{-1})	0.94×10^{6}	1.4×10^{6}
Nuclear charge (14)	57.25	41.7
Effective atomic charge	16.30	21.80

1.2.2. Passage of the fission fragment through the medium

At first the fragment will be travelling too fast to be affected by the electrons and nuclear potentials of the atoms in the medium. Due to its high effective charge, the fragment looses energy, mainly through Coulomb interaction with the electrons. This causes ionisation and electronic

Fig 1·3
VARIATION OF CHARGE WITH ENERGY FOR FISSION FRAGMENT ^{133}I



excitation of the medium. About 80 - 85% of its energy is dissipated in this way. At lower velocities, its charge is reduced as it starts to capture ionised electrons along its path.

This situation can be considered, in the frame of reference of the fission fragment, as a cloud of electrons moving towards it with its own velocity (6). The fragment will loose its electrons to the cloud when their binding energy is less than the kinetic energy of the cloud electrons with respect to the fragment. It will collect electrons when their kinetic energy is less than the binding energy of the electrons on the fragment. It can be seen that the velocity of the fragment determines its effective atomic charge throughout the slowing down process. At first, the rate of slowing down is fast due to the high charge involved in the Coulomb interactions. As the effective charge on the fragment decreases, due to electron pick-up, the rate of slowing down also decreases.

During the slowing down process, the fragment will reach a stage, firstly, where it is unable to ionise and, secondly, where it is unable to cause electronic excitation. These energies are given by the approximate relationship

$$E \simeq \frac{MI}{m} \qquad (1.10)$$

M is the fragment mass

m is the electron mass

I is the ionisation potential or the lowest excitation potential of the valency electron.

The energy above which ionisation losses are predominant is given for insulators by (15)

$$E_c = 1/8\,(MI/m) \qquad (1.11)$$

Here, I is the lowest electronic excitation energy. This was taken as the sum of the energy of absorption for F

centres in KCl and the thermal ionisation energy for F centres, i.e. 2.463 eV (16). Therefore for a fission fragment of average mass 116.75 amu passing through KCl,
$E = 6.62 \times 10^4$ eV.

As the fragment reaches the end of its path and the electronic excitation becomes small, direct collisions with the nuclei of the stopping medium begin to predominate. These are inelastic at first, and can be described by Rutherford's scattering law. Normally, this describes the collision between two point charges and masses with central fields of force. This is not the case for a fission fragment and an atom. The real situation can be considered by replacing the Coulomb potential of Rutherford scattering by a function that allows for the screening effect of the bound electrons.

$$V(r) = (Z_1 Z_2 e^2/r) \exp(-r/a) \qquad (1.12)$$

where a is a screening parameter

$$a = a_o/(Z_1^{2/3} + Z_2^{2/3})^{\frac{1}{2}} \qquad (1.13)$$

a_o is the Bohr radius of the hydrogen atom.
Rutherford's law holds for weak screening which occurs at high fragment velocities. At such velocities the collision diameter b is much smaller than the screening radius a

$$b = 2Z_1 Z_2 e^2/\mu V^2 \qquad (1.14)$$ where μ is the reduced mass

As the fission fragment slows down, b increases. When b is much greater than a, Rutherford scattering no longer applies and hard sphere collisions predominate.

The energy, E_A, at which Rutherford collisions equal hard sphere collisions can be calculated. This is when the collision diameter equals the screening radius. Then (17),

$$E_A = E_r \left[\frac{2(M_1 + M_2)}{M_2}\right] Z_1 Z_2 (Z_1^{2/3} + Z_2^{2/3})^{\frac{1}{2}} \qquad (1.15)$$

$$= 4.56 \times 10^5 \text{ eV}$$

This is calculated for an average fission fragment $M_1 = 116.75$, $Z_1 = 49.9$ passing through a medium of mass $M_2 = 37.275$, $Z_2 = 18$ (the average for K and Cl), E_r is taken as 13.6 eV, the Rydberg energy (the energy of an electron in the first Bohr orbit of the hydrogen atom).

The energy, E_B, below which all collisions lead to displacement can also be found from (17).

$$E_B = 4E_r^2 Z_1^2 Z_2^2 (Z_1^{2/3} + Z_2^{2/3}) M_1/M_2 E_d \qquad (1.16)$$

where E_d is the minimum displacement energy, taken here as 25 eV (see section 1.3.1.).

$\therefore$ $E_B = 1.527 \times 10^9$ eV for an average fission fragment passing through KCl.

To summarize, if the fragment's energy is above E_c the main process of energy loss is electronic. When the energy falls below E_A, hard sphere collisions predominate and displacement occurs by this process until the energy reaches E_d, the minimum for displacement. E_B is the energy below which all collisions lead to displacement. It need not be less than E_c, but it has to be greater than E_d.

1.2.3. Range of fission fragments

The range of a fission fragment in a crystal is related to the rate of energy loss, or stopping power, by

$$R(E_o) = \int_o^{E_o} dE/(-dE/dx) \qquad (1.17)$$

In general, the stopping power has contributions due to electronic, nuclear and radiative processes. For heavy energetic ions, such as fission fragments, radiative losses are negligible. The greatest contribution to the stopping power is due to electronic excitation, since the fragment loses most of its energy in this way. At the end of its range the fission fragment has a more slowly varying charge,

electronic excitation is less, and nuclear collisions are its main mechanism of energy loss.

An approximate ratio of the energy loss due to nuclear collisions to that due to electronic collisions for any value of the velocity of the fragment is given by (17)

$$\frac{(-dE/dx)_{\text{nuclear}}}{(-dE/dx)_{\text{electronic}}} = \frac{Z_2 m_e}{M_2} \left(Z_1/Z_{1\,\text{eff}}\right)^2 \qquad (1.18)$$

with usual notation.

This ratio increases greatly at the end of the range as $Z_{1\,\text{eff}}$ decreases, and is greater than unity at a fragment energy of several MeV. This agrees with the observation of a heavy deposition of energy at the end of the fission fragment track, amounting to between 5 and 10% of the total energy release.

The above formula allows $Z_{1\,\text{eff}}$ to be calculated for a fission fragment where electronic processes account for 80 - 85% of the energy loss mechanism (see section 1.2.2.). A fission fragment of average mass 116.75 amu and probable charge 49.9 (14) is taken as the energetic particle in KCl. $Z_{1\,\text{eff}}$ is found to be 2.4. This shows that when the fragment has reached a charge of approximately 3+, nuclear processes become significant.

There is no one formula to evaluate the electronic stopping power over the complete range of energy and mass. Chadderton (17) reviews the various equations and their regions of applicability. For this reason, range is usually determined experimentally. This has been simplified by the observation of several useful correlations. One such correlation relates the electronic range of the fragment or heavy ion to the range of an α-particle which has the same initial velocity V as the fission fragment in the material in question (13).

$$\frac{R_{electronic}}{R_{\alpha}} = 7.5\, M_1 Z_1^{-2/3}\, (V_o/V)^2 \qquad (1.19)$$

V_o is the velocity of an electron in the first Bohr orbit of the hydrogen atom with energy 13.6 eV. M_1 and Z_1 are the mass and nuclear charge on the fragment. This form is convenient because R_α has been plotted as a function of velocity or energy for many materials. Heavy fragments in substances with medium atomic numbers gave results that agreed best with experiment.

An empirical relationship that gives a better description of the ranges of plutonium fission fragments in air at 15°C and 760 mm pressure is (6)

$$R \propto M_1^{-1/6}\, E^{1/2} \qquad (1.20)$$

A useful observation by Segré and Wiegand was that the relative thickness of absorber and aluminium required to reduce fission fragment recoils by a given amount is constant over most of the range. Also the atomic stopping power was found to be roughly proportional to the square root of the atomic number of the material.

Using this last statement, it is possible to predict the maximum range for fission fragments in a tablet of KCl by comparison with their range in Al. The atomic stopping power is expressed as g mol m^{-2}. The average range of a fission fragment in Al was found from (18). A value of 3.73×10^{-7} gm^{-2} was taken since this is the mean of the ranges for the average light and heavy fragments. This was converted to g mol m^{-2} by dividing by the molecular weight of aluminium. A typical KCl tablet is of mass 0.3 g and volume 0.1906×10^{-6} m^3

Since $X_1 \sqrt{Z_1} = X_2 \sqrt{Z_2}$

where X_1 is in g mol m^{-2} for Al

evaluation of this equation gives 27μ as the average range for a fission fragment through KCl. The range for the average light fragment is 31μ and that for the average heavy fragment is 23.8μ. These values agree with the experimental range for fission fragments of 15μ which was found by Young (19).

The range for ^{131}I in Al is given as 3.48×10^{-7} g m^{-2} (18). Using the above formula, the corresponding range in KCl is 25.6μ. Therefore, in the context of this thesis, there is little difference between the range of ^{131}I and the average range for a fission fragment in KCl.

So far, consideration has been given to the linear range. Due to atomic scattering, the penetration of the fragment will often be less than this value. Figure 1.4 shows several types of ranges that can be considered.

R_L is the total path length, measured along the path of the incident particle.

R_V is the vector distance between start and finish.

R_P is the projection of the vector range onto the initial direction of motion. This gives the penetration.

R is the lateral spread of the particles.

Good and Wollan (20) investigated the slight variation in ranges for certain fission products in gases, often called the range straggling. They identified straggling as resulting from electronic and nuclear stopping and variations in the energy of the fission process. The electronic stopping was considered negligible as it amounted to 0.2%. Using Bohr's expression (13) for the nuclear range straggling, they were able to relate the total straggling to that contributed by the fission process. They found values of 8 MeV and 3.5 MeV for the full width at half maximum for light and heavy fragments. These values, although obtained from

Fig 1.4 DIAGRAMATIC REPRESENTATION OF VARIOUS RANGE MEASUREMENTS

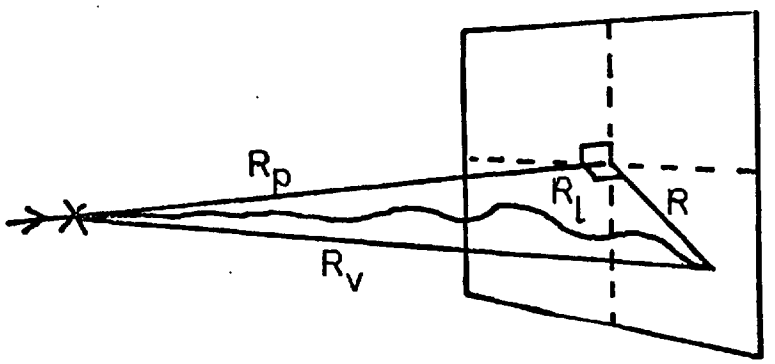
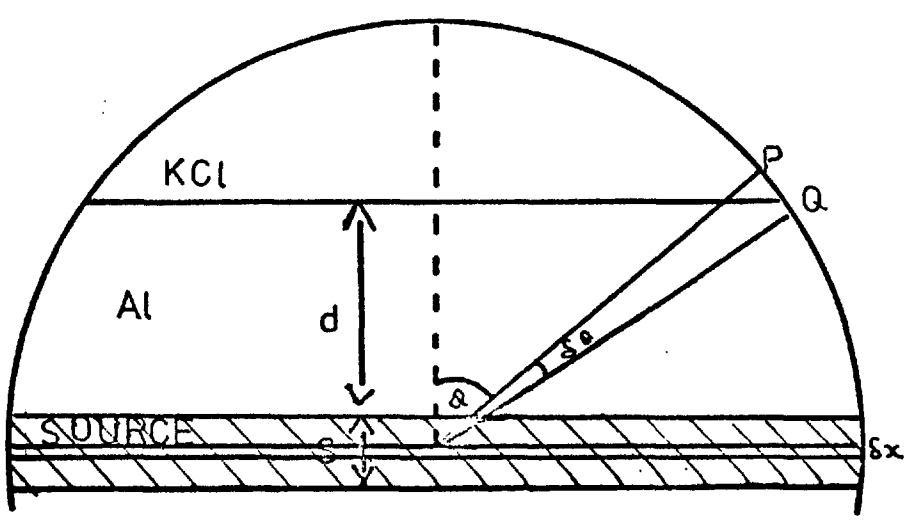


Fig 1.5 DIAGRAM FOR CALCULATING THE NUMBER OF FISSION FRAGMENTS ENTERING THE TABLET OF KCl



scattered results, were reported to agree well with theoretical values of 8 MeV and 5.6 MeV derived by Fong.

An investigation into the penetration distribution of ^{85}Kr in Al for ions with different energy by Davies et al (21) revealed a tailing off in the penetration depth which increased at higher energies. Such 'straggling' was found not to occur in amorphous solids such as Al_2O_3 and WO_3 , and so this property was attributed to crystalline solids only. This implied that the geometry of a crystal lattice can also influence the stopping of fragments and be responsible for long range transport of fragments, and their associated damage. This is discussed in section 1.3.5. Thus, it should be noted that some fragments would be able to travel further than the ranges calculated above.

1.2.4. A calculation of the number and energy of fission fragments entering KCl.

(a) Theory (22)

The fission fragments are created in a source of U_3O_8 of film thickness S and pass through an aluminium screen of thickness d before entering the tablet of potassium chloride, as shown in figure 1.5. Let the source have an area A and thickness δx. If the number of fission fragments generated per cm^3 in the source is N_o then, total number of fragments generated is $N A\delta x$. The number of particles emitted through $\angle\theta$ with range r is given by the number arriving on the surface of a band, generated by revolving PQ about x.

Surface area of band = $r\,\delta\theta\; 2\pi\, r\sin\theta$

But $N_o A\delta x$ particles will fall on an area $4\pi r^2$

$\therefore$ number falling on surface area of band = $\frac{1}{2}N_o A \sin\theta\;\; \delta\theta\;\; \delta x$

Let d be the thickness of Al film and S the thickness of the source. Fragments will not be emitted at angles

larger than $\cos^{-1}\frac{x+d}{R_o}$ to the normal, where R_o is the range.

(i) The total number of fragments N_t emitted from a source of thickness S through an absorber of thickness d

This is given by:

$$N_t = \int_{x=0}^{x=S} \int_{\theta=0}^{\theta=\cos^{-1}\left(\frac{x+d}{R_o}\right)} \tfrac{1}{2} A N_o \sin\theta \, d\theta \, dx$$

$$= \tfrac{1}{2} A N_o \int_0^S 1 - \frac{(x+d)}{R_o} \, dx$$

$$= \tfrac{1}{2} A N_o \left[\frac{-x^2}{2R_o} - x\frac{(d - R_o)}{R_o} \right]_0^S$$

$$= \tfrac{1}{2} A N_o S \left(1 - \frac{S + 2d}{2 R_o}\right) \qquad (1.21)$$

(ii) The total energy E_t of fragments emitted from a source of thickness S through an absorber of thickness d

The energy emitted is related to the residual range R by

$$E = f(R)$$

where

$$R = R_o - \frac{x+d}{\cos\theta}$$

The total energy carried by all the fragments emitted from the absorber is given by

$$E_t = \int_{x=0}^{x=S} \int_{\theta=0}^{\theta=\cos^{-1}\left(\frac{x+d}{R_o}\right)} \tfrac{1}{2} A N_o f\left(R_o - \frac{x+d}{\cos\theta}\right) \sin\theta \, d\theta \, dx$$

Now $E = aR^2$ (6)

$$\therefore E_t = \frac{aAN_o}{2} \int_{x=0}^{x=S} \int_{\theta=0}^{\theta=\cos^{-1}((x+d)/R_o)} R_o^2 \sin\theta + \left(\frac{x+d}{\cos\theta}\right)^2 \sin\theta - 2R_o\left(\frac{x+d}{\cos\theta}\right) \sin\theta \, d\theta \, dx$$

Integration and evaluation w.r.t. θ gives

$$E_t = \frac{aAN_o}{2} \int_{x=0}^{x=S} R_o^2 + 2R_o(x + d)\ln\left(\frac{x + d}{R_o}\right) - (x + d)^2 \, dx$$

Integration of the second terms is by parts, giving

$$E_t = \frac{aAN_o}{2} \left[R_o^2 x + R_o\frac{(x + d)^2}{2} \left\{ 2\ln\left(\frac{x + d}{R_o}\right) - 1 \right\} - \frac{(x + d)^3}{3} \right]_{x=0}^{x=S}$$

Evaluation and rearrangement gives

$$E_t = \frac{aAN_o}{2} \left[R_o^2 S - \tfrac{1}{3}\left\{ (s + d)^3 - d^3 \right\} + R_o s(s + 2d) \left\{ \ln\frac{(s + d)}{r_o} - \tfrac{1}{2} \right\} + R_o d^2 \ln\left(\frac{s + d}{d}\right) \right] \quad (1.22)$$

b) Calculation

The source thickness, S, was found from the density of U_3O_8, its mass, and the area covered by the film.

Density of U_3O_8 (23) = 8.38×10^3 g mm^{-3}

Weight of U_3O_8 = 200×10^{-6} g

Diameter of film = 10 mm

The diameter of the platinum disc is 12.72 mm but its surface area was not covered completely by the film.

Area of source A = 78.5 mm^2

$\therefore$ S = 3.04×10^{-4} mm

The absorber thickness of aluminium was obtained by weighing a known area

d = 7.62×10^{-3} mm

The number of fission fragments generated per mm^3 in the source, N_o, is obtained from a typical experiment, using 200×10^{-6} g for mass U_3O_8. (Experiment no.17 at 100^{0}C). Irradiation was for 2 hours.

If the number of fission fragments per s = 8.12×10^{8}

N_o(fission fragments) = 2.45×10^{14}

The cumulative yield for ^{131}I is 2.9% of the heavy mass fragments emitted

$\therefore N_o(^{131}I) = 3.55 \times 10^{12}$

The constant a is found from the relationship $E = aR^2$. The average energy deposited by a fission fragment is found from table 1.1. It is assumed that approximately half the fission products β and γ ray energy will be dissipated in the source.

$\therefore$ E(fission fragments) = 93 MeV

The average range R = 27×10^{-3} mm (section 1.2.3)

$\therefore$ a(fission fragments) = 1.28×10^{6} MeV mm^{-1}

The energy E for ^{131}I = 72 MeV (section 1.1.1)

range R (section 1.2.3) = 25.6×10^{-3} mm

$\therefore a(^{131}I) = 1.099 \times 10^{6}$ MeV mm^{-1}

These values are substituted into equations above to give:

for fission fragments $N_t = 2.08 \times 10^{12}$

$E_t = 5.46 \times 10^{13}$ MeV

$\therefore$ Average energy of a fragment entering KCl = 26.25 MeV

for ^{131}I $N_t = 2.95 \times 10^{10}$

$E_t = 5.62 \times 10^{11}$ MeV

$\therefore$ Average energy of ^{131}I entering KCl = 19.03 MeV

1.3. Fission Damage - The Host Atoms

1.3.1. Displacement and replacement of atoms

If the atoms in the medium receive sufficient energy, they can be displaced from their lattice sites. This kinetic energy can arrive from the high thermal and electronic excitation of the atoms in the wake of the fission fragment. Such displacements are secondary processes arising from the electronic energy of the fragment. At high energies below the ionisation limit, the fragment undergoes Rutherford scattering and some displacement atoms are produced. Below a certain energy given by (17)

$$E_B = 4E_r^2 Z_1^2 Z_2^2 (Z_1^{2/3} + Z_2^{2/3}) M_1/M_2 E_d \qquad (1.16)$$

all collisions produce displacements until E falls below E_d, the displacement threshold.

a) Replacement Energy

E_r is the minimum replacement energy, where

$$2E_r \simeq E_d \qquad (17)$$

Its value is taken as 13.6 eV (the Rydberg energy). Replacement occurs after a head-on collision between two neighbouring atoms where most of the energy is transferred to the second atom. The primary knock-on is left with insufficient energy to escape the potential field of the vacancy it has created. This is a case of dynamic interstitialcy interchange. Through a series of exchanges with atoms in normal sites, an interstitial can drift through the crystal. This can be expected to promote quite a considerable amount of disorder in a binary material such as KCl.

b) Displacement Threshold

E_d is a crystallographic property of the material. A

temperature dependence is introduced by the vibration of the atoms on their lattice sites which produces variations $\simeq kT$ in the value for E_d. k is the Boltzmann constant. A directional dependence for E_d can be understood if one considers that the displaced atom has to pass through a barrier of atoms in the crystal. The resulting interaction potential will depend on the angle of ejection and the configuration of the lattice. A rough value for E_d can be found from the sublimation energy of atoms in solids, which is $\simeq$ 5eV. This is a surface property and since internal sites are being considered, at least twice this value would be expected. Neighbouring effects, which oppose displacement, also have to be considered. Thus the energy required to remove the atom from its site to an interstitial position is taken to be $\simeq$ 25 eV.

1.3.2. Displacements in KCl

Computational experiments for KCl (5) have illustrated the dependence of displacement threshold on the direction of motion. For a K^+ ion displaced in the $\langle 110 \rangle$ direction, E_d lies between 25 and 30 eV. In this direction, displacement is assisted by the surrounding ions of opposite charge which form a lense. An ion moving with $E > 30$ eV can perturb the ionic lense so that the ions move out. However, they are soon reflected back by their own strong interaction with their neighbours and are in time to prevent the K^+ ion from returning to its lattice. Below approximately 25 eV, the interaction is not so strong, and the K^+ ion is able to return.

For a K^+ ion displaced in the $\langle 100 \rangle$ direction, E_d is computed to be $>$150 eV. In this case the K^+ ion is displacing

its neighbour, a Cl^- ion. Therefore, it requires a larger amount of energy to overcome the opposing potential energy and has no ionic lense motion to assist in the displacement. E_d, for a chlorine knock-on, was found to have a similar variation, due to the high lattice symmetry and the comparable size with a potassium atom.

A value for the number of displaced atoms by fission fragments passing through KCl is worked out in section 1.3.4.

1.3.3. Energy transferred in collisions

The probability that a certain amount of energy will be transferred from the particle to the atom is measured by the differential cross-section for energy transfer. This is given by the area of a ring shaped region, in which the path of the incident particle must lie, in order for this energy transfer to occur.

The energy transferred to an atom from radiation damage will range from zero to a maximum value T_m, which corresponds to the energy transferred in a head on collision.

$$T_m = 4 \left[M_1 M_2/(M_1 + M_2)^2 \right] E \quad (1.23)$$

The differential cross-section for the transfer of energy between T and T + dT in Rutherford scattering is given by

$$d\sigma = A(dT/T^2) \quad (1.24)$$

where

$$A = 4\pi a_o^2 \frac{M_1}{M_2} Z_1^2 Z_2^2 \frac{E_r^2}{E}$$

a_o is the Bohr radius, 0.52917 Å

E_r is the Rydberg energy, 13.6 eV

This holds for energies of T_m to the lower limit E_d, where electronic screening cannot be neglected

$$\therefore \quad \sigma_d = \int_{T = E_d}^{T = T_m} \sigma d$$

$$= A \left(1/E_d - 1/T_m \right)$$

$$= 16\,\pi\, a_o^2 Z_1^2 Z_2^2 \frac{M_1^2}{(M_1 + M_2)^2} \frac{E_R^2}{T_m^2}\left(\frac{T_m}{E_d} - 1\right)$$

The average energy transferred in Rutherford collisions is

$$\bar{T} = \int_{T=E_d}^{T=T_m} T\, d\sigma \Big/ \int_{T=E_d}^{T=T_m} d\sigma$$

$$= \frac{E_d T_m}{T_m - E_d} \ln(T_m/E_d) \qquad (1.25)$$

This shows that $\bar{T} \ll T_m$ and illustrates the preference for low energy transfer in Rutherford collisions.

In hard sphere collisions all energy transfers are probable.

$$d\sigma = B\, dT \qquad (1.26)$$

where $B = \pi a_1^2 / T_m$

a_1 is the diameter of the effective hard sphere and approximates to the screening radius.

The transfer from Rutherford collisions to hard sphere collisions is not definite and so a cross section for intermediately screened Coulomb collisions is used in this region.

$$d\sigma = T^{-n} dT \text{ (where n is 1-2)} \qquad (1.27)$$

The approach to the hard sphere approximation does not seem to follow from this. However it can be used to describe displacement cascades because they are insensitive to the form of the energy transfer cross-section.

1.3.4. Number of displacments

There will be an increase in displaced atoms when both atoms have $E > E_d$ after the collision.

This leads to an expression

$$\nu(E_p) = E_p / 2E_d \qquad (1.28)$$

where $\nu(E_p)$ is the number of displaced atoms arising, on the average, from a single primary, energy E_p. Values obtained from this expression are higher than those observed experimentally because the reduction in available energy of E_p after every displacement has not been included. Also, E_d is not a sharply defined value, due to lattice effects. Other more rigorous expressions have been derived, but all give poor agreement with values obtained from resistivity, semiconductivity and density experiments. Displaced atoms can fall into vacant lattice sites to reduce the number of displacements. Other factors exist which are associated with the concentration of damage into a small atomic volume and the overlap of damaged regions. This shows that displacement is a complicated many body process which cannot be described completely.

The total number of displaced atoms is given by

$$n_d = n_p \bar{\nu} \qquad (1.29)$$

where n_p is the number of primary knock-ons

and $\bar{\nu}$ is the average number of displaced atoms due to primary knock-ons of average energy.

It is assumed that $\bar{\nu} = \nu(\bar{E}_p)$ which is true when $\nu(E_p)$ is proportional to E_p.

The number of primary knock-ons is given by

$$n_p = \phi \; t \; n_o \sigma_d \qquad (1.30)$$

where ϕ is the flux

t is the time of bombardment

n_o is the density of atoms

σ_d is the displacement cross-section for Rutherford scattering.

From the equations in this section and the previous section, the total number of displaced atoms produced by fission fragments of average energy 26.25 MeV (see section 1.2.4) travelling through KCl can be estimated.

As in other calculations, the fission fragment is taken to have average mass 116.75 and probable charge 49.9 MeV

$$T_m = 19.26 \text{ MeV}$$

$$A = 6.261 \times 10^{-13} \text{ mm}^2$$

$$\therefore \quad \sigma_d = 2.504 \times 10^{-14} \text{ mm}^2 \text{MeV}^{-1}$$

The number of fission fragments emitted in this case (ϕt) is given in section 1.2.4, since only those that pass through KCl need be considered

$$\therefore \quad \phi t = 2.08 \times 10^{12}$$

The density of atoms in the sample is obtained from section 1.4.1

i.e.

$$n_o = 1.272 \times 10^{19} \text{ atoms mm}^{-3}$$

$$n_p = 6.63 \times 10^{17}$$

From section 1.3.3

$$\bar{\nu} = \bar{T}/2E_d$$

$$= 6.78$$

Due to concurrent annealing, it is probable that only 1/4 of this value will be left (17).

$$\therefore n_d = 1.3 \times 10^{18} \text{ atoms}$$

1.3.5. Crystal Lattice Effects

A particle, either a fission fragment or primary knock-on, will interact with the atoms in a crystal according to its energy. Effective interaction is possible at high energies because the primary is able to penetrate quite close to the atoms in the medium. At lower energies, $\sim$ 60 eV, interaction is less. The lattice is able to impose rigid conditions upon the possible modes of momentum transfer, and it assists in long range transferance of energy and mass. Two processes by which this is accomplished are focusing and channelling.

(a) Focusing

At lower energies, the primary finds that its motion is inhibited by the potential fields of the crystal lattice atoms. It finds that it can transfer energy only by collision with its neighbours in the lattice. These collisions are propagated along a close packed row of atoms until the energy packet is dissipated as vibrational energy of each atom. This could be described as generating a mild thermal spike in the lattice (see section 1.4.1) and could be enhanced by thermal vibrations. Atomic displacement, through lattice vibrations, can also help in dissipating energy out of the line to neighbouring atoms. Energy loss is more rapid for binary materials where the masses are different. It increases in crystals with an increased number of impurity atoms, dislocations and stacking faults.

Let the angle between the momentum vector and line of centres of the two atoms be θ . From a consideration of the hard sphere model of the interaction, conditions can be derived for a focused collision sequence where successive collisions reduce the initial angle θ to zero (17). Collisions become head-on and a component of the initial momentum is focused into the line of centres of the atoms. This is called a focuson and, in theory, should never escape. In practice, a portion of the energy in each collision is retained by each atom and is expended as vibrational energy. If θ increases with successive collisions, momentum and energy will soon be dissipated to neighbouring close-packed rows.

Focused replacements can occur when the energy is within certain limits. In this case, matter is propagated down the line as a dynamic crowdion. This describes the

situation when an extra atom is packed into a line of atoms already sufficient to fill the number of lattice sites in the row. There is a smearing out of the interstitial over the neighbouring atoms, resulting in perhaps five lattice sites being shared by six atoms. Such motion implies that a vacancy is left behind at the beginning. When the energy falls below the lower limit, E_r, the extra atom is deposited as an interstitial, and only energy is continued to be transported.

The result of focusing depends on the direction of the primary atom in the crystal. A collision along $\langle 100 \rangle$ in a face centred cubic crystal, such as KCl, will experience a symmetrical potential distribution of the neighbouring rows of atoms. A collision along $\langle 100 \rangle$ in a body centred cubic crystal will experience marked asymmetrical focusing due to the potential distribution of the diamond shaped rings of neighbouring atoms.

(b) Channelling

This effect is observed at predominantly higher energies than the focusing effect, of about 10 keV. It is due to the passage of a particle through open channels that exist in certain directions in a regular lattice structure. The particle has very little interaction with the lattice after entering the channel and only loses energy through loose interactions with the bordering lattice atoms. There is a central axis of symmetry along the length of the channel, and the net force acting on the primary from the potential of the neighbouring atoms is only a component along the x axis. Usually, the atom will bounce between two adjacent rows of atoms, but the amplitude of this transverse motion can decrease with distance along the channel.

The particle experiencing channelling (the channelon) is responsible for the transport of matter and energy over large distances. This gives rise to the possibility of fission fragments and knock-ons being transported over large distances in the crystal matrix, and could explain the reduction of expected radiation damage in a particular region (21). However, although the initial process of introducing the atom into the channel is not understood, this effect would seem to be less favoured than focusing, and this is observed in practice.

Experiments have not, as yet, been conducted with single crystals of KCl, and this discussion on focusing and channelling is not directly relevant to the experiments discussed here. However, it is presented for completeness, as these effects will certainly occur in the individual crystals which constitute the polycrystalline tablet.

1.3.6. Other sources of damage

By far the most damage associated with the fission process is created by the passage of fission fragments through the medium. The majority of the damage is due to fission spike formation (section 1.4) and the associated displacement and replacement of atoms (section 1.3.1). In order to complete the picture of radiation damage, the effect of electromagnetic, β -ray and neutron irradiation will now be considered.

(a) Neutron irradiation damage

This source of radiation will occur while the sample is in the reactor. Since neutrons carry no charge, their mechanism for damage is by direct interaction with the

nuclei of the host medium. Both fast and thermal neutrons are present during pile irradiation. Fast neutrons are more likely to collide with the nuclei and damage is due to direct displacements by these neutrons. Thermal neutrons are more likely to be captured by the nuclei of the medium, with subsequent transmutations of the nuclei and emission of excess energy as β- and γ-rays. Transmutations are responsible for the existence of certain impurity atoms in the lattice. Table 1.4 shows the effect of thermal neutron capture on isotopes of potassium and chlorine present in KCl. However in most pile irradiations far more atoms are displaced by fast neutrons than are transmuted by thermal neutrons.

Table 1.4

Effect of thermal neutron capture in KCl

Atomic Number	Mass Number							
	35	36	37	38	39	40	41	42
16		S stable						
		1.9%						
17	Cl →	Cl (3.1×10^5 y)		Cl → 95% Cl 0.74 s; 5% Cl 37.3m				
		98.1%						
18		Ar stable		Ar stable		Ar stable		
						11%		
19					K →	K (1.26×10^9 y)	K →	K 12.4h
						89%		
20						Ca stable		Ca stable

The neutrons produced in fission have energies between 0 and 15 MeV with an average value of 2 MeV. The energy of the neutrons reaching the lattice will depend on intervening moderating materials. For neutrons, all recoil energies between 0 and T_m are equally possible.

$$\therefore \qquad \bar{T} = \tfrac{1}{2} T_m$$

where $\bar{T}$ is the mean energy transferred

If the maximum energy is taken to be 2 MeV,

$$\bar{T} = \left(\frac{4}{A}\right)\left(1 + \frac{1}{A}\right)^{-2} \qquad (1.31)$$

This assumes that fast neutron scattering is isotropic and collisions are elastic. This is not true in practice and corrections reduce $\bar{T}$ by $\frac{1}{2}$ or $\frac{2}{3}$. This has more significance at high neutron energies.

(b) Damage due to electromagnetic radiation

γ-and X-ray irradiation produce ionisations in all solids and there is evidence that γ-rays can produce displaced atoms in solids, although the efficiency is low. X-rays are generally of lower energy and so effects will be discussed in terms of γ-rays.

The main sources of γ-ray energy in solids are from fission product decay and the decay of transmuted lattice atoms. The energy ranges from keV to 10 MeV, with an average energy of 1 MeV. γ-rays interact with matter by three processes: photoelectric effect at low energies, the Compton effect at intermediate energies and pair production at high energies. For a given energy, the atomic cross-section for each process is proportional to the atomic number of the absorber. The Compton effect is dominant for fission product sources, γ-rays from the reactor and ^{60}Co sources.

This process causes electrons to be ejected with a spectrum of energies related to the incident γ-ray energy. Thus the solid medium is bombarded internally with fairly energetic electrons. Most of this energy causes further ionisation, but elastic collisions occasionally displace atoms. Displacement becomes more frequent for in pile radiations where the electron energies produced by the fission γ-flux are more likely to be above the threshold energy for displacement, E_d. In this case, because of its small mass, the electron is travelling at relativistic velocities. The maximum energy transferred in a collision between an electron of mass m and an atom of mass M_2 is given by

$$T_m = \frac{2(E + 2mc^2)E}{M_2 c^2} \qquad (1.32)$$

where c is the velocity of light, $m << M_2$ and $E << M_2c^2$. This reduces to the nonrelativistic formula for energy transfer when $E < mc^2$. The penetration and energy loss of relativistic electrons in matter is complicated by relativistic effects and radiative losses.

Dienes and Vineyard (15) derived a formula for the number of displaced atoms by electrons emitted from the Compton effect. For a γ-ray energy $\leqslant$ 1 MeV, the number of displaced atoms is a maximum in very light elements and declines rapidly with increasing Z. It becomes zero at M $\simeq$ 125 for a displacement threshold energy (E_d) of 25 eV and a 1 MeV γ-ray energy. At higher energies the number is a maximum for intermediate or heavy elements.

A similar calculation for displacement by photoelectrons showed that the Compton effect was more important. Calculations also showed that fast reactor neutron radiation would be two to three orders more effective at causing

displacements than reactor γ-ray radiation. However, two other processes exist which can convert the electronic excitation energy to displacement energy, and these could help to increase the effectiveness of γ-ray radiation in causing displacements. They are most effective in insulating crystals such as KCl.

The first process was introduced by Seitz (24) and suggests that excitons, which are localised regions of electronic excitation, wander about in the crystal until they reach a lattice irregularity, where they discharge their energy and create a local hot spot. Such sites might be jogs in dislocation lines. If a jog is heated in this manner, it can induce dislocation climb and this is accompanied by vacancies boiling off at the jog. The energy expended in this way is $\simeq 10$ eV which is sufficient to produce a vacancy. Free electrons and holes created by ionizing radiation can also liberate energy at these sites through recombination. Excitons are produced by U.V. light as well as γ-and X-rays. However no calculations have been published in support of this process.

The second process is the Varley mechanism (25). If a negative ion is stripped of two or more electrons, it becomes positively charged. The electrons move through the crystal. The ion will be ejected to an interstitial site since, as a positively charged ion surrounded by other positive ions, it is in a highly unstable state on the negative ion lattice site. The ion now captures enough electrons to be neutral and the vacant lattice site has the opportunity to capture an electron and become an F centre. Diffusion of the neutral interstitial can occur at a high enough temperature and it can eventually become trapped at a defect. This mechanism can provide an important

contribution to the number of atomic displacements in the crystal. It also provides an explanation for the observation that the experimentally observed cross-section for displacement in alkali halides is 30 times larger than that predicted for direct collisions between electrons and atoms (Relativistic Rutherford Scattering). The mechanism requires a largely ionic lattice, a large cross-section for multiple ionisation, and a recombination time $> 10^{-13}$ s to allow ejection of the ion which must be far enough to prevent it from returning to the lattice site on neutralisation. Multiple ionisation could occur through direct interaction of the γ-rays with more than one outer electron, or through an Auger cascade effect.

A recent computer simulation by Chadderton and Torrens (5) has shown the Varley mechanism to be unlikely. A reasonable theoretical life time for the ionized state was assumed, but replacement was found to occur and, after recombination, the ion settled down in its own lattice site. Pooley suggested that F centres are produced by the separation of a vacancy and interstitial through a $\langle 110 \rangle$ replacement sequence following a radiationless electron-hole recombination. However,Chadderton and Torrens again showed this to be unlikely,since the true threshold for production of a permanent displaced ion is well in excess of the recombination energy of 5 eV and, on account of the ionic lens influence, is likely to exceed 20 eV. It has been suggested that the F centre mechanism is due to the formation of neutral atoms or molecules and their participation in replacement sequences through positive hole tunnelling. However, this has yet to be verified by

computer simulation.

(c) Damage due to β- irradiation

β -rays are also associated with decay of fission products and transmuted atoms of the host lattice. β-decay has been described generally in section 1.1.4, and from this it can be seen that any energy up to a maximum value can be expected. The maximum energy for β -particles generally varies between 0.1 MeV and 10 MeV. When account is taken of the difference between their energies, β-particles have a similar effect on material as electrons produced by γ-interaction with the material. β -particles have a greater probability for interaction with the host atoms but these effects are less uniform than for γ-ray interaction. β -particles penetrate further than fission fragments, due to their small size and charge, but have a range much shorter than that for γ-rays in the same material.

The total energy absorbed by the medium is complicated to calculate and it is usual to take values from experimental curves, such as those produced by Moteff (26) for γ-ray energy emitted from irradiated Uranium for various times after shut down. Allen (14) has published curves showing the power output, due to β-and γ-radiation of fission products from Uranium irradiated at a given neutron dose rate for different times, after various cooling times. The use of these curves is demonstrated in section 4.2.3.

1.4. Fission Spikes

So far, consideration has been given to the individual atomic collisions in the undisturbed lattice. These processes describe secondary effects and are important in considering the final state of the lattice. However, the primary fission product damage in the lattice affects the atoms as groups. Such damage, centred around the fission fragment path, is called a fission spike. This term includes the concepts of thermal and displacement spikes and their associated plasticity spikes. Processes most likely to be affected by spikes are those which nearly go of their own accord at ambient temperature. Instances of nucleation and phase change have been reported.

1.4.1. Thermal Spikes

A thermal spike describes the localised redistribution of the energy involved in damage, which is produced by a fission fragment or knock-on, and is not expended in the displacement of the knocked atom. A fast particle moving through the lattice first loses energy through ionisation. This reappears as thermal vibrations of the lattice in a time that depends on the rate of transfer of excitation from the electrons to the lattice. This occurs through electron-electron collisions and interaction with the lattice vibrations (electron-phonon interactions). The rate of transfer determines the temperature profile of the spike. In an insulating crystal, such as KCl, the rate of transfer is fast and so the electronic excitation is transferred to the lattice in a short time. The corresponding temperature profile is narrow and sharply peaked since the thermal effect dies away as quickly as it is created.

The rate of transfer for metals is much slower and the temperature profile is broader and flatter.

Thermal spikes are also created by collisions which transfer just sufficient energy to cause large amplitude vibrations without displacement of the atoms. The atomic vibrations are shared with neighbouring atoms and the region is heated to a high temperature. This effect is of little importance, when compared with the total heating effect, since only a small fraction of the fission fragment energy is lost in this way.

In both cases the region expands rapidly, and there is an accompanying drastic decrease in temperature. Such rapid heating and quenching of a small volume of material is typical of a thermal spike.

If the atom responsible for starting the spike has high energy, its interaction with the lattice atoms is well separated. These spikes can be described as individual spherical regions or local hotspots at sites where collisions occur. As the moving particle slows down, its interactions become more closely spaced and the individual spikes begin to overlap. At this point, the energy in the spike is assumed to be uniformly distributed along the track of the particle, and so the subsequent temperature distribution has cylindrical symmetry. From the formula for the maximum energy, T_m, transferred in a head on collision (section 1.3.3) it can be seen that energy for spherical spike overlap increases with the atomic numbers of the moving particle and lattice.

It is usual to consider the spreading and subsequent diminishing of the excitation as a form of heat conduction. In fact, the excited region is never in equilibrium with

itself. It exists for approximately 100 lattice vibrations and should not be characterised by a temperature. Also the distances and times involved are so small that the macroscopic laws of heat conduction are not strictly valid. In spite of its shortcomings a model based on the law of heat conduction gives a qualitative picture of the situation (15).

As a first approximation, the medium is considered to be homogeneous. If a moving particle transfers QeV/Å to the lattice, this energy is considered to have been suddenly liberated as heat energy in a localised area of a continuous medium. It then spreads out according to the classical laws of heat conduction. If the medium has a thermal diffusion coefficient D and a temperature T (r,t)at each point r and at time t, the temperature after the beginning of the spike is expressed as

$$\nabla^2 T = \frac{1}{D}\left(\frac{\partial T}{\partial t}\right) \qquad (1.33)$$

where $D = k/C_p d$

k is the thermal conductivity of the lattice

C_p is the specific heat

d is the density

The temperature dependence of D is ignored.

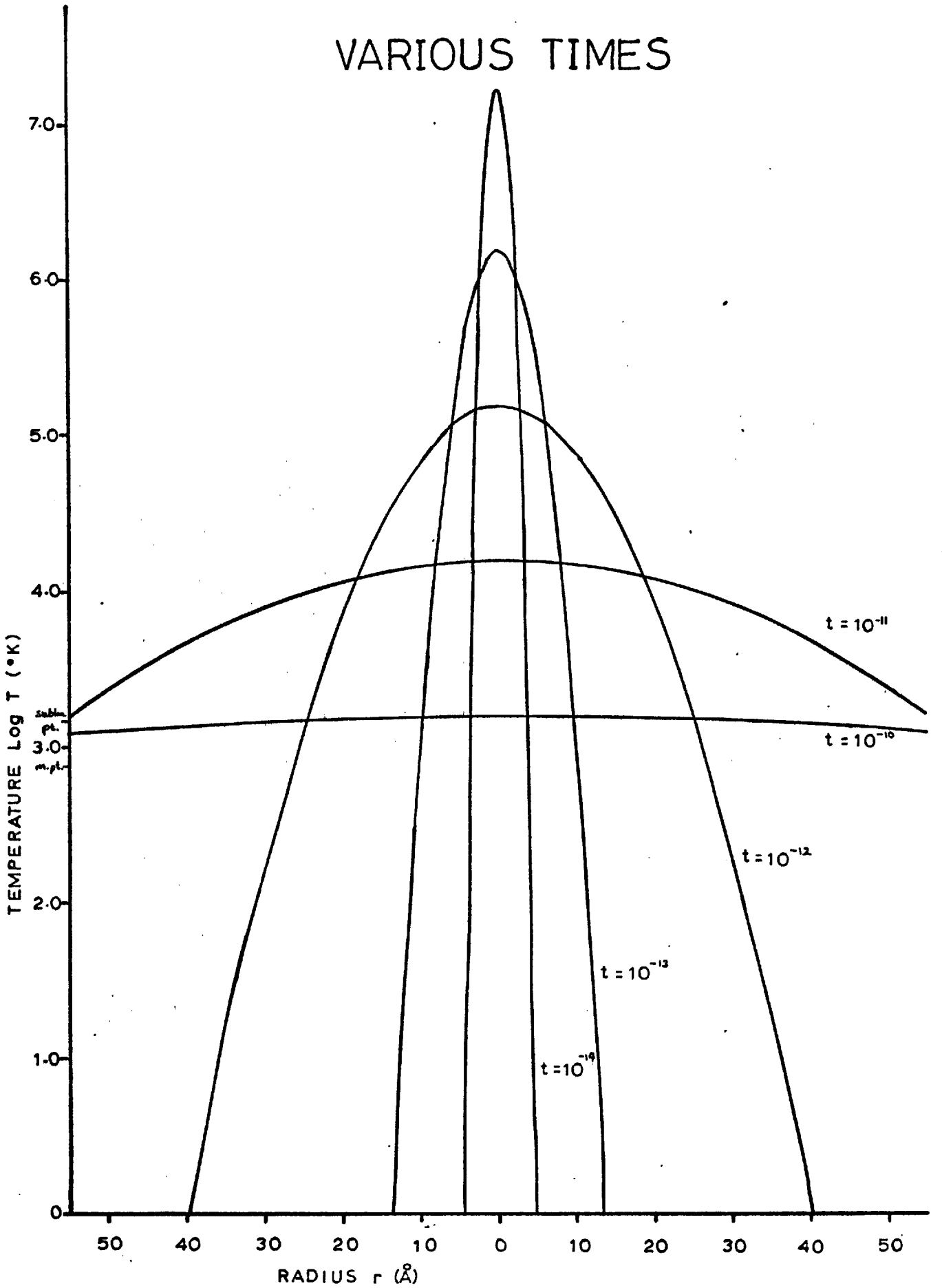
The cylindrical solution to this is

$$T(r,t) = T_o + Q/4\pi C_p d \times \frac{1}{Dt} e^{-r^2/4Dt} \qquad (1.34)$$

and corresponds to the liberation of Q eV/Å along the axis when t = 0 and the lattice temperature is T_o. r is the perpendicular distance from the point of observation to the axis of the spike.

These curves are plotted in figure 1.6, using the following values for a fission fragment of mass 131 and

Fig 1·6 TEMPERATURE DISTRIBUTION IN A TYPICAL THERMAL SPIKE AT VARIOUS TIMES



energy 26.25 MeV passing through a KCl lattice.

Fission fragment path length (19) = 15×10^{-4} cm

Energy liberated per cm, Q = 2.804×10^{-9} joules cm^{-1}

Weight of typical tablet = 0.3 g

Volume of typical tablet = 0.191 cm^3

For a typical tablet, d = 1.574 g cm^{-3}

Diffusion coefficient D = 3.3×10^{-3} cm^2 s^{-1}

Specific heat C_p = 20.922 joules $degree^{-1}$ $molar\ vol^{-1}$

The value chosen for D is that typical of a metal as a condensed gas.

C_p was obtained from the gas equation for an ideal gas. (γ = 1.66 for a monatomic gas)

From figure 1.6, it can be seen that, 5×10^{-13} s after the fragment has entered the tablet, there is damage along its path, 3 Å in radius. This is of the order of a bond length and so, in this time, only immediate neighbours will be affected. The temperature reached by the spike after this time is 4.26×10^3 °K, which is well above the sublimation point for KCl. The temperature at any time has a maximum at the centre of the spike, and this drops as time increases, in proportion to t^{-1}.

(a) Calculations

(i) To find the volume of tablet made molten

The volume of KCl which has been raised above the melting point by the passage of the spike can be found from equation 1.34. If T = 1049 °K (the melting point for KCl) T_o = 300 °K and r = 0, substitution in equation 1.34 gives

$$t = 2.04 \times 10^{-10} \text{ s}$$

This is the time after which no part of the tablet will be raised above the melting point. The volume of tablet which

is molten up to this time from the instant of spike formation is given by

$$V = \int_{t=0}^{t=2.04 \times 10^{-10}} \pi r^2 l \, dt$$

r^2 can be found from equation 1.34 in terms of t when $T - T_o = 749\ ^oK$. If l is taken as the path length of a fission fragment

$$V = \pi \times 15 \times 10^{-4} \int_{t=0}^{t=2.04 \times 10^{-10}} -29.45t - 1.32 \times 10^{-2} t \ln t \, dt$$

Integration of the last term by parts gives

$$V = 6.36 \times 10^{-15} \text{ cm}^3$$

The total volume of the tablet to be raised above the melting point continually during irradiation is given by the product of the volume of the spike, its duration above the melting point and the number of fission fragments emitted per second. A value for the last factor has been found by two different processes. The first involved calculating the energy of a fission fragment and the number entering the tablet after fission, as in section 1.2.4. This gave 2.89×10^8 as the number of fragments per second to enter the pellet. The second process involved calculating the number of fission fragments per second from the experimental value for the activity of ^{131}I and its fission yield, using equation (4.9). A value of 7.93×10^7 fragments s^{-1} was obtained using this method. Both values agree well with the theoretical value of 8.12×10^8 fragments s^{-1} obtained from the amount of fissionable uranium and neutron flux. An average of the first two values give

Number of fragments s^{-1}	=	1.84×10^8
Total vol. melted continually	=	2.39×10^{-16} cm^3 s^{-1}
For comparison, volume of tablet	=	0.19 cm^3
Volume of tablet containing fission fragments (15μ tracks)	=	1.9×10^{-3} cm^3

It can be seen from the last two values that the fractional volume that is molten during irradiation is extremely small.

(ii) To find the number of atoms raised above the melting point

The number of atoms brought to the molten state can be found as follows:

Volume of unit cube (each containing 11 atoms) = 2.49×10^{-22} cm

Number of unit cubes in a spike = 2.55×10^{7}

$\therefore$ Number of atoms affected = 2.81×10^{8}

However, this value is slightly greater than the true value, due to a density factor

Number of atoms calculated by cube method = 8.41×10^{21}

Number of atoms calculated from weight = 4.85×10^{21}

$\therefore$ density factor = 1.74

$\therefore$ True number of atoms affected = 1.61×10^{8}

Total number of atoms damaged continually = 6.04×10^{6}

In practice this last value would be expected to be less, due to the high probability that spikes will overlap.

Due to the confining effect of the surrounding material, the heated volume may not reach a true liquid state. For this reason, the area is referred to as a superheated solid, although true melting may occur at the centre.

(b) Diffusion of ions

Calculations have been made to find the effect of thermal spikes on the diffusion of ions in the lattice (27). As the heating is intense, brief, and over a small volume, the kinetics are not known precisely, and such calculations are only rough guides. The usual rate equation is assumed for an ion jumping to a neighbouring site or interstitial.

$$\nu = \nu_0 \exp(-E/kT)$$

where E is the activation energy

ν_o is the effective frequency

If there are n_o atoms per unit volume, the extra number of jumps Δn induced by the spike is found by integrating the above equation. A complicated expression is obtained. Taking simple solutions, Seitz et al showed that

$$\Delta n = 0.016(\nu_o r_s^2/D)(Q/E)^{5/3}$$

where $r_s = \left[(3/4\pi n_o)\right]^{1/3}$

$\nu_o r_s^2/D$ can be regarded as the ratio of atomic diffusivity to a lattice thermal diffusivity. Values obtained from this were an order of magnitude down on experimental results obtained for the disordering caused by a displaced atom. They concluded that radiation disordering was not primarily due to thermal spikes. Similarly, it has been concluded by other investigators that the production of Frenkel defects (vacancy - interstitial pairs) is not important when compared to their production by displacement cascades and spikes.

1.4.2. Plastic Spikes

Within the central region of the thermal spikes there is the possibility of plastic flow and the subsequent formation of dislocation loops. This is due to the expansion of the material by the heating effect, which causes a region of stress around the spike.

Consider a typical spike of radius r_e which is heated uniformly and neglect heating outside the spike (15). If the flow of heat is slow compared to the velocity of elastic waves, a system of stresses is built up which obey static elasticity theory. In an isotropic material the compressive stress in a radial direction is given by p where

$$p = p_o \quad \text{if } r < r_e$$

$$p = p_o r / r_e^3 \quad \text{if } r > r_e$$

r is the distance from the centre of the spike and

$$p_o = \frac{4(1+\sigma)}{3(1-\sigma)} \mu \frac{\Delta l}{l}$$

where σ = Poisson's ratio

μ = sheer modulus

$\Delta l/l$ = the fractional linear expansion in the absence of pressure

A knock-on with energy 300 eV, passing through copper, was calculated (15) to heat a region of 15 Å diameter to its melting point in 5×10^{-12} s. For such a spike, the compressive stress has been calculated to be $\simeq 10^{10}$ newtons m^{-2} This is sufficient to cause plastic deformation in perfect crystals.

Stress decreases rapidly with increasing radius. At 10 r_e, it is sufficient to move existing dislocations, but cannot initiate plastic deformation in perfect crystals. Since dislocations have to end on a crystal surface, those produced in the interior of a crystal lattice will have the form of a loop. Calculations have shown that the equilibrium diameter for a loop is $\sim$ 10 Å, where the self stresses in the loop are balanced by the thermal stress field in the material. As the spike cools, the material stress decreases and the loop contracts because its energy content is proportional to its length. If contraction is the exact inverse of formation, no plastic spikes remain. In reality, the loops tangle to produce permanent plastic displacements. The system under investigation here is in the form of a compressed powder. Thus, many dislocation loops would be expected, resulting both from compression of the powder and from fission damage. In most irradiated

polycrystalline solids the dislocation density

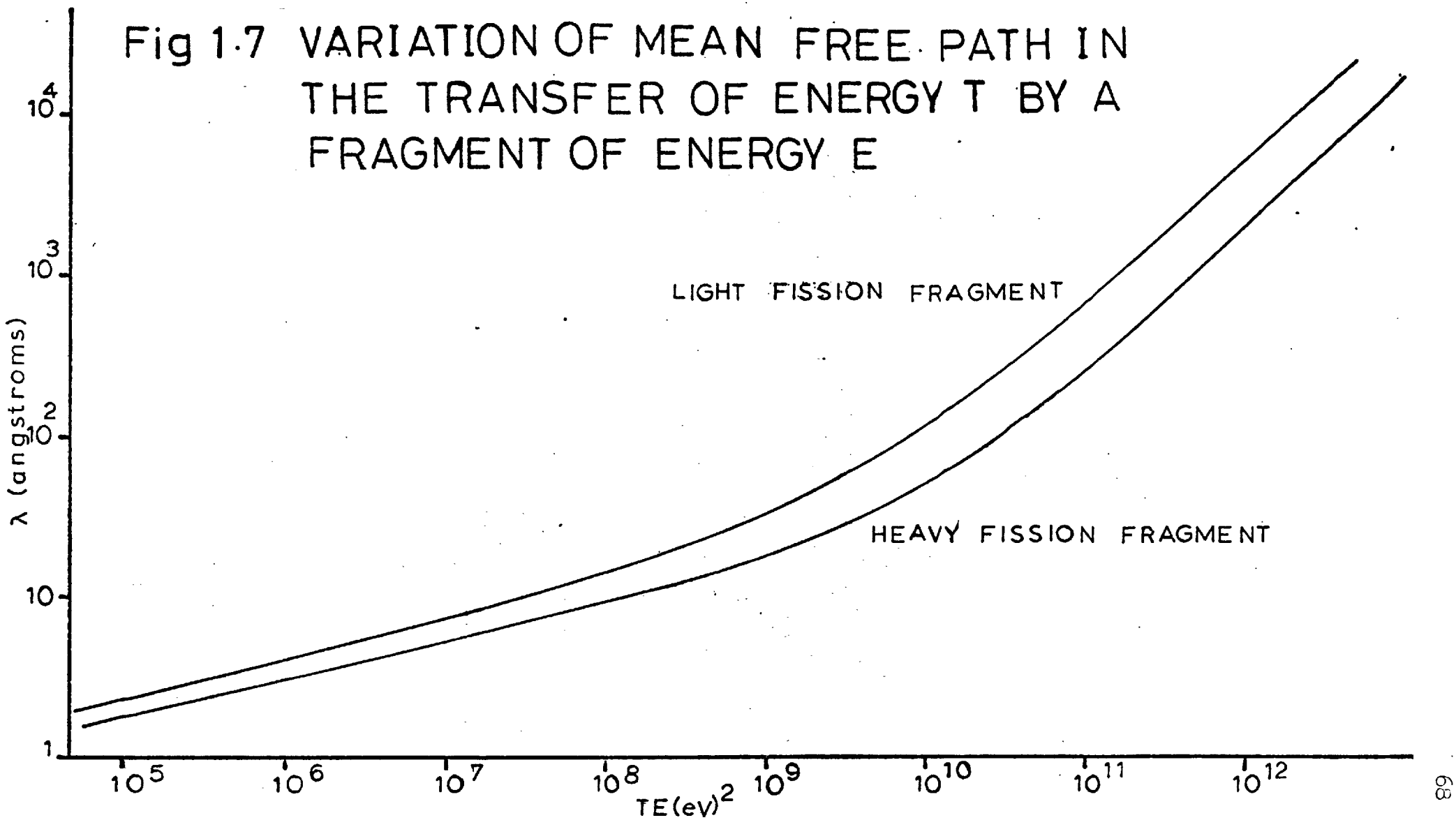
$N_d = 10^{10} - 10^{13}\ m^{-2}$ (28).

1.4.3. Displacement Spike

As the energy of the fragment or knock-on slows down, the mean free path between collisions becomes less than the atomic spacing in the lattice. Provided $E \geqslant E_d$, this leads to the concept of a multiple displacement of neighbouring atoms at the end of the track.

The concept is due to Brinkman (29) who obtained an expression for the relationship between the mean free path λ of a fragment, its energy E and the minimum energy transferred in a collision T. The relationship was displayed graphically to give a universal curve from which the mean free path could be found for a transfer of any energy T by a fission fragment with any energy E. A typical curve for fission fragments in uranium is shown in figure 1.7. From this it can be seen that, if T = 25 eV (the displacement threshold) an atom with energy $\sim 10^3$ eV will transfer energy greater than T with a mean free path less than one interatomic distance, thus producing a multiple displacement. It was suggested that the multiple displacement would exist for a short time as a shell of interstitials surrounding a multiple vacancy core. The surrounding interstitials would increase the normal atomic density by $\sim$10%. The central core would be under great pressure of approximately 10^{10} newtons m^{-2} and this would result in raising it to a high temperature. The combined effect of temperature and pressure could influence the atoms between the interstitial shell and core to fall into the vacancy region. This could be followed by

Fig 1.7 VARIATION OF MEAN FREE PATH IN THE TRANSFER OF ENERGY T BY A FRAGMENT OF ENERGY E



a refilling of their lattice sites by some of the interstitials. Seeger has suggested that focused collision sequences (see section 1.3.5) could also act to separate the interstitials from the multiple vacancy region. This would result in a depleted zone, which would be composed of a high local density of vacancies around the stationary knock-on, with a few nearby interstitials. Figure 1.8 is a schematic two-dimensional representation of the Seeger depleted zone and its environment in a face-centred cubic crystal.

In a binary compound such as KCl, a displacement spike creates a very disordered region, and strains on the surrounding lattice will be expected. Extended defects, such as regions of mismatch and tangles of dislocation loops, may also be formed by an aggregation of point defects.

Due to the high pressures associated with a displacement spike there is a possibility of thermal and plastic spike formation. Figure 1.9 is a schematic representation of the fission spike. At first, thermal spikes are prevalent, and this corresponds to the high electronic excitation of the lattice atoms, since the energy due to non-displacement collisions and associated thermal spikes is negligible. As the fragment picks up electrons, so the intensity of the thermal spike decreases. The intensity at any point along the track is depicted in (a) as the radius of a right circular cone. When the charge on the fragment approaches zero, elastic and inelastic collisions begin to take precedence. (c) shows the increased frequency of displacement spike formation as the fragment slows down and there is a gradual transition from "Rutherford" to "hard sphere" collisions. More primary knock-ons are created at lower energies and the occurrence of displacement spikes becomes

more probable. (b) shows the formation of a displacement spike by an energetic knock-on deriving from a collision between the fragment and a lattice atom.

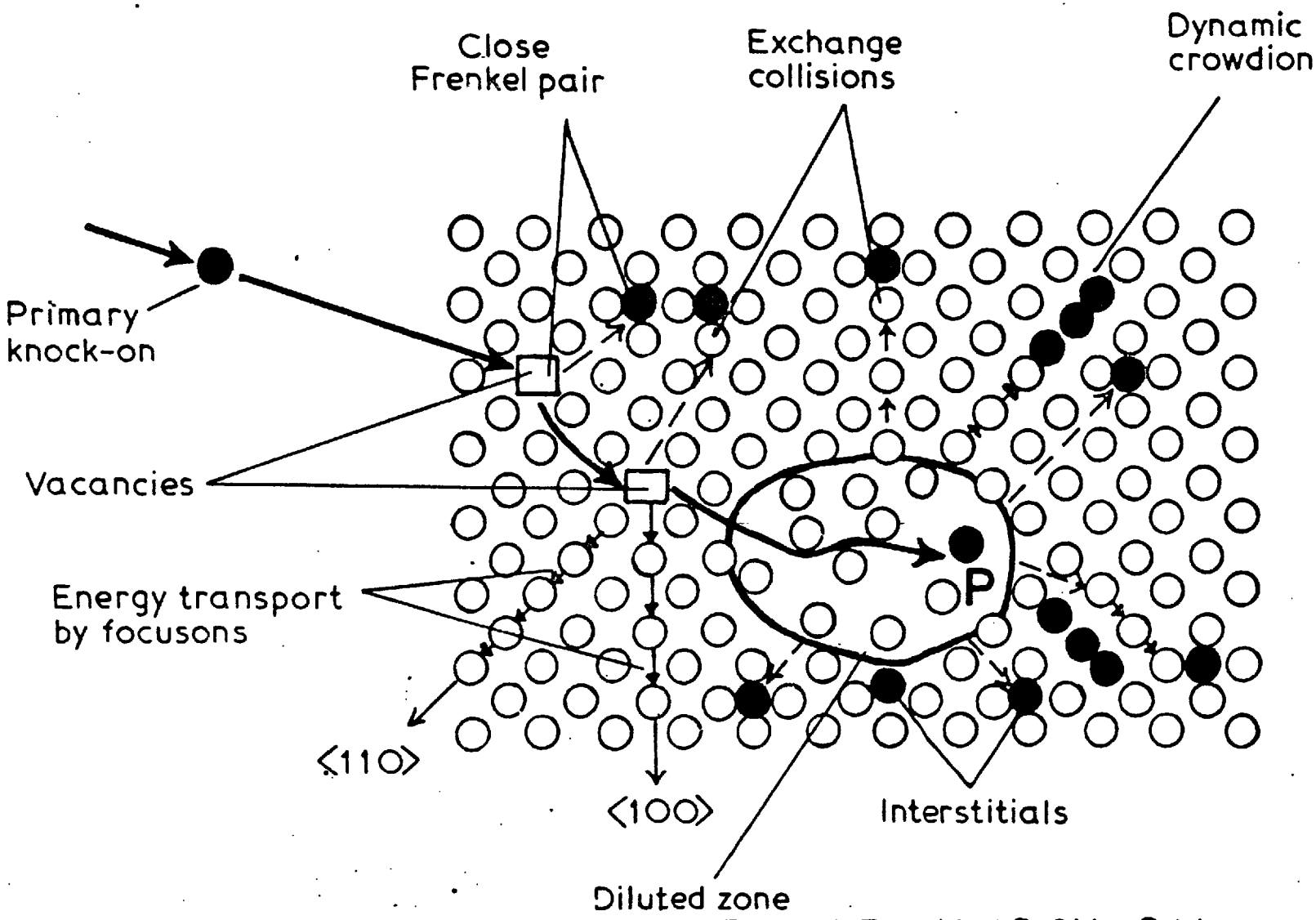


Fig 1.8 DAMAGE CREATED BY PRIMARY KNOCK ON IMPINGING FROM THE LEFT AND COMING TO REST AT P

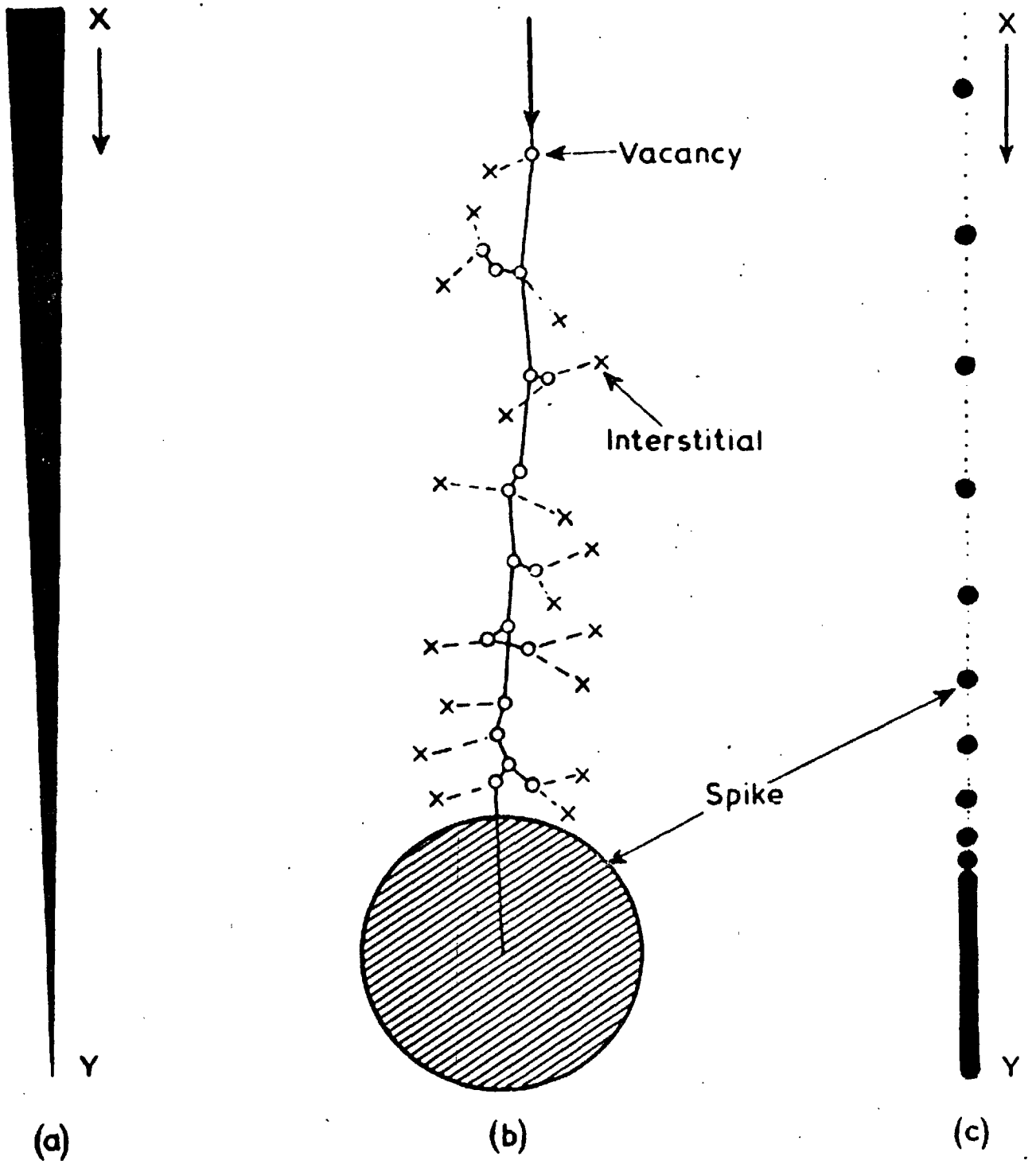


Fig 1.9 SCHEMATIC REPRESENTATION OF THE FISSION SPIKE

(SEE TEXT FOR DISCUSSION)

Chapter 2. Reactor Technology.

Contents:

2.1	Introduction	74
2.2	Molten Salt Reactors	75
2.3	Molten Salt Breeder Reactors	78
2.3.1	The need for chemical processing of the fuel and coolant	78
2.3.2	Description of MSBR	79
2.3.3	Problems with MSBR technology	82
2.3.4	Advantages of the system	84
2.4	The Molten Salt Fast Breeder Reactor System	86
2.4.1	Introduction	86
2.4.2	Problems associated with a molted chloride salt (a) The compatibility of a chloride melt with container materials (b) Oxide behaviour	87
2.5	Fast Reactor Fuel	96
2.5.1	Redistribution phenomenon	96
2.5.2	Fission product behaviour	99

CHAPTER 2

REACTOR TECHNOLOGY

2.1. Introduction

The passage of a fission fragment through a solid and the associated phenomenon of thermal spikes has been reviewed in Chapter 1. Many thermal spikes will be expected in the system under investigation. Calculations suggest that a tiny portion of the solid penetrated by 26.25 MeV fission fragments will be in the molten state at any one time. The molten state created by each spike lasts for only 2×10^{-10} s and affects a region of radius 7 Å. At this time, the volume of the tablet, which has been raised above room temperature, has a radius of 422 Å. This heating effect lasts for 5×10^{-7} s in each spike.

Continual fission product bombardment, while the sample is in the reactor, could result in some areas remaining for some time at, or above, the melting point for KCl. Such a situation will be very nearly a simulation of the passage of fission fragments through a molten salt coolant in a molten salt reactor when KCl is the salt. Thus the final state of a fission fragment in the molten salt reactor can be compared to that adopted by the same isotope when it comes to rest in the KCl tablet.

2.2. Molten Salt Reactors

The possibility of using a reactor fuel and coolant as a homogeneous phase in the core was first investigated in 1947 for possible use in nuclear powered aircraft. Molten fluoride salt fuels were considered to have particular advantages. Their chemical stability was much greater than other reactor systems at that time, which either operated at high pressures or had gaseous coolants circulating at high temperatures. Furthermore, uranium is highly soluble in fluoride salts and such a system has good physical properties.

The success of the project initiated an investigation into its use for civilian power generation. The system was found to have many advantages over its solid fuel rivals. These are as follows:

(1) High temperatures can be achieved at low pressure operations. At present turbines can only operate at approximately 500 ^{o}C and so this advantage cannot be demonstrated. However, higher temperatures mean greater power, and this can only be achieved in other systems by raising the pressure, or using difficult materials such as molten metal.

(2) The canning problems that exist with other reactor systems are avoided,since the fuel is distributed uniformly throughout the core as a molten salt.

(3) Molten salt materials are stable to the high irradiation fluxes. This is not the case in water reactors where radiolysis is a problem. Also, there are no structural materials in the core that could suffer damage. In the CANDU and SGHW systems, the pressure tubes in the centre

of the core have to withstand very high neutron fluxes. High fluxes and penetration of fission products into the tubes contribute to the failure of these materials. If a pressure tube fails it can buckle and severely restrict the flow of coolant and moderator past the fuel, with serious consequences.

(4) The molten salt system has a large negative temperature coefficient of reactivity. This makes it particularly safe in the event of an accident, such as a pump failure, which would otherwise result in overheating of the core.

(5) The maximum temperature gradient is low and the temperature fluctuation in the can and fuel, which is observed in other reactors, is avoided.

(6) On-load processing of the fuel is possible. Thus, safety problems such as radiation build-up can be reduced, along with the fission product inventory of the core. The neutron economy will also be improved, since less would be lost in absorption by fission products.

In addition to these point, a good solution of fuel components could produce a mixture that has:

(7) Low corrosion of structural materials.

(8) Low vapour pressure.

(9) Low parasitic neutron capture.

(10) Adequate solubility of both fissile and fertile materials.

Preliminary investigations resulted in the Molten Salt

Reactor Experiment (MSRE) at Oak Ridge National Laboratory (1965-1969). The 7.4 MWt reactor had a total operating time of 2½ years with molten salt circulating at 650 °C and the experiment proved to be very successful. The fuel was $^{7}LiF-BeF_2-ZrF_4-UF_4$ (66-29-5-0.2 mole %). This was circulated through a 1.4 m diameter core of graphite moderator. The salt vessels and piping were of Hastelloy N which is a nickel base alloy with 16% Mo, 7% Cr and 5% Fe. An intermediate coolant, $LiF-BeF_2$, transferred heat from the fuel salt, and was itself cooled by air.

During the final year ^{233}U was used as the fuel with Pu as make-up fuel for part of the time. This made the reactor the first in the world to be fuelled with ^{233}U. The information gathered from the experiment helped in the progress of the next stage - the Molten Salt Breeder Reactor (MSBR).

2.3. The Molten Salt Breeder Reactor (MSBR)

2.3.1. The need for chemical processing of the fuel and coolant

The MSRE demonstrated the operability of a fluid fuel system using ^{233}U as fuel. When ^{233}U is used in a thermal reactor, breeding is possible. The number of neutrons produced for every thermal neutron lost in fission is, on average, 2.3. Neutron losses to the reactor materials and through leakage are typically 0.2 to 0.25 per fission. Thus, with such a fuel, it is possible to sustain the chain reaction with one neutron and, at the same time, create a fissile atom through capture of the other neutron in a fertile isotope such as ^{232}Th. This eventually decays to ^{233}U.

$$^{232}Th + n \longrightarrow {}^{233}Th \xrightarrow{\beta^-} {}^{233}Pa \xrightarrow{\beta^-} {}^{233}U$$

Protactinium (Pa) and the rare earths have significant σ_n values, and they could seriously impare the breeding performance of a thermal breeder by increasing neutron losses so that the net number of neutrons available from each fission process is below 2. The following process for extracting these poisons has been envisaged. It is based on the tendency for Bi containing a reductant such as Li to separate Pa from Th and the rare earths, and then to separate fission products from Th. The equilibrium distributions are given in table 2.1 (30).

Table 2.1

Equilibrium Distributions (mole fractions)

	Fuel Salt	Bismuth	LiCl
Th	0.12	0.0025	0.33×10^{-7}
Pa	0.35×10^{-4}	0.9×10^{-3}	0.83×10^{-10}
La	0.55×10^{-5}	0.27×10^{-6}	0.38×10^{-6}

The steps in the process are:

(1) Uranium is removed as volatile UF_6.

(2) The salt is contacted with liquid Bi containing dissolved Li to extract Pa. This is transferred to a separate salt and held until it decays to U.

(3) This is the 'metal-transfer process' where the salt is in contact with a captive volume of Bi into which rare earths and other fission products transfer. Th and Be are left behind in the salt.

(4) The UF_6 produced is converted to UF_4 and fed back into the system. Any excess can be sold.

(5) The waste products are fluorinated to recover any U that has passed through the process. They are then stored prior to disposal. This scheme is shown in figure 2.1.

2.3.2. Description of MSBR (see figure 2.2)

The core is an array of bare graphite moderator bars with open channels that allow circulation of the salt. The single fluid consists of UF_4 and ThF_4 (0.3, 12 mole %) dissolved in ^7LiF-BeF_2 (72, 16 mole %) as coolant. It has a melting point at 450 °C. By passing upwards through the core, it is heated to 700 °C. It is then pumped to a heat

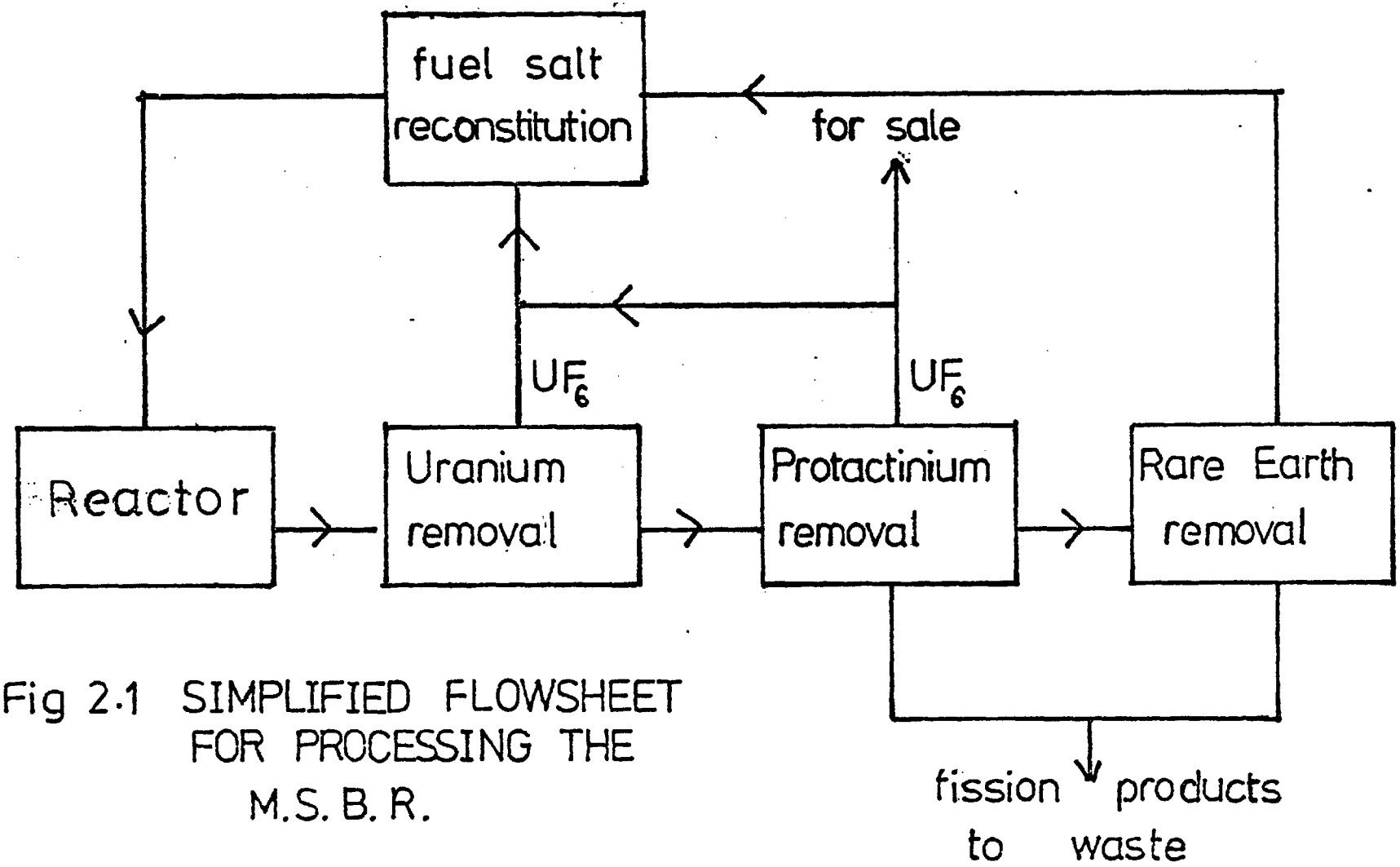
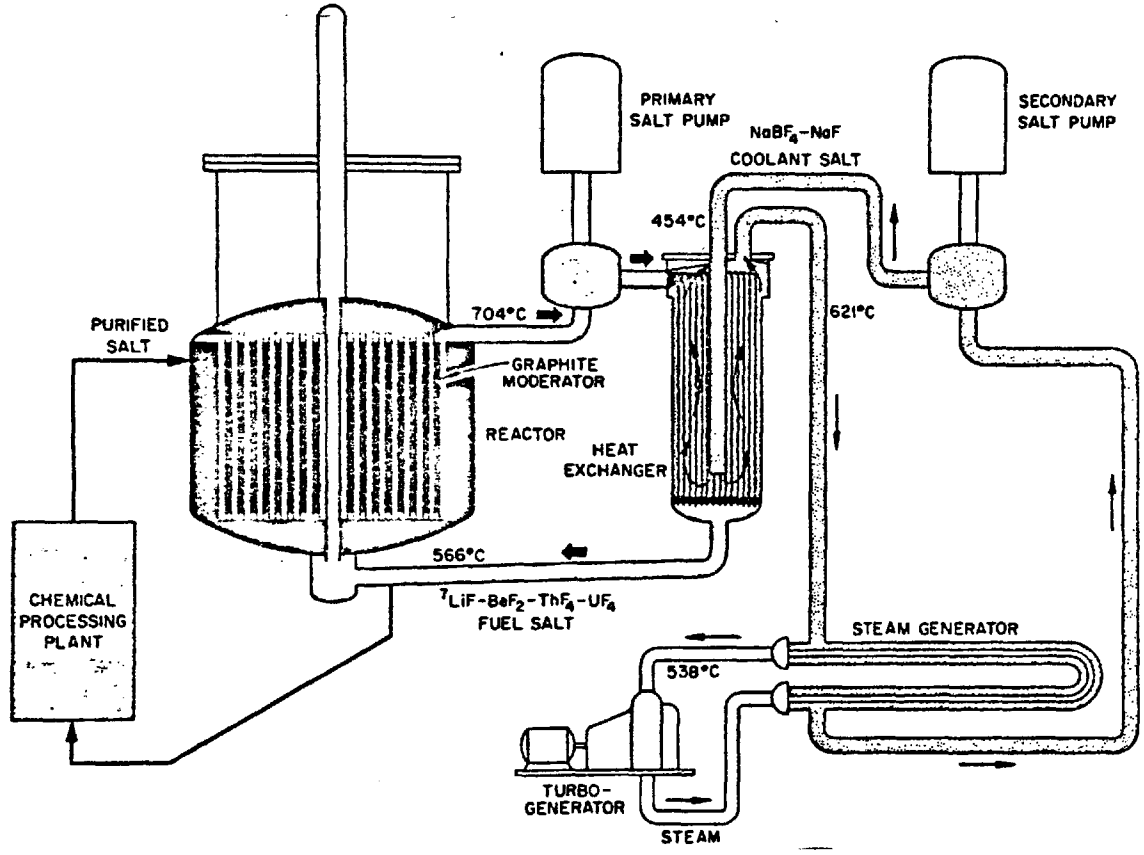


Fig 2.1 SIMPLIFIED FLOWSHEET FOR PROCESSING THE M.S.B.R.

Fig 2.2

SIMPLIFIED FLOW DIAGRAM FOR A MOLTEN-SALT BREEDER-REACTOR



exchanger. The heat is transferred by an intermediate coolant, $NaBF_4$-NaF, to a steam system generating supercritical steam at 540 °C. The overall thermal efficiency is 44%. Bubbles of He are injected into a small side-stream of fuel to remove ^{135}Xe and other noble gases. This stream then passes into the chemical processing plant at a rate of 1.0 gpm. This rate allows a recycle time of 10 days for a 1,000 MWe reactor (2250 MW th). Power and temperature are regulated by movable graphite rods that displace fuel salt near the centre of the core. The annulus has a higher salt volume fraction than the core and is undermoderated. Displacement of more salt towards the edge of the reactor will result in increased undermoderation and less thermal neutrons will be available for fission. Long term reactivity control is achieved by adjusting the fuel concentration. During shutdown, the fuel is safely stored in a drain tank having a thermal convection cooling system.

2.3.3. Problems with MSBR technology.

The molten salt breeder concept is still in a theoretical stage and the reactor is not yet much of a reality. This is because there are several problems associated with such a system that require further developments in nuclear technology for their solution.

The first problem concerns the material, Hastelloy N, which is used to construct reactor cores and pipes. At the end of the MSRE small surface cracks were found in one of the fuel pipes after it had been strained at room temperature. Experiments indicated that they were due to fission product Te contamination. Another problem with this material is that neutron irradiation lowers its

ductility. The longer irradiation times and higher temperatures envisaged in the MSBR operation would help to increase these effects. The development of a new or modified alloy is required, and this must also have a low corrosion rate and high radiation resistance.

There are problems associated with the graphite moderator. Commercial supplies of graphite do not have sufficient radiation resistance for use in a MSBR. Prolonged radiation results in shrinkage and then swelling of the material. The in-reactor lifetime for present materials is four years. Thus, it would be economically advantageous to develope a better graphite which has a longer lifetime. Diffusion of fission product ^{135}Xe into the graphite must also be avoided. ^{135}Xe has a high σ_n value and build up in the graphite would impare the breeding performance of the reactor. Methods of sealing the graphite with pyrolytic carbon are being investigated.

The fuel processing cycle also has problems. It is based on a liquid Bi extraction procedure, but this material is incompatible with most conventional structural materials. The fluorination steps also result in a corrosive mixture of fluorine and fluoride salt. However, the Hastelloy N could be protected from this by the deposition of a frozen wall of fuel salt. In general, the levels of radiation and fission product activity in the processing system and primary coolant loop will be so high that remote systems for surveillance and maintenance will have to be developed.

There has been no experience in generating steam with high-melting salts, and the fluoroborate coolant, which has been chosen for this system has a melting point above conventional feed water temperatures. Therefore, if

this salt is used, it will freeze in conventional steam generators. Alteration of the steam cycle to allow an increased inlet temperature could result in a small loss in efficiency and more cost in equipment.

In a 1,000 MWe reactor, over 2,400 Ci/dy of tritium will be produced. This is almost fifty times the amount produced in the LWR or LMFBR. It is produced from ^{6}Li and ^{7}Li by n,α reactions, and it also occurs as a fission product. It diffuses through Hastelloy N at high temperatures and so it is possible for it to reach the steam system and then to be discharged into the environment. Oxide films on the steam side of steam generators have been found to reduce the diffusion by several orders of magnitude. This needs to be demonstrated under realistic reactor conditions. The other troublesome fission products, I and Sr, form stable fluoride salts and are contained in this system.

Other effects such as moisture, steam in-leakage and the mixing of fluoroborate and fuel will also have to be investigated. The proposed fuel salt is reported to have the best properties for the MSBR but it has a low oxide solubility at 30 ppm O^{2-}. Successful operation of the reactor will require the minimum ingress of air and moisture. However, experience with the MSRE has shown that the oxide content varied little during the plant life, although this included periodic opening of the reactor for insertion and removal of corrosion specimen.

2.3.4. Advantages of the system

The advantages of the MSBR from safety considerations are enormous. Several lay groups in Britain and the U.S.A. have recently expressed their concern, publicly, that

present commercial reactor systems are unsafe and that it is only a matter of time before the occurrence of a major nuclear disaster. In view of the present hot climate of public opinion and its possible adverse effect on the progress of nuclear reactor technology, such a potentially safe system should be given serious consideration. Provided that the problems mentioned above are overcome, it should also prove to be economically equal to the LWR. There is a relatively small fissile inventory, a breeding ratio of 1.06, and no fuel fabrication or construction materials in the core. The major expenditure will be in replacing the graphite every few years. The development of a better graphite material could overcome this cost.

However, general opinion is that the development of the MSBR system is too late for the thermal power market, but may have a future in the fast reactor technology, where systems have not yet been developed to such an extent.

The fast reactor concepts taken to design stage are:

1. Molten sodium coolant for U/Pu system (LMFBR).
2. Gas cooled Helium at high pressures (GCFBR).
3. Molten sodium chloride (MSFBR).

Of these, only the molten sodium system has been developed on a commercial scale. It is considered that the MSFBR is intrinsically the safest of the three systems and should be developed, in prudence, as a back-up system to the LMFBR.

2.4. The Molten Salt Fast Breeder Reactor System (MSFBR)

2.4.1. Introduction

In order to obtain a good breeding ratio, the fuel will have to be based on the U-Pu cycle for a fast reactor, instead of the Th-U cycle in a thermal reactor. A higher density of fissile material is required to achieve criticality. This poses cooling problems, and extra circulation through external circuits will result in a substantial hold-up of fuel salt, thus increasing the fuel inventory and increasing costs. Alternative methods have been suggested, such as injecting a stream of lead drops around the periphery of the core (31). The high interfacial area and relative velocity between the salt and lead help to remove the heat very efficiently.

An alternative to fluorine is required in a fast reactor system because, due to its low atomic weight, there is some moderating and a subsequent softening of the neutron spectrum. Molten chlorides are considered to be suitable salts, with Pu as the fuel and U as the internal breeder. ^{35}Cl has a high neutron absorption cross-section for fast neutron energies, and so the fuel mixture should be enriched in ^{37}Cl. All previous experience has been with fluoride salts containing a low concentration of 1 mole % U. This experience cannot be applied to chloride melts which have a much higher concentration of heavy elements at 20 - 50 mole %. Furthermore, little is known about the chemical behaviour of chloride fuel salts at temperatures between 550 ^{o}C and 750 ^{o}C. The state of oxidation of iodine in KCl can vary from a highly reduced condition as iodide to a highly oxidised condition as iodate. It is

considered that its oxidation state might act as a kind of "indicator" for the "redox" potential in such fuels.

2.4.2. Problems associated with a molten chloride fuel salt

The chemical problems of a molten chloride salt system can be divided into two categories (32). They are its compatibility with proposed container materials and the behaviour of oxide introduced into the system.

(a) The compatibility of a chloride melt with container materials

The reaction between a container material and a multivalent component, dissolved in the melt, can be written as

$$MCl_x(d) + X_{(s)} = XCl_y(d) + MCl_{(x-y)}(d) \quad (2.1)$$

Reduction of the melt component to metal will occur when $x = y$. The reaction can be considered as occurring in two stages:

$$MCl_x(d) = MCl_{(x-y)}(d) + \frac{y}{2} Cl_2(g) \quad (2.2)$$

$$\frac{y}{2} Cl_2(g) + X(s) = XCl_y(s) \quad (2.3)$$

This analysis leads to a general expression for either a container metal A or a melt component ACl_Z

$$\frac{1}{Z} A(s) + \tfrac{1}{2} Cl_2(g) = \frac{1}{Z} . ACl_Z(d) \quad (2.4)$$

The equilibrium constant K_A is given by the activities of the reactants

$$K_A = \frac{\left[a_{ACl_Z} \right]^{1/Z}}{\left[a_{A(s)} \right]^{1/Z} \left[a_{Cl_2} \right]^{\frac{1}{2}}}$$

The activity of Cl_2 in a multicomponent system is its partial pressure. The other activities are related to their concentration by

$$a_i = \gamma_i x_i$$

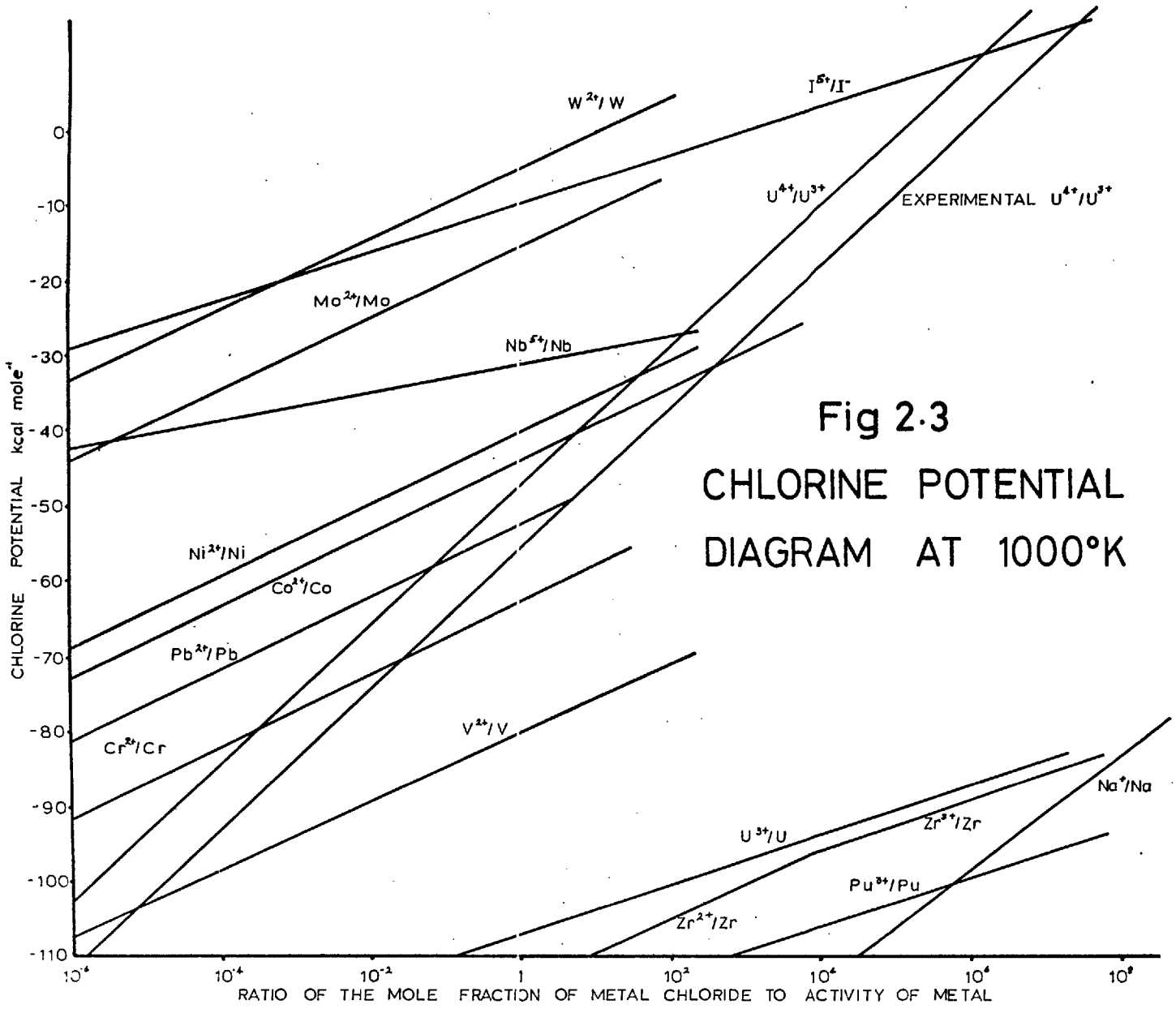


Fig 2.3

CHLORINE POTENTIAL DIAGRAM AT 1000°K

where γ_i is the activity coefficient and x_i is the concentration. K_A is related to the free energy of formation of ACl_Z by

$$-\Delta F^f(ACl_Z) = RT \ln K_A$$

$$= \frac{1}{Z}.RT \ln(a_{ACl_Z}/a_A) - \frac{1}{2} RT \ln p(Cl_2)$$

$$RT \ln p(Cl_2) = 2\Delta F^f(ACl_Z) + \frac{2}{Z} RT \ln \gamma_{ACl_Z} + \frac{2}{Z} RT \ln (x_{ACl_Z}/a_A)$$

This is an expression for the chlorine potential, RT ln $p(Cl_2)$. If the pure liquid salt is taken to be the standard state of unit activity, the second term is zero. Harder, Long and Stanaway plotted the chlorine potential at 1000 ^oK as a function of the ratio of the mole fraction of the chloride to the activity of the metal, for several metals that were likely to be in contact with the chloride melt. The redox reaction

$$UCl_3(d) + \tfrac{1}{2}Cl_2(g) = UCl_4(d)$$

was also plotted on the graph. In this case the abscissa became the concentration ratio of the two species. See figure 2.3, which includes an experimental value for fission product iodine. This is discussed in section 4.2.3.

The graph showed that high levels of UCl_4 are very corrosive for most possible container materials. Therefore, melts rich in UCl_3 are to be preferred; but some UCl_4 is required to prevent disproportionation of UCl_3 with subsequent deposition of U. The presence of metals such as Ni and Pb lowers the activity of U by compound formation, and will increase the tendency of UCl_3 to disproportionation. It was predicted that corrosion of available structural

materials should be acceptably low between -90 to -60 k cal $mole^{-1}$ of chlorine potential. Alkali and alkaline earth chlorides are suitable salts for use as diluents and are also stable towards reduction in this range. The chlorine pressure can be maintained during reactor operation by suitably adjusting the ratio of UCl_4 to UCl_3.

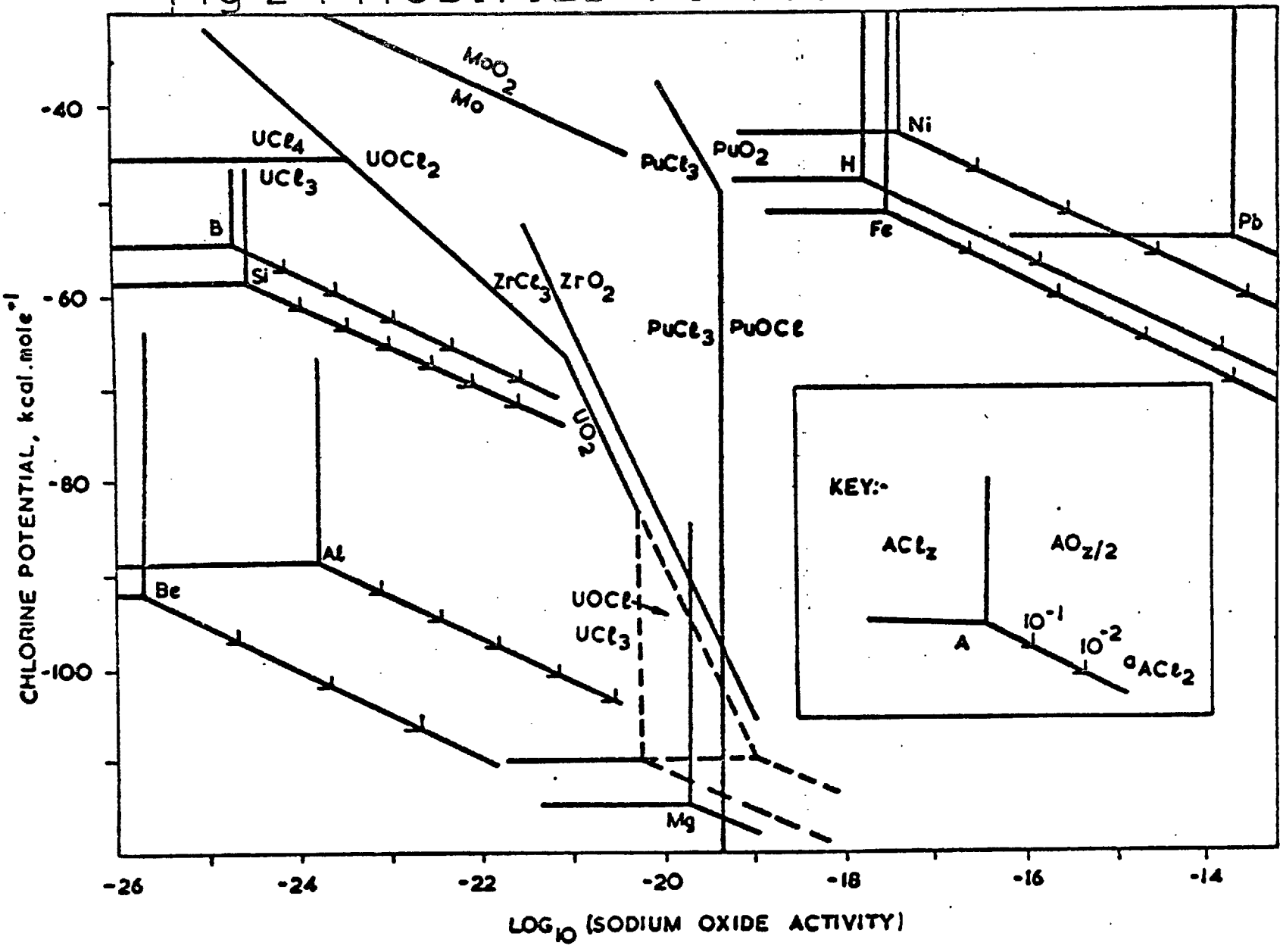
The valency state of the important stable fission products in the melt can be predicted from the graph for this range of chlorine potential. See table 2.2. The net valency of the fission products is predicted to be less than 3+ which is the valency of uranium present as UCl_3. Therefore the melt will become more oxidising with increasing burn-up. Since the most easily oxidised substance present will be UCl_3 , this compound can act as a buffer against large sudden changes in potential. However, some method of reducing the UCl_4 that accumulates will be required.

(b) Oxide Behaviour

The introduction of oxygen into the system could result in the precipitation of the oxide of one of the components of the salt mixture or in corrosion of the container metals. Since it is difficult to ensure the complete absence of oxygen in the reactor core, a prediction of its effect on the melt and materials in the reactor is essential for reactor control.

Harder, Long and Stanaway used a modified Pourboix diagram for predicting the behaviour of oxide in chloride melts, shown in figure 2.4. The abscissa is the activity of a convenient oxide such as Na_2O in melts containing NaCl. The ordinate is the chlorine potential. These two variables are independent of each other. Areas exist on the diagram

Fig 2.4 MODIFIED POURBAIX DIAGRAM



in which one of several phases is stable for each element. The metal-metal chloride boundary was defined by equation 2.4. It is independent of oxide activity but is dependent on the concentration of metal chloride. The metal-metal oxide boundary is defined as

$$\tfrac{1}{2}Cl_Z(g) + \frac{1}{Z}A(s) + \tfrac{1}{2}Na_2O = \frac{1}{Z}AO_{Z/2}(s) + NaCl(d)$$

This depends on the chlorine potential and oxide activity, but is independent of the metal chloride.

The metal chloride-metal oxide boundary is defined as

$$\frac{1}{Z}ACl_Z(d) + \tfrac{1}{2}Na_2O(s) = \frac{1}{Z}AO_{Z/2}(s) + NaCl(d)$$

This depends on the activity of the metal chloride and is independent of the chlorine potential.

Boundaries for oxychlorides were calculated in a similar manner. If oxidation occurs in producing the oxide or oxychloride, then the oxide-chloride boundary must depend on the chlorine potential.

As in the previous section, consideration of the free energy of formation and equilibrium constants for each boundary reaction leads to an expression for the activity of the metal oxide in terms of the chlorine potential and the activity of Na_2O. The activities of sodium chloride, metal and metal chloride are taken to be unity.

The result of decreasing the activity of the metal chloride in decade steps is indicated along the metal-oxide boundary. The dashed line indicates uncertainty in the stability of UOCl.

The diagram enabled several predictions to be made about the oxide behaviour. Firstly, UO_2 or $UOCl_2$ will be precipitated first when the oxide activity is increased. The diagram also shows that uranium need only be used in experiments on a suitable melt since, at all chlorine potentials above -90 kcal $mole^{-1}$, uranium will precipitate

before Pu.

The diagram suggests a method of oxide removal by the introduction of B, Si, Be or Al chloride into the melt. These oxides are all more stable than UO_2 and will precipitate first. An adequate addition of one of these chlorides will ensure that uranium will not precipitate out of the melt as UO_2. However these chlorides are corrosive vapours at reactor temperatures and normal pressures, and maintenance of an adequate concentration in the melt could be a problem. The presence of these chlorides and uranium also ensures that the container metals, Ni, Fe, Mo, are not corroded by oxide formation. If the melt did not contain stable oxide forming chlorides, the activity of Na_2O would increase until it was sufficient to attack the container. In the melts under consideration, corrosion is determined only by the chlorine potential, and sufficient uranium will control this and also the oxide activity.

A prediction of the solubility of oxide in the melt is not possible from the diagram. This is an important value because the melt will have to be reprocessed at a sufficient rate to avoid oxide precipitation, if a method for keeping the volatile halide in the melt is not found.

Harder, Long and Stanaway investigated the stability of UCl_4 in a NaCl, UCl_3 melt (70, 30 mole %). They found it to be less reactive in the melt than in its own liquid. They also reported an independence of melt composition from the activity coefficients of UCl_4 and UCl_3. The activity coefficient for UCl_3 = 0.25 ± 0.1 and that for UCl_4 = 0.025 ± 0.01. This suggests that melts containing UCl_4 will be less oxidising than predicted and is shown by the broken line

in figure 2.3.

They investigated the solubility of oxide (UO_2) and found it varied slightly with the temperature and concentration of UCl_4. However, at the oxide values reported, it would be possible to process the melt at an acceptable rate in order to avoid precipitation.

Experiments with Ni and Pb predicted that these metals would behave almost ideally in the melt.

The results of the investigation implies that uranium chloride-alkali chloride mixtures are definite possibilities as reactor fuels. However, the experiments have been performed under laboratory conditions. The performance of the melt under burn-up conditions will depend on the behaviour of the fission products. The reactor operation of single fluid uranium fuels depends on the U^{3+}/U^{4+} ratio. Fluctuations in this value are due to the final oxidation state of the fission products in the fuel. The valence state of the normal element can be predicted for any chlorine potential from figure 2.3. Table 2.2 shows the chlorine balance of the major stable fission products.

Table 2.2 (32)

Chlorine Balance of the Major Stable Fission Products

Fission Product	Yield, atoms per 100 fissions	Valency in $NaCl:UCl_3$	Cl atoms reacted
Xe, Kr	25	0	0
Rb, Cs	19	1	19
Sr, Ba	10	2	20
Rare Earths	46	3	138
Zr	22	3	66
Nb, Mo	2	0	0
Te, I	6	0	0
Pd, Ru, Rh, Ag, Cd	61	0	0
Total Cl atoms reacted out of 300 available:			243

It implies that the melt becomes more oxidising as burn-up proceeds, since a number of chlorine atoms are left unreacted out of the 300 available per 100 fissions. Fission products cannot be considered as normal atoms of an element. From previous discussions, it is seen that the slowing down period is a complicated process and only predictions based on probability can be made about its final state. The absence of satisfactory methods for measuring the U^{4+}/U^{3+} ratio, with the reactor on load, emphasises the need for information on the behaviour of fission products in such melts, and their possible use as "indicators". The results presented in this thesis show that fission product iodine will be expected to be in an oxidised state of +0.2 , in contrast to the value given in table 2.2 .

2.5. Fast Reactor Fuel

A recent report on the burn-up of fuel in the prototype fast reactor (PFR) at Dounray has indicated that the behaviour of fuel and fission products is dependent on the oxidising atmosphere inside the fuel pin (1). The fuel for the fast reactor is a mixture of PUO_2 and $^{238}UO_2$. Both plutonium and uranium undergo fission in the fast neutron flux. The cross-section for inelastic scattering of ^{238}U is higher than that for fission and so many neutrons are reduced to energies below that required for fission and these are captured by ^{238}U nuclei. The mixed oxide (20% Pu) is contained in fuel rods which are canned in stainless steel. These are made up into hexagonal subassemblies, each containing 325 fuel rods. The core contains 78 subassemblies, plus another 42 containing depleted uranium from thermal reactors which are distributed around the edge of the core for breeding. The coolant is molten sodium.

2.5.1. Redistribution phenomenon

A redistribution of fuel and fission products was found to occur in the fuel rods after irradiation. See figure 2.5. A tubular central hole was found along the rod axis. This was surrounded by a region of radially-elongated columna grains. The portion of the pin on the outside next to the cladding developed equiaxial graining. Experiments related this phenomenon to the initial stoichiometry of the fuel. See figure 2.6. A decrease in the O_2/metal ratio produced a decrease in central Pu concentration. When the O_2/metal ratio was reduced from a normal value of 2.01 down to 1.935, the normal segregation curve was

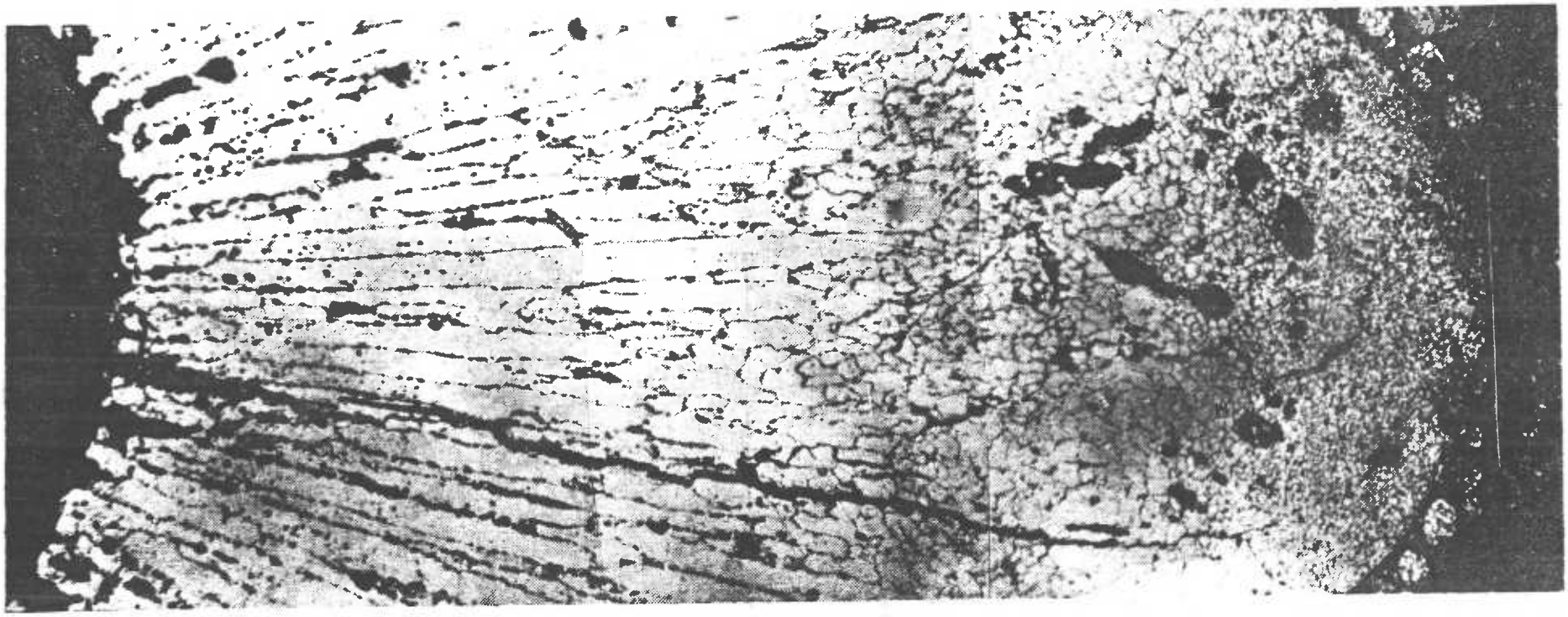
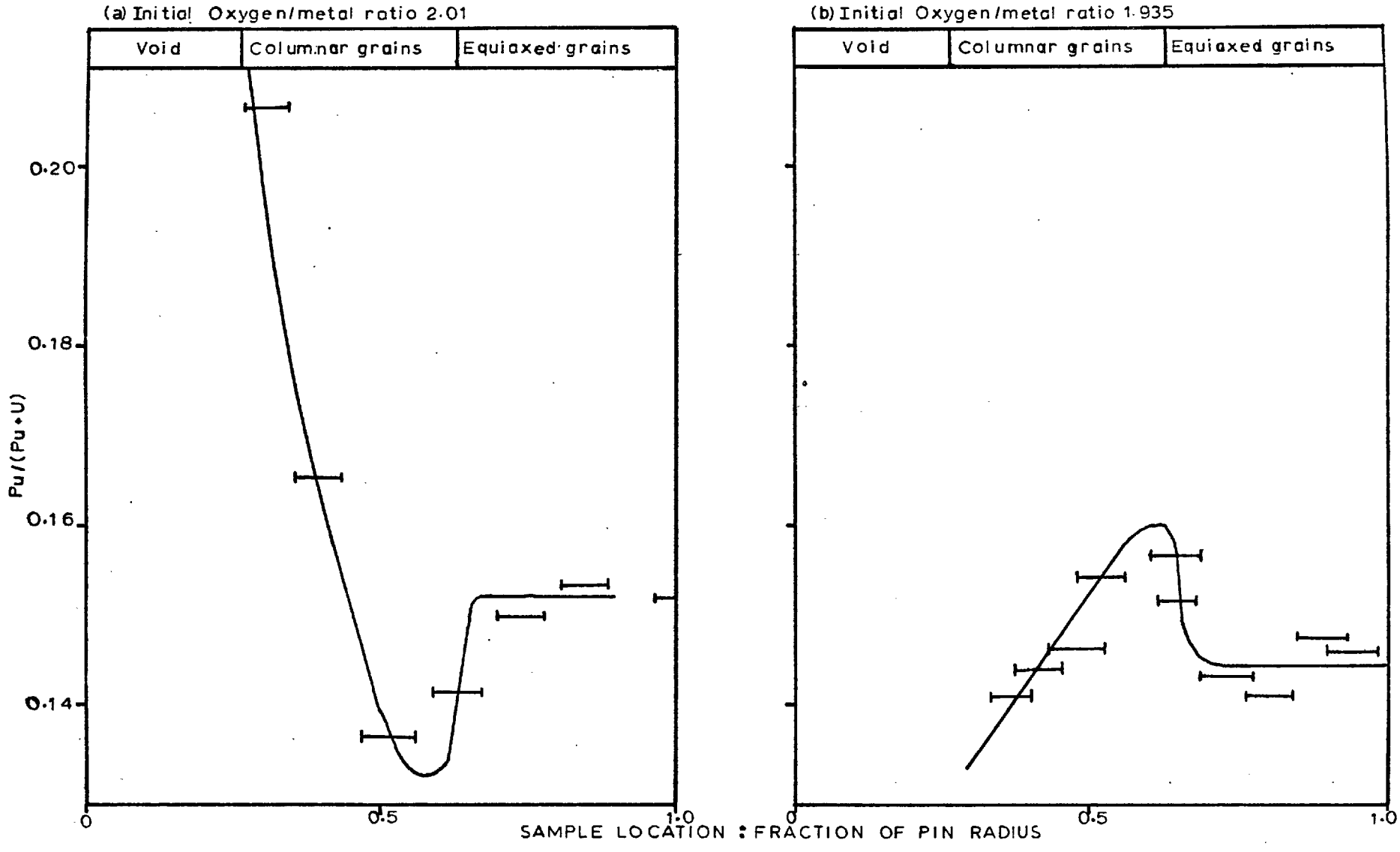


Fig.2.5Part of a transverse cross section of an irradiated mixed oxide fuel pin showing (left to right) the axial hole, the columnar grain growth region, the equiaxed grains and (dark, extreme right) the cladding. Magnification: × 75.

Fig 2·6 Pu/U SEGREGATION ON D F R MIXED OXIDE FUEL PINS



inverted.

A mechanism, that explains the results in part, is that there is preferential evaporation and migration of one species from the hot centre which is at 2,000 °C. The vapour phase generated by the fuel near the centre consists almost entirely of uranium trioxide and oxygen, with minor amounts of uranium and plutonium dioxides. A decrease in the O_2/metal ratio has little effect on the partial pressures of the dioxides, but results in a marked decrease in uranium trioxide pressure and an increase in PuO pressure. This helps to increase the central temperature of the fuel and thus vary the neutron absorption cross-section. This depends on the velocity of the neutrons which,in turn,depends on the temperature. The authors maintain that these are not serious effects. A central plutonium concentration 50% higher than average would raise the central temperature by only 100 °C (5%). Even so, the report shows that,due to incomplete knowledge of the chemistry at high temperatures, such unforeseen effects can occur.

2.5.2. Fission product behaviour

The chemical environment into which the fission products are released is determined by the O_2/metal ratio. Each fission event is accompanied by the release of two oxygen atoms. The fate of these is very important in predicting the state of the fission products.

The fission products can be grouped into those elements that form stable oxides in the fuel and those that are likely to be present in elemental form. The oxide-forming elements can be subdivided according to solubility in the fuel matrix. This classification suggests that the alkali

metals and halogens might exist in elemental form, with a probability of alkali halides involving caesium being formed. However, if the O_2/metal ratio is greater than 2.03 at 1000°K, caesium oxide might be formed. As there are uncertainties in estimating the free energy of formation, this ratio might be as low as 2.01. There is migration of both caesium and iodine towards the cooler ends of the pin and one would expect CsI. The low vapour pressure of this compound at fuel cladding temperatures does not support this and, so far, no quantitative analysis has been made.

Iodine has been identified as a major product diffusing from irradiated uranium metal. Since iodine is the most electronegative of all the longer lived fission products, any compound formation between the different fission products could be expected to involve iodine. Therefore, a study of this fission product might suggest the general conditions prevailing inside an irradiated fuel pin of uranium metal or oxide.

As indicated in the Introduction, the commercial viability of the fast breeder will depend on its fuel inventory. The minimum cooling times associated with maximum decontamination factors will be highly desirable. ^{131}I will be particularly troublesome as it has a high fission yield and will be present to an appreciable extent due to its 8 day half life. Allowing the isotope to cool to an acceptable level of activity will no longer be possible. Thus identification of its chemical state in a fuel melt could help enormously in this field. This state, in turn,

is determined by the redox conditions prevailing inside the reactor core when the fission fragment has reached thermal velocities.

The choice of iodine as a fission product to be studied is discussed in section 4.1 from the analytical point of view.

Chapter 3. Literature Survey

Contents:

3.1	Introduction	103
3.2	Valence State Distribution	104
3.2.1	Fission product iodine	104
3.2.2	Impurity atoms in KCl and related subjects	108
	(a) Methods used to introduce impurity atoms into the host lattice	
	(i) Ion implantation	
	(ii) Radiation induced nuclear transformations	
	(iii)Filiation	
	(b) Impurity ions	
	(i) Sulphur	
	(ii) Phosphorus	
3.3	Influence of the Host Medium on the Recoil Atom	115
3.3.1	Moisture effect	115
	(a) Water of crystallisation	
	(i) Oxygen bond formation and dissolution in water of crystallisation	
	(ii) Donor-acceptor mechanisms	
	(b) Effect of dissolution	
3.3.2	pH effect	122
3.3.3	Effect of gases, especially oxygen	125
3.4	Determination of the Nature of Precursors in the Crystal	131
3.4.1	Annealing techniques	131
3.4.2	Annealing mechanisms	134
3.5	Defects	143

CHAPTER 3

LITERATURE SURVEY

3.1. Introduction

The experimental work described in this thesis is concerned with the ratio of the oxidised to reduced species of iodine formed as a fission fragment in KCl. Some study is given to the effects of moisture, pH, pressing load and annealing, since it is thought probable that these variables can influence the results.

The moisture effect is discussed in terms of water of crystallisation. Although KCl forms no known hydrates, some of the mechanisms proposed can be applied to the system under investigation. The importance of the dissolution step in determining the valence state is reviewed. The pH effect on the valence state of ^{32}P and ^{35}S atoms in alkali halides is surveyed, mainly with respect to KOH doping. The effect of gases, such as O_2, was reviewed. This effect was not considered in the analysis. It was thought that any effect on the valence distribution would be similar for all experiments conducted in air. Section 3.4 is a review of annealing results, some of which bear a resemblance to the experimental results reported later. It is seen that many annealing mechanisms are proposed in terms of electron donor and acceptor sites in the crystal. However, it is felt that defect centres resulting from fission damage will have a greater effect on the valence state distribution of fission product iodine. Several relevant defect centres are discussed in section 3.5.

A summary of the review with respect to the experimental results is presented in section 5.3.1.

3.2. Valence State Distribution

3.2.1. Fission Product Iodine

No reference has been found in the literature to the system described in this work - that of fission product iodine in a potassium chloride polycrystalline matrix solid. However, the behaviour of fission product iodine in uranium metal and salts has been reported. Inferences from these reports will have to be tentative since, in these systems, the uranium undergoing fission is part of the host medium for the iodine fragments.

Walton et al (33) have reported on the chemical states of fission products in irradiated uranium metal before dissolution in acid. No evidence was found for combination of the radioactive iodine and alkali metals. Iodine appeared to be present in some form, other than iodide, which showed preferential extraction into hexane. It was suggested that the iodine fragment released in fission is present, as an isolated, positively charged atom, in the matrix of the metal. Thermodynamical considerations show that it can extract electrons from the metal surface to become a neutral atom. It would not be expected to exert a strong coulombic force with electrons or uranium ions in the metal. It would be expected to behave as a rare gas atom in the lattice.

Hall and Walton (34) have studied the valence states of fission product iodine formed in uranyl iodate. Values for the oxidised fractions were 86% (^{131}I), 63% (^{132}I), 82% (^{133}I), 33% (^{135}I). The results were interpreted in terms of the independent yields of the isobars and electron affinities of the outer electrons. The latter determined

the electronegative character for each mass which increased with atomic number along each decay chain. These considerations explain the decreasing order in oxidation with increasing atomic mass, observed for all the isotopes except ^{132}I. The decay scheme for this isotope shows that it exists mainly as ^{132}Te which is easily reduced. It exists for only a short time as Sn and Sb which are reduced with greater difficulty. On the other hand, ^{131}I and ^{135}I exist for longer relative times as Sn and Sb. These appeared to be more oxidised. ^{135}I has no identified precursors and could be expected to be formed directly from fission. Its appearance, mainly in the reduced state, was taken as evidence that the initial electron stripping process of the fission fragment has no major effect on the final state adopted. If a contribution were expected, the fission product closest to the original fragment would be in the most oxidised condition. It was concluded that since the fission fragments arise as isolated atoms, their subsequent behaviour is more likely to be described by atomic properties such as electron affinity, polarisability and ionic radii than by thermodynamical properties of the host material.

Experiments with uranyl iodate irradiated at high neutron doses of $\sim 10^{16}$ n cm^{-2} s^{-1} gave sharply increased values for the reduced iodide fraction. This was attributed to decomposition of the iodate salt at such high fluxes and the creation of oxygen depleted regions. Fractions were constant over a wide range for doses below this value. Other previous experiments had proved that, if the overall decomposition of iodate was small relative to the amount of iodate present, radiation induced exchange and recombination

were not important factors in the distribution.

Bellido and Wiles (35), conversely, showed that transfer annealing reactions did occur in KIO_3 and $NaIO_3.H_2O$ doped with ^{131}I as iodide. In a short time the iodide was converted to iodate by heating to 200 and 300° C and by γ-radiation at 35 °C, -78 °C and -196 °C. In these experiments the total activity was found to decrease quite dramatically. In experiments at 100 °C and 200 °C active iodide was found to be escaping from the system after being oxidised to volatile iodine. The decrease at lower temperatures was explained by iodine being in a chemical state which does not exchange with either of the carriers present (I^- and IO_3^-) under the conditions used for analysis. A similar decrease in total activity was observed by Kaucic and Vlatkovic (36). However, such an effect was not observed in the results presented here. See section 5.1.3.

Experiments by Brown and Wahl,(37) on the distribution of fission product Sn in irradiated uranyl salts and solutions,produced results which discounted the electron affinity concept proposed above. The irradiated solutions gave better reproducible results because, unlike the solid samples, they contained carriers which were able to stabilise the newly formed fragment in a short time, and minimise the possibility of reaction with impurities and radiolysis products in the solutions. The Sn atoms, newly formed in the solid matrix, were available for chemical reactions with components of the solid and trace impurities for several hours before dissolution and analysis. ^{121}Sn was found to be mainly oxidised while ^{125}Sn exhibited the opposite behaviour. These isotopic differences were related

to the different modes of formation. ^{121}Sn is formed 88% by the β^--decay, while ^{125}Sn is formed 70% independently. Since ^{121}Sn would most probably be present in solution as 3+, β^--decay would result in Sn(IV). The recoil energy of 25 eV is too low for Sn to pick up electrons, and so 35% found as Sn(II) must result from chemical reduction of the excited Sn(IV) atoms by the medium. Primary Sn fission products have initial energies of $\sim$ 70 MeV. These are more likely to be stabilised with charges of 0 or +1, due to electronic exchange with the medium before the energy is low enough for chemical reaction. Therefore ^{125}Sn occurs in a predominantly reduced condition. The Sn(IV) fraction can be accounted for by assuming that newly formed Sn ions of low charge are excited and that some are oxidised to Sn(IV) by the medium before becoming chemically equivalent to Sn(II) carrier.

Spiridou and Călușaru (38) have studied iodine fission products in a uranyl nitrate medium. A similar isotopic trend was observed with the percentage of reduced forms being increased considerably by lowering the irradiation temperature. All salts were dehydrated prior to irradiation. A variation in dehydration temperature did not have an important effect on the initial value. Oxidised values for salts which had been dehydrated at 51°C and irradiated at room temperature in a flux of $\sim 10^{11}$ n cm^{-2}sec^{-1} for 20 m. are 64.78% (^{131}I) 58.18%(^{133}I) 29.4%(^{135}I). It was deduced from the similarity of the results with those for uranyl iodate (35) that the valence state distribution of the fission product may be determined at an early stage in the process and is not the consequence of simple thermal reactions in the different matrices.

The results presented in this thesis reveal a larger iodate fraction for ^{132}I than for ^{131}I and ^{133}I, in contrast to Hall and Walton's work (34). This can be explained by thermodynamical considerations and is discussed in section 5.1.3.

3.2.2. Impurity atoms in KCl and related subjects

(a) Methods used to introduce impurity atom into the host lattice

It is generally difficult to predict the initial chemical state of a fission fragment from an analysis of the valence distribution in a host medium. The debris caused by its passage through the solid, the initial crystal defects and those produced by the accompanying radiation, all help to promote additional redox reactions, prior to analysis, between the thermalised fragment and entities in the crystal. Also the method of analysis could alter the valence distribution.

(i) Ion implantation:

Other techniques have been used which allow a certain amount of control to be exercised over variables introduced by reactor irradiations. Radioactive atoms can be introduced into a matrix by bombarding with impurity ions at high energies. Whereas the fission fragment entering the lattice can have a distribution in energy, the energy of the bombarding ions can be predetermined. Use of this technique has shown that variations in the initial fragment energy is of little importance in the final valence distribution adopted.

Ladrielle et al (39) have obtained similar annealing results with 25 MeV protons and 11 MeV deuterons although highly different primary disorder regions must have been created. They attribute the results to annealing of the

defects during bombardment by the beam.

Both chromium ions implanted in potassium chromate (40) and sulphur ions implanted in alkali chlorides (41) give the same species and redox transformations as those produced by (n,p)reactions in a reactor. This suggests that the solid state processes do not depend on the particular nuclear process which produces the atom.

(ii) Radiation induced nuclear transformations

Impurity atoms can be introduced into the matrix by in situ methods. Different radiation can initiate a variety of nuclear reactions in the lattice atoms. The daughter recoil atoms can be found as another chemical element. Implantation by nuclear transformations eliminates the large amount of damage produced by fission fragments. Only the damage introduced by the radiation flux and recoiling atom need by considered. Each nuclear transformation will generate recoil atoms with energies characteristic of that nuclear process, and it could be expected that such differences would affect the valence distribution.

Ambe and Saito (42) have reported such an effect in the oxidation states of recoil iodine atoms after $^{127}I(n,\gamma)^{128}I$ and $^{127}I(n, 2n)^{126}I$ reactions in iodates. Retentions after the (n, 2n) reactions are lower. Although the authors site other inorganic systems where similar observations have been made, they mention that no effect has been observed in the related system, sodium bromate. They suggest that other factors could be producing the effects observed. They also found that similar retention values were obtained in sodium and potassium iodates irradiated with neutrons from a cyclotron or in a reactor.

(iii)Filiation

A neat method which permits analysis of the impurity atom in cleaner surroundings is one of filiation. This method reduces the damage to a level which would be expected in a normal crystal at thermal equilibrium. The method has been used by Ladrielle et al (39) in two ways, in an effort to find the role played by the surrounding in the oxidation of Cr(III) to Cr(VI). In the first, element A (a major constitutent in the crystal) is transformed by nuclear reaction on irradiation to a radionuclide of B. Heating will stabilise B* and reduce the irradiation damage. B* decays to A* which is now an isotopic doping species in the sample and need not be in the same state as A. The second method involves extraction of B* from the target. This is used to label a compound containing B as a major constituent. Decay of B* into A* provides a dopant of another element in the matrix. The filiation $Cr \rightarrow Mn^* \rightarrow Cr^*$ was used. The experiments showed that the environment of the doping species is the most important and also the limiting factor that leads to the possible conversion of ^{51}Cr(III)to ^{51}Cr(VI).

(b) Impurity ions·

The results discussed in this report have been concerned with the valence state of a foreign atom introduced into an alkali chloride lattice. Experimental results, obtained from ^{35}S and ^{32}P generated in the crystal by (n,p) and (n,α) reactions in ^{35}Cl, have shown that the valence state is determined by the number and nature of the oxidising and reducing impurities and point defects in its vicinity. Its situation as an interstitial or at an anionic or cationic site is also important. In these systems, the method of

introduction is liable to produce a variety of other defects in the lattice which will be greater than the concentration of foreign atoms. However, these effects can be eliminated by introducing ^{35}S and ^{32}P using the alternative methods described above.

(i) Sulphur

Results for the valence states adopted by the ^{35}S impurity atom have produced conflicting evidence for the presence of different species. Abdel-Rassuol et al (43) have reported the presence of thiosulphate (S^{2+}) and others have failed to find sulphite (S^{4+}). It is generally agreed that sulphide (S^{2-}) and sulphate (S^{6+}) exist, and several workers have reported the presence of sulphur.

Kasrai and Maddock (44) have made a detailed study of the effects of the medium on the species present for analysis. They have distinguished sulphide, sulphur stabilised as CNS^-, sulphite and sulphate. From these, they have identified precursors in the crystals as S^o and S^- or S^{2-} which give sulphide, and entities such as SCl, SCl_2^-, SCl_2, which contribute to sulphite and sulphate fractions. The latter are more likely to occur than the oxidation of $^{35}S^+$ by acquiring three or four oxygen atoms from trace oxygen in the KCl matrix. Also Cl_2^- and Cl_3^- ions are known to be produced by irradiation of alkali chlorides (16).

Adloff and Meyer (45) have shown that if no carrier is present, a fraction of the activity is lost which arose from zero-valent sulphur. The same fraction appears as thiosulphate if the irradiated crystals are dissolved in concentrated sulphite solution. This indicates that S^o will be oxidised by water or alkaline solutions in the absence of a carrier. Therefore a carrier for thiosulphate

is unnecessary if one is present for sulphur.

Owen and Hobbs (46) investigated the chemical states of ^{35}S produced by the ^{35}Cl (n,p) ^{35}S reactions in solid KCl-KBr solutions. The relative yields in the four fractions varied with treatment and composition. The dependence of the latter was attributed to the associated varying concentration of oxidising and reducing defects. Following the Maddock-Mirsky model, they identified three precursors S^+, S^o, S^-, and established a correlation between the yields of the last two and the F centre concentration. It was suggested that the variation in yields was due to competition between the species for V or F centres or their derivatives. They reported that the oxidising effect reached a plateau after 12 hours annealing, and this corresponded to a depletion in V centre concentration. The observation of a plateau for the oxidising effect agrees with the results presented in this thesis (figure 5.1).

Kasrai et al (47) have compared the behaviour of ion implanted ^{35}S with (n,p) reactions in NaCl irradiated in a reactor flux. They found that the same ^{35}S species are produced by either process, but ion implantation gives higher yields of the lower oxidation states of sulphur. No difference was observed for the distribution with 40 or 100 KeV implantation. The results correlate with the fact that less hole damage is introduced through ion implantation. Most of the remaining holes are probably due to concurrent Cl^+ implantation which was unavoidable in the experiments reported. They suggest that sulphur is present at cationic and anionic sites. The latter are preferred because of the large size of the sulphur atom in relation to the Na^+ ion. An interesting observation

was made of a tail to the penetration of ^{35}S during the ion implantation process. This sulphur was expected, through channelling, to have reached a region of the crystal where there is no damage from the incident-ion beam. It was found to be mainly in the reduced state.

(ii) Phosphorus

Similar experiments have been made to find the valence distribution of ^{32}P in KCl. In this system the identity of the crystal species are not so well established. Generally, three fractions have been reported in aqueous solutions of the irradiated salts. These are P(I), P(III) and P(V). Bogdanov and Murin (48) have shown that the P(I) fraction consists of two chemically distinguishable ^{32}P species, a P(III) and a P(I) generating fraction. Andersen and Baptista (49) have also obtained evidence for two precursors to the P(I) fraction. Chandratillake et al (50) have recently studied ^{32}P in neutron irradiated ammonium hypophosphite using aqueous, non-aqueous and thin layer chromatographic analyses. They established that the P(V) state is a hydrolytic product, P(III) has an independent precursor in the solid state, and that at least three precursors for the P(I) valence state exist.

The decay of the F centre band has been correlated with an increase in the P(I) fraction by some (49) (51). However, Bogdanov et al (52) demonstrated that there is no strict correlation between F centre formation and content of P(I). They suggest that the behaviour of the fraction depends on the rates of formation of different types of defects and rate of colour formation during bombardment. It was also proposed that vacancies can exist as bundles, which are ineffective in the capture of electrons

resulting from the decay of F bands.

Several workers have shown that the dissolving medium determines the valency states obtained by chemical analysis. This is discussed in section 3.3.1.

Many experiments have been performed on nuclear transformations in more complicated systems such as the phthalocyanines, acetylacetonates, complexes of rhenium, osmium, iridium, rhodium and of cobalt, iron and chromium. Retention in these systems will be expected to be influenced by steric factors and radiolysis products of the parent molecule. Its affinity for ligands in the damaged medium will also be important. In many of these complexes, oxygen will exist as a radiolysis product of one of the ligands and it will be expected to have an oxidising effect on the products. As before, the effects observed are interpreted in terms of electron donating and accepting fragments.

3.3. Influence of the host medium on the recoil atom

3.3.1. Moisture Effect

A search through the literature has not revealed any reports of an observed moisture effect in the annealing studies of fission products. However, several reports have been made of effects due to water in other recoil chemistry studies of solids. The water was present either as water of crystallisation or as an aqueous medium in which the solid was dissolved before analysis. The effects are most often discussed in terms of the retention of the target atom.

(a) Water of crystallisation

(i) Oxygen bond formation and dissolution in water of crystallisation

Arnikar et al (53) observed the effect of annealing on the retention in cadmium bromates after (n,γ) processes, initiated by reactor irradiation. At 150 °C there was complete dehydration of the hydrated salts. These showed 100% retention at this temperature but the anhydrous salt only produced 53% retention. It was suggested that irradiation of the bromate ion produced species such as BrO_2^-, BrO^-, Br^- and radiolytic oxygen. Of these, BrO_2^- would be most likely to reform the bromate ion by oxidation during annealing. If some of the oxygen escapes or is trapped at sites inaccessible to BrO_2^-, annealing retention values will be lowered. The presence of water in the lattice seeemed to hold the oxygen during irradiation, and the following reactions were proposed.

Anhydrous crystals $BrO_3^- \longrightarrow BrO_2^- + O$ (3.1)

Hydrated crystals $(BrO_3.H_2O)^- \longrightarrow (HO.BrO_2.OH)^-$ (3.2)

On annealing at 150 ^oC $(HO.BrO_2.OH)^- \longrightarrow BrO_3^- + H_2O$ (3.3)

Ladrielle et al (39) have reported the importance of the environment of the doping species for the conversion of $^{51}Cr(III)$ to $^{51}Cr(VI)$ in doped manganese compounds. An increase in the number of water molecules in going from $MnSO_4.H_2O$ to $MnSO_4.7H_2O$ decreased the conversion by 50%. This effect was attributed to an oxygen bond reorientation from S to Cr, which is less favoured for $MnSO_4.7H_2O$ due to steric hindrance. The percentage conversions for $MnSO_4.7H_2O$ and $MnCl_4.4H_2O$ were similar. The oxidation of the latter must have proceeded by way of the water molecules and was explained by a lowering of the melting point, due to the water, and transfer reactions taking place in a concentrated aqueous solution where oxygen is more mobile. No transfer was found for MnS because there was no oxygen present in this compound.

Stamouli (54) has invoked an oxygen bridge effect, liquid phase reactions and acceptor sites to explain the annealing effects observed after irradiation of $Na_2Cr_2O_7$, Na_2CrO_4, $Na_2Cr_2O_7.2H_2O$ and $Na_2CrO_4.4H_2O$. There was a decrease in the ratio of Cr(III) species appearing as monomers (M) to Cr(III) polynuclear species (DP), in both hydrated salts when compared with the anhydrous salts. It was suggested that water was acting as a bridging agent to enhance the formation of polynuclear species.

Above the dehydration temperature $Na_2Cr_2O_7.2H_2O$ was observed to dissolve in the water of crystallisation, and was accompanied by DP being oxidised to $^{51}Cr(VI)$ species.

A similar effect was observed in $Na_2CrO_4.4H_2O$ by slow evaporation of the water of crystallisation. Heating above the dehydration temperature at 110 ^{o}C for 1 h gave retention values of 79.4 and 87.3% for the anhydrous and hydrated salts.

(ii) Donor-acceptor mechanisms

The DP species in neutron irradiated $Na_2CrO_4.4H_2O$ was found to be very unstable and quickly underwent oxidation to Cr(VI). This did not happen in samples dehydrated at room temperature in vacuo. An electron transfer reaction was invoked between the DP species and acceptor sites in the crystal produced by radiation damage. Dehydration could result in lattice changes involving the acceptor sites, or in reactions of the crystal phase precursor of the DP species with water molecules, or both.

Ackerhalt et al (55) have reported that trace impurities such as water in crystals of KCl and NaCl have a marked effect on the valence state assumed by 100 KeV ^{208}Tl atoms produced in the α-decay of ^{212}Bi.

Bellido and Wiles (35) observed high retention values in the transfer annealing reaction for hydrated sodium iodate doped with ^{131}I as iodide. They proposed the existence of deep lying electron traps in $NaIO_3.H_2O$, and postulated a reaction mechanism which involved successive electron and oxygen ion transfer.

Ambe and Saito (42) observed low retentions for neutron irradiated hydrated sodium iodates. This is in contrast to the above results for transfer annealing and the observation(35) of a strong similarity between transfer and recoil annealing results for other experimental systems. See section 3.4.1. Ambe and Saito inferred that the water molecules act as

reducing agents for the recoil iodine atoms, as proposed by Harbottle and Sutin (56). The retention was not altered by deuteration, and this indicated that it was not a steric effect. However, a cationic effect was observed in experiments with iodates of transition metals. These hydrates gave higher retentions than were obtained for $NaIO_3.H_2O$. It was inferred that transition metal ions were less able to react with unstable electrons produced along the track of the recoil atom. An alternative explanation was that the coordination of the water molecules to the crystal might be important. Water molecules in the crystal may exist as ligands coordinated to a metal ion, or as hydrogen bonded to iodate ions. They conclude by suggesting that changes in crystal structure, and the extent of packing caused by the introduction of water molecules into the lattice, must also be taken into account in a comparison of recoil reactions in anhydrous and hydrated salts.

KIO_3 does not form hydrates and so the latter explanation could not apply to this compound. Experimental results reported later show that iodate values increase with moisture. This most probably reflects the unusual state of fission product iodine in the lattice, and suggests that reactions on dissolving the lattice are important.

In a study of the Ir (p, 3p xn) Re reaction, generated with 660 MeV protons, Ianovici and Zaitseva (57) found that water of crystallisation and ammonium ions favoured the higher oxidation state Re(VII). This could be due to sites with both acceptor and donor properties such as $OH^{\cdot}$, $H^{\cdot}$, $NH_2^{\cdot}$ which are radiolysis products, formed by proton irradiation. They interpreted the results with an "electronically

excited exchange" model which involved detrapping of electrons (holes) from multi-depth traps.

Peixoto and Maddock (58) have reported similar effects. The observation of both higher and lower retentions in hydrated and ammonium salts can be reconciled as follows. The observed differences in initial retention are due to differences in energies required to promote electrons from different centres to the conduction band. They can then be trapped at other centres in the crystal.

Al-Siddique and Maddock (59) have attempted to correlate differing results in another way, by suggesting that the initial retention values could be affected greatly by room temperature annealing. Lower temperature irradiations and storage often produce lower retentions in crystals which had exhibited high retentions at room temperature. This is due to acceptor sites being less mobile below room temperature. Compounds, still exhibiting higher hydrate retention values, are assumed to be extremely susceptible to radiation annealing, even at liquid nitrogen temperatures.

Walton (60) provides an explanation for the effect of water of crystallisation. He suggested that the presence of water of crystallisation increases the ease with which electrons can be promoted to the conduction band in atoms excited by neutron irradiation. This allows valency bonds to be disrupted more easily than in anhydrous compounds. Bonds in solids and liquids could then become much more labile than in gases. This idea is supported by the observation of a wide variety of products formed in irradiations of organic molecules, and by the observation that optical configurations are retained in nuclear transformations. This observation cannot be reconciled if atoms

move around, but is easily understood if activation is associated mainly with bonds. Such a mechanism helps to correlate the results for neutron irradiations (39) (58) and explains the difference in results for (35) and (42).

Borshagovskii et al (65)have similarly deduced that the effect of an aqueous medium is to promote electronically excited exchange. This is discussed in the next section.

(b) Effect of dissolution

Conventional radiochemical methods of analysis for fission products in solids have required dissolution in a carrier solution. This presents two problems. The first is that the carriers must be present in the same oxidation state as the dissolved fission fragment in the solution. The second problem is that the process of dissolution could change the oxidation states of the fragments that were present in the solid, through greater mobility of the point defects. This could lead to erroneous deductions, concerning the state of the precursors in the solid, from the valence states observed in the solution.

Maddock and Mahmood (61) have invoked the effect of the dissolving medium to explain the difficulty that experimentors have had in the past in determining the nature of ^{32}P species present in neutron irradiated, ion implanted or chemically doped chloride crystals containing atomically dispersed phosphorus. The P(I), P(III) and P(V) fractions were usually identified in aqueous solutions. Dissolution in liquid ammonia revealed the presence of P(-III) which had been reported by some, and P(0) which had not been observed in aqueous solutions. The fractions of P(I), P(III) and P(V) were correspondingly reduced. This was evidence for the theory that water is capable of oxidising atomic

phosphorus by means of the V-centre derivatives formed in the irradiation.

Kasrai and Maddock (44) have shown that, in investigation of ^{35}S produced by neutron irradiations of alkali chlorides, the oxidised products obtained (SO_3^{2-}, SO_4^{2-}) do not occur as a result of oxidation by the solvent. They are more likely to be produced by point defects introduced into the crystal during irradiation. They suggested that oxidizing point defects, produced in the alkali chlorides by irradiation, behave as chlorine atoms or perhaps Cl_2^- upon solution. Precursors in the crystal might be SCl, SCl_2^-, SCl_2. These are analogous to Cl_2^-, Cl_3^- centres etc., which are produced by irradiation of alkali chlorides.

Meyer (62), in a study of the chemical forms of ^{37}S produced by a $^{36}S(n,\gamma)$ reaction on ammonium sulphate, sulphite and hyposulphite salts in the solid state and aqueous solutions, has found similar distributions. This was taken to imply that the recoil distribution for solids is affected by the dissolution step involved in the analysis.

Meyer (63) has also investigated the chemical form of ^{37}S from neutron irradiations of LiCl in methanol solutions. He found that S^o gave sulphate in aqueous solutions and sulphite with reducing mediums.

$$^{35}S^o + 4H_2O \longrightarrow {}^{35}SO_4^{2-} + 8H^+ + 6e^- \qquad (3.4)$$

In carrier solution

$$^{35}S^o + S^{2-} \longrightarrow {}^{35}SS^{2-} \qquad (3.5)$$

$$^{35}SS^{2-} \longrightarrow {}^{35}S^{2-} + S^o \qquad (3.6)$$

Solutions with 100% alcohol still had 16% as SO_4^{2-}, although S^- has been extracted. This was taken to indicate the existence of another precursor S^+, as suggested by other

researchers.

Ambe et al (64) reported that in the electron-capture decay of ^{119m}Te in H_6TeO_6, the distribution of ^{119}Sb between the Sb(III) and Sb(V) states was dependent on the oxidation state of the parent atom in the compound and on the medium used to dissolve the sample. H_6TeO_6 samples, stored as aqueous solutions, gave higher amounts of ^{119}Sb(III) than those stored as solids.

Borshagovskii et al (65) reported the effect of moisture on insoluble Prussian Blue powder $Fe_4\left[Fe^{II}(CN)_6\right]_3$. A small amount of $^{57}FeCl_3$ solution was added giving a singlet in the Mössbauer spectrum corresponding to $^{57}FeCl_3$. After several days, three lines were obtained. These were associated with the exchange of $^{57}Fe^{3+}$ both with the position inside and outside the sphere. They suggested that the effect was due to moisture. Water is a highly polarisable group and will increase the dielectric constant of the matrix. The depths of donors (acceptors) will be reduced and this will lead to electronically excited exchange.

From the results discussed in this section, it is seen that the valence states obtained by analysis are dependent on the point defects in the crystal lattice and their subsequent modification by the dissolving medium.

3.3.2. pH effect

Several researchers have reported the effect of pH on their analyses.

Finn et al (66) have reported that the distribution of ^{14}C between $^{14}CH_4$, $^{14}CN^-$, $^{14}CN^{2-}$ in neutron irradiations of Mg_3N_2 depend on the pH of the solvent. Gutlich et al (67) have reported the pH of the solvent to be one of the

factors determining the distribution of ^{51}Cr activity in irradiated crystalline chromates. Kulikov et al (68) found that the Fe^{3+}/Fe^{2+} ratio in glasses after ^{57}Co decay was affected by the hydrogen ion concentration. These ions are electron acceptors and so the ratio increases with their increased concentration. When hydrogen ions are not present, the Fe^{3+} fraction is determined by electron traps in the matrix.

Bračoková and Cífka (69) studied the effect of KOH concentration in the valence distribution of ^{32}P and ^{35}S atoms in KCl crystals irradiated at dry ice temperature in a reactor. Both distributions favoured the lowest oxidation states during thermal annealing at room temperature throughout the whole range of KOH concentration. The ^{35}S atoms were more affected. The percentage of reduced species of ^{35}S decreased in the range 0.001 to 0.01 mole % KOH and increased in the range 0.01 to 0.1 mole %. The lowest oxidationstates for the ^{32}P species increased in both ranges. Although experiments were not performed at concentrations greater than 10 mole %, it seemed as though high concentrations would result in more highly oxidised species. The authors suggested that P-OH and S-OH bonds were formed and this increased the amount of highly oxidised species. OH^- impurities also increased the sensitivity of crystals to ionising radiation. F centre formation is proportional to the OH^- concentration, and the decay of F centres is easier than in pure KCl crystals. These facts explain the fast reduction of ^{35}S species heated to room temperature and the increase in reduced species between 0.01 to 0.1 mole % KOH. The authors compared their results with those obtained by Baptista et al (70), where a change in

concentration from 10^{-5} mole% to 3 - 7 x 10^{-4} mole % produced an increase in the percentage of ^{32}P as P^{+5} from 23 to 90%. They noted that comparisons were not meaningful because irradiations had been at different temperatures and the concentrations of KOH were of different orders of magnitude.

Kasrai and Maddock (44) studied the effects of pH in relation to aerial oxidation of aqueous solutions containing dissolved irradiated alkali chlorides. Acidic solutions, with H_2S as carrier and exposed to air, produced more oxidised species of ^{35}S as SO_3^{2-} and SO_4^{2-} than those kept and analysed in a vacuum. For these the S^{2-} concentration was greater. However, reproducibility of results was poor in the presence of air. The absence of air and carriers led to complete oxidation, which could only have occurred by the water or by the point defects produced in the crystal during irradiation. Such processes are responsible for oxidising sulphide or its precursors which are normally stable in water. Neutral and alkaline solutions, with no carrier and in a vacuum, have appreciable proportions of reduced forms. A mechanism was used in which the oxidising point defects behave as Cl atoms, as proposed by Rabe et al (71), or as Cl_2^- ions. In alkaline solutions, oxidation will proceed more slowly if

$$Cl + OH^- \longrightarrow ClOH^- \qquad (3.7)$$

Also the reaction

$$OH + Cl^- \longrightarrow Cl + OH^- \qquad (3.8)$$

in aqueous solutions is much slower in neutral solutions than in the acid. This could be reversed in alkaline solutions, and both $ClOH^-$ and OH might be slower in oxidising S^{2-} than Cl.

The effects of pH discussed in (69) and (70) are for crystals with differing pH prior to irradiation. The effect described in (44) applies to irradiated crystals which are analysed in solutions of differing pH. The former describe solid state processes which are modified by dissolution. The latter discussion is applicable to reactions in solution. The effect of an alkaline pH solution is to react chemically with oxidising point defects in the solvated crystal, and to prevent them from otherwise reacting with the species to be analysed. An acid pH will promote the oxidised valency states through the ability of the H^+ ion to act as an electron sink.

3.3.3. Effect of gases, especially oxygen

Several double complexes seem to be susceptible to oxygen. Positive oxygen effects have been reported by Lazzarini and Lazzarini (72) in the annealing of cis- and trans- $\left[Co(en)_2(NO_2)_2\right]\left[Co(edta)\right].nH_2O$. A similar effect was also observed in the substitution of Cr(III) oxinate and Co(III) oxinate crystals doped with Co^{2+} (73). A positive oxygen effect was reported by Kishore and Venkateswarlu (74) in the anion annealing of ^{60}Co recoil species in $\left[Co(III)(NH_3)_6\right]\left[Co(III)(gly)_2(NO_3)_2\right]$. Thomas (75) reported a similar effect with NO in the thermal annealing of $Co(acac)_3$.

An oxygen effect was observed by Podeanu and Costea (76) when they annealed irradiated K_2CrO_4 crystals at temperatures above 180 °C. The crystals had been heated to 650 °C prior to irradiation and it was assumed that this treatment had enhanced the density of surface defects and promoted a higher adsorption of oxygen. Oxygen acts as a deep electron

trap. At higher temperatures during thermal annealing, the electrons will become detrapped and reduce the concentration of free holes which are responsible for oxidising Cr(III) to Cr(VI). This will retard the thermal annealing. Collins et al (77) have proposed a mechanism for hole-induced annealing through stepwise oxidation.

$$Cr^{3+} + 3(CrO_4)^{-} \longrightarrow Cr^{6+} + 3CrO_4^{2-} \qquad (3.9)$$

Several groups working on the neutron irradiation of copper phthalocyanine, e.g., Odru and Vargas (78), Scanlon and Collins (79) have tried to account for the influence of ambient gases (O_2, H_2) and crystal phase on isochronal annealing. Oxygen blocks annealing in the β phase at all temperatures. In the α form, oxygen blocks annealing only above 300 ^{o}C and favours annealing at lower temperatures. On the other hand, hydrogen has been found to enhance the annealing of both, with a greater effect on the β form. This has been attributed to the introduction of electrically active centres.

It is suggested (80) that there is an experimental distribution of electron traps. At temperatures below 100 ^{o}C in an oxygen free atmosphere, there is n conductivity (extrinsic). At higher temperatures, intrinsic hole conductivity begins to dominate, because holes have greater mobility than electrons. If oxygen is present at lower temperatures, its acceptor levels will compensate the donor levels. Less electrons are available for conduction. If the concentration of oxygen is high as in the phase, the type of conductivity changes from electron to hole. At higher temperatures, there is still hole conductivity, but more electrons are released from traps. Less holes are available and annealing is retarded.

One view of the oxygen effect has been proposed by Scanlon and Collins (79). Holes could inhibit annealing by inactivating the recoil atom sites through interaction with them. Thus, the hole conductivity of the oxygenated α-form above 300 ^{o}C would relate directly to a greater hole inactivation of annealing in the α-form.

Anderson and Baptista (81) have reported an oxygen effect in the annealing of n-irradiated K_2CrO_4. In a vacuum M$\rightarrow$Cr(VI) but in air only DP$\rightarrow$Cr(VI).

The radiolysis of labelled K_2CrO_4 was studied by Yung et al (82). The radiolytic yield of Cr^{3+} seemed to be inhibited by oxygen.

Kudo has shown (83) that isothermal annealing and initial retentions are greatly increased in a sandwich of pellets of α-Cu (pc) pressed between two pellets of α-H_2(pc), where pc = phthalocyanine. This can be explained by Cu(pc) absorbing more oxygen than H_2(pc). The higher concentration of electrons in the latter compound transfer to Cu(pc) and are trapped by the oxygen. In this arrangement, there is less surface of Cu(pc) exposed to oxygen, and so more electrons are available for triggering exchange during thermal treatment.

Nath (84) has also shown that retention values are increased when a polycrystalline sample of n-irradiated $Co(acac)_3$ is completely covered by an excess of unirradiated $Co(acac)_3$ powder before thermal treatment in air. This is attributed to shielding of the surface of the microcrystallites from oxygen.

Ianovici and Zaitseva (57) have reported that oxygen retards the annealing of Re to Re(VII) produced from Ir (p, 3pxn) Re reaction in several iridium compounds.

No significant effect was reported (64) on the distribution of Sb(III) and Sb(V) resulting from electron capture decay of $H_6{}^{119m}TeO_6$, which was dissolved in 1.5 M HCl saturated with O_2 or free from O_2.

Kasrai et al (47) have discussed the distribution in valence states of ion-implanted ^{35}S in NaCl, resulting from pre-bombardment influences of O, S and Cl. Preimplantation of a large excess of oxygen or sulphur produced little change in the oxidised fractions, even after annealing. However, both treatments increased S^0 at the expense of S^{2-}. This was explained by assuming that bombardment fills a large proportion of the existing anionic vacancies and reduces the number of sites for S^{2-}. Alternatively, it reduces the supply of electrons in the first 10^{-4} cm of crystal and makes S^{2-} formation more difficult.

Chlorine implantation resulted in direct increases in the oxidised fractions and this was enhanced by annealing. There was no evidence for atmospheric oxidation during low temperature annealing in air, even though $^*S$ is very close to the surface. The results showed that as the $^{35}Cl/^{35}S$ ratio fell, the $^{35}S^{2-}/^{35}S$ ratio grew. This implied that electrons on the sulphide ions are easily transferred to deeper traps, such as those provided by the electron-deficient centres formed by the chlorine atoms.

Venkateswarlu (85) has found that the role adopted by oxygen in the annealing of chromates depends on the system. Reduction in the annealing by O_2(86) was taken as evidence for an electronic mechanism, where the O_2 molecule is an electron trap in competition with the recoil species. Its dual role was explained by adduct formation between ambient gas and Co(II) chelate. There is exciton-stimulated

exchange between the $^{60}Co^{2+}$ recoil and a Co(III) complex to give the ^{60}Co(II) complex. This can then undergo one of many possible reactions. If this is the formation of a bridged oxygen carrier, the results would depend on the reactivity of the complex and the reversible nature of the formation of the bridged oxygen adducts.

No oxygen effect was reported by Rusi and Călușaru (87) in the annealing of n-irradiated $K_4\left[Fe(CN)_6\right]$. It was deduced that an electronic effect is not important in the annealing of Fe(II).

A reaction sequence was proposed for the annealing of ammonium sulphate which involved an oxygen atom as a reactant or an electron acceptor (88).

Kasrai and Maddock (44) have found evidence to suggest that aerial oxdiation plays a part in the analysis of ammoniacal carrier free solutions of irradiated KCl.

Anderson and Baptista (49) investigated the valence distribution of ^{32}P atoms, generated by (n,α) processes in oxygen doped KCl single crystals. The concentration of oxygen centres was less than 10 ppm. They found that the onset of a very fast oxidation process ccincided with the decay of the O(III) - O(IV) centres (89). Their behaviour is similar to that of excess electron centres. When they are removed, oxidative processes involving thermal decay products of V centres can take pla ce. Therefore, the thermal destruction of V-type centres is the rate determining step for ^{32} P oxidation in pure KCl.

Samples of MgO, subjected to pre-irradiation annealing in H_2, exhibited a large change in colour centre concentration after reactor irradiation, compared with un-annealed crystals. Henderson et al (90) attributed this to vacancies diffusing to

large voids produced by the annealing treatment.

There is little doubt from these results that oxygen has an effect on annealing. Its varying effect is attributed to its role as a deep electron trap. At higher temperatures these electrons are detrapped and reduce the concentration of free holes in the lattice. The effect of electrons and holes on annealing is discussed in the next section.

3.4. Determination of the nature of precursors in the crystal

3.4.1. Annealing behaviour

Study of annealing reactions has led to considerable progress in the field of nuclear transformations. Changes in the distribution of the valence states are usually observed, which vary according to the method, time and character of the annealing. This implies that the radioactive fragment under observation is taking part in chemical reactions with entities in its environment. Rate constants can be found for the reactions and, from these, the identity of the initial unreacted fragment can be deduced. Annealing reactions usually promote the formation of the parent species or the oxidised fraction, and can be induced by heating, ionizing irradiation, illumination, ultrasonic irradiation and pressure.

Dimotakis et al (91) has investigated the thermal annealing effects in irradiated crystalline cobaltic trisethylenediamine nitrate. His results are represented by a series of undulating curves. A three dimensional plot of isothermal curves as retention-time-temperature displays ridges and valleys. Similar curves were obtained for linear tempering, that is, heating samples at a constant temperature gradient and examining them after different times. Although the planes containing the thermal and linear tempering curves intersected, the curves did not, and different retention values were observed at the temperature and time of intersection. This was expected since both systems were not in equilibrium and retention was not a unique function of time and temperature. The similarity of both curves supports the hypothesis that a general

mechanism involving the damaged lattice is concerned in all thermal annealing. The existence of steep maxima and minima suggests that competitive processes involving recombination and microdecomposition are occurring. Therefore, the flattened region in linear temporing curves should not be interpreted as regions where one reaction is complete, while others corresponding to higher temperatures have not yet begun.

It was found that irradiations at low temperatures lead to more pronounced maxima and minima in the annealing isotherms, which shifted to shorter times with increasing annealing temperature. The occurrence of oscillating isothermals appears to be independent of the chemical constitution of the irradiated solid, and to be a general property of the lattice.

No similar curves have been reported by other workers. In fact, most have reported an increase in retention, which reaches a plateau value after some time. However, several have reported a maximum or minimum at the beginning of annealing.

Bracokova and Cifka (92) have produced a curve for the thermal annealing of P^{5+} in pure KCl at 150° C which resembles those reported in Chapter 5. However, its shape was not discussed. An initial reduction period was also shown by them in the thermal curve at 10 °C of ^{35}S recoils in $BaCl_2$ doped with 0.077 mole % monovalent metal chloride (93).

Several research groups, in an effort to find a mechanism for thermal annealing of recoil damage have adopted the technique of transfer annealing. This makes solid state processes more controllable and reproducible.

It entails doping crystals with a radioactive tracer that will eventually exchange with its non active element in the crystal lattice. Often, the results obtained correspond to those obtained through irradiation of the crystal sample (35). Such an experiment has been carried out by Khorana and Wiles (94). Their results for transfer annealing in ^{131}I doped $CsClO_4$ and $CsIO_3$ strongly resembles the annealing curves reported in this work. There was evidence in both compounds for the formation of IO_3^- and IO_4^- on thermal annealing. The participation of correlated defects, formed as a consequence of recoil, does not seem to be a dominant characteristic, since IO_3^- is detected in this experiment. More likely bulk defects, those formed due to concomitant γ-radiation and those existing in the unirradiated solid, are responsible. However, it was proposed that recoil shifts the activation energies so that reactions can take place which would otherwise occur only at elevated temperatures. This implied that the kinetics of transfer annealing and thermal annealing need not be identical. They proposed two mechanisms for the results: the isotope exchange model of Nath et al, and the stepwise oxidation model proposed by Apers et al. The results also showed that annealing had little effect on IO_4^- which had a steady concentration of 18% of total activity.

Spiridou and Călușaru (38) have produced curves for the change in the percentage of reduced forms with heating for the ^{131}I isotope in enriched uranyl nitrate. Irradiationsand annealings have been performed at various temperatures, and the results, again, qualitatively represent those reported in Chapter 5. They suggest that the phenomena are dependent on the thermodynamic properties of

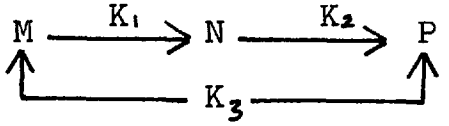
the matrix and a sequence of chemical reactions must be assumed.

Bogdanov and Olevski (95) have investigated the effect of pressure on the valence distribution of phosphorus recoil atoms in alkali halide crystals. A change in the distribution was only observed above a 1.3 % deformation, when the concentration of dislocations had increased 10 fold. This was characterised by an increased in the P(I) fraction. If the dislocations capture electrons released from F centres by irradiation, strongly deformed crystals might show less of a P(I) increase. There was no evidence for this, and it seemed that the capture of electrons on dislocations does not compete with capture by other lattice defects.

3.4.2. Annealing mechanisms

Milenković et al (96) have used computer simulations in order to find a satisfactory model to explain the annealing of recoil atoms in solids. The annealing reactions of radioactive chromium (^{51}Cr) in K_2CrO_4, either pure or doped by alkali halide, were studied. Various reaction schemes were proposed,which incorporated general diffusion controlled kinetics with multistep reactions in localised disordered centres. A great diversity of defects was expected,due to γ-radiation of 10^7 - 10^8 rads from the reactor and the recoiling atom. Vacancies, interstitials, defect dislocation loops, electrons and positive holes will all help to determine the interaction of the recoil atom with its surroundings. Seven possible mechanisms were considered which involved transitional forms and various positional energies of the initial atom. Successive and

parallel processes were considered. A set of criteria was postulated and a computer analysis of the reactions revealed that only one mechanism satisfied this criteria



N is the transitional form (3.10)

Low activation energies and rate constants were obtained for the doped samples and were taken to be the consequence of extrinsic factors in these reaction steps. The pure samples showed greater thermal sensitivity which suggested a "chemical" nature of the processes in pure chromates. The low energy reactions in doped samples were more likely to be due to diffusion of lattice defects and charge carriers. The activation energies for these processes do not exceed 1 eV in most crystals. A certain amount of agreement with ESR measurements was reported.

Anselmo (97) has suggested that an exploding lattice model can explain the results obtained in n-irradiated orthophosphates MH_2PO_4 and orthophosphates MH_3PO_3 where M is an alkali metal. The retention of ^{32}P increases with increasing size of M, and steric factors are considered to be responsible. The recoil ^{32}P is able to break through the primary cage of the tetrahedrally arranged O_2 and H_2 atoms. The probability of its escape from the secondary cage of cations depends on their size. If the cations are smaller than ^{32}P, its probability of escape is greater and retentions are lower.

Baptista et al (98) have studied the effect of γ-irradiation on the valence distribution of radiophosphorus in KCl single crystals produced by $^{35}Cl(n,\alpha)^{32}P$. Oxidation processes were interpreted as involving reactions between ^{32}P and hole species in the solid. However, the final

chemical state will also be determined by processes during dissolution

$$^{35}Cl + n \longrightarrow {}^{32}P_H \longrightarrow {}^{32}P_T \quad (3.11)$$

$$\gamma \longrightarrow S, L, X \quad (3.12)$$

$$^{32}P_H + S \longrightarrow {}^{32}P(ox) \quad (3.13)$$

$$^{32}P_H + L \longrightarrow {}^{32}P(ox) \quad (3.14)$$

$$^{32}P_T + S \longrightarrow {}^{32}P(ox) \quad (3.15)$$

$$S + X \longrightarrow \text{inactive species} \quad (3.16)$$

^{32}P = low valence ^{32}P species before it has lost all its kinetic energy (hot reaction)

$^{32}P_T$ = low valence ^{32}P species in thermal equilibrium with the KCl lattice

S = short-lived hole species

L = long-lived hole species

X = long-lived hole trapping species

Pre-γ-irradiation was ineffective but post-γ-irradiation was very effective at ambient temperature. This suggested that short lived rather than long lived species were responsible for oxidative reactions. The observation of ineffective post-γ-irradiation at 77 ^{o}K implied that an activation energy existed for S which prevented reaction at a low temperature. However, a large increase in the oxidised species was obtained with reactor irradiations at 77 ^{o}K. This can be explained by equation (3.13). Neutron damage was found to be relatively unimportant. The decrease in the rate of oxidation for samples that had been reactor irradiated at room temperature is explained by equation (3.16). The reducing effect of pre-γ-irradiation can be explained by a gradual inhibition of oxidation reactions (3.13) and (3.15) as the concentration of X increases.

Similar ideas have been proposed by Maddock et al (99) to explain post-γ-reactions in chromates.

Baumgärtner and Maddock (100) have investigated the effect of thermal and ionising radiation on retention in potassium chromate. Results for reactor irradiation annealing at different temperatures exhibited a strong dependence on temperature. Similarly, thermal annealing was more efficient when the material had been pre-irradiated with ionising radiation. It was found that room temperature annealing,after low temperature ionising irradiation,leads to a much smaller increase in retention than an equal dose of ionising radiation at room temperature. It was suggested that initial retention values should be regarded as plateau values, for annealing under conditions of temperature and dose of the ionising radiation prevailing during neutron irradiation. Such values will only reflect the hot fragment reactions at very low temperature neutron irradiations, in the absence of ionising radiation.

Previous results have shown that annealing reactions are oxidations and results by others indicate that they are accelerated by gases such as O_2 and alcohol vapour at moderate temperatures. These points and the above results suggest that annealing incorporates two processes. The first involves the removal of an electron from the fragment. This can be achieved by ionising radiation either directly or, more likely, through the creation of acceptor sites in the vicinity of the fragment. The second step is a thermally activated recombination or exchange between the fragment and its surroundings. This can be interpreted for chromates as

$$*CrO^{3+} - e^- \xrightarrow[\text{acceptor site}]{} *CrO^{4+} \qquad (3.17)$$

Recombination $*CrO^{4+} + 3O^{2-} \longrightarrow *CrO_4^{2-}$ (3.18a)

Exchange $*CrO^{4+} + CrO_4^{2-} \longrightarrow *CrO_4^{2-} + CrO^{4+}$ (3.18b)

The thermal process 3.18(a) or 3.18(b) is in competition with other processes which could fill the acceptor site.

Such a framework has been adopted by Bellido and Wiles (36) to explain the results of transfer annealing in alkali iodates with γ and thermal irradiation. There can be an initial electronic step, followed by a thermal step, or a series of both steps following one another. The mechanism for iodates was described in more detail, following Costea's (101) interpretation of recoil reactions in chromates.

$$IO_3^- + \text{photon} \longrightarrow IO_3^0 + \text{electron} \quad (3.19)$$

$$IO_3^- + \text{heat} \longrightarrow IO_3^0 + \text{electron} \quad (3.20a)$$

$$IO_3^0 + \text{electron} \longrightarrow IO_3^- + \text{photon} \quad (3.20b)$$

$$IO_3^0 + *I^m \longrightarrow IO_3^- + *I^{m+1} \quad (3.21)$$

$$IO_3^- + *I^n \longrightarrow IO_{3-x}^{2x-1} + *IO_x^{n-2x} \quad (3.22)$$

The concentration of the oxidising species IO_3^0 is controlled by the depth of the electron traps in the crystal matrix. If the traps are deep, reaction 3.21 will occur. In these experiments, the total activity was found to decrease during annealing. This can be understood if, in 3.21, m = -1 (iodide). Atomic I^0 will be formed and could combine with another atom to produce iodine, which could then escape from the system. Reaction 3.21 could also produce radioactive atoms in intermediate oxidation states. These could escape detection by polymerising, since such forms will be slow to exchange with the carriers. This provides an explanation for the intractable fraction which they

found to exist below the boiling point of iodine.

The exchange mechanism was confirmed by Mahieu et al (102) in a study of $^{51}Cr^{3+}$ doped $(NH_4)_2CrO_4$. The total amount of Cr^{3+} remained constant during thermal treatment, but $^{51}Cr^{3+}$ was transformed into $^{51}CrO_4^{2-}$.

Earlier, Nath et al (103) had proposed that thermally detrapped electrons or holes could electronically excite the recoil species and trigger exchange with a neighbouring molecule. This accounts for the formation of polynuclear species in $^{51}Cr^{3+}$ doped CrO_4^{2-}, and of $^{51}CrO_4^{2-}$ in $^{51}Cr^{3+}$ doped K_2SO_4 and KIO_3. In these systems, the electronically excited recoil atom or dopant can interact with more than one neighbouring molecule, resulting in a transfer of ligands from more than one molecule. Some of the excitation can be converted into vibrational energy, which will enhance ligand transfer.

Several authors have used the concept of electron donors and acceptors to describe isothermal annealing results. This interpretation is verified by observations that electron acceptors such as O_2 and NO retard thermal annealing, while electron donors such as C_2H_5OH and CH_3COCH_3 enhance annealing (76) (104). During annealing, electron acceptors act as donors and will release electrons, and thus reduce the holes available in the solid for oxidation. Costea et al (105) have used these ideas to explain the effects observed in pure lanthanum and phosphate doped K_2CrO_4 crystals. La^{3+} has three possible acceptor levels due to charge compensation and the formation of cation vacancies. These reduce the activation energies of hole production and thus the activation energies of thermal annealing.

$$La^{3+} \longrightarrow La^{3+}_{K+} + 2\,\square_{K^+} \qquad (3.23)$$

$$La^{3+} \longrightarrow La^{2+}_{K^+} + \square_{K^+} + \oplus \qquad (3.24)$$

$$La^{3+} \longrightarrow La^{+}_{K^+} + 2\oplus \qquad (3.25)$$

where $\square_{K^+}$ = cationic vacancy

$La^{3+}_{K^+}$ = substitutional ion on a potassium site

$\oplus$ = free hole

The holes can be trapped by dichromate ions, which can then migrate in the lattice.

$$\oplus + CrO_4^{2-} \longrightarrow [CrO_4]^- \qquad (3.26)$$

$$[CrO_4]^- + CrO_4^{2-} \longrightarrow CrO_4^{2-} + [CrO_4]^- \qquad (3.27)$$

where $[CrO_4]^-$ = trapped hole

Annealing is retarded by phosphate impurities

$$PO_4^{3-} \longrightarrow (PO_4^{3-})_{CrO_4^{2-}} + \tfrac{1}{2}\square_{CrO_4^{2-}} \qquad (3.28)$$

$$PO_4^{3-} \longrightarrow (PO_4^{2-})_{CrO_4^{-}} + \ominus \qquad (3.29)$$

where $\square_{CrO_4^{2-}}$ = anionic vacancy

$(PO_4^{3-})_{CrO_4^{2-}}$ = substitutional ion on a dichromate site

$\ominus$ = free electron

The free electrons can be trapped by the anionic vacancies, which have an effective positive charge.

$$\ominus + \square_{CrO_4^{2-}} \longrightarrow \square^{-}_{CrO_4^{2-}} \qquad (3.30)$$

$$\ominus + \square^{-}_{CrO_4^{2-}} \longrightarrow \square^{2-}_{CrO_4^{2-}} \qquad (3.31)$$

During thermal annealing, the electrons are detrapped from these electron donors and reduce the concentration of free holes. This reduces the concentration of trapped holes (CrO_4^-) and retards thermal annealing. Doping of $La_2(CrO_4)_3$ with Ba^{2+} and K^+ had no effect. This was thought to be, because the concentration of charge carriers was not altered by the doping.

Veljković (28) has shown that the annealing kinetics of recoil atoms in chromates, arsenates and bromates which have undergone (n,γ) reaction can be described by the equation for the diffusion controlled segregation of new phases in solids.

$$1 - X = \exp (- kt^n) \qquad (3.32)$$

where k is the velocity constant

n is $\frac{1}{2}$ or $\frac{2}{3}$, and depends on the elastic interactions in crystals

X is the relative yield of the annealing

X depends on the diffusion coefficient of migrating vacancies, the dislocation density, and the range of mutual interaction between vacancies and dislocations. This implies that the annealing reactions are dominated by dislocations and radiation-induced irregularities. There is limited diffusion of the reacting species in hot zones, whose reactions are most intensive at the border zones of the loops. This explains why first order kinetics does not apply.

The mechanisms reported here have been concerned with the role of electrons and holes in the annealing phenomenon. It is suggested that, since a large amount of radiation damage will be present in the lattice, it might be an oversimplification to consider single accepting and donating

entities. In this case, it might be more appropriate to consider the effect of point defects and their aggregates on the valency state of fission product iodine. See the next section and chapter 5.

3.5. Defects

Many interpretations of valence distributions, found on analysis and from annealing curves, have been based, in a general way, on the interaction of electrons and holes with the recoil atom in the lattice. Such a simple explanation might not be a true representation of the reactions, and such processes might well occur with participation from more complicated centres, which could be composed of lattice atoms associated with vacancies or electrons. Techniques such as absorption, fluorescence, ESR, ENDOR spectroscopy have been very useful in characterising these centres. Also reirradiation in the F band region and monitoring the effect on the optical spectrum can provide additional information.

Anderson and Baptista (89) have made a thorough investigation of the oxygen centres in doped KCl crystals. The reaction

$$Cl^- + O_2 \longrightarrow O_2^- + \tfrac{1}{2}Cl_2 \qquad (3.33)$$

had been proposed, but they found evidence for an O_2^{2-} molecule ion. This would most likely be associated with an anion vacancy, in order to fit into a chloride position. They named this the O(I) centre. An O(II) centre was also identified. From the enhancement of F centre production, it was thought to be an association of an O(I)-interstitial chlorine. The O(I) centres were acting as stabilizers for interstitial halogen atoms, decreasing their rate of recombination with the electrons produced at the same time, and increasing the probability of electron capture by anion vacancies to form F centres. Other centres, O(III) and O(IV) were also found. These seemed to set up an equilibrium with O(II) during irradiation with X rays, but their exact nature was not determined. They were

thermally annealed in the temperature interval 50 °C to 200 °C.

Although these centres were formed in oxygen doped samples, similar entities might exist in multi-crystalline samples irradiated and annealed in air. Cifka and Bračoková (93), however, discounted the possibility that oxidation processes are due to oxygen in the sample because their irradiated crystal, $BaCl_2$, formed negligible BaO on melting. They attributed the comparatively easy oxidation of ^{32}P and ^{35}S recoils in $BaCl_2$, to the enhanced formation of free chlorine in the former crystals as compared to KCl. The percentage of the reduced species was related to the number of anionic vacancies, since values increase with the mole % of alkali metal chloride. This suggested a correlation with F centre concentration, although an immediate correlation has been discounted by Bogdanov et al (52).

Kasrai et al (47), in accounting for the existence of an oxidised sulphur formation in NaCl, have proposed the formation of SCl^- by a sulphur recoil atom at a cationic site. This could trap a hole to form SCl_2^- . A centre, analogous to the V_k centre, and composed of interstitial ^{35}S and SCl_2^- , was proposed. However, it was thought that, like the V_k centre, it could be unstable at room temperature.

Kasrai and Maddock (44) have interpreted their results for ^{35}S recoils in neutron irradiated potassium chloride as indicating the presence of oxidised sulphur precursors such as SCl, SCl_2^- , SCl_2 and similar species, rather than S^+ ions. These centres are analogous to Cl_2^- , Cl_3^- , which are known to be produced in the irradiation of alkali chlorides.

Baptista and Marques (106) have also suggested the existence of PCl_2^- and SCl_2^- centres as precursors to the phosphate and sulphate fraction in pure and OH^- doped reactor irradiated KCl crystals.

Rabe et al (71) have suggested that oxidising point defects, produced in the alkali chloride through irradiation, behave as chlorine atoms, or perhaps Cl_2^- ions, upon solution.

Many types of centres exist at very low temperatures in alkali halide crystals, and have been characterised with ENDOR, ESR techniques and optical spectra. They can be divided into two categories: those that are electron deficient centres,such as V centres,and those that are electron excess centres, such as F centres. Many of these are unstable at room temperature. Electron excess centres which exist at room temperatures are R_1R_2M and N centres (16) and are different combinations of electrons with vacancies. At 100 ^oC the vacancy mobility is greatly increased and a variety of combinations of electrons with groups of vacancies are found, e.g. R_1^-, R_2^-, M^- centres.

Of all the electron deficient centres that have been proposed (16),only four have been identified from optical spectra , viz V_k, H, F^- and V_1 centres, and only four have been identified with ESR techniques viz V_K, H, V_F and V_t centres. These are shown in figure 3.1.

All of these are reported not to be present at room temperature. However, they could be thermally decomposed, and their products could be responsible for the oxidation products observed.

There is a possibility of defect centres arising from the impurity iodine. Schoemaker (107) has discussed the ESR spectra of V_k type I_2^- centres in KI and V_k and V_F

Fig 3.1 MODELS OF THE CENTRES V_K(A), H(B), V_F(C), V_t(D) IN KCl

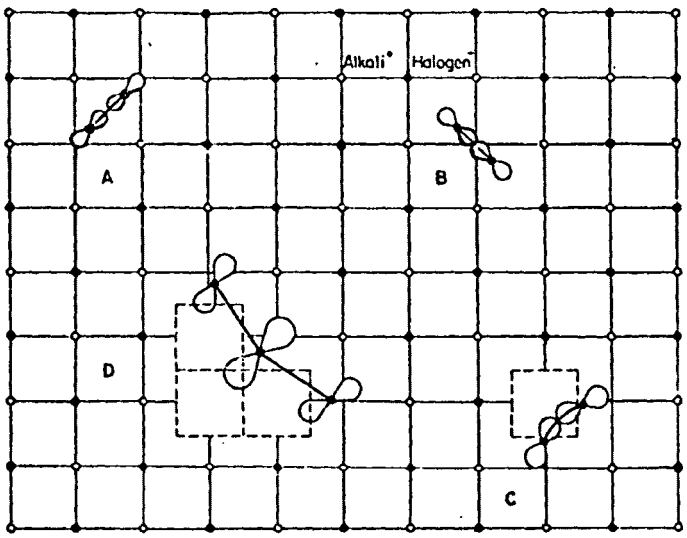
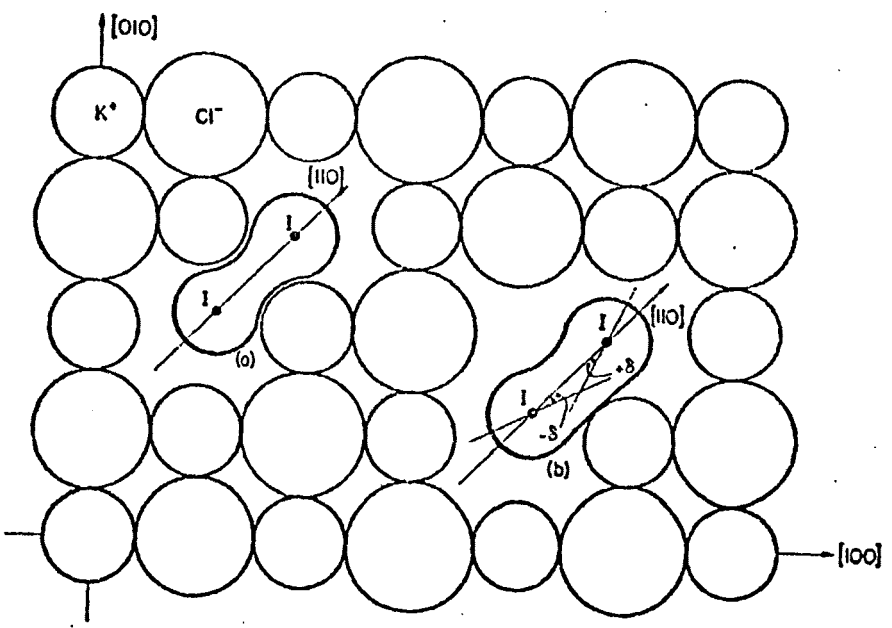


Fig 3.2 MODELS OF A V_K(a) AND V_F(b) TYPE I_2^- CENTRE IN Pb^{++} AND I^- DOPED KCl LATTICE

THE MOLECULE IONS ARE REPRESENTED BY AN APPROXIMATE CONTOUR OF THE TOTAL ELECTRONIC DENSITY



type I_2^- centres in Pb^{++} doped KCl:KI. See figure 3.2. The KCl crystals were strongly doped with I^- ions, and Pb^{++} ions were present as electron traps. Irradiation creates electrons. These are trapped by Pb^{++} and holes, which are self trapped, to form V_k type Cl_2^- centres. Other holes are trapped by I^- ions and form ICl^- centres. Above -100 °C, Cl_2^- centres or holes become thermally unstable and move through the lattice. These holes are trapped and stabilised by I^- ions with enhanced formation of ICl^- and I_2^-. Doping with Pb^{++} has provided positive ion vacancies in the lattice due to charge compensation, and these react with the I_2^- centres to form the V_F type I_2^- centre. This is an I_2^- molecule associated with a positive ion vacancy. In this system, the $I_2^-V_k$ centre was found to be converted to the I_2^- V_F centre between -50 °C and 0 °C. In KCl:KI crystals, doped with NO_2^-, the $I_2^-V_k$ centre decayed at 120 °C, Meistrich and Goldberg (108) have reported that the ICl^-V_k centre decays at 35 °K.

In contrast to this system, the iodine produced from fission will be of a much smaller concentration in the KCl samples used for the experiments reported in Chapter 4, and such defect centres will not be major contributors to the effects observed. However, one can imagine analogous chlorine centres being formed.

The existence of a ClO_2 centre in irradiated $KClO_4$, which is stable up to 150 °C, has been investigated by Byberg et al (109). However, trapped oxygen is not sufficient to account for its formation.

Chapter 4. Experimental.

Contents:

4.1	Introduction	150
4.2	Assembly used for Irradiation	152
4.2.1	Preparation of triuranooxide U_3O_8 film	153
	(a) Alpha-counting	
	(b) Self absorption of α-particles	
	(c) Calculation of uranium oxide weights and errors in values	
4.2.2	Preparation of tablets	169
	(a) Effect of compression	
4.2.3	Description of the London University Reactor	173
	(a) Activity of samples	
	(b) Fission product calculations	
4.3	Experimental Method	178
4.3.1	The carrier solution and exchange reactions	178
4.3.2	Analysis	181
	(a) Method	
4.3.3	Modifications	184
4.3.4	Explanation of calculation	185
	(a) Section A. To find experimental activities from count rates	
	(b) Section B. To find the theoretical activities of isotopes	
	(i) Neutron flux n	
	(ii) Fission rate F	
	(c) Section C. Specific and fractional activities	
	(i) To find the specific activities	
	(ii) To find the fractional activities	
	(iii) Modification	
4.4	Counting Methods	193
4.4.1	Decay schemes for iodine isotopes	193
	(a) Decay chains	
	(b) The isotopes used and their decay schemes	
	(i) Calculation of the primary yield for $^{130}_{53}I$	
	(c) Decay curves	

4.4.2	Counting apparatus	200
	(a) Lithium Drifted Germanium detector	
	(i) Method of fabrication	
	(ii) Analysis of spectrum	
	(iii) Characteristics of a Ge(Li) detector	
	Resolution	
	Efficiency	
	(b) Experimental efficiency determination	
4.5	Other Experiments	212
4.5.1	Moisture experiments	212
4.5.2	The effect of pH	213
	(a) Method	
	(b) Results	
4.5.3	Chlorine experiments	216
	(a) Preparation of sodium hypochlorite solution (NaOCl)	
	(b) Spectrophotometric analysis of samples	
	(c) Sample analysis	

CHAPTER 4

EXPERIMENTAL

4.1. Introduction

Fission product iodine is particularly suited to chemical analysis because of two points:

i) Iodine isotopes are easily identified by their γ-ray spectra, especially ^{131}I which has a relatively long $t_{\frac{1}{2}}$ of 8 days. This is not the case for many other fission products.

ii) A characteristic of the halogen family is that its members form a complex with CCl_4. The chlorine isotopes are short lived. The only bromine isotope present with a half life of sufficient length to be detected is ^{82}Br ($t_{\frac{1}{2}}$ = 35.87 h). However, this isotope has a very small independent fission yield of 3.8×10^{-5} and occurs as a shielded nucleus. In the presence of fission product iodine, its concentration is negligible. Therefore, the use of a CCl_4 extraction method allows a fairly clean separation of iodine from other fission products.

The oxidation state of fission product iodine in KCl was analysed by dissolving a tablet of KCl powder containing the fission products in an aqueous carrier solution containing inactive iodine in oxidised and reduced forms. By this means, the iodine was trapped, at the instant of dissolution, in the oxidation states of the carriers. It was shown that all the iodine present adopted either one of two forms. None of the iodine was present in a form that did not exchange, such as an organic iodo compound (35, 36, 117).

The following experimental section covers the majority of the work, which is an investigation of the

annealing effect on the valency states of fission product iodine in a polycrystalline KCl medium. Experiments were also performed on the effect of moisture, pH of the medium, the compressible load on the powder, and the existence of free chlorine. As discussed in section 4.4.1, the different isotopes of iodine arise from fission in different ways. Experiments were carried out to discover if these different modes of origin had any influence on the proportions entering the reduced and oxidised forms.

4.2. Assembly used for irradiation

The source of fission fragments was a uranium film of enriched U_3O_8. The film was required to be uniform and of such thickness that the self absorption of the fission product iodine became insignificant; that is, much less than 10 mg/cm^2, the maximum range of fission products in U_3O_8(6). However, there needed to be sufficient uranium to produce a measurable amount of fission product iodine in the sample at the end of irradiation (about 10^{12} atoms for ^{131}I). Too much could interfere with the reactor operation or present a post irradiation handling problem (section 4.2.3). In view of the last two requirements, a suitable weight of uranium oxide was calculated. Then the film thickness was determined by the surface area of the backing platinum discs, of diameter 12.72 $\pm$ 0.01 mm and thickness 0.113 $\pm$ 0.001 mm.

A backing disc was required since the uranium film was very thin. Platinum was chosen because it does not corrode in the acid used to mount the film. It has a melting point of 1769 ^{o}C(see section 4.2.1), will not oxidise at this temperature, and any activation products are short lived.

A tablet of compressed KCl crystals, with the same diameter as the Pt disc and 1-2 mm thick, was placed on top of the uranium film. During the fission process, material tends to be spluttered or ejected from the surface of the material in which it occurs (110). The object of this investigation was to study the form of iodine arising as a fission fragment in the potassium chloride, and not the forms that may arise in the uranium oxide itself. Accordingly, a thin layer of aluminium was placed across

the top of the uranium film to prevent spluttered material being transferred from the oxide surface to the potassium chloride. The fission fragments would be expected to penetrate the aluminium with miniuum interference from other induced activity. The foil thickness had to be smaller than the maximum range of the fis sion particles in Al, 3.7 mg/cm^2 (6), so that an insignificant number were absorbed before they reached the target. See section 1.2.3 for typical range calculations. A fine Al foil disc 0.0076 mm thick was used. The assemblage was kept together by an aluminium clip of thickness 0.1499 $\pm$ 0.0025 mm which was shaped like a cross and wrapped around the tablet and disc. The samples were irradiated in sealed standard polythene capsules in the ICIS position of the University of London Experimental Nuclear Reactor (section 4.2.3). There were two samples to each capsule and these were separated by a flux monitor of cobaltous chloride, $CoCl_2.6H_2O$. This was contained as a powder in a smaller capsule. "Blackness" calculations were made to ensure that the assembly was not shielding the uranium film from the reactor flux.

The Al foil was a special beating of standard thickness supplied by G.M. Whiley Ltd., Ruislip, Middlesex. The dimensions of the tablet and platinum disc were measured with a micrometer screw gauge. The film thickness of U_3O_8 is discussed in the next section.

4.2.1. Preparation of triuranooctoxide film (U_3O_8)

Initial experiments to find a method of coating the surface of a platinum disc with a uniform layer of U_3O_8 were based on references (111) and (112).

The best films were obtained by first etching the Pt disc in aqua regia, with heat, until the polished surface had disappeared and the grain boundaries could be seen. These probably provided an anchorage for the first layers of atoms. The disc was rinsed with distilled water, degreased with CCl_4, and dried. It was then heated in a furnace at $\sim$ 800 °C for five minutes, in order to expel any impurities on the surface, and allowed to cool.

The source of U_3O_8 was a uranyl sulphate solution, 80% enriched and of strength 3.7 mg/ml in 0.2 M H_2SO_4. This solution had been prepared in the laboratory from a mixture of uranium dioxide and trioxide, of enrichment 80%, which was supplied by The Atomic Energy Authority at Dounray, Scotland.

The uranyl sulphate solution (10 λ) was pipetted onto the surface of the disc. The micropipette was washed out with distilled water and the washings were added ($\sim$10 λ). A solution of polyvinyl acetate in acetone, 0.005 g/ml, was added (10 λ) and this acted as a spreading and adhesive agent. The disc was dried under a heat lamp for 10 minutes, and then transferred to a furnace at $\sim$ 800°C for 5 minutes. The P.V.A. was expected to volatilise at such a high temperature. No direct reference could be found for the action of heat on uranyl sulphate solution. However, uranyl salts of volatile or unstable acids can be converted directly to U_3O_8 by heating (113). Oxides of uranium result from ignition of any uranium oxide and almost all uranium compounds in air. The colour of U_3O_8 ranges from olive-green to black-green. U_3O_8 is thermally stable in the temperature range 650 - 900 °C, and complete conversion to uranium dioxide (UO_2) does not occur below 2000 °C (114).

The disc was cooled and rubbed lightly with a tissue. The amount of U_3O_8 firmly deposited was counted with an alpha counter. More solution was deposited onto the disc, and the procedure was repeated, until a suitable amount of U_3O_8 was recorded.

(a) Alpha-counting

The α-counting apparatus consisted of a Twentieth Century, partially depleted, silicon surface barrier, radiation detector. The pulses were analysed with a multi-channel pulse height analyser. This had been calibrated with an americium source containing α-energies in the region of interest. Figure 4.1 is a typical α-spectrum obtained with the apparatus. Figure 4.2 is the calibration curve, plotted from the data in table 4.1. Increased resolution was achieved by counting at pressures of the order of 0.01 mm Hg and below. At such pressures the mean free path of the α-particle is not reduced significantly by the air particles in the counting chamber.

Table 4.1

Data for standard Americium source

Isotope	$t_{\frac{1}{2}}$ (y)	Principal α Energy (MeV)	Intensity %	Channel Number
^{239}Pu	2.44×10^4	5.107	11.5	947
		5.145	15.1	986
		5.157	73.3	
^{241}Am	458	5.389	1.3	1166
		5.443	12.7	1204
		5.486	86.0	1236
^{244}Cm	17.6	5.766	23.3	1449
		5.808	76.7	1481

Fig 4.1 ALPHA SPECTRUM

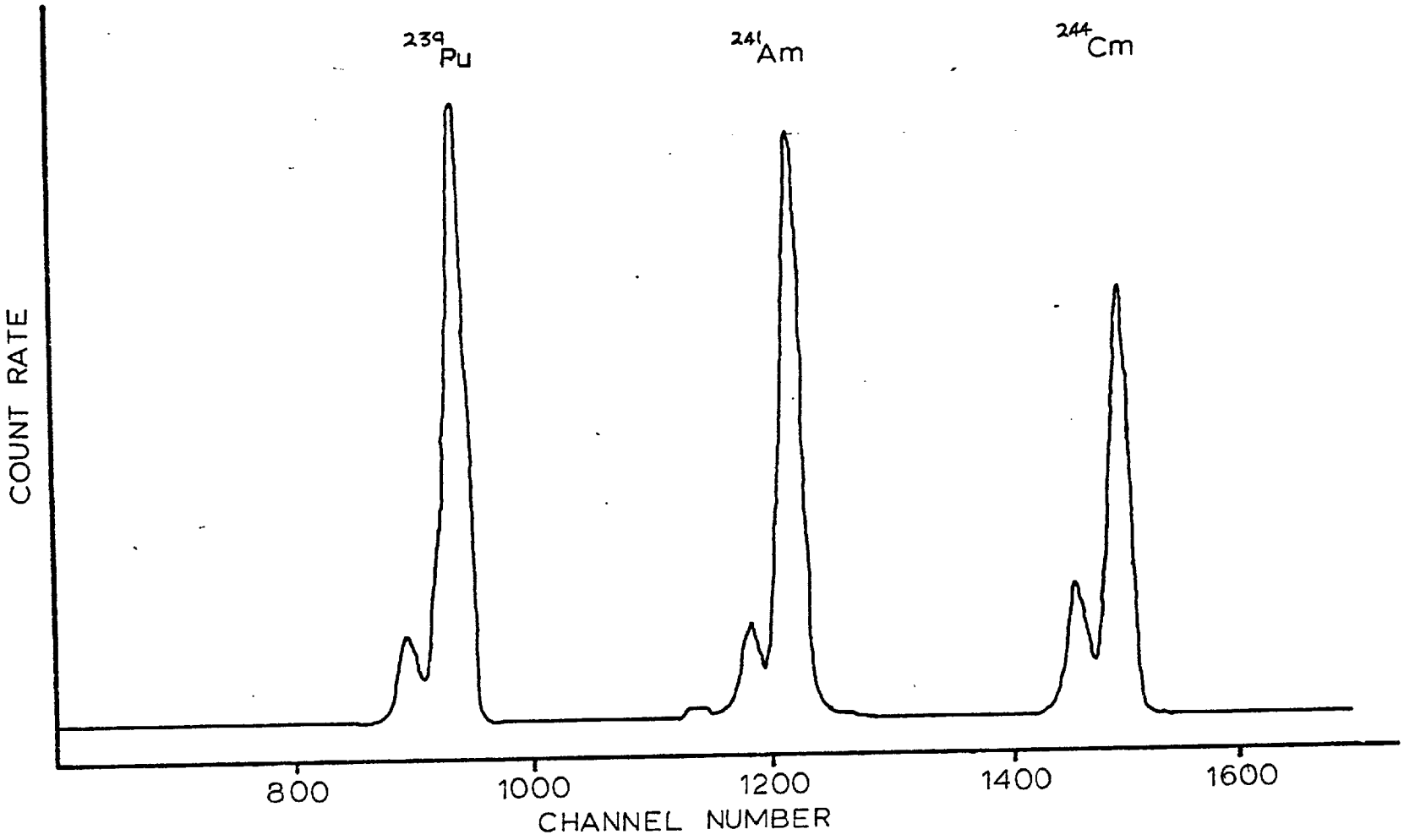
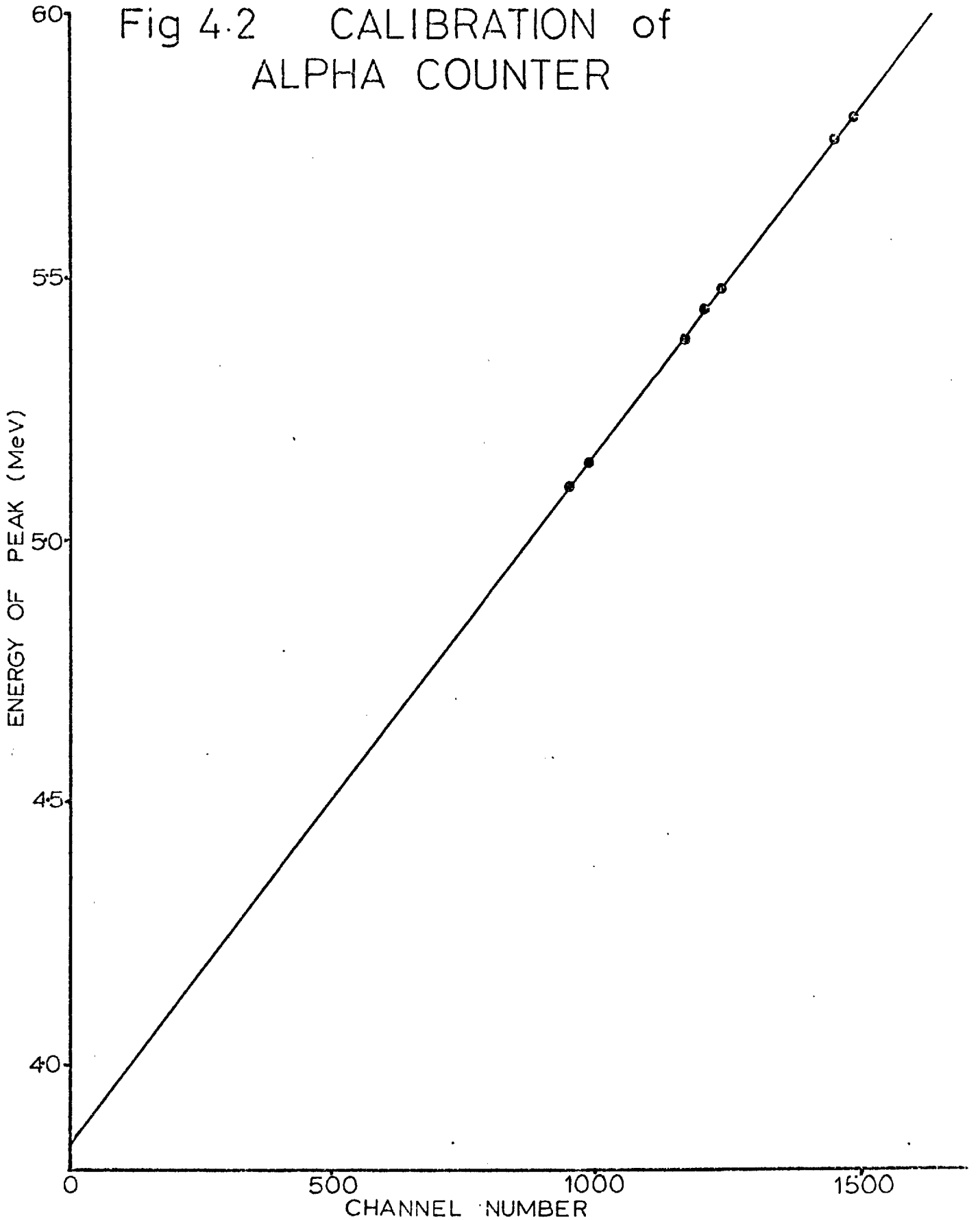


Fig 4·2 CALIBRATION of ALPHA COUNTER



However, the α-spectrum for U_3O_8 did not resolve sufficiently well for identification of ^{235}U, and so the number of fissile nuclei present could not be obtained directly from the spectrum. The prominent peaks in the spectrum are due mainly to ^{234}U, but the amounts of the other isotopes cannot be found from these peaks, because enrichment with ^{235}U includes the addition of an unknown amount of ^{234}U, and this amount depends on the isotopic separation process used to obtain ^{235}U. Thus, ^{234}U is no longer present in its natural abundance.

The amount of U_3O_8 present in each sample was found by a comparison of areas under the curve with the spectrum obtained from a known amount of U_3O_8. The peaks for successive spectra occurred at the same channel numbers and so the total areas under the curves were compared. The enrichment is known to be 80%, and so the number of ^{235}U atoms which undergo fission can be found indirectly. Although a more rigorous analysis of the spectrum can be achieved with spectrum stripping, this method was considered to be of sufficient accuracy for the experimental work, since the weights of uranium are not concerned directly with the final results, as discussed in section 5.1.2. For convenience in identifying the peaks in the spectrum, a relative intensity value of 100 was assigned to the intensity of the 4.773 MeV peak of ^{234}U and the intensities of the other peaks were adjusted accordingly, as in table 4.2.

Table 4.2

Data for α spectrum observed in uranium sample

Isotope	$t_{\frac{1}{2}}$(y)	Energy (MeV)	Relative intensities for each isotope %	Relative intensities for all isotopes %
^{234}U	2.47×10^{5}	4.773	72	100
		4.722	28	38.90
		4.590	0.35	4.86×10^{-1}
		4.265	4.5×10^{-5}	6.25×10^{-5}
		4.130	3.0×10^{-5}	4.17×10^{-5}
^{238}U	4.51×10^{9}	4.198	77	7.28
		4.150	23	2.17
		4.038	0.23	2.17×10^{-3}
^{235}U	7.1×10^{8}	4.597	4.6	6.88×10^{-1}
		4.556	3.7	5.53×10^{-1}
		4.502	1.2	1.79×10^{-1}
		4.445	0.6	8.97×10^{-2}
		4.415	4.0	5.98×10^{-1}
		4.396	57.0	8.53
		4.366	18.0	2.69
		4.344	1.5	2.24×10^{-1}
		4.323	3.4	5.09×10^{-1}
		4.266	0.6	8.97×10^{-2}
		4.216	5.7	8.52×10^{-1}
		4.157	0.5	7.48×10^{-1}

(b) Self absorption of α-particles

The self absorption of α -particles is illustrated by figures 4.3 and 4.4, which show the deterioration in resolution as the film thickness is increased. Figure 4.3 corresponds to a film of weight 24.13 μg U_3O_8 and figure 4.4 corresponds to one of weight 160.8 μg. The latter sample is nearer the weight of the samples used in the experiments.

The self absorption was investigated to find the degree of significance of this type of error in estimating the weights of the heavier samples. It should be noted that the films obtained were not very uniform and, although the overall areas covered by U_3O_8 on the discs were similar, the degree of self absorption for each disc could vary by more than the experimental value of self absorption for that weight of material.

Since such an investigation into absorption relies on accurate pipetting techniques, 10λ portions of a ^{60}Co solution were pipetted onto aluminium (Al) discs in groups of six, and counted until the results for a group did not display any marked deviation from a Poissson distribution of the counts. Table 4.3 gives the results for six equal volumes of ^{60}Co solution. The counts were corrected for dead time, taken as 1.25×10^{-8} s^{-1}. The third column gives the variation of each corrected count (m_i) from the mean count ($\bar{m}$) for the six samples (n = 6) where $\bar{m} = \frac{\Sigma m_i}{n}$. The fourth column gives the square of each difference in the third column.

Fig 4.3 ALPHA SPECTRUM

U_3O_8 ENRICHED 80 %(1x10λ addn. of soltn.)

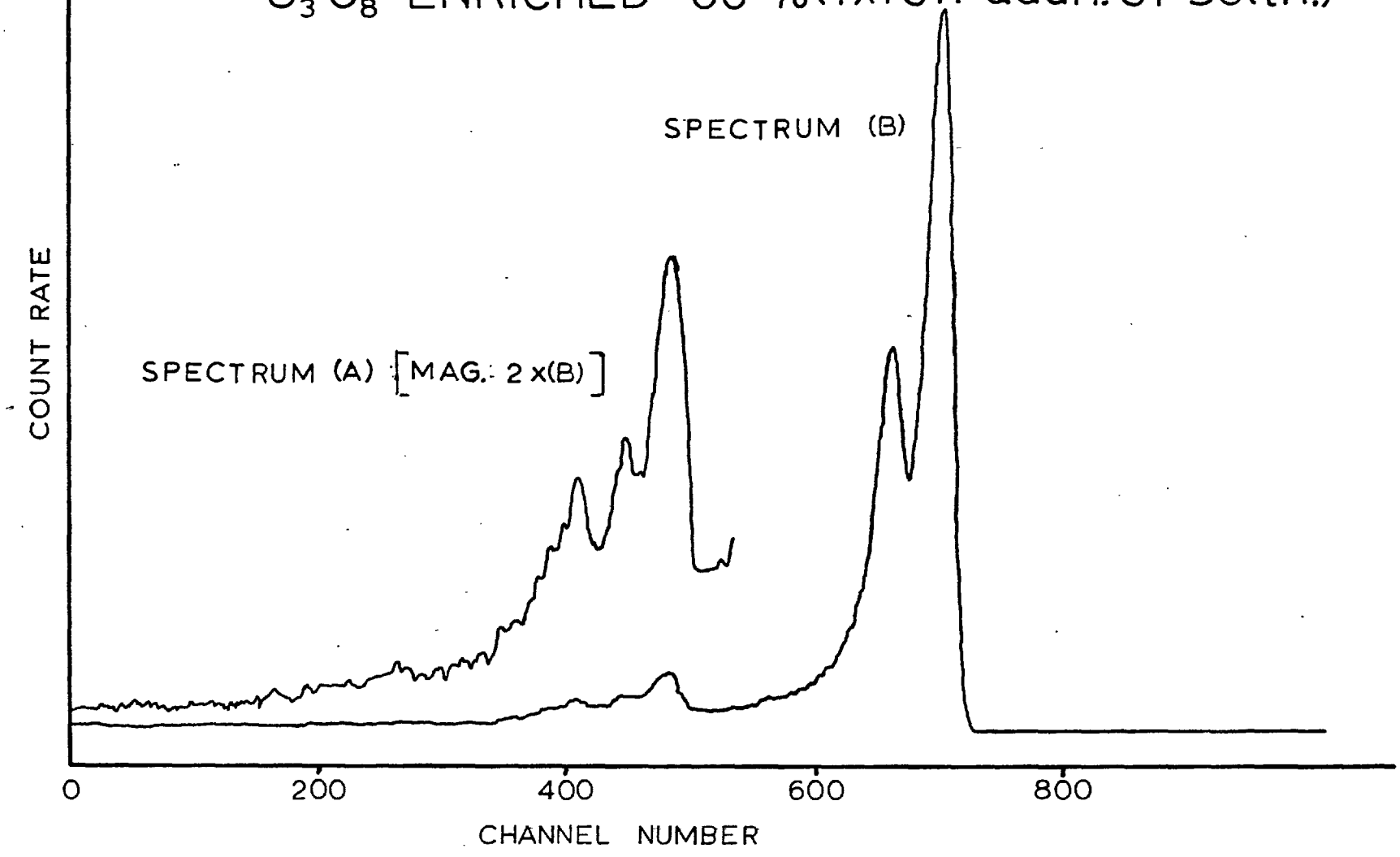


Fig 4.4 ALPHA SPECTRUM

U_3O_8 ENRICHED 80% (6x10λ addn. of soltn)

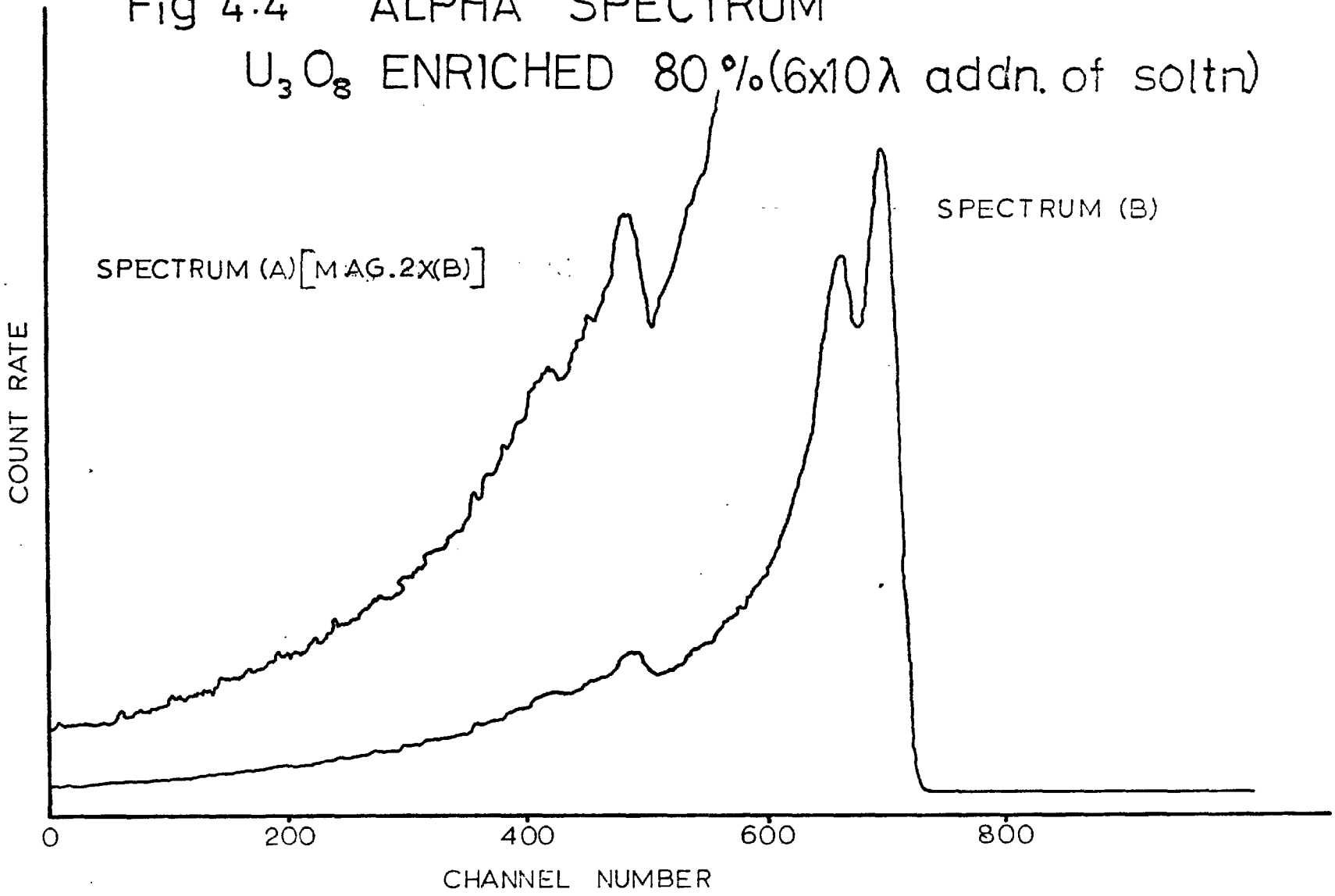


Table 4.3

Pipetting results for equal portions of ^{60}Co solution

	Counts (50 s)	Counts corrected for dead time m_i	$\lvert m_i - \bar{m} \rvert$	$(m_i - \bar{m})^2$
1	58,244	68,170	555.67	308,769
2	57,957	67,778	947.67	898,078
3	59,584	70,014	1,288.33	1,659,794
4	58,887	69,053	327.33	107,145
5	59,219	69,509	783.33	613,606
6	57,996	67,830	895.67	802,225

The standard deviation $$\sigma = \left[\sum_n \frac{(m_i - \bar{m})^2}{(n-1)} \right]^{\frac{1}{2}}$$

$$= \pm 937$$

The deviation of the mean $$\bar{\sigma} = \frac{\sigma}{n^{\frac{1}{2}}}$$

$$= 383$$

For the Poisson distribution to be a true representation of the counts,

$$\sigma = \bar{m}^{\frac{1}{2}}$$

$$= 262$$

$$\bar{\sigma} = \left[\sum_n \frac{m_i}{n} \right]^{\frac{1}{2}}$$

$$= 107$$

Since no immediate correlation could be established with these figures, Pearson's Chi-squared test was applied to the results. This determines the probability that a repetition of the observations will show greater deviation from the frequency distribution which is assumed for the data.

$$\chi^2 = n \sum_n \left(\frac{(m_i - \bar{m})^2}{\sum m_i} \right)$$

$$= 63$$

From special tables (115) a figure of 63 for 5 degrees of freedom gives a probability of deviation from a Poisson distribution $<<$ 1%.

Three standard samples were made up which had 10 λ of the sulphate solution deposited onto each Pt surface. The procedure described for making up samples of U_3O_8 was followed, but the samples were not rubbed down after heating. They were each counted in the α-counter and an average value for the count rate produced by 10 λ sulphate solution (37 μ g) was obtained. This was taken to be the count rate with no absorption. The average count rate was 2.617 counts s^{-1} (σ = 0.021 counts s^{-1}).

One Pt disc had increasing amounts of U_3O_8 deposited onto it in 10λ portions of solution. Again, the disc was not rubbed down between additions. Figure 4.5 is a graph of the self absorption of α-particles in the uranium oxide. The values used to plot this are given in table 4.4.

Comparison of the first three results for U_3O_8, before absorption becomes evident, shows that the true error in values, as revealed by the discrepancy between the two methods of working out the amount of U_3O_8 present, is much bigger than the calculated error associated with each method. This could be due to the surface area covered, which varies with each sample, and to the non-uniformity of the layers of U_3O_8. The discs used in the reactor experiments were rubbed down before each

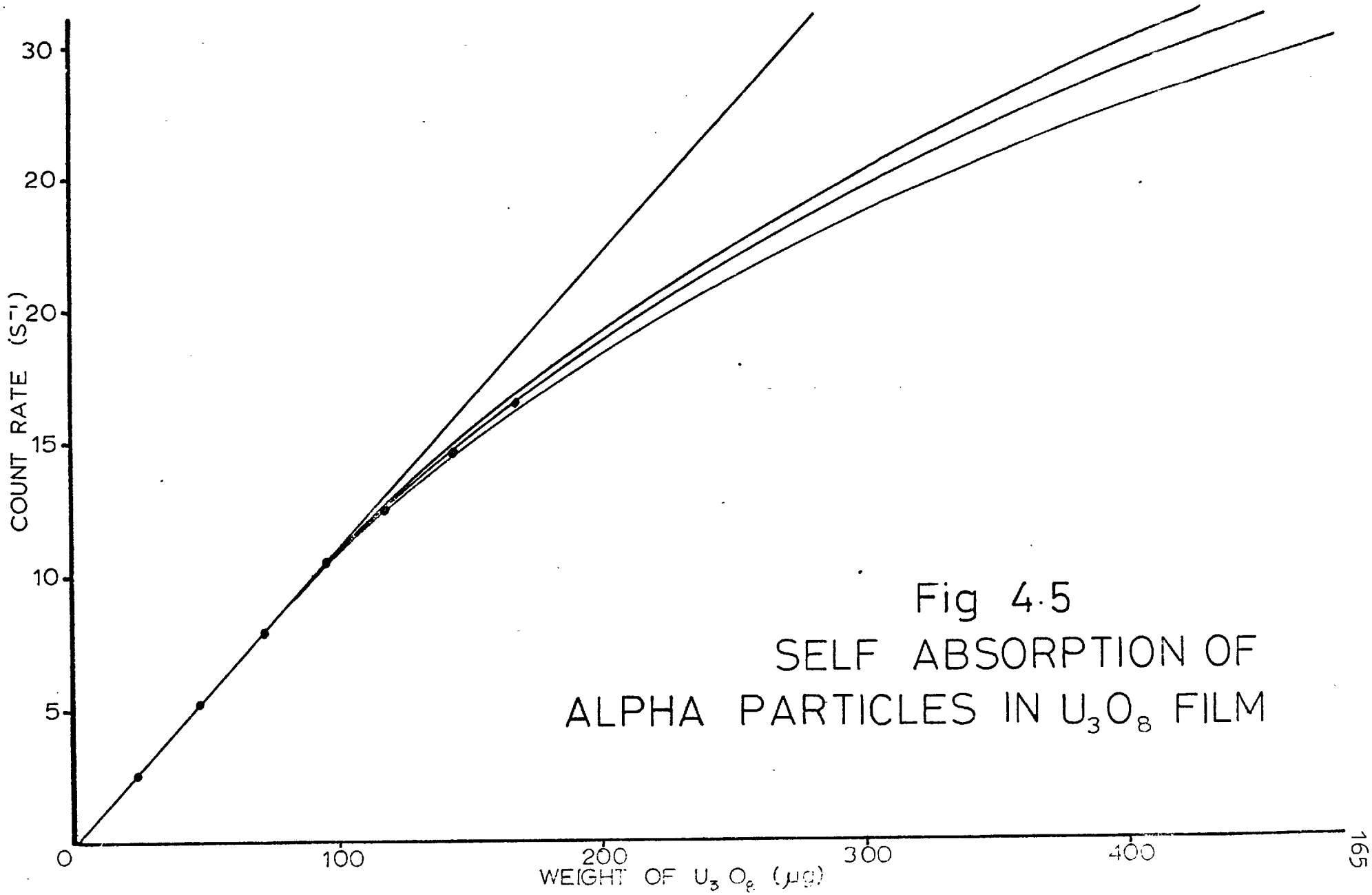


Fig 4.5
SELF ABSORPTION OF
ALPHA PARTICLES IN U_3O_8 FILM

Table 4.4

Self absorption of α-particles in U_3O_8 film

Uranyl sulphate (μg)	U_3O_8 from sulphate conversion (μg)	Count rate s^{-1}	U_3O_8 from count rate conversion (μg)
37	24.1 ± 0.2	2.606 ± 0.005	24.0 ± 0.008
74	48.3 ± 0.3	5.375 ± 0.009	49.6 ± 0.008
111	72.4 ± 0.35	8.042 ± 0.01	74.2 ± 0.008
148	96.5 ± 0.4	10.65 ± 0.01	98.2 ± 0.008
185	120.6 ± 0.45	12.49 ± 0.02	115.2 ± 0.008
222	144.8 ± 0.5	14.61 ± 0.03	134.8 ± 0.008
259	168.9 ± 0.55	16.55 ± 0.03	152.7 ± 0.008

successive addition of solution, in an effort to provide a uniform surface.

The divergence from linearity, observed in figure 4.5, can be explained by a simple consideration of the isotropic emisssion of α-particles with range R_o from a plane source of thickness S and area A (22). This is discussed in section 1.2.4. d, in this case, is the distance in a low vacuum between the foil and the detector.

(c) Calculation of uranium oxide weights and errors in values

The amount of U_3O_8 formed from the uranyl sulphate solution was found as is shown below, and the values obtained for each sample were recorded in tables 4.4, 4.6.

From table 4.5,the average atomic weights for three enrichments have been calculated.

Table 4.5

Natural and enriched abundances of uranium isotopes

Isotope	Weight	% natural abundance	% enriched abundance I	% enriched abundance II
235	235.0439	0.7196	80.0	80.0
238	238.0509	99.276	19.9989	19.8723
234	234.0409	0.0057	0.0012	0.1277

Uranium,natural enrichment = 238.029 a.m.u.

Uranium, enrichment I = 235.6453 a.m.u.

Uranium, enrichment II = 235.6402 a.m.u.

Average I and II = 235.6428 $\pm$ 0.0026 a.m.u.

Enrichment I is for ^{235}U 80% enriched and with ^{234}U present in its natural abundance ratio with ^{238}U.

Enrichment II is for ^{235}U 80% enriched and with ^{234}U present, increased by the same fraction as ^{235}U over its natural abundance ratio.

The ^{234}U enrichment in the uranyl sulphate solution is not known but, most probably, is somewhere between its natural enrichment ratio with ^{238}U (enrichment I) and its value after having been enriched by the same amount as ^{235}U (enrichment II). This gives enrichments of 0.00115% and 0.1277% respectively. Either enrichment value has little effect on the average atomic weight for uranium. However, other atomic weights used in the following calculation are given accurately (116) to four decimal places and so an average of 235.6428 was employed

for uranium.

In equation 4.1, which represents the effect of stoving on uranyl sulphate, 37μg uranyl sulphate were found to be equivalent to 24.1294 ± 0.0001μg U_3O_8.

$$3(UO\,SO_4.3\tfrac{1}{2}H_2O) \xrightarrow{650.\ ^{o}C - 900^{o}C} U_3O_8 \qquad (4.1)$$

Three separate results for pipetting and counting 37μg of sulphate solution gave a standard deviation in the count rate of 0.8%. Columns 2 and 4, in table 4.4, show values for U_3O_8 which have been found by different methods. Column 2 gives values derived from the weight of sulphate solution, and the values in column 4 were found from the count rate of the sample (see previous text). The onset of absorption, which occurs in sample 5, is apparent by a reduction in the weight recorded in column 4 when compared with column 2. Samples 1-4 (no absorption) show a slight variation from the values in column 2. This was taken to be a meaningful indication of the errors in the method. The errors are only slightly less variable than a Poisson distribution, thus indicating that the errors are random. The average deviation in results was 1.16μg with σ = 0.86. A maximum error of ± 3μg was assigned to each value in column 4.

Table 4.6 is a record of the samples used for the experiments. The standard error in the count rate was taken as the square root of the total count. The errors in the values taken for the absorption curve were estimated from the graph. There is a bigger error associated with the weight of sample 8,since the absorption curve (figure 4.5) had to be extrapolated for this reading.

Table 4.6

Record of samples used in experiments

Sample Number	Count rate s^{-}	U_3O_8 /µg (from count rate)	U_3O_8 /µg (from absorption curve)
1	18.132 ± 0.067	167.2072 ± 0.0088	188.5 ± 8
2	18.959 ± 0.067	174.8335 ± 0.0088	200 ± 12
3	18.981 ± 0.069	175.0364 ± 0.0088	200 ± 12
4	11.601 ± 0.054	106.9805 ± 0.0093	109 ± 1
5	15.474 ± 0.062	142.6960 ± 0.0091	154 ± 5
6	14.041 ± 0.059	129.4814 ± 0.0091	137 ± 3
7	16.240 ± 0.064	149.7598 ± 0.0089	164 ± 6
8	31.337 ± 0.0089	288.9792 ± 0.0085	428 ± 80

4.2.2. Preparation of tablets

The KCl crystals were pressed in a mould using an "Instron" machine. This is normally used as a tensile testing machine but was adapted for use as an electrically operated press. Employing a cross head speed of 0.1 cm min^{-1}, the samples were compressed to 450 kg with the machine on cycle, so that the time spent under maximum compression was the same for all samples.

The diameter of the mould was slightly greater than that of the Pt discs. This meant that the area of the tablets would be greater than the area of uranium oxide film. This helped to minimise edge effects. If the tablets had been smaller, less efficient use would have been made of the U_3O_8 film, because not all the fission iodine emitted would have been trapped in the tablet and the edge effect would have been enhanced. The thickness of the tablets was limited by the Reactor safety rules

(see section 4.2.3), especially with regard to the amount of chlorine which produces a high energy γ-radiation of 2.147 MeV (this is 47% of the γ-disintegrations for ^{38}Cl) with a half life of 37.3 min. Thus, the total activity produced by ^{38}Cl is rather high at the end of a 2 hr. irradiation. However, the thickness had to be greater than the range of fission product iodine entering the tablet. See section 1.2.3. A thickness of 1-2 mm was employed.

The crystals were of analar grade A. Except as discussed below for experiments in the effect of pH and hydrolytic conditions, one batch of KCl was used throughout to eliminate variations that might occur in the impurity content of different batches. The crystals were ground lightly with a glass pestle in a mortar and kept in a silica-gel dessicator prior to use. It has been suggested that organic compounds such as methyl iodide will be formed when radio-iodine is released in the presence of traces of organic matter (117). In order to ensure that a fraction of fission product iodine will not be lost in this way, the mould and platform were rinsed in CCl_4 before use and the tablets were handled with tweezers in order to keep them grease-free. Similar amounts of KCl were inserted into the mould and the tablets were pressed in air, one at a time. They were put into a dessicator and stored until required for making up samples to be irradiated. The tablets were weighed before use, but this gave only a rough guide to similarity since the tablets often crumbled around the edges, an effect more common in the lighter samples. This was thought to be due to traces of powder from the previous pressings remaining on the inside of the mould, and to corrosion and deformation of the mould, which was

made of mild steel.

(a) Effect of compression

Although the tablets were pressed to the same load, it might have been possible to have had unequal loads within the tablet, resulting from an uneven level of powder before pressing. This could have led to non-reproducibility of results. With this in mind, experiments were carried out to find how a variation in the applied load would affect the valency states of the fission product iodine.

Tablets were pressed at different loads ranging from 200 kg force to 3000 kg force. Tablets could not be pressed below 200 kg force, and 3000 kg force was well in excess of the working load of 450 kg force. Attempts were made to ensure that the powder was level in the mould before pressing.

It was observed that heavily pressed pellets at 3000 kg force load exhibited glassy patches which indicated a certain amount of crystal fusion. After irradiation, the F centre colouring of the tablets increased with the load applied, and the heavily pressed tablets appeared dark purple. This, too, implied an increasing amount of crystal damage with load.

In spite of these visible signs, no correlation could be made between the load applied in pressing and the iodine valency states adopted in the tablet. See table 4.7. Several tablets pressed at lighter loads were more brittle than those pressed at heavier loads. After irradiation, these tablets were found to be in pieces in the containers. In these cases only portions of tablets which had kept their original geometry with respect to the uranium film during irradiation were used in the analysis. These

were broken into two approximately equal pieces. One was kept at room temperature and the other was isothermally annealed at 150 °C. They were analysed consecutively, usually within 40 min. An increasing amount of damage, producing F centres, might favour the reduced state but there was no difference from the ratios found for samples pressed under normal conditions, when room temperature results were compared. The annealing results also appeared to be scattered and no definite trend was observed. Bogdanov and Olevskii (95) reported similar results when they observed the distribution of phosphorus recoils in single crystals of KCl, which had undergone deformation by uniaxial compression.

Table 4.7

Variation of iodate fraction with tablet pressing load

Load kg force	Weight of tablet before irradiation (g)	Room temperature sample Fractional iodate value
200	0.3181	0.179
225	0.3387	0.161
450	0.3427	0.117
625	0.3630	0.137
1,000	0.2717	0.160
3,500	0.3427	0.144

4.2.3. Description of the London University Reactor

The London University Reactor, sited at Ascot, is a light water experimental reactor of 100 kW (thermal) maximum power. It has several tubes at different locations - these pass down into the core and allow samples to be irradiated under different conditions, since the radiation profiles vary at different points inside the core. The ICIS (In Core Irradiation System) tube facility was used to provide maximum flux irradiations for two hour periods. In the experiments reported, irradiation conditions were reproduced at closely as possible.

The samples had irradiation levels of above 1R/h. immediately after irradiation and were too hot to handle. They were allowed to cool to a more acceptable level and transported to Imperial College. The time interval between irradiation and use was approximately one to two days and longer in some cases.

A flux monitor of cobaltous chloride powder was included with every irradiated capsule because the flux could vary according to the operating conditions and nature of other samples being irradiated at the same time. The thermal neutron flux in the ICIS position was found to be of the order of 2×10^{12} neutron/cm^2 s. The following additional information was supplied by the Reactor Manager:

background γ- radiation	$\simeq$	10-20 MR/h
fast neutron flux	=	1×10^{12} neutrons/cm^{2}s
temperature in ICIS	=	46 - 49 ^{o}C

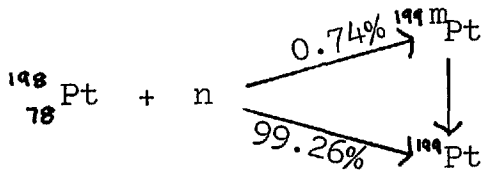
The fast neutron flux calculation assumed that the fast neutron spectrum corresponded to the fission spectrum. The figure supplied for background γ- radiation resulted

from experiments with dyed perspex. The perspex was coloured with an orange dye, and the changes in the absorption bands, due to the γ-irradiation, were measured. A 'Thermindex' indicator strip provided the temperature measurement. Its operation depended on a colour change of dots along the strip. The temperature measurement was made 4 h. 34 m. after start-up, the indicator having been left in ICIS for 1 h. of full power operation. The temperature in ICIS will vary with the ambient temperature of water in the tank which varies with the time of year since, in order to maintain steady temperature, the bulk water is circulated through an external air-cooled radiator.

(a) Activity of samples

The amounts of materials irradiated at any one time were restricted by an operating condition: the total activity after irradiation was not to exceed 100 MeV x mCi. Consequently, the size of KCl tablets irradiated in the reactor at any one time was limited.

The principal radioactive isotopes for each element in the sample irradiation capsule were found to be ^{42}K, ^{38}Cl, ^{199}Pt, ^{28}Al and fission products. A typical calculation for activity immediately after irradiation follows. Consider the thermal neutron capture by ^{198}Pt to form ^{199}Pt.



$t_{\frac{1}{2}}$ = 14.1s

$t_{\frac{1}{2}}$ = 30 m

The thermal neutron cross-section capture for Pt^{198}, σ_c $= 4.03 \times 10^{-24} cm^2$

Neutron flux, n $= 2 \times 10^{12}$ neutrons/cm^2s

Time of irradiation, t $= 2$ h

Weight of Pt $= 0.7$ g

Abundance of ^{198}Pt $= 7.21$ %

Avogadro's Number $= 6.023 \times 10^{23}$ atoms/g-atom

Atomic weight of Pt $= 195.09$ g/g-atom

$\therefore$ number of atoms of ^{198}Pt, x $= \frac{7.21}{100} \times \frac{0.7}{195.09} \times 6.023 \times 10^{23}$

$= 1.558 \times 10^{20}$

Atoms ^{199}Pt formed per sec, R, is given by

$$x n \sigma_c = 1.256 \times 10^9$$

Rate of formation of the atoms during irradiation is given by

$$\frac{dN}{dt} = R - \lambda N \qquad (4.2)$$

$$\lambda N = R(1 - e^{-\lambda t}) \qquad (4.3)$$

λ is the decay constant, and if the half life ($t_{\frac{1}{2}}$) is 30 m.

$$\lambda = \frac{\ln 2}{30} \times 60 \; n^{-1} \text{ by definition}$$

$\therefore \lambda N = 1.177 \times 10^9$ atoms/sec at the end of a 2h irradiation

By definition, 3.7×10^7 disintegrations = 1 mCi of activity

$\therefore \lambda N = 31.82$ mCi

The activity after irradiation at time t can be found by applying the well known decay law for activity

$$\therefore \lambda N_t = \lambda N_o e^{-\lambda t} \qquad (4.4)$$

when t = 0.25 h

$\therefore \lambda N = 22.46$ mCi

Calculations for the other isotopes were similar.

(b) Fission product calculations

Fission product activities are due to a range of fission

products, each with a small probability of occurrence in the fission process. They have a variety of half lives and γ-radiation energies, and so it is more convenient to use experimental graphs from the literature to predict their total activity immediately after irradiation and 15 minutes later (as required for the London University Reactor Centre sample irradiation proposal form).

Weight of uranium as U_3O_8 = 0.4 mg

^{235}U enrichment = 80%

Time of irradiation = 2 h

Flux = 2×10^{12} neutrons/cm^2 s

Capture cross-section for ^{235}U = 580×10^{-24} cm^{-2}

Atoms of ^{235}U = $\frac{0.4}{100} \times \frac{80}{100} \times 6.023 \times 10^{23} \times 3/842.09$

= 6.866×10^{17}

Fissions per second = 7.9650×10^{8}

The energy produced by one fission is $\sim$ 200 MeV

1 eV = 1.602×10^{-19} joules

$\therefore$ the energy produced by 7.97×10^{8} fissions s^{-1}

= $7.97 \times 10^{8} \times 200 \times 10^{6} \times 1.602 \times 10^{-19}$ watts

= 2.55×10^{-2} watts

A graph of γ-power for fission products of 1 g uranium irradiated at 1 MW/T for I seconds is given in ref. 14.

Since 1 tonne = 10^6 g

the fission energy = $\frac{2.55}{0.4} \times 10^{-2} \times 10^{-6} \times 10^{9}$

= 63.75 MW/T

Using the graph, a value was interpolated for the γ-power

from 1 g of uranium irradiated at 1 MW/T for 2 h. This was 8.5×10^{10} MeV s^{-1}. The γ-power from 0.4 mg U_3O_8 produced immediately after irradiation for 2 h

$$= 63.75 \times 8.5 \times 10^{10} \times \frac{0.4}{1000} \text{ MeV s}^{-1}$$

$$= 2.1675 \times 10^{9}$$

The energies for seven principal groups of γ-rays between 0.1 and 2.9 MeV immediately after irradiation were given in ref. 26. An average γ-ray energy was found by a weighted average to be 0.7155 MeV.

The power radiated from C curies emitting E MeV/disintegration $= 5.94 \times 10^{-3}$ E C watts (26). The γ-power produced from 0.4 mg U_3O_8 after a 2 h irradiation

$$= \frac{2.168 \times 10^{9} \times 1.602 \times 10^{-19} \times 10^{6} \times 0.7155}{5.94 \times 10^{-3}} \text{ Ci}$$

$$= 4.184 \times 10^{-2} \text{ Ci}$$

$$= 41.84 \text{ mCi}$$

Fifteen minutes after irradiation, the γ-power for 1 g uranium irradiated at 1 MW/T for 2 h has reduced to 1.5×10^{10} MeV/s. The graph of γ-ray energies is plotted in days. After fifteen minutes cooling time the average energy is assumed to remain the same, and the activity by simple proportion is found to be 7.384 mCi.

To ensure that the 100 MeV x mCi restriction was not exceeded, the activities due to all possible isotopes were calculated, and the products of activity and γ-ray energy were summed.

4.3. Experimental method

4.3.1. The carrier solution and exchange reactions

Fission product iodine is present in such small quantities of 10^{10} atoms or 10^{-11} M that no chemical analysis can be achieved. If a carrier solution containing iodine in the same oxidation states as the active iodine in the aqueous solution is added, exchange will take place between active and inactive atoms in the same oxidation state. This results in an active solution which is of sufficient concentration to be analysed by chemical means.

Iodine can exist in aqueous solution as I^-, I_2, IO_3^-, IO_4^- (118). Exchange has been reported between the different oxidation states. The results are shown in table 4.8 (119), where f = gram formula weight per litre.

Table 4.8

Exchange reactions for iodine ions in aqueous solutions (119)

Reactants	Temp. °C	Other conditions	Separation method	$t_{\frac{1}{2}}$ exchange
$IO_3^- - I^{*-}$	50.0	Neutral solution	Acidified I_2 in C_6H_6	>30 y
$I_2 - I^{*-}$	Rm	-	I_2 in ether	<15 s
$IO_3^- - I_2^*$	25.0	0.099f HIO_3, 7×10^{-4}f I_2	I_2 in $CHCl_3$ or CCl_4	280 ± 4h
$IO_3^- - I_2^*$	25.0	0.020f $NaIO_3$, 6.7×10^{-4} f I_2 1.00f $HClO_4$	I_2 in CCl_4	208 h
$IO_3^- - I_2^*$	25.0	0.01f $NaIO_3$ 0.001f I_2, 1.5f H_2SO_4	I_2 in $CHCl_3$	216 ± 8h

It can be seen that exchange is unlikely between IO_3^- and I^- but is almost instantaneous between I_2 and I^-.

Some early experiments were carried out with molecular

iodine, iodide, and iodate present as carriers. Confirmation of the exchange reaction between I_2 and I^- was obtained by adding a second fresh carrier solution containing I_2, KI, KIO_3 to the first, active I_2 extract. (See section 4.3.2. for method of analysis). A subsequent analysis of this second carrier solution revealed no activity in the iodate fraction but both the I_2 and KI fractions were active. As was expected, the results of subsequent experiments, not using iodine carrier, showed that the iodide fraction obtained was the sum of the I_2 and I^- fractions obtained in these earlier experiments. Table 4.9 gives the fractional activities for early experiments with I_2, KI and KIO_3 carrier. Experiments, using carrier KI and KIO_3 only, gave a value for the fractional amount of KI present at room temperature of 0.823 (σ = 0.046). See section 5.1.1.

Table 4.9

Distribution of ^{131}I activity in carrier solution (KI, KIO_3, I_2)

Run	Fractional Activities		
	I_2	KI	KIO_3
9	0.507	0.281	0.212
10	0.579	0.284	0.138
11	0.409	0.371	0.220
12	0.545	0.266	0.189
13	0.489	0.329	0.182
14	0.599	0.210	0.191

Confirmation, for the absence of exchange between the iodide and iodate fractions, was found in a similar manner, by adding a carrier solution containing KI and KIO_3 to

the final fraction extracted from the original solution. The activity in this fraction is due entirely to KIO_3.

Possible reactions involving the periodate ion have yet to be discussed. Exchange between iodide and periodate fractions would not be expected from the results in table 4.1. Any periodate present was expected to be extracted with the iodate fraction. This was suggested in part from the literature and in part by experiment.

Samples of organic solvent and aqueous residue were analysed for iodine activity after the extraction procedure, with negative results. This indicated that the carrier solution of iodide and iodate was sufficient,and that no appreciable amount of fission product iodine was being lost,either as an organic iodo compound,or as iodine in an unusual oxidation state in the aqueous solution. This was confirmed by the observance of an acceptable level of correlation between the amount of active iodine found and the amount calculated to be present for each tablet analysed.

From the literature,it was found that in the presence of excess iodide (this occurs when iodide is added to liberate the remaining iodate according to equation 4.7) periodate is reduced to iodine, according to the following equation (120):

$$IO_4^- + 7I^- + 8H^+ \longrightarrow 4I_2 + 4H_2O \qquad (4.5)$$

However, evaluation of the rate constant with experimental concentrations gave

$$-\frac{d\,[IO_4^-]}{dt} = 5.7 \times 10^{-9}\ M/min$$

It can be seen from this value that negligible reduction would be expected.

The first step in the above reaction is the intermediate

formation of iodate

$$IO_4^- + 2I^- + H_2O \longrightarrow IO_3^- + I + 2OH^- \qquad (4.6)$$

It was found (119) that when radioactive iodide was used, the iodine produced was also active but the iodate remained completely inactive. This proved that it was produced entirely from inactive periodate. Since no activity remained in the original solution after analysis (as discussed above), it was assumed that any periodate present would be reduced to iodate.

4.3.2. Analysis

It was found that most extractions of fission product iodine, reported in the literature, used an oxidation/reduction process between an aqueous layer and CCl_4. Iodine forms a unique complex with CCl_4, which is characterised by a strong pink colour, and is visible to concentrations of 2.54 ppm (121). Repeated extractions between fresh aqueous and organic volumes allow almost 100% separation from other fission products. The iodine is usually precipitated as AgI, and counted.

Carrier solutions of analar grade A KI and KIO_3 were prepared. These contained sufficient iodine to visibly change the colour of CCl_4, but not too much to saturate the organic phase. A neutral solution of KI and KIO_3 has been reported to be quite stable, but air oxidation of iodide increases rapidly with decreasing pH and is catalysed by strong sunlight (121). Separated volumes of each carrier solution were made up and stored in the dark, in order to eliminate any possible reactions.

(a) Method

0.0083 M KI (5 ml) and 0.0051 M KIO_3 (5 ml) were pipetted

into a beaker and diluted with H_2O (10 ml). The active tablet was added to the solution and allowed to dissolve. After approximately 10 minutes, the solution and washings were added to analar grade A CCl_4 (10 ml) in a separating funnel in a fume cupboard. 0.05 M H_2SO_4 (6 ml) were added to acifify the solution, according to equation 4.7 and following calculations.

$$5I^- + IO_3^- + 6H^+ \longrightarrow 3I_2 + 3H_2O \qquad (4.7)$$

Iodate carrier was present in sufficient quantity to permit all the iodide activity to be extracted as iodine in the CCl_4 layer. This was separated out with two more 10 ml portions of CCl_4, which were collected in a stoppered flask with the first CCl_4 extract. By this means two fractions were obtained: one, the organic layer, containing the fission product iodine with carrier in the reduced form A and the other, the aqueous layer, containing the iodine with carrier in the oxidised form B. However, the activity in fraction A was not due to purely iodide activity. According to the equation, a fraction of iodate activity will also be oxidised to iodine. For all experiments, this fraction was small, as can be seen from table 4.10. See section 4.3.4 (c)(ii) for notation.

The organic layer A was added to 0.2 M Na_2SO_3 solution (15 ml) in order to reduce the organic complex to iodide. The organic layer, now free of I_2, was discarded. A mixture of HNO_3 and $NaNO_2$ was added to oxidise the iodide to iodine, which was extracted with a fresh CCl_4 solution. This was repeated twice to effect a pure separation of I_2 from the fission products. The final aqueous layer was acidified slightly with 0.1 N HNO_3 and a fewdrops of 0.1M $AgNO_3$ were added to precipitate the iodide as AgI. The

Table 4.10

Carrier solutions that were used in the analysis

No.	Iodide x_1 mg/ml	Iodate x_2 mg/ml	Iodide x_3 mg/ml	% iodate extracted with iodide	% correction for solution B
1	6.855	5.14	15.675	34	16.6
2	6.915	5.78	16.17	31	3.7
3	6.87	5.505	16.05	32	9.1
4	6.84	5.57	16.15	32	7.9
5	6.885	5.54	16.23	32	9.4
6	6.93	5.555	16.205	32	9.2
7	6.948	5.734	15.884	31	3.3
8	6.806	5.577	16.101	31	7.3

solution was heated to coagulate the precipitate, and filtered through a suction filter. This was manufactured specially to provide easy handling of the active filters and decontamination of the stick. The precipitate was washed with three 5 ml portions of alcohol and dried with the same amount of ether. It was mounted on a planchette, dried under a heat lamp and weighed to constant weight. Finally, it was covered with cellotape to prevent powder from being lost, and reweighed.

The aqueous volume B containing iodine with carrier in the oxidised form was washed with CCl_4 (10 ml) and used to extract the iodate as iodine. CCl_4 (10 ml) was added and then a solution of KI (5 ml) of sufficient concentration to extract the iodate according to equation 4.7. The same procedure as above, for purifying and precipitating the AgI, was adopted.

4.3.3. Modifications

Sometimes it was noticed that chemical yields were greater than 100%. This indicated that Ag_2SO_4, resulting from SO_2 in the solution, was precipitating out as well. Addition of acid and rapid boiling before adding $AgNO_3$ should expel SO_2, but there is also a possibility that a large fraction of the iodine will be lost as HI. To overcome these difficulties, an aqueous solution of SO_2 was used as the final aqueous extraction phase. Before using the solution, a blank of similar concentration was mixed with 0.1N $AgNO_3$ (1 ml) to see if a precipitate would form. This maximum concentration of SO_2 for no precipitation was then diluted with an equal volume of water before use.

In most of the experiments reported, the purifying and precipitation procedure was discarded altogether, since no adverse effect on the results was found by counting samples immediately after the first organic extraction. See table 4.11. (* These values have larger errors, due to lower counts).

Table 4.11

Samples counted as $CCl_4.I_2$(solution) and AgI (solid)

^{131}I:	KI		KIO_3	KI/KIO_3
Run 24	$CCl_4 I_2$	4.47×10^6	1.49×10^6	3.000
	AgI	6.01×10^6	2.06×10^6	2.917
Run 25	$CCl_4 I_2$	1.61×10^6	5.53×10^4	29.10*
	AgI	2.11×10^6	1.26×10^5	16.74*
^{133}I:	KI		KIO_3	KI/KIO_3
Run 24	$CCl_4 I_2$	1.07×10^8	3.57×10^8	0.299
	AgI	1.14×10^8	3.66×10^7	0.311
Run 25	$CCl_4 I_2$	3.75×10^7	8.49×10^5	44.0
	AgI	4.64×10^7	1.05×10^6	44.2

Specially made glass containers were used which could be opened easily for filling and cleaning. Each container was manufactured from a glass cone and matching socket. These were both cut down to size. The container was made by fitting the glass cone into the socket and glueing a glass plate across each of the other unground ends. PTFE sleeves were used to provide a good seal between the two parts of the containers.

This modification had several advantages: the extraction time, measured from the instant the tablet was added to the carrier solution to the time at which the last fraction was extracted, was reduced from four hours to thirty minutes. It became possible to deal with many more samples and reduce the time delay between the analysis of an annealed sample and its room temperature analogue. It was possible to find the amount of active iodine present without correcting for yield. Thus, errors introduced by precipitating AgI and weighing the precipitate were eliminated. Also, using this method, no iodine was lost as HI.

The effect of geometry and absorption in counting the liquid sample is discussed in section 4.4.2.

4.3.4. Explanation of calculation

The calculation required to find the distribution of the active iodine atoms between the iodide and iodate states can be divided into three sections. Section A shows how the experimental activities are found from the count rates observed. Section B explains how the theoretical fission product iodine activity is found. Section C combines the previous data in finding the specific and fractional activities. (The calculation is worked through for a

typical run (153) in appendix 1).

(a) Section A: To find experimental activities from count rates

The count rate produced by a γ-ray energy is recorded by the Ge (Li) detector as a number of pulses of a characteristic energy and this is stored in a channel number location. A plot of pulses against channel numbers produces a spectrum, where each peak can be assigned to a particular γ-ray energy. The peaks are analysed by the method of summing under the peak and subtracting the background Compton effect. The latter is found by averaging the first and last channel number in the peak and multiplying by the number of channel numbers used.

Each γ-ray has an associated γ-ray intensity which can be obtained from the literature. It is the percentage probability of the disintegrations occurring with that energy.

The efficiency of the machine in registering the number of disintegrations must also be considered. This is an intrinsic property of the counting equipment and must be found with standards of known activity before the counting is begun. However, as it is a slowly varying property, one calibration is usually sufficient for several months work. By means of an efficiency curve, the associated efficiency for any peak in the energy range can be found. It is expressed as a percentage.

Let the (area of the peak-background)/count time = a

% efficiency of the peak = eff

% intensity of the peak = int

then the activity immediately after counting, $\lambda N = \frac{a}{\text{eff} \times \text{int}}$

It is usual to take the end of irradiation as a reference point, and so all activities are worked back to this time using equation 4.4.

(b) Section B: To find the theoretical activities of isotope

The theoretical activity is found from the fission rate F, which is obtained from the neutron flux n.

(i) Neutron flux n

The neutron self shielding in the sample was estimated to be negligible. Therefore, the neutron flux monitor must have been subjected to the same flux as that encountered by the samples. During bombardment, ^{59}Co (in the monitor) captured neutrons and formed ^{60}Co, which is a radioactive isotope. Its nuclear energy is lost by emitting two γ-rays of energy 1.173 MeV and 1.333 MeV. The activities of these peaks were found according to section A and were averaged to give X.

Next, the number of atoms of ^{59}Co(Y) is found from the weight of cobalt chloride (x g) and its formula $CoCl_2.6H_2O$

$$Y = x \times \frac{6.023 \times 10^{23}}{237.93}$$

Finally, the thermal neutron capture cross-section σ_c for ^{59}Co is found from the literature.

The number of atoms of ^{60}Co at the end of irradiation for T hours is N_o where

$$N_o = \sigma_c \times Y \times T \times n \qquad (4.8)$$

But $$\lambda N_o = X$$

$$\therefore \quad n = \frac{X}{\sigma_c \times Y \times T \times n}$$

(ii) Fission rate F

The value for neutron flux, found above, together with the number of atoms of ^{235}U and its capture cross-section, allows the fission rate, F, to be found.

Let the weight (in grams) of U_3O_8 be y and the enrichment

be 80%. The number of atoms of ^{235}U is U, then

$$U = 0.8y \times 6.023 \times 10^{23} \times 3/834.9236$$

The fission cross-section for ^{235}U depends on the neutron energy. The value used of 580×10^{-24} cm^2 may not represent the true situation since the phenomenon of resonance makes possible the capture of neutrons with energies above thermal values. However, using this value

$$F = U \times 580 \times 10^{-24} \times n$$

During irradiation fission products are continually being formed, and each atom then decays with its isotopic half life. At the end of irradiation the situation is expressed as

$$N\lambda = \alpha F (1 - e^{-\lambda T}) \qquad (4.9)$$

This is similar to equation 4.3 with R replaced by αF.

$N\lambda$ is the activity of the isotope after T hours of irradiation

α is its probability of occurring through fission

λ is its decay constant.

Equation 4.9 gives the theoretical primary yield of the isotope immediately after irradiation.

(c) Section C: Specific and fractional activities

(i) To find the specific activities

The specific activity for each state is defined as the activity per g iodine in the carrier solution for that state.

First, the activities in the two extracted solutions A and B are computed according to section A. The activity in B is due entirely to iodate; that in A is due to iodide ions and a small amount of iodate ions. The activity is separated as follows:

Let carrier solution P (KI) be x_1 g/ml

Q (KIO_3) be x_2 g/ml

R (KI) be x_3 g/ml

$$IO_3^- + 5I^- + 6H^+ = 3I_2 + 3H_2O \qquad (4.7)$$

According to this equation

1 g KI reacts with 0.258 g KIO_3

$\therefore$ x_1 g $x_1 \times 0.258$ g KIO_3

i.e. C g KIO_3

KIO_3 remaining in solution is $(x_2 - C)$ g

i.e. C_1 g

Furthermore, C_1 g KIO_3 requires $\frac{C_1}{0.258}$ g KI to be liberated as iodine, according to equation 4.7.

Thus, the activity of solution B is due to C_1 g iodate.

$\therefore$ the iodate activity of solution A = $\frac{C}{C_1}$ x activity of solution B

Subtracting this from the total activity in solution A gives the activity due to iodide ions. The iodide and total iodate activities are each divided by the weight of iodine (in grams) in the iodide and iodate carrier solutions P and Q. This gives the specific activity in each state.

In the above calculation, no account was taken of the fact that in extracting the remaining iodate as solution B, x_3g KI are added where x_3 exceeds the required amount of $\frac{C_1}{0.258}$ g obtained by calculation.

Iodine atoms in B solution before extraction = $x_3 \times \frac{126.904}{166.006}$ g + $C_1 \frac{126.904}{214.0042}$ g

= $0.7645 \times x_3$g + $0.5930 \times C_1$ g

I_2 in CCl_4 after extraction = $\frac{C_1}{0.258} \times \frac{126.904}{166.004}$ g + $C_1 \frac{126.904}{214.0042}$ g

= $3.556\ C_1$ g

$$I_2 \text{ left in aqueous solution} = \left(x_3 - \frac{C_1}{0.258} \times \frac{126.904}{166.006} \right)$$

$$= 0.7645\ x_3 g - 2.963\ C_1 g$$

If this iodine had undergone exchange with the active iodate atoms, then the count rate for solution B should be increased by the following fraction

$$\frac{\text{Iodine atoms in soluction before extraction}}{\text{Iodine atoms extracted into } CCl_4} = \left(\frac{0.7645x_3 + 0.593C_1}{3.556\ C_1} \right)$$

This gives an upper limit to the correction which depends on the nature of the equilibrium between I_2 and I^- under the conditions present in the solution. The correction is of the order of 8.3% (σ = 4.1). See table 4.10.

(ii) To find the fractional activities

It is conventional to divide the activity in each state by the theoretical yield. This gives a_1 for iodide and a_5 for iodate. The sum ($\Sigma_a = a_1 + a_5$) is the ratio of the iodine activity found experimentally to that expected from calculation. The geometry of the sample during irradiation suggests that this value is < 0.5. The fractions of the activity due to iodide and iodate ions are expressed as a_1/Σ_a and a_5/Σ_a respectively.

The calculation was carried out for each of the isotopes ^{131}I, ^{133}I, ^{135}I. ^{132}I has a precursoe ^{132}Te with a relatively long half life of 77.7 h. It was assumed that all the activity for ^{132}I at the time of counting had originated from ^{132}Te

(see section 4.4.1. - Decay schemes for iodine isotopes) and the calculation was modified accordingly.

(iii) Modification

During irradiation for 2h there is negligible decay of Te. After irradiation ^{132}Te decays to ^{132}I.

$$^{132}_{52}\mathrm{Te} \xrightarrow{\beta^-} {}^{132}_{53}\mathrm{I}$$

A B

$$\frac{dA}{dt} = -\lambda_A A \qquad (4.10)$$

$$\frac{dB}{dt} = \lambda_A A - \lambda_B B \qquad (4.11)$$

$$e^{\lambda_B t}\left(\lambda_B B + \frac{dB}{dt}\right) = \lambda_A A\, e^{(\lambda_B t - \lambda_A t)}$$

$$\frac{d\left(B\, e^{\lambda_B t}\right)}{dt} = \lambda_A A_o\, e^{(\lambda_B t - \lambda_A t)}$$

$$B e^{\lambda_B t} = \frac{\lambda_A}{\lambda_B - \lambda_A} A_o e^{(\lambda_B - \lambda_A)t} + \text{const}$$

At end of irradiation $t = 0$ and $B = B_o = 0$

$$\therefore \text{const.} = -\frac{\lambda_A}{\lambda_B - \lambda_A} A_o$$

$$\lambda_B B = \frac{\lambda_B \lambda_A A_o (e^{-\lambda_A t} - e^{-\lambda_B t})}{(\lambda_B - \lambda_A)} \qquad (4.12)$$

This gives the iodine activity at the time of dissolution of the tablets, t hours after the end of irradiation. $\lambda_B B$ is found from the measured activity of ^{132}I by using the equation for radioactive decay (4.4). In this case t is the time between dissolution and count. In calculations for the other isotopes, the time between the count and end of irradiation has been used.

The tellurium activity at the end of irradiation, which has produced the iodine activity $\lambda_B B$ at dissolution, can be found from equation 4.12. This value is compared with the theoretical yield for ^{132}Te, and the rest of the calculation is the same as before.

The results were computed on a PDP8 machine with a program written in FOCAL language. This is shown in appendix 1.

4.4. Counting Methods

4.4.1. Decay schemes for iodine isotopes

Due to the energetics involved in nuclear fission, the isotopes of iodine formed contain more neutrons than the stable iodine isotope ^{127}I. These have excess neutron energy and decay to a more stable nucleus by β-particle emission. This decay can be considered as a neutron in the nucleus changing into a proton and emitting an electron. The daughter nucleus will have the same mass number as the parent, but the nuclear charge will be increased by one unit. This process is repeated until a stable nucleus is reached. The series of decay isotopes is called a chain. β- decay often results in a highly excited daughter nucleus, which loses energy through photon emission as γ-rays. The photons have either a single energy or a group of discrete energies which identify the nucleus. See section 1.1.4.

(a) Decay chains

As discussed in section 1.1.3 the mass and charge yields for thermal neutron fission of ^{235}U have similarly shaped curves. The most probable charge for mass A can be obtained from the empirical formula (14)

$$Z_p = 46 - \frac{Z_{A_2} - Z_{A_1}}{2} \qquad (1.3)$$

where

$$A_1 + A_2 = A - \nu \qquad (1.4)$$

ν is the average number of neutrons emitted in fission

Z_{A_1} is the most stable charge for the mass in question.

This assumes that light and heavy fragments are equally far away from stability; and this is observed in practice.

Using this value, the independent yields for isobars in the same decay chain can be calculated. They are found to

form a normal distribution about the most probable charge Z_p. In the thermal fission of uranium, the width of the distribution is similar for all masses. The independent yield is the yield of the isobar relative to the total yield of all the isobars of the same mass. It is given by

$$P = \frac{1}{\sqrt{c\pi}} e^{-\frac{(Z - Z_p)^2}{c}} \qquad (1.2)$$

where $1/\sqrt{c\pi}$ is the normalising factor. This is required because the sum of all the independent yields for a decay chain must equal unity and

$$\int_{\pi = 0}^{\pi = \infty} e^{-x^2/c} = \sqrt{c\pi}$$

This value, multiplied by the mass yield, gives the primary yield for that isotope. The mass yield is read from the mass-yield curve for the appropriate mode of fission.

A third yield, which is often quoted, is the cumulative yield. This is the sum of the primary yields of all the previous isotopes in the decay chain. The total cumulative yield equals the mass yield, since the sum of the independent yields is unity.

(b) The isotopes used and their decay schemes

The samples were not analysed until at least 24 hours after irradiation, and so the isotopes used in the experiments were required to have half lives greater than a few hours. The suitable isotopes are shown in table 4.12 which was compiled from reference 122. The γ-ray energies that were used in the analysis are underlined. ^{128}I, ^{134}I, $^{136-141}$I have half lives that are too short. The half life for ^{129}I is too long. ^{130}I is a shielded nucleus, its precursor having a closed nuclear shell, and so the

primary yield is extremely low.

(i) Calculation of the primary yield for $^{130}_{53}I$

Equations (1.3) and (1.4) are employed to find the most probable charge for mass 130. For thermal fission of ^{235}U, $\nu = 2.5$. Since A = 236 and $A_1 = 130$, then $A_2 = 103.5$. The most stable charges for these masses can be found from tables (14)

$$Z_{130} = 53.9$$

$$Z_{102.5} = 45.4$$

$$\therefore \quad Z_p = 50.25$$

The independent yield of charge 53 is found from equation 1.2 with C = 0.82.

$$P = 6.16 \times 10^{-5}$$

The yield for mass 130 is also found from tables (14) and is found to be 2×10^{-2} for thermal fission of ^{235}U.

$\therefore$ the primary yield for $^{130}_{53}I$ is 1.2×10^{-6}

Table 4.13 gives the decay scheme for each isotope in table 4.12. Cumulative yields were calculated using the method described above.

The precursors for ^{133}I, ^{135}I should have all decayed away at the time of analysis, and so the correct values to use for the fission yields for these isotopes will be their cumulative yields. ^{131}I has a precursor Te^m which could be present 24 h after irradiation. Its small concentration can be neglected as this will not alter appreciably the cumulative yield for ^{131}I at the time of analysis. ^{132}I has a precursor Te ($t_{\frac{1}{2}}$ 77.7 h). This should be considered when establishing the yield for $^{132}I_2$ since the fission yield at the time of analysis is significantly less than the cumulative yield. In the calculation, the activity of Te required to

Table 4.12 (122)

Data for iodine isotopes which are suitable for analysis

Isotope	Half life	Principal photon energies (MeV)	% total disintegration
^{131}I	8.05 y	Xe X-rays	
		0.08	2.6
		0.284	5.4
		0.364	82
		0.637	6.8
		0.723	1.6
^{132}I	2.26 h	0.24	1.0
		0.52 (complex)	20.0
		0.67 (complex)	144.0
		0.773	89
		0.955	22.0
		1.14 (doublet)	6.0
		1.28	7.0
		1.40 (complex)	14.0
		1.45	1.0
		1.91	1.3
		1.99	1.3
^{133}I	20.3 h	0.53	90.0
		(Daughter radiations from ^{133}Xe, ^{133m}Xe)	
^{135}I	6.68 h	0.42	7.0
		0.86	11.0
		1.04	9.0
		1.14	37.0
		1.28	34.0
		1.46	12.0
		1.72	19.0
		1.80	11.0
		(Daughter radiations from ^{135m}Xe, ^{135}Xe)	

Table 4.13

Decay schemes for isotopes (14)

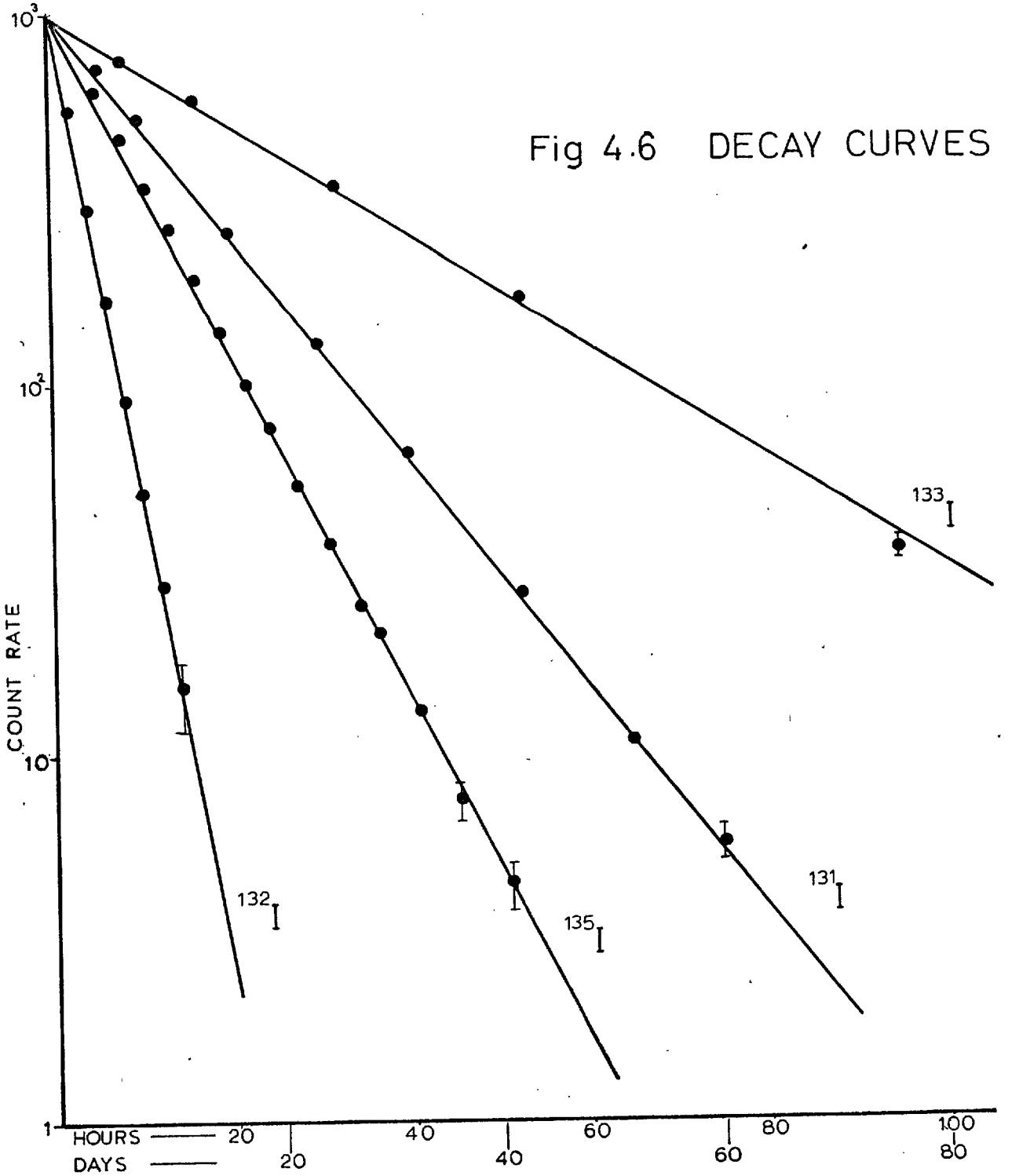
Mass No.	Atomic No. 51	52	53	54	55	56
131	21.0 mSb (2.7) ~15% → 30 hTe 0.44 → 24.8 mTe 2.9; ~85% → 24.8 mTe 2.9		8.05 dI 2.9	1% → 12 dXe 0.03 → Stable Xe; 99% → Stable Xe		
132	1.9 mSb (3.4)	→ 77 hTe 4.4	→ 2.4 hI 4.4	→ Stable Xe		
133	4.1 mSb (3.8) ?% → 63 mTe 4.6 → 2 mTe 6.0; ?% → 2 mTe 6.0		20.8 hI 6.5	2.4% → 2.3 dXe 0.16 → 5.27 dXe 6.5; 97.6% → 5.27 dXe 6.5	→ Stable Cs	
135		< 2 mTe (4.2)	→ 6.68 hI 5.9	30% → 15.6 mXe 1.8 → 9.13 hXe 6.2; 70% → 9.13 hXe 6.2	→ 3.0×10^6 yCs 6.2	→ Stable Ba

produce the measured ^{132}I activity was found and compared with the theoretical activity of Te present immediately after irradiation. Only the fission yield for Te was required, which is the cumulative yield.

(c) Decay curves

Decay curves were plotted for each isotope to show that the peaks used were assigned correctly and were isotopically pure. The activity decays exponentially according to its half life. It is usual to plot the count rate against time on log-linear graph paper. If the decay is due purely to the isotope in question, the plot will be a straight line, and the half life is read directly as the slope of the line. If any other isotope is present, the decay line becomes a curve. This can be resolved into its component lines corresponding to each isotope present. The slope of the last portion of the curve corresponds to the half life of the longest lived isotope. The tangent to the curve is constructed, and the remaining curve is drawn where these linear values have been subtracted from the original curve. The new curve now has a final portion with a slope that corresponds to the half life of the second longest lived isotope. The procedure is repeated until the whole curve is analysed.

The decay curves for the isotopes used in the experiments are shown in figure 4.6. The samples were counted at characteristic γ-ray energies as I_2 in CCl_4. No interference from other isotopes with similar γ-ray energies was detected.


Fig 4.6 DECAY CURVES
COUNT RATE
10^3
10^2
10
1
^{133}I
^{131}I
^{135}I
^{132}I
HOURS
DAYS
20
40
60
80
100
20
40
60
80

4.4.2. Counting apparatus

The detectors that are available for detection of radiation can be characterised by the nature of the interaction of radiation with the detector. Detectors such as ionization chambers, proportional counters, Geiger-Müller counters, semiconductor radiation detectors, cloud chambers and spark chambers, operate through the ionization produced by the passage of charged particles. Uncharged particles such as neutrons and γ-rays can also be detected, since they produce ionization as secondary processes. Scintillation detectors, however, depend on the excitation of the scintillator atoms; and chemical detection systems are sensitive to chemical reactions promoted by the radiation.

The counters that were employed to count the samples were the Geiger-Müller counter and the Lithium drifted Germanium detector. These both belong to the first category of detectors. Initially, the samples were counted with the Geiger-Müller counter. In this detector, the incident radiation is not resolved according to its energy. A total decay curve is obtained which can be resolved into its component half-lives by the method described in section 4.4.1.

For a more detailed account of detectors see (123, 124, 125, 126). ^{131}I has a long half life of 8.05 d and so each sample was counted for several weeks in order to establish the final slope of the total decay curve.

The Ge (Li) detector, on the other hand, gives immediate resolution of incident energies. Although the efficiency of this detector is less, this method of counting was adopted because of its speed in counting and analysis. If peaks are assigned their correct energies then single counts

are sufficient in the analysis of each sample, provided the set-up remains the same.

(a) Lithium drifted Germanium detectors

Ge (Li) detectors fall into the class of semiconductor radiation detectors. Primarily, they are used for γ-ray spectrometry. Due to their good resolution, they have surplanted sodium iodide scintillator detectors in this field. Their operation depends on the properties of a depletion region in the semiconductor material. All trapping impurities due to the p-type dopant are compensated for by the Lithium that drifts into this region.

(i) Method of fabrication

P-type germanium is made by doping a very pure crystal with indium or gallium. The resulting material has a low dislocation density, high carrier lifetime and a uniform distribution of acceptor centres. Lithium, a donor impurity, is diffused into one side. Li is a very light ion with a high diffusion coefficient and, in the presence of an electric field, it can drift through the crystal. Diffusion will mask the ion drift effect for most impurities but, for Li, the drift effect predominates between 100 ^{o}C and 400 ^{o}C. It is drifted for several months under carefully controlled conditions of reverse bias current, temperature and heat dissipation. The increased thermal energy generates carriers which are responsible for most of the reverse current. Space charges are also set up. These are a function of the distance from the centre of the depletion zone and are responsible for leakage currents which reduce the resolution of the counter. At these high temperatures and wide depletion layers, the Li compensation for acceptor and space charges becomes less accurate. The final stage

of the drifting process is to gradually lower the temperature to values where the mobility of Li is still high while the generation current is only a fraction of its value during the drift. This is the clean-up drift.

The Li ions are very mobile at room temperature and will undrift in the absence of a reverse bias voltage. They may precipitate out in the crystal or move to a surface and be lost. In order to prevent this, the crystal must be stored under reverse bias voltage and kept at liquid nitrogen temperature.

(ii) Analysis of the spectrum (127)

In every γ-ray spectrum for monoenergetic γ-rays, there is a full energy peak, backscatter peak, Compton continuum and Compton edge. Bremsstrahlung is also evident if the source emits β-rays. Escape and annihilation peaks occur when the γ-ray energy exceeds approximately 1.2 MeV.

The interaction of γ-rays with matter has been discussed in section 1.3.6. Of the three main processes, the photoelectric effect is responsible for the full energy peak. This is so named because all of the γ-ray energy has been converted by a single process to produce an electron with the same energy minus its binding energy. The electron is of a characteristic energy and loses this in creating a proportional number of charge carriers in the depleted region.

The Compton effect reduces the initial energy of the γ-ray by varying amounts and the energy of the scattered electron is recorded as the number of charged carriers produced in the detector. The γ-ray can undergo multiple Compton collisions until its energy is reduced to zero. If some of these γ-rays are near the surface, they can

escape from the detector. A spread in energy is observed, which is less than the incident γ-ray energy, and this gives rise to the Compton continuum. The Compton edge is the maximum electron energy that can be recorded from this process with a correspondingly minimum energy for the photon. The electron is scattered in the same direction as the incident photon and the re-emitted photon is scattered through 180°. The scattering of this photon with minimum energy gives rise to the backscatter peak. It has contributions from photons that have passed through the crystal without collision but are returned by back-scattering from the materials near the detector. The backscatter energy is given by

$$E_{BS}(\bar{\theta}) = \frac{E_{\gamma}}{1 + (E_{\gamma}/0.511)(1 - \cos\theta)} \qquad (4.13)$$

where $\bar{\theta}$ is the effective scattering angle (from $\sim 150^{\circ}$ to 180°)

E_{γ} is the crystal incident photon energy

0.511 MeV is the rest mass energy of an electron

The sum of the energies of the back-scattering peak and Compton edge gives the energy of the original γ-ray.

γ-rays with energies above 2 MeV have a high probability for pair formation. The spectra for these γ-rays contain annihilation peaks at 1.02 MeV below the full energy peak. Annihilation is the recombination of an electron-hole pair. It does not occur until all the positron kinetic energy has been dissipated by ionization or radiation processes. Two annihilitation photons, each with 0.511 MeV energy, are emitted at approximately 180° with respect to each other. This leads to the possibility of two escape peaks at 0.511 MeV intervals. If appreciable

external pair production is occurring in the vicinity of the crystal, a single 0.511 MeV photon may be scattered into the crystal. This can undergo photoelectric absorption to give the observed peaks.

Bremsstrahlung is the breaking radiation observed where there is negative acceleration of a charged particle produced by the Coulomb field of a nucleus. A continuous spectrum of X-rays, from zero to the maximum kinetic energy of the particle, is produced. This radiation can be minimised by surrounding the detector with an absorber to prevent the entry of external electrons.

The detector was used in the analysis of γ-rays with energies between 0.364 and 1.28 MeV. A typical spectrum obtained from the samples is shown in figure 4.7 . The full peak area is used for absolute or relative intensity determinations because, for a given detector system and γ-ray energy, it is proportional to the intensity of the corresponding radiation.

(iii) Characteristics of a Ge (Li) detector

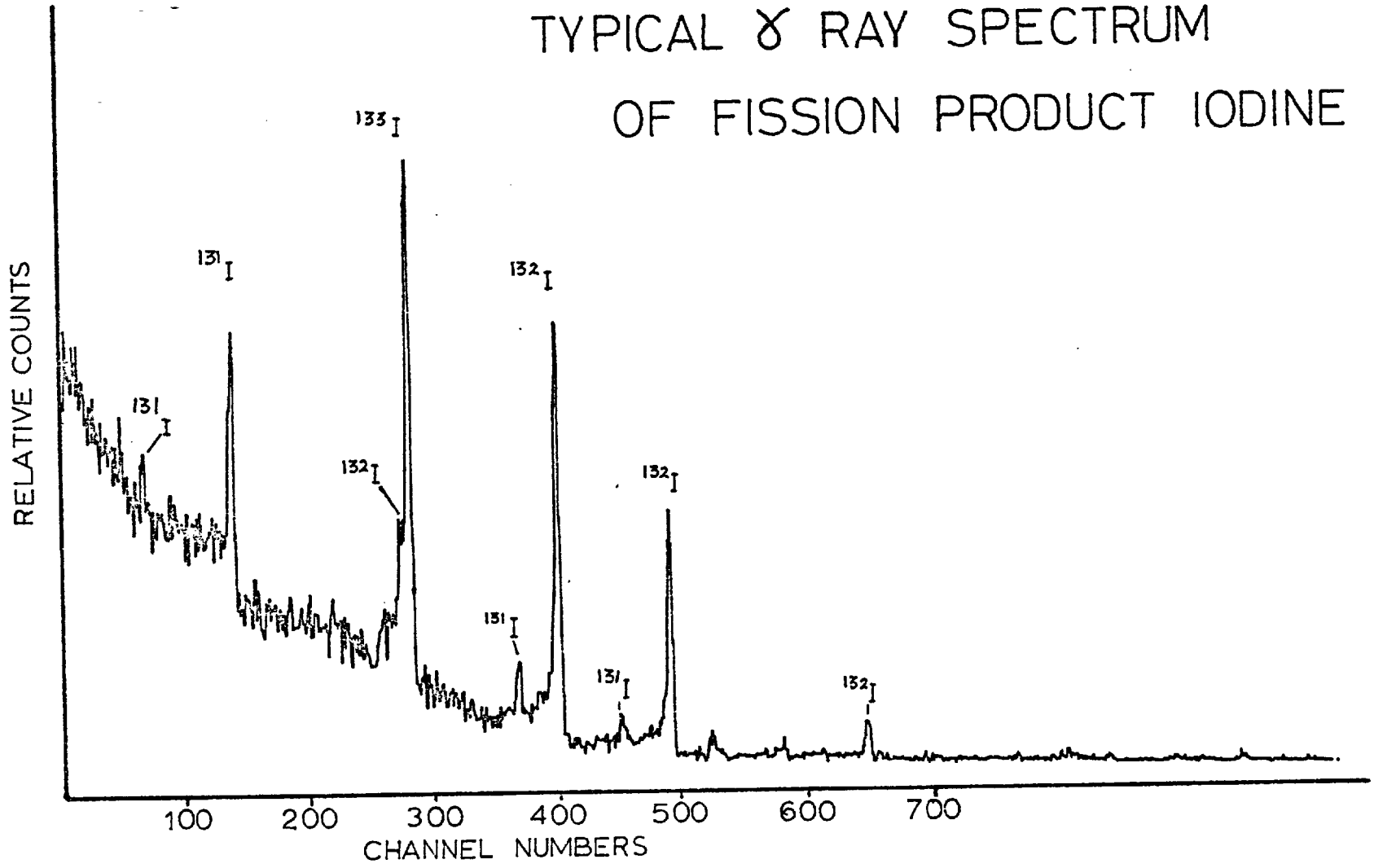
There are two important characteristics of a Ge (Li) detector. These are its resolution and efficiency.

Resolution:

This is usually expressed as the full width at half maximum height of the peak (FWHM). Factors which broaden the line corresponding to total energy loss are multiple Compton scattering, non-linearity in the electron energy to pulse height conversion, wall effects and pulse pile-up. The last factor expresses the situation when two γ-rays interact with the detector within the resolving time of the pulse amplitude determining circuit. Only one pulse is stored with an amplitude that is the sum of the

Fig 4.7

TYPICAL γ RAY SPECTRUM OF FISSION PRODUCT IODINE



pulses. This can be minimised by reducing the source strength and having a fixed dead time - a period when no pulses are registered. Many multichannel analysers have an optional built-in dead time correction,and live time is measured in preference to clock time. This technique was used in the experiments reported in this thesis. Pulse pile-up is an activity dependent distortion and alters the shape of the spectra. The rest are statistical intensity-independent distortions which effect the low-energy side of the, otherwise, Gaussian peak.

The resolution of the detector also depends on the statistical fluctuation in the number of electrons produced by the γ-rays, the intrinsic noise effects in the detection system and the channel width of the spectrometer.

The resolution of the Ge(Li) detector is much greater than that of its competitor, the NaI crystal detector, which is a scintillation counter. The energy for producing an electron-hole pair in the Ge(Li) detector is two orders of magnitude less than that required to produce a photo-electron in the NaI crystal which will reach the first dynode of the photomultiplier tube. The higher number of charge carriers per unit γ-ray energy leads to a higher number of statistical processes and smaller relative statistical fluctuations.

Efficiency:

This can be found experimentally and accounts for the discrepancy between the true disintegration rate of the source and the count rate registered by the detector and associated electronics. It varies with the γ-ray energy, and so it is usual to obtain an efficiency curve over the range of energy required by plotting efficiency against

the γ-ray energy of several standard sources. A list of the sources used in the calibration together with their principal γ-ray energies, is given in table 4.14. For a discussion of errors, see section 5.1.2. A typical efficiency curve for the experimental work is shown in figure 4.4.

Table 4.14

Standard sources used for calibration

Isotope	Half life	Principal photon energies MeV	% total disintegration
^{133}Ba	10.8 y	0.276	7.1
		0.303	18.7
		0.356	61.9
		0.384	8.9
^{137}Cs	30.1 y	0.662	85.1
^{57}Co	270.5 d	0.122	85.2
		0.136	11.1
^{60}Co	5.27 y	1.173	99.86
		1.333	99.98
^{54}Mn	312.5 d	0.835	100.0

The reference efficiency and resolution energy for Ge(Li) detectors is 1.33 MeV and the standard source-to-detector distance is 25 cm. The Ge (Li) efficiency is generally expressed as the photopeak counts relative to the corresponding 3" x 3" NaI (Tl) photopeak counts. The ratio of the peak height to Compton edge is also quoted by manufacturers. Table 4.15 shows these values for the two detectors used during the experimental work.

The first detector was used for the 100 °C annealing results and the investigations associated with efficiency.

Table 4.15

Characteristics of detectors used for experimental work

Configuration	Resolution (KeV)	Peak to Compton	Efficiency %
True coaxial right circular cylinder open at both ends	2.17	21.7:1.0	5.5
Trapezoidal	5.1	6.1:1.0	10.0

(b) Experimental efficiency determination

An efficiency curve was obtained by counting solid standard point sources at 4.9 cm from the surface of the detector. All samples were placed centrally under the crystal. The ^{60}Co flux monitors, essentially point sources, were counted at this distance. Thus, the efficiency curve gave an accurate value for the efficiency of the Co peaks. However, the samples were solutions and could not be considered as point sources, since the containers were of radius 2.75 cm and the liquid filled them to a level of 1.7 cm. The top of the liquid was 4.3 cm from the detector head. In view of these complications, it was considered necessary to find the variation of efficiency with distance, and the effect on count rate of sources displaced slightly from an axial position.

A study of displacement and count rate for both solid and liquid samples at these distances showed no alteration in the count rate for maximum credible accidental displacements. In table 4.16 it is seen that a solid sample, 4.9 cm from the surface of the detector, showed a decrease in count rate when moved 1.3 cm. This was taken to be the

maximum credible accidental displacement in a horizontal plane. Similar results were obtained when the disc was moved the same distance in two perpendicular directions. This proved that the disc was centrally placed for counting before the displacements. Movement of the liquid sample through a distance of 1.38 cm in the horizontal plane had no effect on the count rate. Even though the top of the

Table 4.16

Displacement of samples in the horizontal plane

Solid = 4.9 cm from detector: liquid = 4.3 cm from detector

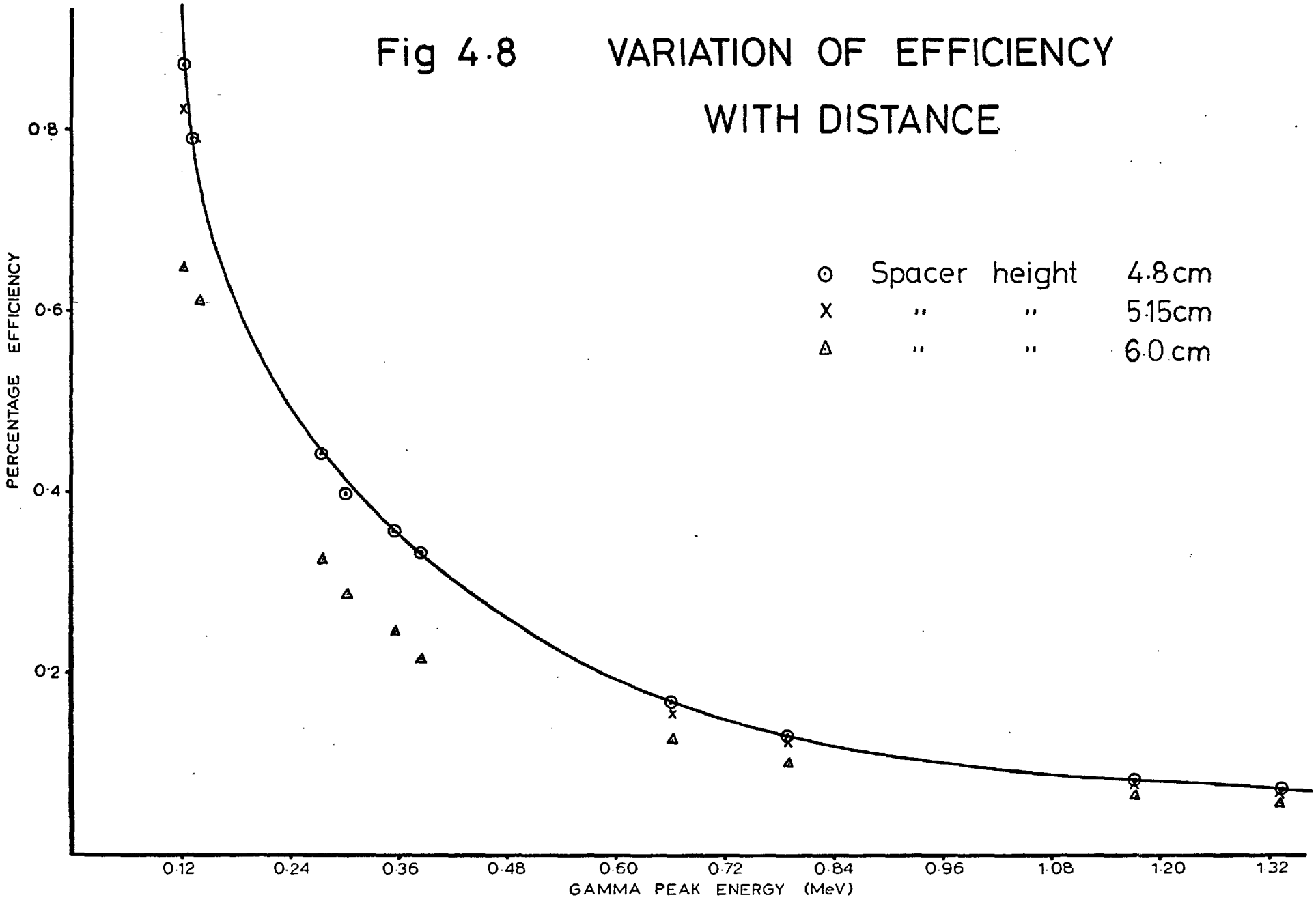
Displacement	Count rate	Isotope	State
0	61.43 ± 0.39	^{60}Co	solid
1.3 cm, x axis	58.04 ± 0.38	"	"
1.3 cm, y axis	58.54 ± 0.38	"	"
0	1.114 ± 0.06	^{131}I	liquid
0.85 cm, x axis	1.048 ± 0.06	"	"
1.38 cm, x axis	1.102 ± 0.06	"	"
0.85 cm, y axis	1.102 ± 0.06	"	"
1.38 cm, y axis	1.112 ± 0.06	"	"
0	1.146 ± 0.06	"	"

liquid is nearer the detector, the count rate is less than that for the solid sample. There is an error of 5% in these count rates, which is ten times the error in the count rate for solid samples, and masks any effect of an accidental displacement. The accuracy to which the source can be placed under the detector will be expected to have more significance as the count rate increases. ^{133}I in the B fraction is usually the most active isotope at the time of analysis. It has an error in the count of $\sim$ 1%.

The efficiency was found to vary linearly with the source distance. This is shown in figure 4.8. All the liquid samples have similar attenuation coefficients, since they are all of the same volume and nature, and so the correction for distance should be a constant factor. The efficiency curves plotted with point sources do not represent the absolute efficiency of the liquid samples. However, this is not required in the final analysis of the samples and will not affect the results, since it is a constant factor throughout.

It is concluded, from these results and discussion, that the use of liquid samples, instead of solid ones, for counting has no adverse effects on the accuracy of the results obtained.

Fig 4.8 VARIATION OF EFFICIENCY WITH DISTANCE



4.5. Other Experiments

4.5.1. Moisture experiments

Initially, annealing experiments were conducted with the tablet sealed in a glass tube. The glass was shaped like a test tube, which was 30 cm long, in order to avoid heating the sample during sealing. The tablet was transferred to the tube and the top was sealed with an oxymethane flame. The annealing experiments gave scattered results, using this method. It was often observed that, after heating, the tablet appeared moist, and this observation correlated with very high iodate fractions. The tablets were sealed so that gases in the tablet, diffusing to the surface, would be trapped. Later, experiments in which the tablets were heated in air without any containment gave results that did not differ significantly from those obtained with containment. The results are shown in table 4.17, where D = dessicator.

Table 4.17

Effect of sealing the tablets

Conditions			Fractional Iodate Value (p.226)
pre-annealing	annealing	post-annealing	
sealed	24h, 100°C	sealed	0.088
air	" "	air	0.153
sealed	20h, 100°C	sealed	0.072
D	" "	D	0.103

The tubes were dried in silica gel dessicators prior to use, but even then some tablets appeared wet after heating. This could have been due to moisture entering the system during the sealing process. It was decided to investigate

this effect. Tablets were not sealed or kept in a dessicator. For some experiments the tablet was split in two. One half was wetted and the other was kept in laboratory conditions for the same length of time. 5 λ portions of water were pipetted onto the surface of the tablet, which was then left for varying times before being added to the carrier solution. It was observed that the wetted pellets always showed the higher iodate fraction. Experiments were also carried out to find the effect of a moist atmosphere on the tablets. Both sets of results are shown in table 4.18 where D = dessicator and H = humidity vessel (a glass vessel, saturated with water vapour). The tablets are affected by moisture only if it is introduced just before analysis. The time of contact with moisture and the time between irradiation and analysis had no effect.

The importance of wetting the side nearer the U_3O_8 film is demonstrated by the following results. One half of a tablet was wetted on this side and the other was wetted on the opposite side. Values of 0.314 and 0.217 respectively were obtained for the iodate fractions.

Another interesting experiment was performed in which one portion received approximately 1 M Rad of γ-radiation prior to wetting. A value of 0.632, compared with 0.373 for no post-reactor irradiation, was obtained.

4.5.2. The effect of pH

Occasionally, results were obtained that differed noticeably from the majority. It was thought that the reactions occurring might be highly sensitive to pH. Any change, such as a fresh stock of distilled water with

Table 4.18

Moisture Results

Run	Conditions for wet/heated tablet			Fractional iodate values for ^{131}I (p.226)	
	Pre-annealing	annealing	post-annealing	Wet/heated	Dry(room temp.)
1	-	-	2m, 5 λ H 0	0.450	0.187
2	-	-	5m, 5 λ H 0	0.343	0.111
3	-	-	10m, 5 λ H 0	0.500	0.190
4	-	-	15m, 5 λ H 0	0.504	0.234
5	-	-	20m, 5 λ H 0	0.433	0.182
6	D	17h, 200°C	H, 1h 7m	0.552	0.130
7	D	" "	D	0.449	0.149
8	D	14h, 200°C	D	0.385	0.168
9	H, 31 m	" "	D, 22m	0.365	0.150
10	D	2h, 200°C	H, 1h	0.309	0.196
11	D	" "	D	0.230	0.149
12	D, 5h 43m	" "	H, 1h 19m	0.600	0.211
13	H, 5h 42m	" "	D, 1h 23m	0.488	0.200

a variation in pH, might be responsible for these "odd" results. The method of neutralization employed by the manufacturers in producing the KCl crystals could also effect the resulting pH. The crystals could have resulted from neutralisation from a slight excess of acid or alkali. However, this source of varying pH would only occur if different batches of the powder had been used, which was not the case for these experiments. Nevertheless, such considerations gave rise to an easy method of preparing a medium with controlled extremes of pH.

(a) Method

Approximately 1N HCl (20 ml) was neutralised with 1N KOH solution in a burette, using methyl red as indicator. 21.9 ml KOH solution was required. Acid and alkali solutions were prepared with 20.9 ml and 22.9 ml KOH respectively. The solutions were evaporated on an electric heater with a steam bath being used for the final stages. The crystals were kept in a dessicator which contained both silica gel and pellets of KOH. The latter was required to prevent carbon dioxide from reacting with the slightly basic salt to form potassium carbonate. After drying for several days, the powders were pressed into tablets under the usual conditions and irradiated in sealed capsules. In order to check that no reactions were occurring during this time, two dummy acid and alkali tablets were kept in containers which were sealed and later opened along with the sample containers. There was no change in weight for the dummy tablets. The irradiated tablets were halved and each portion was analysed for iodide and iodate activity. The usual procedure was adopted except that since the acid tablets would react immediately with the

carrier solution to liberate iodine, they were added to the carrier in the separating funnel with CCl_4 present.

(b) Results

The first set of results indicated a slight increase of iodate in the alkali pellets, but the opposite effect was obtained for the second set of results. These are shown in table 4.19.

Table 4.19

Acid/Alkali results

Run	Condition	Fractional Iodate Value for ^{131}I (p.226)
1	acid	0.147
2	alkali	0.234
3	acid	0.174
4	alkali	0.116

The results are within the range of experimental error and typical for room temperature samples. The tablets were dissolved in 10 ml of water and 10 ml carrier solution. Therefore, the acid tablets had a pH of 1.3 in solution, and the alkali tablets had a pH of 12.7 in solution.

The results, discussed above, show that pH does not have an appreciable effect within the range of variation expected.

4.5.3. Chlorine experiments

The following experiments were carried out to find the level of free chlorine present in the samples after irradiation and annealing. It was felt that the presence of chlorine could influence the behaviour of the iodine

atoms in the medium.

A titometric analysis was adopted, to prepare standard solutions of sodium hypochlorite solution containing known amounts of free chlorine. These solutions were used to plot a Beers Law curve for a Pye Unicam spectrophotometer, which was set to record the transmission at λ = 353, the wave length of the I_3^- ion.

(a) Preparation of sodium hypochlorite solution (NaOCl)

Commercially available NaOCl contains an indefinite amount of free chlorine. The iodometric method (121) for the determination of the available chlorine in bleaching powder was adopted,to establish the amount of free chlorine in a solution of NaOCl containing approximately 1 x 10^{-4} g Cl_2 per ml. The analysis required a standard solution of sodium thiosulphate ($Na_2S_2O_3$). This was prepared as described in (121) by titrating against a known weight of potassium iodate. Excess iodide was added to the acidified solution and I_2 was liberated according to equation 4.7. Starch solution was used as indicator near the end point. Standard solutions of $Na_2S_2O_3$ have to be prepared by titration methods because, as there is uncertainty in the exact water content of the crystal, one cannot make a known solution by simple weighing. The calculations depends on the amount of iodate present, and so the iodide had to be free from iodate contamination. This was checked by adding dilute H_2SO_4 and starch to separate portions. No colour change was observed in each case, proving that the iodide was iodate free. The solution of $Na_2S_2O_3$ was 0.0998 $\pm$ 0.0002 N.

The chlorine analysis of NaOCl depends on the liberation of iodine from an excess solution of iodate-free potassium iodate. Acid was added. The titrant was standard

$Na_2S_2O_3$ solution, diluted to a suitable strength (0.01 N). The indicator was starch. The equations for the reactions are as follows:

$$OCl^- + 2I^- + 2H^+ \rightleftharpoons Cl^- + I_2 + H_2O \qquad (4.14)$$

$$2S_2O_3^{=} + I_2 \longrightarrow S_4O_6^{=} + 2I^- \qquad (4.15)$$

The NaOCl solution was found to contain 47 ppm free chlorine.

(b) Spectrophotometric analysis of samples

The spectrophotometer had to be calibrated prior to use. The stock solution of NaOCl was suitably diluted to different amounts in the range 1 to 50 μg/ml, and a Beers' law plot was obtained of transmission against concentration of solution. Each solution was compared with a reference containing the same volume of water as the NaOCl solution in the sample cell. Each cell also contained an equal amount of KI solution, acidified to promote the formation of the I_3^- ion.

$$I_2(aq) + I^- \rightleftharpoons I_3^- \qquad (4.16)$$

The iodide ion is displaced from solutions of its salts by the free chlorine that is present. The concentration of free chlorine is given by the amount of transmitted light at the absorption wavelength of the I_3^- ion, 353 λ. Instantaneous transmission readings were taken, and the light source was switched off quickly, in order to minimise any degradation of the solution by the photons. The Beers' Law curve obtained is shown in figure 4.9.

An attempt was made to correlate these readings directly with a titre. The titration was carried out immediately after the transmission reading had been obtained. Concentrations were near and below the limit of detectability and depended very much on the volume of

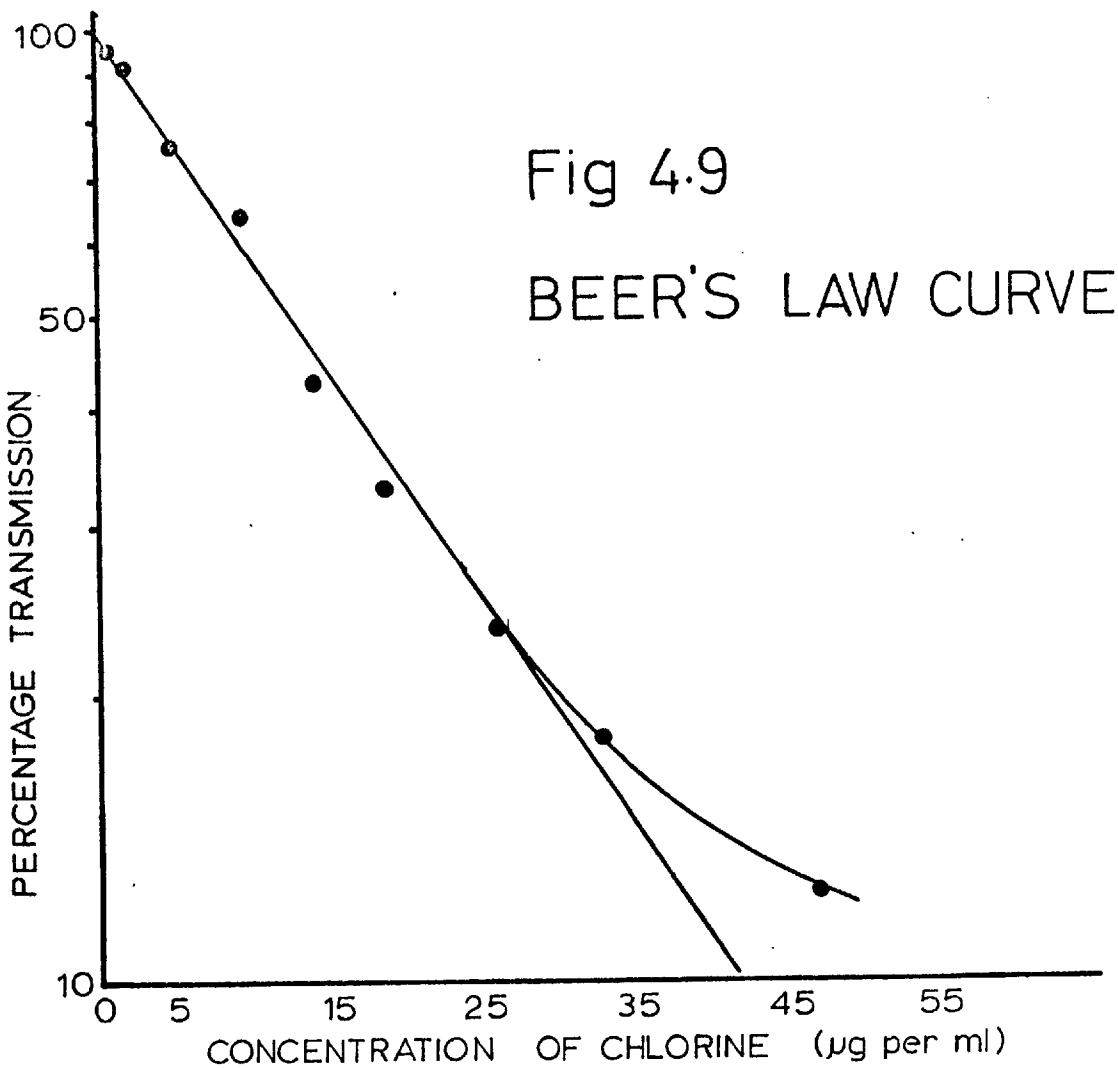


Fig 4.9

BEER'S LAW CURVE

solution in the sample cell. With a volume of 10 ml, the first solution that could be titrated was one that gave a transmission of 64%. The titre corresponded to two drops of $Na_2S_2O_3$ solution (0.001 N) from a 1 ml burette. It was felt that lower dilutions would have been too inaccurate to use. In smaller cells requiring only 4 ml solution, the sample giving a transmission of 92% was titrated with one drop of $Na_2S_2O_3$ solution. These results are shown in table 4.20. Large cells were used, in preference to small ones. Boundary effects are less, and the large volume permits greater dissipation of any heating effect produced by the light source. Transmissions were correlated with the concentration of chlorine, calculated from the concentration of the stock solution.

Table 4.20

Calibration curve values for the spectrophotometer (Beers' Law Curve)

Run	Transmission %	Titre(1) ml	Titre(2) ml	Conc(1) g/ml x 10^{-6}	Conc(2) g/ml x 10^{-6}	Conc(3) g/ml x 10^{-6}
1	95	-	-	-	-	0.941 ± 0.009
2	92	-	0.04	-	1.4	1.88 ± 0.02
3	75.7	-	0.10	-	3.5	4.71 ± 0.05
4	64.0	0.10	0.17	3.5	6.1	9.42 ± 0.09
5	42.2	0.22	-	7.9	-	14.10 ± 0.1
6	33.0	0.40	-	14.1	-	18.80 ± 0.2
7	26.0	0.44	-	15.6	-	23.5 ± 0.2
8	18.0	0.66	-	23.4	-	33.0 ± 0.3
9	12.5	0.87	1.09	30.9	38.3	47.1 ± 0.5

(1) are results for solutions of 10 ml volume.

(2) are results for solutions of 4 ml volume.

There is a maximum error of 0.04 ml in the titres (the volume of one drop).

The corresponding error in the concentrations, calculated from the titres, is 1.6×10^{-6} g/ml.

The last column gives the concentration, calculated from the dilution of the standard solution. The total standard error from pipetting, making up solutions, and the end point, was estimated to be 1%. These values are more accurate, and so a Beers' Law curve was plotted, using these in preference to the values obtained from titrations.

(c) Sample analysis

The portions of tablets used in the experiments were weighed prior to use. They were dissolved in the cells in 4 ml H_2O. 3.7×10^{-3} N KI and 0.1 N acetic acid were added and the solutions were analysed with a short burst of radiation, for reasons explained previously. The reference cell contained a tablet which had not been irradiated and was of comparable weight to that of the samples. Portions from the same tablet were compared. One was kept at room temperature. The other was heated for 6 h at 150 ^{o} C, when conditions corresponded to an increasing amount of iodate after an initial decrease (see figure 5.1). The samples were each compared with the reference, and then they were compared together. In the latter case, every time the heated sample was placed in the reference side, the transmission was less than 100%. This implied that the heated sample contained less free chlorine than the room temperature sample. This trend was independent of the slight differences in weight. However, if the

chlorine is responsible for the oxidation state adopted by the iodine as discussed in section 5.1.3, and since fission fragments penetrate to a depth of 15 μ (19) which is much less than the tablet thickness, any effects observed would be more likely to be proportional to surface area and not weight. The results are given in table 4.21. Values were read to ± 0.2 of a division.

Table 4.21

% Transmission values for KCl tablets

Run	Reference vs. Sample sample at room temp.	sample annealed	Annealed sample vs. room temp. sample
1	89.8	97.7	-
2	95.2	98.7	96.2
3	90.3	98.2	91.9
4	89.8	98.0	90.4
5	94.0	100.0	93.7
6	90.0	100.0	90.1

A value for the amount of free Cl_2 present in the room temperature samples was found from the Beers' Law curve. The average transmission for a heated sample was 91.5 (σ = 2.4). This corresponded to 1.8 μg Cl_2/10 ml. with a 20% to 40% error calculated from the curve. The number of chlorine molecules present was approximately 1.5×10^{16} .

Chapter 5. Results and Discussion.

Contents:

5.1 Results 225

5.1.1 Summary of annealing results 225

5.1.2 Error analysis 231

(a) Errors in estimating the flux

(i) Timing

(ii) Peak activity

(iii) Weighing

(iv) Efficiency

(v) Half life and capture cross section

(b) Errors in estimating the theoretical activity

(i) Flux

(ii) Values from the literature

(iii) Weight of U_3O_8

(iv) Fission cross-section for uranium

(v) Enrichment

(c) Errors in estimating disintegration rates

(d) Errors in estimating specific and fractional activities

(i) Carrier solutions

(ii) Specific activities

(iii) Fractional activities

5.1.3 A comparison of the results with those in the literature 238

(a) Annealing results

(b) Isotopic effect

(c) pH effect

(d) Pressure effect

(e) Water effect

(f) Chlorine effect

5.2 Discussion of Temperature Results 244

5.2.1 Theoretical discussion 244

(a) The basis for a model

(b) The model

(c) Fitting of model to experimental points

(d) Evaluation of rate constants

(e) Annealing at room temperatures

(f) Isotopic effect

5.2.2 Variation of concentration with chlorine potential 251
(a) Calculation of chlorine overpotential
(b) Calculation of concentration ratio
(c) Theoretical considerations
5.2.3 Thermodynamics 255
5.2.4 The ionic picture and diffusion 258
(a) Calculation of distances between species in the tablet
(b) The diffusion of V_K centres
(c) The diffusion of Cl^- ions

5.3 Effect of Water 265
5.3.1 Results and discussion 265

CHAPTER 5

RESULTS AND DISCUSSION

5.1. Results

5.1.1. Summary of the annealing results

The results of isothermally annealing the tablets at 100 °C, 150 °C and 200 °C is shown in figure 5.1. and table 5.1 for ^{131}I. The ordinate is a_5 which is the fraction of the total activity of the isotope (in question at a given time) that is formed as iodate at the same time. The abscissa shows the annealing time. Half of the table was kept at room temperature while the other portion was annealed, and so each point has an associated room temperature value. In order to relate all the points to each other,an average room temperature value of 0.177 ± 0.011 was found from all the room temperature results. Each a_5 value was adjusted by multiplying by the ratio of the average room temperature value to the room temperature value associated with each annealed fractional value. The errors on the figure are for one standard deviation in the adjusted a_5 value. These were calculated as discussed in section 5.1.2. The samples annealed at 100 °C were more active when analysed than those annealed at 150 °C and 200 °C. This reduced the error in the count rate, and thus the error in the a_5 values. Errors of $\sim$ 15% were found for samples annealed at 100 °C, whereas those annealed at other temperatures gave errors of $\sim$ 20-30%. Where several values for the same temperature and time had been obtained, their average value was included on the graph.

Fig 5.1 ISOTHERMAL ANNEALING CURVES FOR ^{131}I

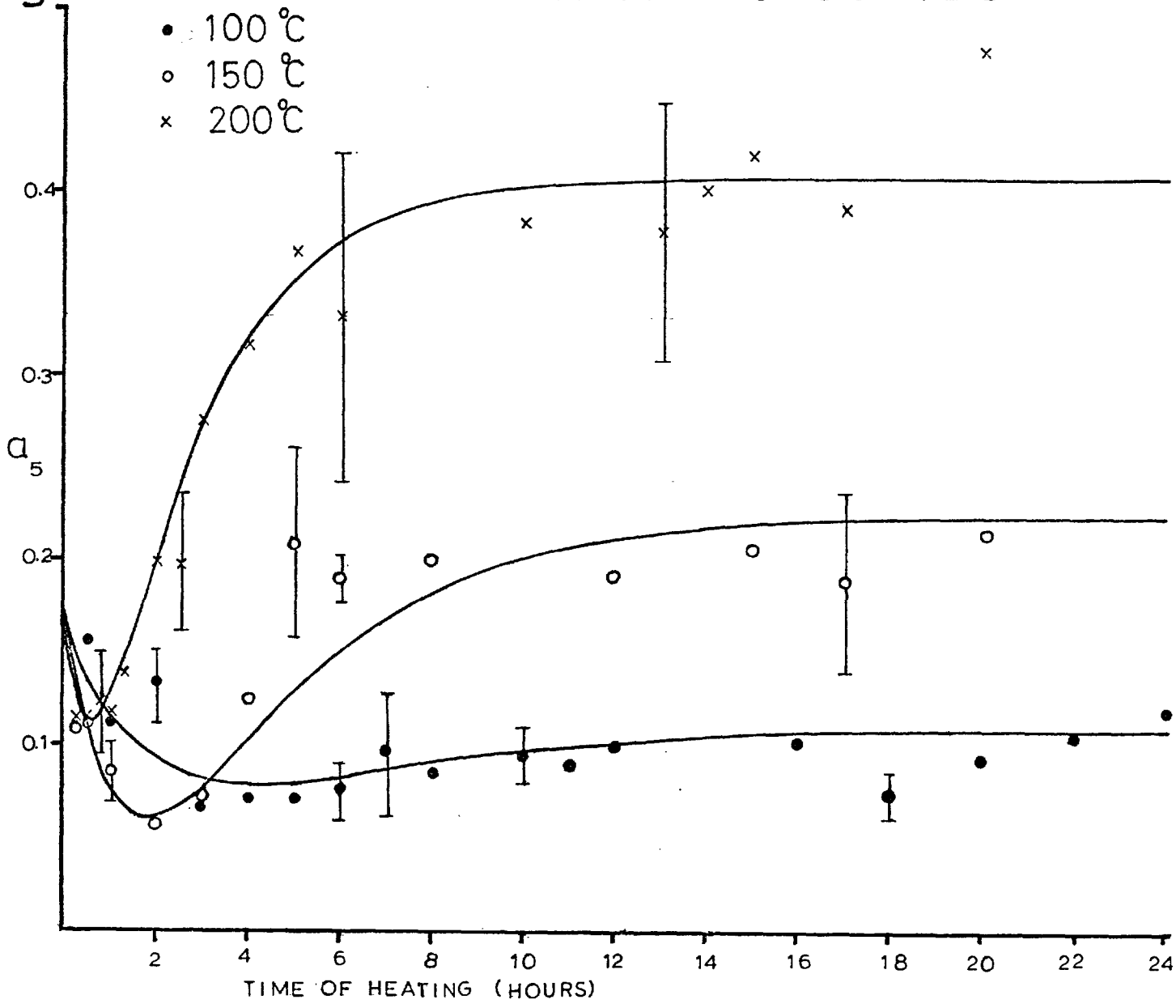
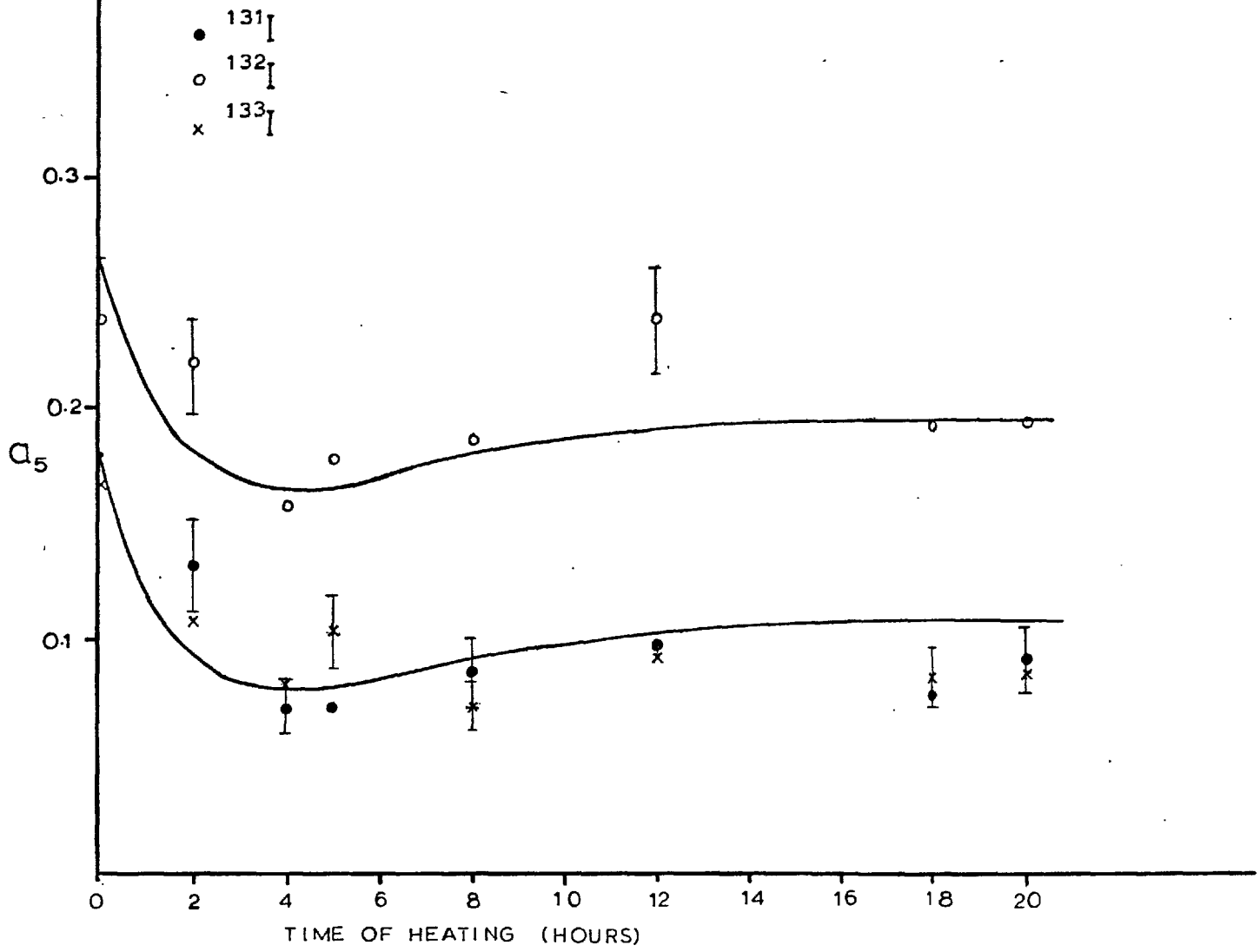


Fig 5.2 ANNEALING AT 100 °C FOR ^{131}I, ^{132}I, ^{133}I



The curves reveal an unexpected trend of an initial decrease in iodate fraction, followed by an increase for curves at 150 ^{o}C and 200 ^{o}C. This is consistent with the model proposed in section 5.2.1. The continuous lines shown in figure 5.1 and 5.2 are theoretical lines based on this model.

Where possible, values for ^{135}I, ^{132}I, ^{133}I were compared with the results for ^{131}I. The same general trend was observed for ^{132}I and ^{133}I, with ^{132}I exhibiting a constant increased iodate fraction. This is discussed in section 5.1.3 and shown in figure 5.2. Table 5.2 gives the values used to plot these curves. Values for ^{135}I were too scattered to be meaningful. This was because most analyses were carried out 40 hours after irradiation, when very little ^{135}I remained to be analysed. This problem did not arise with ^{132}I because, up to the time of analysis, it was being produced from the decay of its precursor ^{132}Te. As discussed in section 4.3.3 (c), the Te activity at the end of irradiation, which had produced the iodine activity at dissolution, is found and compared with the theoretical yield for ^{132}Te. ^{133}I has a long half life of 20.8 h, and little will have decayed before analysis.

Occasionally, a few results for annealing gave unusually high values. The pH investigation indicated that these observations were not related to variations in the acidity of the carrier. Similarly, the results for varying loads in compression of the tablets showed no similar trend. Since all tablets were irradiated under similar conditions in the reactor for the same length of time, the effect was not produced by radiation anomalies. The only effect investigated and revealing a similar trend was

that due to moisture.

Table 5.1

Isothermal annealing results for ^{131}I

	Time(h)	a_5(adjusted)	error(1σ)
	0	0.177	0.011
100°C			
	0.5	0.160	0.021
	1.0	0.112	0.004
	2.0	0.134	0.020
	3.0	0.068	0.005
	4.0	0.072	0.012
	5.0	0.072	0.011
	6.0	0.077	0.015
	7.0	0.098	0.036
	8.0	0.087	0.015
	10.0	0.097	0.015
	11.0	0.090	0.014
	12.0	0.100	0.016
	16.0	0.102	0.016
	18.0	0.076	0.013
	20.0	0.093	0.014
	22.0	0.107	0.016
	24.0	0.120	0.020
	40.0	0.122	0.017
150°C			
	0.25	0.109	0.032
	0.5	0.110	0.040
	1.0	0.087	0.016
	2.0	0.059	0.021
	3.0	0.076	0.038
	4.0	0.126	0.039
	5.0	0.211	0.052
	6.0	0.191	0.013
	8.0	0.200	0.015
	12.0	0.191	0.055
	15.0	0.208	0.049
	17.0	0.190	0.050
	20.1	0.214	0.057
	40.0	0.237	0.069

Table 5.1 (cont'd)

	Time(h)	a_5(adjusted)	error(1σ)
200°C			
	0.25	0.116	0.003
	0.5	0.115	0.015
	0.75	0.124	0.028
	1.0	0.119	0.026
	1.25	0.140	0.027
	2.0	0.201	0.038
	2.5	0.200	0.037
	3.0	0.277	0.059
	4.0	0.320	0.086
	5.0	0.370	0.11
	6.0	0.334	0.089
	10.0	0.390	0.10
	13.0	0.381	0.070
	14.0	0.404	0.079
	15.0	0.423	0.076
	17.0	0.394	0.082
	20.0	0.480	0.10
	40.0	0.489	0.09

Table 5.2

Annealing at 100°C for ^{131}I, ^{132}I, ^{133}I, ^{135}I

Time (h)	a_5 value			
	^{131}I	^{132}I	^{133}I	^{135}I
0.0	0.175	0.239	0.167	0.218
2.0	0.132	0.220	0.109	0.213
4.0	0.072	0.158	0.081	0.089
5.0	0.072	0.178	0.104	0.036
8.0	0.086	0.187	0.073	0.175
12.0	0.099	0.240	0.095	0.255
18.0	0.074	0.196	0.085	0.069
20.0	0.093	0.196	0.087	0.104

5.1.2. Error analysis

The error analysis of the annealing results can be divided into four main categories, as was the calculation. These are errors in estimates of a) the flux, b) the theoretical activities, c) the disintegration rates and d) the specific and fractional activities. Each division will be discussed in turn, and the relevance of its associated error to the final results will be indicated.

a) Errors in estimating the flux

Errors associated with this value are those in timing, in summing the activity under the ^{60}Co peak in the γ-spectrum, in the weight of cobalt, and in its γ-peak efficiency.

(i) Timing

Errors involved in timing were due mainly to non synchronisation of clocks at Imperial College with those at the Reactor Centre. The total error was estimated to be less than 5 min. This error will have a negligible effect on the results after the usual minimum cooling time of 24 h.

(ii) Peak activity

There is an error in choosing the correct channel number span and in estimating the background count. These are related to the resolution of the peak and activity of the sample. An account is given by Quittner (127) of several methods of base line construction under the peak. These require the fitting of various polynomial expressions to selected points, fixed distances either side of the peak. These methods are most suitable for samples with high background. In these experiments, the ratio of base line to total peak height was fairly low at $\sim$ 1:10. The simplest method

of baseline construction was used which involved drawing a straight line between the peak boundaries. The peak was assumed to be gaussian, and the background for each channel in the peak was taken as the average of the two counts at the peak boundaries.

The exact location of the boundaries is influenced by various experimental parameters, and the best way to determine them is from the experimental spectra. Slight changes in detector resolution, although not affecting the peak area, might impose statistical fluctuations on the positions of the boundaries, and increase the error in peak area determination. This is eliminated, by using a fixed number of channels for a given γ-energy, when summing the counts.

Let n_1 be the count in the first channel at the beginning of the peak and n_s be the count in the last channel where the peak ends. Let the peak occupy s channels.

$\therefore$ number of counts due to sample $= \sum_1^s n - \frac{(n_1 + n_s)s}{2}$

The error is taken as $\sqrt{\sum_1^s n + \frac{(n_1 + n_s)s}{2}}$

The error in the base area ΔB is larger than the simple statistical error of B counts. More correctly $B \simeq k\sqrt{B}$ where k depends on the method used for baseline construction. For the simple case discussed here

$$\Delta B \simeq \frac{(s - 3)B}{2}$$

In these experimental counts, typical values for s are as follows:

^{131}I, s = 10 and so the error is not underestimated.

^{132}I, s = 10 and the error is underestimated. However, the

discrepancy becomes negligible for small background counts.

^{133}I, s = 13. In this case, the count rate is much higher than in the previous cases, and again the discrepancy becomes negligible.

The error in choosing the correct span was investigated by finding the number of counts and associated error for the "best span" (which was judged by eye) and then for larger and smaller spans involving up to four channels on either side of the peak. The results are given in table 5.3. It can be seen that the "best span" and larger span including two channels either side give the largest number of counts and low associated errors. The error in the best span is slightly smaller. The difference between the two counts is 5.7%, and this is taken as an indication of the error in choosing the correct channel number span. In this case, this is 2% higher than the calculated error.

Table 5.3

Determination of the error associated with choosing the "best span"

		^{131}I		^{133}I	
		count rate	error(1σ)	count rate	error(1σ)
"best span"		7.99	0.31	43.20	0.46
smaller span:					
1 channel each	side	6.41	0.29	40.99	0.46
2 " "	"	3.26	0.27	37.93	0.45
3 " "	"	-	-	37.90	0.44
larger span:					
1 channel each	side	7.17	0.34	44.80	0.46
2 " "	"	8.44	0.36	40.84	0.48
3 " "	"	3.16	0.37	42.13	0.48

All samples were counted for 500 s, which gave a background to peak ratio of 1:10. This was considered to

give a count rate of reasonable statistical accuracy.

As discussed in section 4.4.2 and shown in table 4.16, there was no alteration in the count rate for maximum credible accidental displacements. Therefore, errors in positioning samples were negligible.

Another source of error was thought to be in accidentally shaking the container before the count. This could result in some of the active solution sticking to the top of the counting vessel, and thus remaining a few mm above the main bulk of the liquid during the count. A sample was counted, shaken, replaced on the counting tray, and counted again. This made little difference to the count rate, as shown in table 5.4 where Run 2 is the count after shaking. It was concluded that this source of error was negligible.

Table 5.4

Effect of shaking the sample before the count

Run	count rate ^{131}I	error(1σ)	count rate ^{133}I	error(1σ)
1	7.99	0.31	43.20	0.46
2	8.27	0.31	42.00	0.46

(iii) Weighing

The standard error incorporated into the two weighings of cobalt was 1.4×10^{-4} g, since the balance weighed to 0.0001 g.

(iv) Efficiency

These errors were minimised by using a graphical method for determining the efficiency. Periodical determinations were made on the efficiency of the machine in the range 0.3 to 1.3 MeV. The standard sources employed and their γ-ray energies and intensities are given in table

An error of 10% was deduced from the graph and applied to the samples. See figure 4.5.

(iv) Fission cross-section for uranium

A value of 580 barns was used, although this can vary by as much as 10%, depending on the fast fission flux.

(v) Enrichment

The final source of error is in the enrichment of uranium. An experiment was undertaken to establish the enrichment of the uranium compound from the activity of a selection of fission products, resulting from the irradiation of a known amount of U_3O_8. Errors in weighing and activity, as calculated from the area under the curve in the γ-spectrum, were too great to establish the enrichment precisely. Also, an analysis of the α-spectra was unsuccessful, due to incomplete resolution of the peaks. A value of 80% was used,which was the value supplied with the solution. Any errors in this will only affect absolute results and will not alter comparisons.

c) Errors in estimating disintegration rates

These are due to errors in efficiency values, timing and summing of the peak activity. These have all been discussed above.

d) Errors in estimating specific and fractional activities

(i) Carrier solutions

There is an error associated with the carrier solutions

4.14. These values were supplied by the Radiochemical Centre and agree well with the literature (122).

However, although an exponential relationship was expected between the efficiency and γ-ray energies, this was not apparent for ^{133}Ba. The points calculated for this isotope deviated randomly from the exponential curve, and this implied that errors existed in the relative intensities of the peaks and, possibly, also in their absolute γ-ray energies. See figure 4.8.

The efficiency of the machine was expected to be constant over several months. Efficiencies, taken at the beginning and end of each set of values at a particular temperature, were very similar and were combined to give an average efficiency curve. Therefore, three efficiency curves were used,and each one was employed to calculate the results at the three annealing temperatures.

(v) Half-life and capture cross section values for ^{60}Co were taken from the literature.

b) Errors in estimating the theoretical activity

(i) Flux

One source of error will be in the flux, since this value is used to calculate the theoretical activity.

(ii) Values from the literature

Literature values for fission yields and half lives are well established and their errors were ignored. Provided the same values are used throughout the experimental work, these will be systematic errors and will be of no significance in a comparison of results.

(iii) Weight of U_3O_8

The error in the uranium oxide weight was due to absorption of α-particles by the layer (see section 4.2.1).

P, Q, R. This involves errors in weighing and errors in making up and pipetting out the solutions. The last error was found to be most significant. A 3% error was assumed in the calculation. Later experiments, which involved the weighing of successively pipetted solutions of 5 ml, revealed an experimental error of 0.5% and a systematic error of 0.8%.

(ii) Specific activities

This involved only the error in the total iodate or iodide activity, as calculated from the activity counts, with all the associated errors and the error in the weight of iodine in the carrier solution.

(iii) Fractional activities

The fractional activity has been defined as the fraction of the total activity of the isotope in question at a given time that is formed as iodate at the same time. For a typical calculation (as in appendix 1) the standard deviation associated with the iodide fraction was 6.74% and that associated with the iodate fraction was 7.72%. These values are used in preference to the larger error of~18% which is obtained by working systematically through the calculation. This last error result is computed in the final steps of the program. At this stage the final error has incorporated that error associated with the theoretical activity. However, this theoretical activity cancels out when calculating the value for the fractional iodate activity.

The final error resulted from the sum of the error in the annealed fractional iodate value, and the error in the normalising ratio of room temperature fractional iodate values for that sample. Although the errors, calculated

in this fashion, were large, sufficient experiments had been performed to establish the trend observed in the annealing results.

5.1.3. A comparison of the results with those in the literature

(a) Annealing results

Several workers (36, 96-100) have reported an oxidising effect due to thermal annealing. This observation is also reflected here. The initial increase in reduced species can be compared with variations in annealing observed in refs. 39, 91-94. See section 3.3.

It has been reported by some investigators (35, 36) that the total activity of the samples decreased during thermal annealing. This was attributed to the presence of iodine in a form not present in the carrier solution, which was added after transfer annealing reactions had taken place in KIO_3 and $NaIO_3.H_2O$ doped with ^{131}I as iodide.

No loss in activity was found for the experiments presented here. Table 5.5 is a selection of results for several samples which were heated to 200 ^{o}C for varying times.

As discussed in section 4.3.1, only iodide and iodate states of iodine were expected to be present in any appreciable quantity, under the conditions of the experimental analysis. The mean of the values given in the last column in table 5.5 is 1.056 ($1\sigma = 0.341$). Thus, there seems to be no evidence to suggest that either form of iodine has been lost by heating.

Table 5.5

No form of iodine is being lost by the thermal annealing process

Time of heating (h)	$\frac{A(H)}{A(R.T.)}$	$\frac{B(H)}{B(R.T.)}$	$\frac{A(H) + B(H)}{A(R.T.) + B(R.T.)}$
0.25	0.907	0.547	0.817
0.50	1.190	0.838	1.130
0.75	0.739	0.571	0.707
1.0	1.733	1.082	1.611
2.0	1.098	1.386	1.145
3.0	1.312	2.303	1.465
15.0	0.529	1.813	0.754
40.0	0.500	2.26	0.820

A = fraction of theoretical activity for ^{131}I that is iodide

B = fraction of theoretical activity for ^{131}I that is iodate

H = portion of tablet that was heated

R.T. = portion of tablet that was kept at room temperature

(b) Isotopic effect

All the isotopes studied ^{131}I, ^{132}I and ^{133}I were found to be predominantly in the reduced form. No isotopic effect could be determined between ^{131}I and ^{133}I, within the limits of experimental error. An isotopic effect was observed for ^{132}I which appeared in a more oxidised form throughout the annealing. This is in contrast to Hall and Walton's work (34) where the same isotopes appeared in the mainly oxidised state. However, ^{132}I appeared less oxidised than the other isotopes.

Hall and Walton were investigating the neutron irradiation

of uranyl iodates. The presence of oxygen in the lattice and radiolysis products from irradiation which could act as electron traps might explain the observance of a mainly oxidised form for the isotopes. The observation of an isotopic effect for ^{132}I is probably due to its long lived precursor ^{132}Te ($t_{\frac{1}{2}}$ = 77h). K_2TeO_3(aq) is thermodynamically more stable than KIO_3 (aq), and it could be expected that the same will apply to the solid state. KIO_3 (s) is thermodynamically more stable than KI (s). Therefore, in view of its long existence as Te, ^{132}I might be expected to be more oxidised than the other isotopes, which spend shorter times as Te.

Table 5.6

Thermodynamical values (128, 129)

	H_f^o kJ mole^{-1}
KIO_3(s)	- 508
KI (s)	- 328
KIO_3(aq)	- 481
K_2TeO_3(aq)	-1095

(c) pH effect

Experiments have been reported (69,70) which showed an effect in the annealing of OH^- doped crystals.

Kasrai and Maddock (44) have shown that, in complete absence of both air and carriers, dissolution in an acid medium promotes oxidation of all active sulphur to sulphate. The same conditions, operating on neutral and alkaline solutions, reveal the presence of a substantial amount of sulphide. They attribute such reactions to the presence of a pH dependent reaction involving oxidising point

defects in the crystal.

In the pH experiments reported here, the crystals were doped to 2.3 mole % with KOH. The initial valence distribution was not altered. However, changes in the annealing curves which could have occurred with these samples were not investigated. The concentration of KOH impurity in the KCl powder used (not doped) was estimated to be at a maximum of 0.05 ml N KOH. This represents over 0.05×10^{-3} mole % KOH. From the literature, oxidised fractions are reported to be low at both the concentrations of OH^- used in these experiments (312, 27) and this fact could explain the observation from the results of no significant pH effect.

(d) Pressure effect

Bogdanov and Olevski (106) found no change in valence distribution until a 1.3% compression of the samples was reached, when the density of defects had been increased tenfold. Further increase in pressure produced a slow increase in reduced species.

The relations between this work and the results reported here (section 4.2.2, table 4.7) due to a variation in pressing load is obscure since the % compression and density of defects is not known in the latter case. However, the trend in the results of the former work seem to validate the conclusion from the results reported here, that there is no correlation between the load applied in pressing the tablets and the iodine valency states adopted in the crystal.

(e) Water effect

Many references have been found for the enhancement of retention or increase in the oxidised species by water.

These have been discussed in section 3.3.1. However, water entering the lattice as water of crystallisation is not relevant, since KCl forms no known hydrate.

One can envisage the water moving through dislocations and voids or vacancies to act as a sheath of saturated solution around groups of lattice atoms. Radiolysis due to γ-rays and β- decay of entities in the crystal might cause decomposition of the water molecules viz. $H_2O \longrightarrow e^-$, H^+, $OH^\cdot$, H_2O_2, H_2 and some of these oxidising products might diffuse to neighbouring iodine fragments before recombination reactions occur to create more oxidising forms of iodine.

The lattice order may be destroyed as in references 44, 61. Oxidising entities are rendered more mobile and have a greater chance of reacting with iodine.

The observation from table 4.18 that tablets were affected by moisture only if it was introduced just before analysis, implied that water formed a protective sheath around portions of the crystal during dissolution in the carrier solution. The survival of the $OH^\cdot$ radical would provide an electron sink in the vicinity of the iodine fragment, which would then have a greater chance of combining with the oxidising defects, after the initial protecting action of the water had been dissipated. A reduced fraction is also observed because the water sheath does not protect every iodine fragment. Both electrons and holes are in competition for these fragments.

The importance of wetting the side of the tablet which had been irradiated nearer the U_3O_8 film (section 4.5.1) implies a direct reaction between the water and the iodine fission fragment.

An increase in the oxidised fraction of the wet tablet was observed if it had been γ-irradiated prior to being reactor irradiated. (Section 4.5.1). This effect can be attributed to the creation of oxidising defects by the γ-flux which contributed to the damage produced in the reactor. Fairweather and Fletcher (130) have reported such an additive effect from γ and reactor irradiation of a KCl tablet.

(f) Chlorine effect

Cifka and Brucokova (93) have suggested that an increased oxidation effect in $BaCl_2$, when compared to effects in alkali halides, could be attributed to more free chlorine being produced in the former with ionizing radiation.

Bradbury and Leicester (131) reported that an investigation into the effect of reactor irradiation on KCl pellets showed that more chlorine was produced in pellets that did not suffer concurrent fission product damage. It seemed, from this observation, that fission product damage helped to anneal the damage producing free chlorine.

The results of the chlorine investigation reported here have shown a disappearance of chlorine on annealing of the irradiated sample and a corresponding increase in oxidised fraction. The chlorine might have only been reduced to below the limits of detectability, approximately 1.7×10^{15} molecules of Cl_2. The observed levels of chlorine were at 1.7×10^{17} molecules.

5.2. Discussion of temperature results

5.2.1. Theoretical discussion

(a) The basis for a model

The shape of the annealing curves indicates that at least two competing reactions are occurring. The process which dominates at the beginning of the annealing leads to a more reduced species. After a certain time during the annealing, which depends on temperature, oxidising processes begin to be significant. At this point in the annealing curve, the free Cl_2 concentration falls below the limit of detectability i.e. by at least 100 fold. Thus, it seems that the free chlorine produced by the irradiation, or the mobilization of defects such as Cl_2^- V_K centres, could be responsible for the oxidising effect observed.

Complete oxidation does not occur. A plateau value is reached which is temperature dependent and suggests that, except for ^{132}I at 200 °C, the reduced species predominates for all the isotopes investigated at the three temperatures 100 °C, 150 °C and 200 °C.

A model was set up along these lines which was able to account satisfactorily for the shape of the annealing curves.

(b) The model

The model is based on an initial concentration of defects, such as displaced chloride ions x_1^o, which are able to cause reduction or oxidation of the iodine fragments. The displaced chloride causing reduction (e.g. Cl_2^-) is represented by x_1 and that causing oxidation (e.g. Cl_2) is represented by x_2 where

$$x_1^o = x_1 + x_2 \qquad (5.1)$$

It is further assumed that the reducing form can change into the oxidising form with a rate constant k. Assuming that the defects are in the reducing state initially,

$$\frac{dx_1}{dt} = -k\,x_1 \qquad (5.2)$$

Integrating and letting $x_1 = x_1^o$ when $t = 0$

$$x_1 = x_1^o\, e^{-kt} \qquad (5.3)$$

Similarly for the species causing oxidation

$$\frac{dx_2}{dt} = +k\,x_1 \qquad (5.4)$$

Integrating and letting $x_2 = 0$ when $t = 0$

$$x_2 = x_1^o(1 - e^{-kt}) \qquad (5.5)$$

The results, plotted in figure 5.1, show that the iodine never goes completely to one valency state, but adopts a steady condition in both oxidised and reduced states. This suggests that the labile form, initially present, changes to a non labile form in the course of the annealing. It is proposed that this change could be a first order process, which may be represented by an equation of the form

$$\frac{da}{dt} = -P\,a \qquad (5.6)$$

Integrating and letting $a = a_o$ when $t = 0$

$$a = a_o e^{-Pt} \qquad (5.7)$$

P is the rate at which the labile iodine reacts with its surroundings. It eventually adopts a non labile form, which is insensitive to the redox processes of the displaced chloride.

a_o is the number of iodine atoms in the labile state and present initially.

a is the number of radioactive iodine atoms present in the labile state after a time t of annealing at temperature T °C.
a_1' is the number of radioactive iodine fragments that exchange with iodide carrier after time t.
a_5' is the number of radioactive iodine fragments that exchange with iodate carrier after time t

$$a_o = a_1' + a_5' \qquad (5.8)$$

This equation assumes that there is no loss in iodine activity as another unidentified form, which was true for these experiments.

The values obtained from experiment are the fractional activities a_1 and a_5 (corresponding to P and Q in the computer output)

$$a_1 = a_1'/a_o$$

and

$$a = a_5'/a_o$$

$\therefore$

$$a_1 + a_5 = 1$$

Reduced iodine is produced by reaction between the labile iodine a and the reduced form of displaced chloride ions, and removed by reaction with the oxidised form of displaced ions. This is a second order reaction with a rate constant r and may be expressed as

$$\frac{da_1'}{dt} = r\,(x_1 a - x_2 a) \qquad (5.9)$$

Similarly, whether the oxidised form is produced or not is determined by the following process

$$\frac{da_5'}{dt} = r\,(x_2 a - x_1 a) \qquad (5.10)$$

Substituting for x_1, x_2, a and a_5'

$$\frac{da_5}{dt} = r\,x_1^o(e^{-Pt} - 2e^{-(k+P)t}) \qquad (5.11)$$

Integration gives

$$a_5 = rx_1^o \left(- \frac{e^{-Pt}}{P} + \frac{2}{(k + P)} e^{-(P + k)t} \right) + C \qquad (5.12)$$

where C is a constant of integration

When $t = 0$, $a_5 = a_5^o$

$$\therefore \quad C = a_5^o - rx_1^o \left(\frac{2}{(k + P)} - \frac{1}{P} \right) \qquad (5.13)$$

$$a_5 = a_5^o - rx_1^o \left[\frac{2}{(k + P)} (1 - e)^{-(k + P)t} - \frac{1}{P}(1 - e^{-Pt}) \right] \qquad (5.14)$$

When t is small

$$a_5 = a_5^o - rx_1^o t \qquad (5.15)$$

When t is large

$$a_5^\infty = a_5^o + rx_1^o \frac{(k - P)}{P(k + P)} \qquad (5.16)$$

a_5 is a minimum when

$$\frac{da_5}{dt} = 0$$

i.e. when

$$e^{-kt} = \tfrac{1}{2}, \quad kt = 0.693 \qquad (5.17)$$

(c) Fitting of model to experimental points

Equations 5.15, 5.16 and 5.17 determine the values for r, k, P. The initial value a_5^o, the plateau value a_5^∞, and the time of annealing at which a minimum value for a_5 occurs are found from figure 5.1.

For small values of t, equation(5.15) approximates to a straight line, with slope $- rx_1$. The initial tangent to the curve has a similar slope which is found from $(a_5 - a_5^o)/t$ where a_5 is the iodate value, taken from the line, for small t.

These values are substituted into equation (5.14), which is evaluated for different annealing times t.

An average initial iodate value, found by averaging all the room temperature iodate values, was used. This was 0.177 (σ = 0.011).

The values shown in table 5.7 were found to give the best fit to the experimental points.

Table 5.7

Values used for "best fit" to experimental points

	100°C	150°C	200°C
k	0.173	0.385	1.155
P	0.290	0.322	0.470
rx_1^o	0.077	0.174	0.26
minimum	4.0	1.8	0.6
a_5^∞	0.11	0.225	0.41
ln k	-1.753	-0.955	0.144
ln P	-1.236	-1.133	-0.755
ln (rx_1^o)	-2.564	-1.749	-1.347
ln (r)	-1.194	-0.378	0.024

(d) Evaluation of rate constants

An Arrhenius plot was made of the rate constants. This is shown in figure 5.3. The values used to plot this are given in table 5.7. If x_1^o is taken to be the amount of free chlorine found in the room temperature samples, i.e. 0.254 moles litre^{-1}, then ln r has the values shown in the table. The activation energies, for the reactions associated with each rate constant, can be found as follows.

If the rate constant k is related to the activation energy Q by Arrhenius's equation, then

$$k = A \exp(-Q/RT) \qquad (5.18)$$

where A is a constant and R is the gas constant, and is taken as 8.318 J degree^{-1} mole^{-1}. T is in °K.

$$\ln k = \ln A - Q/RT \qquad (5.19)$$

The activation energy can be found from equation 5.19 for each rate constant, by selecting two values of ln k from

Fig 5.3
ARRHENIUS PLOT

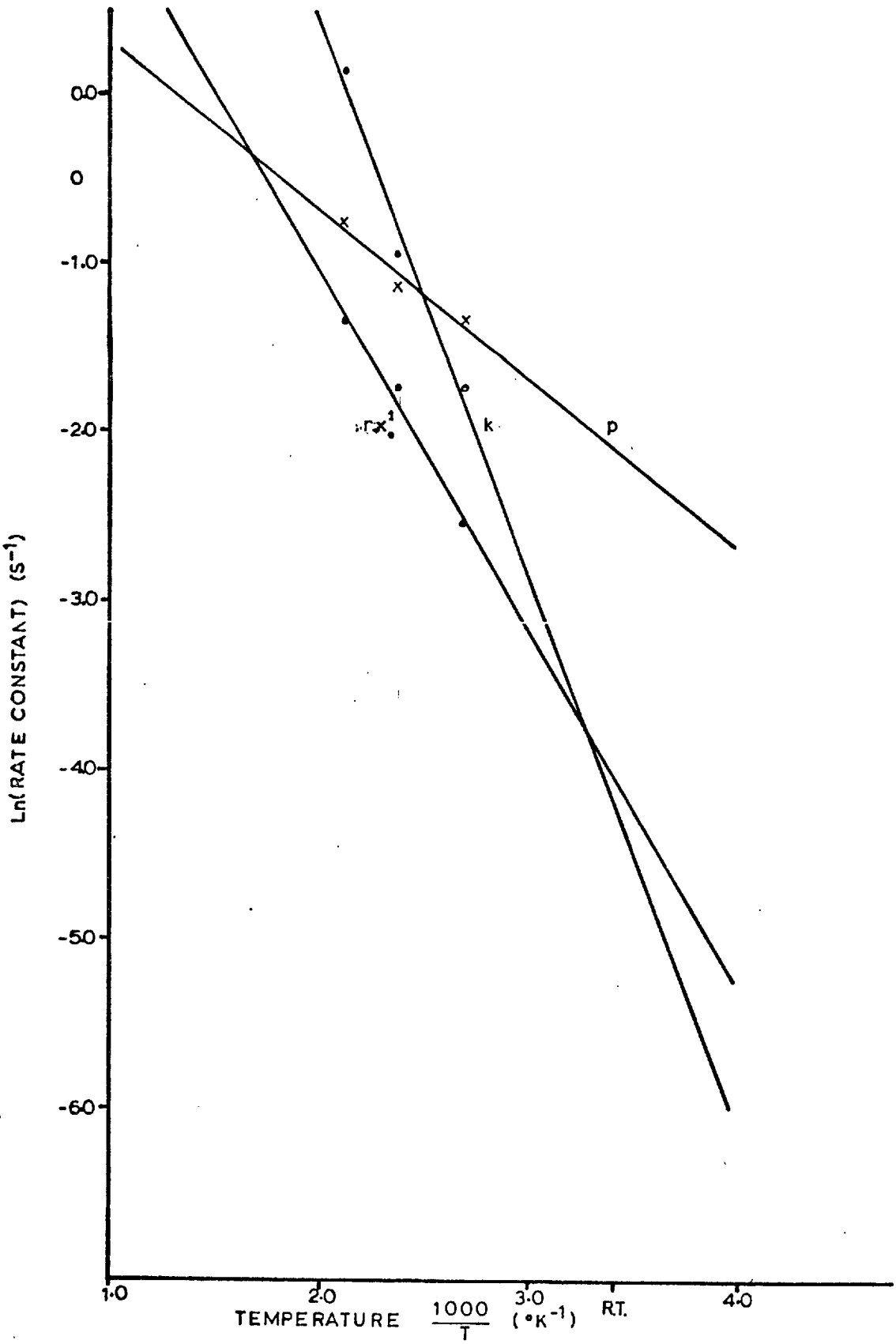


figure 5.3 and substituting each in turn into equation 5.19. Subtraction of the two equations and rearrangement yields a value for Q. The values obtained were

Q_r = 17.58 kJoule ~~degree~~$^{-1}$ mole^{-1} σ = 4.19

Q_p = 8.50 " " " σ = 3.85

Q_k = 27.21 " " " σ = 8.79

(e) Annealing at room temperature

This analysis of the results implies that a certain amount of annealing can take place at any temperature, as has been suggested in the literature. The value for a_5^o used in obtaining these results is, more correctly, the value for a_5 after thermal annealing at room temperature. This is taken as commencing immediately after irradiation. Using the appropriate values for the rate constants k, p and rx_1^o at room temperature, which were obtained from the Arrhenius plot, an annealing curve was plotted for the sample. The total annealing time was taken to be 25 h. which corresponded to the storage time for most of the samples. If T^oK = 294.12, the corresponding value for k is 0.015. Substitution of this value into equation 12 shows that the minimum will occur at t = 46.67 h. The value for a_5^o can be found from equation 9, since it is known that the value for a_5 at t = 25 h. is 0.177, and a_5^o is found to be 0.289. Substitution of this value into equation (11) yields a_5^∞ (0.175). Now the minimum value for a_5 can be found from equation (9), a^{min} = 0.175.

From this analysis, it can be seen that there is an initial decrease in the iodate fraction. This reaches a value of 0.18 - 0.175 at the end of the usual storage time for the samples. The value for a_5^o, obtained from this analysis, still does not reflect the initial state of the

unreacted iodine fragment obtained directly from fission because there will also have been a certain amount of annealing during irradiation, both thermal and radiative.

(f) Isotopic effect

An isotopic effect has been reported for ^{132}I where this isotope seems to have a more oxidised value at the beginning of the thermal annealing curves, but its behaviour is similar to that of ^{131}I and ^{133}I. The isotopic effect can be incorporated into the theoretical model, since it is possible to alter a_5^{∞} and a_5^{o}, while giving all the shape determining parameters the same values they had in the analysis of the annealing curves for ^{131}I and ^{133}I at the same temperature.

Although the analysis is very hypothetical, there does not appear to be a simpler model that is consistent with the experimental observations.

5.2.2. Variation of concentration with chlorine potential

Long and Stanaway (32) have predicted the behaviour of typical reactor materials and uranium salts in a molten salt reactor core. In order to do this, they constructed a chlorine potential diagram (see figure 2.3). This relates the concentration of the elements in question to the chlorine overpotential in the core. Thus, the oxidation states for typical reactor materials at different chlorine concentrations, or chlorine potentials, can be found.

From the results reported in this work, a prediction of the fission product iodine behaviour can also be made, following the method of Long and Stanaway. An equation which describes the oxidation of iodide by free chlorine to iodate

is

$$3Cl_2 + 2KI + 3H_2O \longrightarrow 2KIO_3 + 6HCl \qquad (5.20)$$

The equilibrium constant $K = \dfrac{\left[a_{KIO_3}\right]^2 \left[a_{HCl}\right]^6}{\left[a_{Cl_2}\right]^3 \left[a_{KI}\right]^2 \left[a_{H_2O}\right]^3}$

The free energy of formation for KIO_3 is given by

$$-\Delta F^f(KIO_3) = RT \ln K$$

$$\therefore \quad RT \ln K = 2\,RT \ln\left(\frac{\left[a_{KIO_3}\right]}{\left[a_{KI}\right]}\right) + 3\,RT \ln\left(\frac{\left[a_{HCl}\right]^2}{\left[a_{H_2O}\right]}\right)$$

$$- 3\,RT \ln p\,(Cl_2)$$

The chlorine overpotential is defined as $RT \ln p\,(Cl_2)$ where $p\,(Cl_2)$ is the partial pressure due to gaseous chlorine in the system.

$$\therefore \quad RT \ln p(Cl_2)_e = \tfrac{1}{3}\Delta F^f(KIO_3) + \tfrac{2}{3} RT \ln\left(\frac{\left[a_{KIO_3}\right]}{\left[a_{KI}\right]}\right) + RT \ln\left(\frac{\left[a_{HCl}\right]}{\left[a_{H_2O}\right]}\right)$$

In figure 2.3, the chlorine potential is plotted against the concentration ratio of KIO_3 to KI. This assumes that the chemical activity coefficients are unity, and for simplicity ignores the last term. The equations for the general case of metal A forming chloride ACl_Z is

$$\frac{1}{Z} A(s) + \tfrac{1}{2}Cl_2(g) = \frac{1}{Z} ACl_Z(d)$$

$$RT \ln p(Cl_2) = 2\Delta F^f(ACl_Z) + \frac{2}{Z} RT \ln (a_{ACl_Z}/a_A)$$

From this, it can be seen that the value of Z determines the slope of the line. Also Z represents the difference in oxidation state of the element in its different valency forms. For the case of the oxidation of iodide to iodate by free chlorine, Z = 3. Therefore, the line representing fission

fragment iodine will have a slope equal to other materials with Z = 3, such as the oxidation of metallic uranium to UCl_3. The position of this line can now be defined precisely, since its slope is known and the coordinates of a point on the line can be found from the following calculation.

(a) Calculation of chlorine overpotential

The following experimental results have been quoted elsewhere.

Amount of free chlorine at 20 °C (section 4.5.3) = 1.53×10^{16} molecules

Volume of tablet (section 4.2.2) = 0.95 cm^3

∴ Pressure due to chlorine at 0 °C = 5.96×10^{-4} at.

The pressure at 1000 °K was found in order to compare with the results of Long and Stanaway. In default of any more definitive information, it is suggested that the potential of the chlorine is equivalent to the partial pressure it would exert if it were present as free chlorine within the volume of the KCl tablet.

The gas constant R was taken as 8.318 J $degree^{-1}$ $mole^{-1}$

∴ At 1000 °K

$$RT \ln p(Cl_2) = -51.279 \text{ kJ mole}^{-1}$$

(b) Calculation of concentration ratio

The concentration ratio is given by the fractional radioactivities of each valence state.

$$\therefore \quad \frac{[IO_3^-]}{[I^-]} = \frac{0.177}{0.823} = 0.215$$

This is the ratio of the average room temperature results obtained after 25 h of thermal annealing at room temperature. It has been shown, previously, that room temperature annealing has little effect on the fractional activities, and so these values can be considered as representing the situation

after irradiation. Values at 1000 ^{o}K would be preferred to these, but they were not available. However, a large increase in iodate fraction (as occurs after a relatively short annealing time at 473 ^{o}K) would only change the concentration ratio by an order of magnitude, and would not seriously affect the position of the line on the diagram.

The line represented by these coordinates and of slope Z = 3 was plotted beside Long and Stanaway's results in figure 2.3.

(c) Theoretical considerations

The validity of such a line for iodine on the diagram can be checked theoretically. When the concentrations of the different valency forms are equal (assuming unit activity coefficient) the chlorine overpotential can be found from the free energy of formation of KIO_3.

i.e. $$RT \ln p\,(Cl_2) = \tfrac{1}{3}\Delta F^{f}(KIO_3)$$

Reference 128 gives the free energies of formation for $Cl_2(g)$ and $KIO_3(aq)$ at 298 ^{o}K. Application of the well known relation $\Delta F = \Delta H - T\Delta S$ allows these values to be calculated at 1000 ^{o}K.

$$\therefore \Delta F_{1000}\ (Cl_2)_g = -223.07 \text{ kJ mole}^{-1}$$

$$\Delta F_{1000}\ (KIO_3)_{aq} = -699.90 \text{ kJ mole}^{-1}$$

Reference 129 gives the free energies of formation for the other compounds in the equation at 1000 ^{o}K.

$$\Delta F_{1000}\ (KI)_{liq} = -269.16 \text{ kJ mole}^{-1}$$

$$\Delta F_{1000}\ (H_2O)_g = -192.72 \text{ " "}$$

$$\Delta F_{1000}\ (HCl)_g = -100.85 \text{ " "}$$

$\therefore$ For the reaction represented by equation 5.20

$$\Delta F^{f}_{1000}\ (KIO_3) = -73.09 \text{ kJ mole}^{-1}$$

This corresponds to

$$[IO_3^-]/[I^-] = 1.0$$

The point with these coordinates lies very near the experimental line, and justifies the position of the line on the diagram. This agreement is probably fortuitous, in view of the highly hypothetical assumptions used to find the chlorine activity in (a).

In principle, the diagram can now be used to predict the behaviour of fission product iodine with respect to other materials in the reactor. In practice, the corrosive effects of the fission products on the molten salt containment will be a major development problem.

5.2.3. Thermodynamics

The model discussed in section 4.2.2 suggests that fission fragment iodine is initially present in the thermalised lattice as a localised energetic ion of undetermined oxidation state. The subsequent motion of defect centres determines the valency by reacting with the fission fragment. V_k centres are proposed as being defects that could act in the way described by the model. The thermodynamical validity of such a proposal is now considered.

A V_k centre is described in the literature as a self trapped electronic hole. It can be envisaged as a $(Cl_2)^-$ ion on the site of two halogen ions in the lattice. Therefore the hole belongs predominantly to two neighbouring negative ions. Other similar centres have also been reported, such as the V_H centre, which is created along with the V_k centre, and is chemically equivalent to an interstitial halogen atom. However, these centres will be dismissed for the sake of simplicity.

The reaction of the defect V_k centre to produce

iodide or iodate is represented as follows

$$I + Cl_2^- \longrightarrow I^- + Cl_2 \qquad (5.21)$$

$$5I + 5Cl_2^- \longrightarrow IOCl^- + I^{5+} \qquad (5.22a)$$

$$I^{5+} + 3H_2O \longrightarrow IO_3^- + 6H^+ \qquad (5.22b)$$

The standard heat of formation for I^{5+} was found from the heat of formation of an iodine atom and the fifth ionisation potential. The latter was calculated on the energy required to remove the outer five electrons from the neutral atom. Several of the ionisation potentials needed were not reported in the literature. A graph was constructed (see figure 5.4) which related successive ionisation values to each other for an increase in ionisation. Graphs were drawn for Cl, Br and I. Any missing values were interpolated from the graph, since the halogens have similar electronic structures and can be expected to follow the same trend.

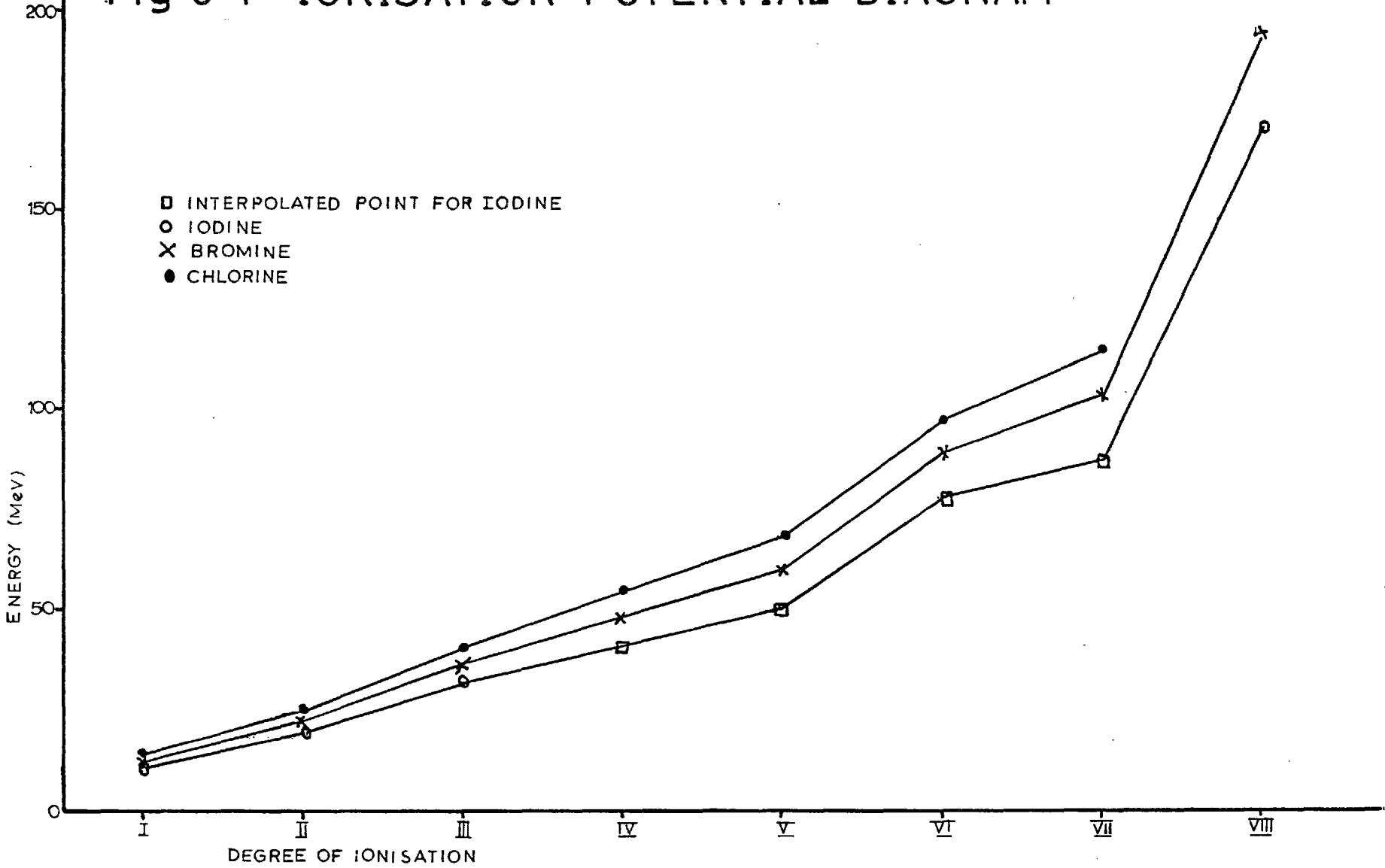
The heat of formation for Cl_2^- was calculated using reference 132. The electron affinity for Cl_2 was given as 29.30 kJ mole^{-1}. The value had been found for Cl_2^- fragments dissociated from CCl_4. Since there is a contribution to the heat of formation from the lattice vibrations, this value would be expected to differ from that for Cl_2^- in KCl. However, in the absence of direct information, the value quoted was expected to indicate the order of magnitude expected.

Values for the heats of formation at room temperature for the other reactants were obtained directly from the literature (128).

Eqn. 5.21:	$I(g)$ +	$Cl_2^-(g)$ ⟶	$I^-(g)$ +	$Cl_2(g)$
ΔH^o kJ/mole	106.67	29.30	-210.14	0

$$\therefore \Delta H_f^o = -346.18 \text{ kJ/mole}$$

Fig 5.4 IONISATION POTENTIAL DIAGRAM



Eqn. 5.22a:

$$I(g) + 5Cl_2^-(g) \longrightarrow I^{5+}(g) + IOCl^-(g)$$

ΔH^o kJ/mole 106.67 29.30 1.481×10^4 - 167.54

$$\therefore \quad \Delta H_f^o = + 1.288 \times 10^4 \text{ kJ/mole}$$

Eqn. 5.22b:

$$I^{5+}(g) + 3H_2O(aq) \longrightarrow IO_3^-(aq) + 6H^+(aq)$$

ΔH^okJ/mole 1.481×10^4 -285.98 -230.23 0

$$\therefore \Delta H_f^o = - 1.418 \times 10^4 \text{ kJ/mole}$$

These calculations show that the reaction represented by equation 5.21 is feasible.

The reaction represented by equation 5.22(a) requires a large positive heat of formation. This reaction is possible because the fission fragment iodine is not a neutral atom in equilibrium with its surroundings and will have a certain amount of positional and internal energy. This could be released in promoting the reaction. The large amount of energy required is offset by the amount of energy released in the reaction 5.22(b). If the two reactions occurred simultaneously, they would have an overall negative heat of formation.

The heat of formation for $I^-(aq)$ is given as -55.97 kJ/mole. When this is compared with heat of formation for IO_3^- (aq) in 5.22(b), it can be seen that I^- ions are less readily solvated than IO_3^- ions.

5.2.4. The ionic picture and diffusion

The proposed explanation can be justified by showing that defects such as V_K centres are sufficiently mobile to react with the iodine fragments, as discussed in the model.

First, calculations were made of the relative concentrations of lattice atoms, chlorine molecules (perhaps originating from V_K centres) and fission fragment iodine atoms. The calculations are shown below and the results expressed in table 5.8.

(a) Calculation of distances between species in the tablet

Penetration depth of fission fragments is $\simeq 15\mu$

This value has been obtained experimentally, (19) and comparable values have been obtained by calculating the range. See section 1.2.3.

The amount of fission fragment iodine present $\simeq 3.27 \times 10^{10}$ atoms.

This is an average experimental result. It is the sum of the numbers of atoms present immediately after irradiation for isotopes ^{131}I, ^{133}I, ^{135}I and ^{132}I (calculated in terms of ^{132}Te).

The total amount of free chlorine found at room temperature $\simeq 1.5 \times 10^{16}$ molecules

This is an experimental result and typical for an average tablet of volume 9.53×10^{-2} cm^3 and thickness 0.15 cm.

$\therefore$ The amount of free chlorine in a 15μ layer $\simeq 1.5 \times 10^{14}$ molecule

Wt. of tablet = 0.15 g

$\equiv 2.012 \times 10^{-3}$ moles KCl

$\equiv 1.21 \times 10^{20}$ ions K^+, Cl^-

This is for a tablet of vol. = 9.53×10^{-2} cm^3

The vol. of a layer 15μ thick = 9.53×10^{-4} cm^3

$\therefore$ This corresponds to wt. = 0.15×10^{-2} g

$\therefore$ In this vol., number of ions K^+, Cl^- = 1.21×10^{19}

Also from section 1.2.4:

Number of fission fragments entering tablet $\simeq 2 \times 10^{12}$

These values permitted the distances shown in table 5.8 to be found between atoms and ions. The distances were found in terms of Cl^- ions and then converted to length since the cube edge for KCl (the Cl-Cl distance) is 6.294 Å.

The distance between free Cl_2 mols. $= \left(\frac{1.21 \times 10^{19}}{1.5 \times 10^{14}}\right)^{\frac{1}{3}} \times 6.294 \times 10^{-1}$

$= 2.71 \times 10^{-8}$ m

The distance between iodine fragments $= \left(\frac{1.21 \times 10^{19}}{3.27 \times 10^{10}}\right)^{\frac{1}{3}} \times 6.294 \times 10^{-}$

$= 4.489 \times 10^{-7}$ m

The distance between fission fragments $= \left(\frac{1.21 \times 10^{19}}{2 \times 10^{12}}\right)^{\frac{1}{3}} \times 6.294 \times 10^{-1}$

$= 1.1409 \times 10^{-7}$ m

The distance between Cl_2 molecules and I $= \left(\frac{1.5 \times 10^{14}}{3.27 \times 10^{10}}\right)^{\frac{1}{3}} \times 2.71 \times 10^{-8}$

$= 4.4902 \times 10^{-7}$ m

The distance between Cl_2 and fission fragments $= \left(\frac{1.5 \times 10^{14}}{2 \times 10^{12}}\right)^{\frac{1}{3}} \times 2.71 \times 10^{-8}$

$= 1.1412 \times 10^{-7}$ m

The distance between fission fragment and I $= \left(\frac{5.85 \times 10^{12}}{3.27 \times 10^{10}}\right)^{\frac{1}{3}} \times 1.1409 \times 10^{-7}$

$= 6.412 \times 10^{-7}$ m

The ionic distance between K^+ and Cl^- $= 3.147 \times 10^{-10}$ m

The ionic distance between Cl^- and Cl^- $= 6.294 \times 10^{-10}$ m

(b) The diffusion of V_K centres

This is given in reference 133 and is for alkali halides at 300 ^{o}K which have been doped with 0.1 mole% Tl^+. It is known that defects and impurities increase diffusion coefficients. The presence of Tl^+ in a volume similar to that of a typical KCl tablet in the above concentration gives rise to 2.9×10^{23} impurity ions. The fission

Table 5.8

Distances (mm) between certain species in the tablet (15 μ layer)

SPECIES	Cl^-	K^+	Cl_2	FISSION FRAGMENT	I
K^+	3.1×10^{-7}	6.3×10^{-7}	3.1×10^{-7}	3.1×10^{-7}	3.1×10^{-7}
Cl^-	6.3×10^{-7}	3.1×10^{-7}	3.1×10^{-7}	3.1×10^{-7}	3.1×10^{-7}
Cl_2	3.1×10^{-7}	3.1×10^{-7}	2.7×10^{-5}	1.1×10^{-4}	4.5×10^{-4}
FISSION FRAGMENT	3.1×10^{-7}	3.1×10^{-7}	1.1×10^{-4}	1.1×10^{-4}	6.4×10^{-4}
I	3.1×10^{-7}	3.1×10^{-7}	4.5×10^{-4}	6.4×10^{-4}	4.5×10^{-4}

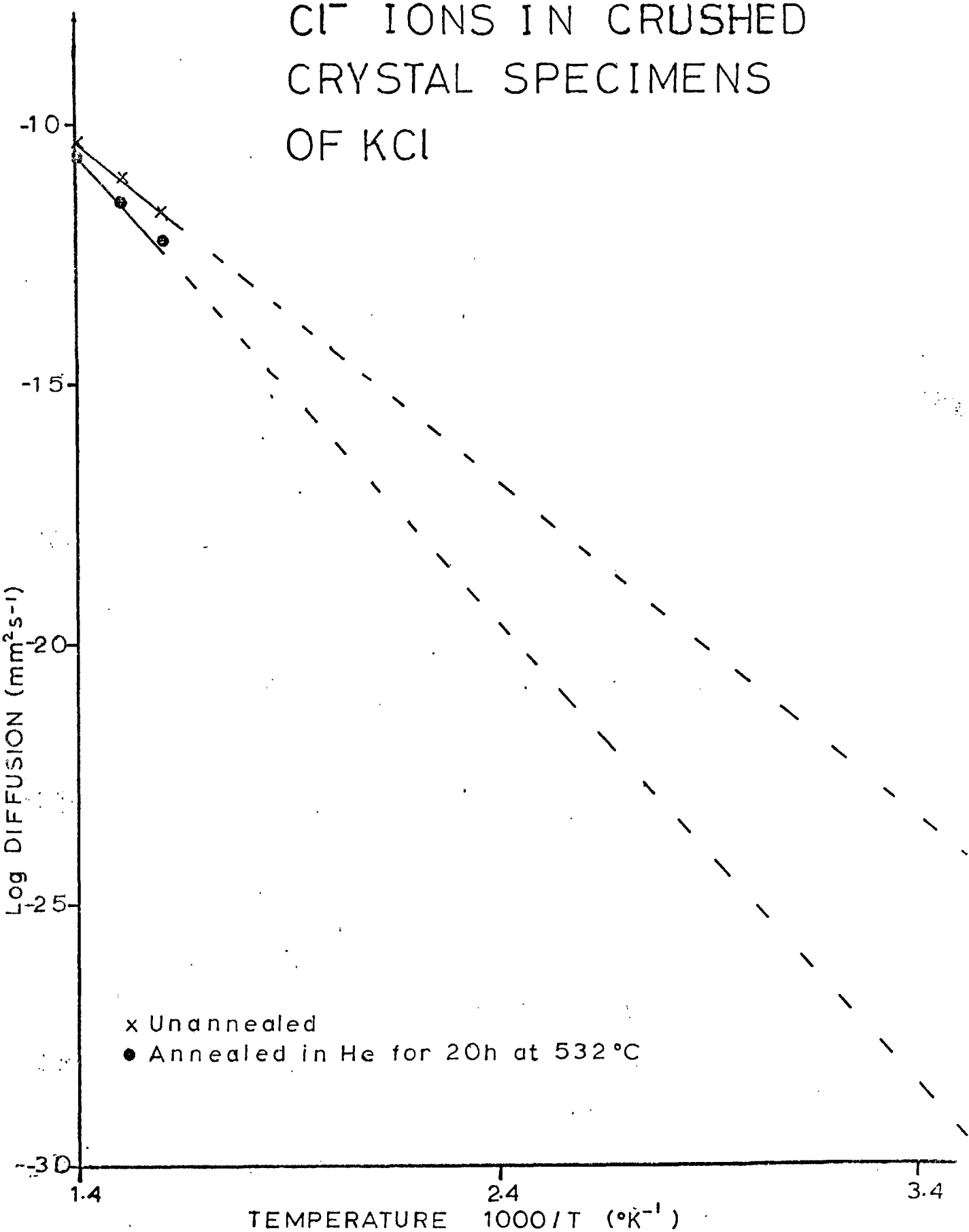
fragment impurity in KCl is $\sim 2 \times 10^{12}$ fragments. In the latter case, other damage will exist such as voids (created by displacement spikes) and dislocations of typical density 10^{6} to 10^{9} cm^{-2} for a material undergoing fission fragment bombardment (28). Therefore, the diffusion rate of 3×10^{-12} cm^{2}/sec (given in reference 133) is not an unreasonable value to take.

From this value, the distances moved in 25 h (average time that tablet is at room temperature) is of the order of 5.2×10^{-6} m. The number of lattice sites moved is approximately 1.64×10^{4}. Diffusion rates are enhanced by temperature rises. Higher rates will be expected for higher temperatures. However, higher temperatures will also lead to faster annealing of the radiation damage. These reactions will compete with each other until all the radiation damage has been annealed. This could result in the creation of vacancies and diffusion might then proceed via anion-vacancy and vacancy-vacancy diffusion, as has been reported for Cl^{-} ions in KCl at temperatures near the melting point (134). Since an appreciable amount of V_K mobility exists at room temperature, and will be expected to increase with higher temperatures, the suggestion that the diffusion of V_K centres might be responsible for the effects observed is not unreasonable.

(c) The diffusion of Cl^{-} ions

This was calculated from reference 135 by extrapolating the graph of log D vs 1/T for unannealed crushed specimens of KCl, see figure 5.5, which was thought to represent the case of a polycrystalline tablet. A very low value of 1.3×10^{-25} cm^{2} sec^{-1} was found. Similar calculations for a crushed crystal specimen annealed in He for 20 h at 532 ^{o}C

Fig 5.5 SELF DIFFUSION OF Cl^- IONS IN CRUSHED CRYSTAL SPECIMENS OF KCl



gave an even lower value of 9.8×10^{-31} cm^2 sec^{-1}. The number of lattice sites moved in 25 h at room temperature (first value) was 3×10^{-3}. Therefore, these results show that the diffusion of Cl^- ions has little effect at room temperature.

In reference 134, the diffusion above 560 °C was interpreted in terms of anion-vacancy and vacancy-pair diffusion. It was noted that below 560 °C diffusion coefficients were too large to be interpreted in these terms. It was suggested that dislocations promote low activation energy diffusion for Cl^- ions in KCl at low temperatures. The values found above have been extrapolated from a graph constructed at much higher temperatures and could be in error by quite a large amount, since at lower temperatures the line was found to have a smaller gradient. At room temperature, its gradient might be much less, resulting in larger values for the diffusion coefficient than those found here. In order to move one lattice site, the diffusion coefficient will have to be $\sim 1.4 \times 10^{-20}$. This is 10^5 greater than the value used here, and represents a shift of 5 units on the y axis, which is not unreasonable. However, movement through one lattice site in 25 h will not cause the annealing predicted by the model at room temperature, and the diffusion of V_K centres is preferred as an explanation.

5.3. Effect of water

5.3.1. Results and discussion

The effect of water is tabulated in terms of the mole% KOH concentration present in the tablet. The calculations are discussed in appendix 2, and the results are shown in table 5.9 and figure 5.6.

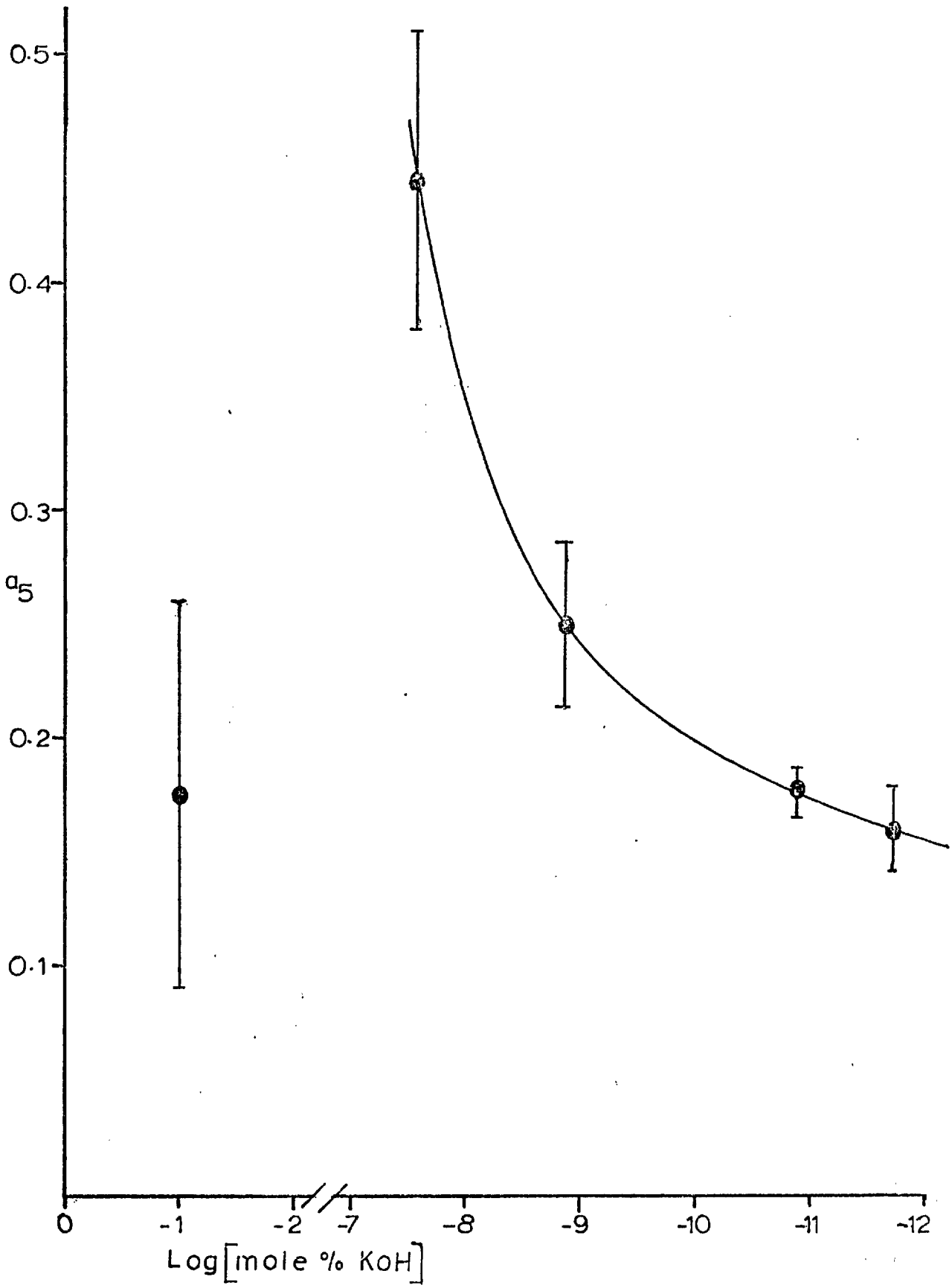
The figure reveals a trend of increased oxidised fraction with increasing concentration of KOH. However, this trend is not followed by the tablet with most KOH, which was made from KCl crystals grown in alkaline conditions. It might be that there is a fluctuating effect of OH^- concentration, as reported in references 69, 70.

The increased iodate fraction occurs for tablets with 5 λ H_2O pipetted onto them and tablets that had been kept in a humidity enclosure. The other results agreed with each other within the experimental error. This suggests that water molecules act in a different way to OH^- ions in the lattice. The presence of water could help in lattice destruction and promote the oxidising effect of Cl_2^- ions by increasing their mobility and, at the same time, acting as a sheath around parts of the lattice to encourage local reactions (53). It has been seen that at room temperatures

$$Cl_2^- \longrightarrow Cl_2 + e$$ is preferred (section 5.2.3)

The electrons released in this reaction can be trapped by the highly mobile vacancies and decomposed dislocations. Radiolysis products of water (due to the γ activity of the fission fragments and transformed lattice atoms) could also help to trap these reducing entities. The chlorine molecule is highly mobile and could easily compete

Fig 5.6 MOISTURE EFFECT



with reducing entities for the fission fragment iodine

$$5Cl_2 + 2I \longrightarrow 2I^{5+} + 10Cl^-$$

It was found that annealing and then wetting prior to analysis produced an increase in iodate fraction. However, wetting, annealing and analysis produced values similar to those obtained for dry tablets (table 4.18). During annealing the lattice structure is re-established and there is less mobility than in solution.

Table 5.9

Moisture Effect

Condition	mole % KOH in KCl	a_5 value (experimental)	σ
Excess alkali	1.14×10^{-1}	0.175	0.084
Excess acid	1.87×10^{-12}	0.160	0.019
Neutral solution	2.16×10^{-6}	-	
$5\lambda H_2O$ to tablet	2.54×10^{-8}	0.446	0.066
Tablet over moisture	1.35×10^{-9}	0.249	0.035
Tablet over silica gel	1.24×10^{-11}	0.177	0.011

This suggests that the presence of the water molecules acts to restrict the motion of the oxidising entities, and thus enhances the probability of reaction with the few iodine fragments in that volume of the tablet. This idea is enforced by the fact that increased iodate fractions are observed when the side with the fission fragment layer is wet, and are not observed when the other side is moistened. Fairweather and Fletcher (130) found that reactor and γ-irradiation damage had an additive effect on the amount of free chlorine found after an aqueous analysis of the tablet. In the moisture experiments, it was found that iodate values were enhanced by

γ- irradiation prior to wetting (section 4.5.1). The extra damage might be in the form of voids and dislocations which could be large enough to permit H_2O or its radiolysis products to surround parts of the crystal lattice and promote local reactions between Cl_2 and fission fragment iodine, as discussed above.

It is suggested that the valence states of iodine have already been determined before reaction with the carrier solution because specific activities were not constant. The valence states can be determined in the crystal or during the process of dissolution where, suddenly, defects have increased mobility and could reach the fission fragment iodine before molecules from the carrier solution. V_K centres would be expected to decompose on solution, and probably give rise to free chlorine (section 4.5.3).

Since Cl_2 is an oxidising agent it might have a similar effect in solution as the oscillatory decomposition of H_2O_2 in the presence of iodate, iodine and iodide(136). Analogous equations to those proposed for the decomposition of H_2O_2 can be derived.

$$H_2O + IO_3^- + Cl_2 \longrightarrow 2Cl^- + IO_4^- + 2H^+ \quad (5.23)$$

$$I_2 + 2Cl_2 + 3H_2O \longrightarrow 2IO_3^- + 6H^+ + 4Cl^- \quad (5.24)$$

$$IO_3^- + 5I^- + 6H^+ \rightleftharpoons 3I_2 + 3H_2O \quad (5.25)$$

$$Cl_2 + 2I^- \longrightarrow 2Cl^- + I_2 \quad (5.26)$$

$$I_2 + H_2O \rightleftharpoons HIO + I^- + H^+ \quad (5.27)$$

$$Cl_2 + H_2O = HCl + HClO \quad (5.28)$$

$$HCl + 2HClO \longrightarrow 3HCl + O_2$$

These equations correspond to equations 2.1 - 2.6 in the

reference. However, these reactions are not expected to occur during the analysis because by the time that there is complete mixing in the carrier solution, the concentration of Cl_2 will be very small when compared with that of KI and KIO_3 in the carrier solution.

Chapter 6. Conclusion.

Contents:

6.1	Summary of Results	271
6.1.1	Annealing experiments	271
6.1.2	Isotopic effect	272
6.1.3	Moisture experiments	273
6.2	Recommendations for Further Work	274

CHAPTER 6

CONCLUSION

6.1. Summary of results

6.1.1. Annealing experiments

The effect of annealing KCl tablets, which have been irradiated by fission fragment iodine, is to promote the formation of oxidised iodine, after an initial period when it promotes reduction. This can be explained by the presence of defect anion centres such as Cl^- ions (V_K or V_H centres). These may react in two ways to produce oxidised and reduced forms.

$$Cl_2^- \longrightarrow Cl_2 + (e)$$

$$5Cl_2^- \longrightarrow 10Cl^- - 5(e)$$

This picture is consistent with thermodynamical considerations and diffusion calculations.

Measurements of free chlorine also show a decrease as the oxidised form increases. This chlorine can be considered to have been formed by the decomposition of V_K centres in solution. One might expect a similar amount of chlorine to be present, as is found in room temperature samples. Its absence can be explained by its being expelled from the lattice, or by its participation in oxidising reactions with other impurities in the lattice, such as iodine. Since it must be present to promote oxidation, either as free chlorine or V_K centres, the former explanation is rejected. It is concluded that the level of free chlorine must be below the limit for detection after annealing, and that it does not leave the lattice.

At first, the oxidised form decreases with an increased rate for higher temperature of annealing. The heating helps to decompose the V_K centres

$$Cl_2^- \longrightarrow Cl_2 + (e)$$

The electrons quickly conduct to iodine fragments, and some are also trapped at dislocations. Sometime after annealing has begun, oxidation processes begin to increase. This can be attributed to reactions with chlorine molecules, which diffuse more slowly than electrons, due to their larger size. Their diffusion rate will be expected to increase with temperature. This could explain the decrease in time for the minimum in the oxidised fraction to occur with increased annealing temperature. Both electrons and chlorine molecules become more mobile with increasing temperature, but the electrons are trapped at vacancies and dislocations which outnumber the iodine fragments. Thus the oxidised fraction is increased. An equilibrium is reached when all the electrons are trapped at dislocations and other electron sinks, which have reduced in number due to temperature/time annealing. There could then be consecutive liberation and retrapping of the electrons at a constant rate since temperature is steady, with some electrons reaching the iodine fragments. This accounts for the fraction that remains reduced at the equilibrium. This is necessarily speculative, but the experimental results appear consistent with this picture.

6.1.2. Isotopic effect

An isotopic effect was observed for ^{132}I which appeared in a more oxidised form throughout the annealing.

Since K_2TeO_3(aq) is thermodynamically more stable than KIO_3(aq), this observation could be attributed to the long existence of ^{132}I as ^{132}Te, its precursor in the decay chain.

6.1.3. Moisture experiments

These experiments have shown that the presence of water in the lattice acts to increase the oxidised form of iodine. It is suggested that the water molecules form a boundary around parts of the lattice, thus promoting local interaction between the decomposed V_K centre and the iodine fragment, on dissolution of the tablet.

6.2. Recommendations for further work

The experiments reported here have been concerned with a determination of the oxidation state of fission fragment iodine in a potassium chloride tablet. Although the results have been modified by the method of analysis, it was possible to propose a crude model for reactions in the solid state.

In the course of this work, ancillary experiments have been carried out, to define the variables acting on the system. Some of these experiments, such as the effect of pH, have not been conclusive. It is suggested that further work of a more controlled nature is carried out in this field. The effect of pressure on the tablet was negligible at room temperature, but could have affected the results of the annealed tablets. This should be investigated. It should also be verified that no chlorine is escaping from the tablet during the annealing process.

The work could be extended to include irradiations and analyses at low temperatures. This would reduce the complication of the annealing of the radiation damage while the tablet is stored at room temperature. Analyses in non aqueous media might yield more information about the valency states present in the solid. Finally, experiments could be carried out to correlate the annealing curves with ESR measurements on the V_K centre or its derivatives. This would help to substantiate the model proposed in this thesis.

References

1. Bramman, J.I. and Powell, H.J., J. BNES, 14, 63, (1975).

2. "Control of Iodine in the Nuclear Industry", Tech. Report No. 148, IAEA, Vienna, (1973).

3. Bohr, N. and Wheeler, J.A., Phys. Rev., 56, 426, (1939).

4. Viola, V.E. Jr., Nucl. Data Sect. A, 1, 391, (1966).

5. Chadderton, L.T. and McC. Torrens, I., "Fission Damage in Crystals", Methuen, London, (1969).

6. Walton, G.N., in "Prog. Nuclear Physics 6" (O.R. Frisch, ed.), Chapter 7, Pergamon, London, (1957).

7. Vandenbosch, R. and Huizenga, J.R., "Nuclear Fission", Academic Press, London (1973).

8. Flynn, K.F. and Glendenin, L.E., Rep. ANL-7749, Argonne Nat. Lab., Argonne, Illinois, (1970).

9. Thomas, T.D. and Vandenbosch, R., Phys. Rev., 133, 976, (1964).

10. Glendenin L.E. et al, NNES, The Fission Products Paper 52, McGraw-Hill, New York, (1951).

11. Wahl, A.C. et al, Phys. Rev., 126, 1112, (1962).

12. Apalin, V.F. et al, Proc. IAEA Symp. Phys. Chem. Fission, Salzburg, 1, 586, IAEA, Vienna, (1965).

13. Bohr, N., Dan. Mat. Fys. Medd., 18, 8, (1948).

14. Walton, G.N. in "Atomic Energy Waste: Its nature, use and disposal" (E. Glueckauf, ed.), Chapter 1, Butterworths, London, (1961).

15. Dienes, G.J. and Vineyard, G.H., "Radiation Effects in Solids", Interscience, London, (1957).

16. "Physics of Color Centers" (W. Beall Fowler, ed.), Academic Press, London, (1968).

17. Chadderton, L.T. "Radiation Damage in Crystals", Methuen, London, (1965).

18. Walton, G.N., Chem. Soc. Quart. Rev., XV, No. 1, (1961).

19. Young, D.A., personal communication.

20. Good, W.M. and Wollan, E.O., Phys. Rev., 101, 249, (1956).

21. Davies, J.A. et al, Can. J. Chem., 39, 611, (1961).

22. Hall, D. and Walton, G.N., J. inorg. nucl. Chem., 10, 215, (1959).

23. Peterson, S. and Wymer, R.G., "Chemistry in Nuclear Technology", Pergamon Press, London, (1963).

24. Seitz, F., Rev. Mod. Phys., 36, 1, (1954).

25. Varley, J.H.O., Nature, 174, 886, (1954).

26. Price, B.T. et al, "Radiation Shielding", Pergamon Press, London, (1957).

27. Seitz, F. and Kochler, J.S., in "Solid State Physics 2" (F. Seitz and D. Turnbull, eds.), Academic Press, New York, (1956).

28. Veljković, S.R., Phil, Mag., 21, 627, (1970).

29. Brinkman, J.A., Nucl. Mat., VI, 1, (1959).

30. Rosenthal, M.W. et al, 4th. Int. Conf. The Peaceful Uses of Atomic Energy, 5, 225, UN and IAEA, Geneva, (1971).

31. Bettis, E.S., U.S. Patent No. 3, 262, 856, (1966).

32. Harder, B.R. et al, Nucl. Mat., 15, USAEC, CONF-69081, (1969).

33. Walton, G.N. et al, 1st. Int. Conf. The Peaceful Uses of Atomic Energy, 7, 155, (1955).

34. Hall, D. and Walton, G.N., J. inorg. nucl. Chem., 19, 16, (1961).

35. Bellido, A.V. and Wiles, D.R., Radiochimica Acta, 12, 94, (1969).

36. Kaučić, S. and Vlatković, M., Croat Chim Acta, 35, 305, (1963).

37. Brown, L.C. and Wahl, A.H., J. inorg. nucl. Chem., 29, 2133, (1967).

38. Spiridou, S. and Călusaru, A., J. inorg. nucl. Chem., 35, 713, (1973).

39. Ladrielle, T.G. et al, Radiochimica Acta, 22, 65, (1975).

40. Andersen, T. and Sorensen, G., Trans. Faraday Soc., 62, 3427, (1966).

41. Freeman, J.H. et al, Chem. Commun., 979, (1967).

42. Ambe, F. and Saito, N., Radiochimica Acta, 13, 105, (1970).

43. Abdel-Rassoul, A.A. et al, Radiochimica Acta, 14, 113, (1970).

44. Kasrai, M. and Maddock, A.G., J. Chem. Soc. (A), 1105, (1970).

45. Adloff, J.P. and Meyer, J.P., Radiochimica Acta, 7, 15, (1967).

46. Owens, C.W. and Hobbs, J.R., J. Phys. Chem., 73, 1956, (1969).

47. Kasrai, M. et al, Trans. Faraday Soc., 67, 2108, (1971).

48. Bogdanov, R.V. and Murin, A.N., Sov. Phys. Sol. State, 9, 180, (1967).

49. Andersen, T., and Baptista, J.L., Trans. Faraday Soc., 67, 1213, (1971).

50. Chandratillake, M.R. et al, J. inorg. nucl. Chem., 38, 199, (1976).

51. Bogdanov, R.V. et al, Radiokhimiya, 11, 612, (1969).

52. Bogdanov, R.V. et al, khim. vysok. Energii, 3, 360, (1969).

53. Arnikar, H.J. et al, Radiochimica Acta, 13, 164, (1970).

54. Stamouli, M.I., Radiochimica Acta, 21, 90, (1974).

55. Ackerhalt, R. et al, Radiochimica Acta, 18, 73, (1972).

56. Harbottle, G. and Sutin, N., "Advances in Inorganic Chemistry and Radiochemistry", Vol. 1, Academic Press, New York, (1960).

57. Ianovici, E. and Zaitseva, N., Radiokhimiya, 14, 319, (1972).

58. Peixoto, J.M. et al, J. inorg. nucl. Chem., 29, 1825, (1967).

59. Al-Siddique, F.R. and Maddock A.G., J. inorg. nucl. Chem., 34, 3007, (1972).

60. Walton, G.N., Radiochimica Acta, 2, 108, (1964).

61. Maddock, A.G. and Mahmood, A.J., Inorg. Nucl. Chem. Letters, 9, 509, (1973).

62. Meyer, J.P., Radiochimica Acta, 15, 88, (1971).

63. Meyer, J.P., Radiochimica Acta, 14, 154, (1970).

64. Ambe, S. et al, Radiochimica Acta, 19, 121, (1973).

65. Borshagovskii, B.V. et al, Izvest Akad. Nauk. S.S.S.R., Ser. khim., 5, 1016, (1971).

66. Finn, R.O. et al, J.Phys. Chem., 73, 3928, (1969).

67. Gütlich, P. et al, J. inorg. nucl. Chem., 33, 307, (1971).

68. Kulikov, L.A. et al, Vestnik Moskov. Univ., Khim., 27, 347, (1972).

69. Bračoková, V. and Cífka, J., J. inorg. nucl. Chem., 32, 365, (1970).

70. Baptista, J.L. et al, Trans. Faraday Soc., 64, 456, (1968).

71. Rabe, J.G. et al, J. Phys. Chem., 1098, (1966).

72. Lazzarini, E. and Fantola-Lazzarini, A.L., J. inorg. nucl. Chem., 35, 2653, (1973).

73. Lazzarini, E., Radiochimica Acta, 13, 156, (1970).

74. Kishore, K. and Venkateswarlu, K.S., Radiochem. Radioanalyst. Letters, 13, 17, (1973).

75. Thomas, V.G., Radiochem. Radioanalyst. Letters, 12, 97, (1972).

76. Podeanu, G. and Costea, T., Radiochem. Radioanalyst. Letters, 6, 57, (1971).

77. Collins, C.H. et al, Radiochimica Acta, 4, 211, (1965).

78. Odru, P. and Vargas, J.I., Inorg. Nucl. Chem. Letters, 7, 379, (1971).

79. Scanlon, M.D. and Collins, K.E., Radiochimica Acta, 15, 141, (1971).

80. Glentworth, P. and Nath, A. in "Radiochemistry Vol. 2", The Chemical Society, London, (1975).

81. Andersen, T.E. and Baptista, J.L., Trans. Faraday Soc., 67, 1203, (1971).

82. Yang, M.H. et al, Radiochem. Radioanalyst. Letters, 13, 173, (1973).

83. Kudo, H., Bull. Chem. Soc. Japan, 45, 392, (1972).

84. Nath, A., unpublished work in "Radiochemistry Vol. 2", The Chemical Society, London, (1975).

85. Venkateswarlu, K.S. and Kishore, K., Radiochimica Acta, 15, 70, (1971).

86. Ras, K.A., Radiochimica Acta, 12, 11, (1969).

87. Rusi, A. and Călușaru, A., Radiochimica Acta, 13, 95, (1970).

88. Kunz, G. and Lieser, K.H., Radiochimica Acta, 11, 72, (1969).

89. Andersen, T. and Baptista, J.L., Phys. Status Solidi, 44, 29, (1971).

90. Henderson, B. et al, J. Phys. (C), 4, 1496, (1971).

91. Dimotakis, P.N. and Yavas, G., J. inorg. nucl. Chem., 32, 1065, (1970).

92. Dimotakis, P.N. and Yavas, G.,J.inorg. nucl. Chem., 32, 1071, (1970).

93. Cífka, J. and Bračoková, V., J. inorg. nucl. Chem., 32, 361, (1970).

94. Khorana, S. and Wiles, D.R., J. inorg. nucl. Chem., 31, 3387, (1967).

95. Bogdanov, R.V. and Olevskii, E.B., Radiokhimiya, 11, 616, (1969).

96. Milenkov, C. et al, J. inorg. nucl. Chem., 33, 1187, (1971).

97. Anselmo, V.C., J. inorg. nucl. Chem., 35, 1069, (1973).

98. Baptista, J.L. et al, Trans. Faraday Soc., 66, 2131, (1970).

99. Maddock, A.G. et al, Trans. Faraday Soc., 59, 924, (1963).

100. Baumgartner, F. and Maddock, A.G., Trans. Faraday Soc., 63, 714, (1968).

101. Costeau, T., Thesis, Paris, (1968).

102. Mahieu, B. et al, Radiochimica Acta, 16, 100, (1971).

103. Nath, A. et al, Indian J. Chem., 4, 51, (1966).

104. Rao, K.A. and Nath, A., Radiochimica Acta, 5, 162, (1966).

105. Costea, T. et al, Radiochimica Acta, 16, 86, (1971).

106. Baptista, J.L. and Marques, N.S.S., J. inorg. nucl. Chem., 36, 1683, (1974).

107. Shoemaker, D., Phys. Rev., 174, 1060, (1968).

108. Meistrich, M.L. and Goldberg, L.S., Sol. State Comm., 4, 469, (1966).

109. Byberg, J.R. et al, J. Chem. Phys., 46, 131, (1967).

110. Erschler, B.V. and Lapteon, F.S., J. Nucl. Energy, 4, 471, (1957).

111. Hudswell, F., "The Preparation of Films and Coatings", AERE C/R 392, (1949).

112. Galley, M.R., "The Fission Fragment Irradiation of Methane", Ph.D., Thesis, Imperial College, London, (1964).

113. Katz, J.J. and Rabinowitch, E., "Chemistry of Uranium", Nuclear Energy Series Division VIII Vol. 5, McGraw-Hill, London, (1951).

114. "Encyclopedia of Chemical Technology" (Kirt-Othmer, ed.), 1st. edn. Vol. 14 (1955); 2nd edn. Vol. 21 (1970).

115. Yule, G. and Kendall, M.G., "An Introduction to the theory of statistics", Griffin, London, (1964).

116. Holden, N.E. and Walker, F.W., "Chart of the Nuclides", Knolls Atomic Power Laboratory, Naval Reactors, USAEC, (1968).

117. Atkins, D.H.F. and Eggleton, A.E.J., "Iodine Compounds formed on release of carrier free-iodine - 131", AERE M 1211, (1963).

118. Blake, C.A. Jnr., "Solvent Stability in Nuclear Fuel Processings", Report O.R.W.C. 4212.

119. Mellor, J.W., "Inorganic and Theoretical Chemistry, Vol. II Supplement 1", Longmans, London, (1956).

120. Abel, E. and Siebenschein, R., Z. Phys. Chem., 130, 631, (1927).

121. Vogel, A.I., "A text-book of Quantitative Inorganic Analysis", Longmans, London, (1961).

122. Lederer, C.M. et al, "Table of Isotopes", 6th. edn., Wiley, London, (1967).

123. Price, W.J., "Nuclear Radiation Detection", McGraw-Hill, London, (1964).

124. Kruger, J., "Instrumentation in Applied Nuclear Chemistry", Plenum Press, London, (1973).

125. Crouthamel, C.E., "Applied Gamma-Ray Spectrometry", Pergamon Press, London, (1970).

126. Siegbahn, K., "Alpha- Beta- and Gamma-Ray Sepctroscopy", Vol. 1, North-Holland Publishing Co., Amsterdam, (1965).

127. Quittner, P., "Gamma-Ray Spectroscopy", Adam Hilger, London, (1972).

128. "Selected Values of Chemical Thermodynamic Properties", NBS Circular 500, U.S. Department of Commerce, (1952).

129. Dow Chemical Company "JANAF Thermochemical Tables", 2nd. edn., NSRDS-NBS 37 U.S., (1970).

130. Fairweather, S. and Fletcher, N., personal communication.

131. Bradbury, T. and Leicester, R., personal communication.

132. Field, F.H., and Franklin, J.L., "Electron Impact Phenomena and the Properties of Gaseous Ions", Academic Press, New York, (1957).

133. Popp, R.D. and Murray, R.B., J. Phys. Chem. Solids, 33, 601, (1972).

134. Fuller, R.G., Phys. Rev., 142, 524, (1966).

135. Barr, L.W. et al, Trans. Faraday Soc., 56, 697, (1960).

136. Matsuzaki, I. and Nakagima, T., in "Physical Chemistry of Oscillatory Phenomena". Symposia of the Faraday Society, 9, The Chemical Society, London, (1974).

137. Handbook of Chemistry and Physics, (R.C. Weast, ed.), 51st edn., The Chemical Rubber Co., U.S.A., (1970).

138. Melville, H. and Gowenlock, B.G., "Experimental Methods in Gas Reactions", Macmillan, London, (1964).

139. Programming Languages, PDP-8, Family Computers, Digital Equipment Corporation, U.S.A. (1970).

APPENDIX 1

PROGRAMS FOR CALCULATING THE RESULTS

INTRODUCTION

CHRIS 1 was the first program to be written. This determined the activities present at the end of irradiation (a convenient reference point) from the experimental activities recorded by the detector after analysis. The activity for each isotope was found from the count rate obtained for a characteristic γ-ray, which was then corrected for detector efficiency and γ-ray intensity. Isotopic activities for oxidised and reduced fractions of ^{131}I, ^{132}I and ^{133}I were calculated in this way. These values were compared with theoretical activities which were calculated from the fission flux, time of irradiation and fission yield for each isotope.

CHRIS 2 was a modification of CHRIS 1 to include an error analysis. It was essentially the same program with error statements inserted after every defined quantity in the program.

CHRIS 3 was a refinement of the program to account for the fact that a large fraction of the cumulative fission yield for ^{132}I will be present as ^{132}Te during the analysis. Since the independent fission yield for ^{132}I is so low as to be negligible, all the ^{132}I that was counted was taken as having decayed from ^{132}Te before the analysis. The amount of ^{132}Te that gave rise to the experimental iodine activity recorded was calculated and compared with the theoretical yield for ^{132}Te.

TABLE A 1.1

Symbol listing for the programs

Variable	Error	Meaning
GROUP 1		
J		Number of isotopes
E1	EA	Efficiency of ^{60}Co γ-peak(1.173 MeV)
E2	EB	" " " " (1.333 MeV)
EN	-	Enrichment of uranium
X1	0.0015 X1	Carrier solution P(iodide) in g
X2	0.0015 X2	" " Q(iodate) " "
X3	0.0015 X3	" " R(iodide) " "
X	1.414×10^{-4}	Cobaltous chloride in g
A1	AA	Detector activity for ^{60}Co γ-peak (1.173 MeV)
A2	AB	Detector activity for ^{60}Co γ-peak (1.333 MeV)
T	-	Time of irradiation in hrs.
U	-	U_3O_8 in g
T2	-	Time between end of irradiation and count from extract A
T3	-	Time between end of irradiation and count from extract B
E3(M)	EC	Efficiency of isotope (M) γ-peak
A3(M)	AC	Detector activity for isotope (M) γ-peak, extract A
A4(M)	AD	Detector activity for isotope (M) γ-peak, extract B
IN(M)	-	Intensity of γ-peak for isotope (M)
Y(M)	-	Fission yield for isotope (M) (cumulative)
TH(M)	-	Half life for isotope (M), hrs.

GROUP 2

CO	DO	Number of cobalt atoms
R1	RA	Activity of ^{60}Co (from the two γ-ray counts, corrected and averaged)
PH	P6	Neutron flux
KF	K6	Fission rate
RK		Correction for count rate of extract B (Incorporated into the program for CHRIS 2 and CHRIS 3)
C	0.03C	Amount of iodate extracted in extract A
C1	CA	Amount of iodate left
D	DZ	Amount of iodide required to extract C1g iodate

GROUP 3

TA(M)	TI(M)	Theoretical activity for isotope(M)
R2(M)	RB(M)	Corrected activity for extract A
R3(M)	RC(M)	" " " " B
R4(M)	RD(M)	Activity due to iodate in extract A
R5(M)	RE(M)	Total KIO_3 activity
R6(M)	RF(M)	" KI "
SI(M)	SJ(M)	Specific iodide activity
SO(M)	SP(M)	" iodate "
B1(M)	BA(M)	Ratio of experimental to theoretical activity (KI)
B2(M)	BB(M)	Ratio of experimental to theoretical activity (KIO_3)
SB(M)	S2(M)	Ratio of total experimental activity to total theoretical activity
P(M)	PP(M)	Fraction of experimental activity as iodide
Q(M)	QQ(M)	Fraction of experimental activity as iodate

Extra Symbols CHRIS 3

GROUP 1

T4	Time from count to dissolution for extract A
T5	Time from count to dissolution for extract B
T6	Time from dissolution to end of irradiation

GROUP 3

H	Function for calculating Te activity at end of irradiation which has produced the iodine activity at dissolution

Explanation of programs

A symbol listing is shown in table A 1.1. The variables are divided into three groups in this table, for convenience in constructing the flow diagram for CHRIS 1, shown in figure A 1.1. The flow diagram for CHRIS 2 is similar. In the program CHRIS 3, T2 and T3 are set equal to T4 and T6 respectively before Group 3 values are calculated.

It should be noted that in CHRIS 1 and CHRIS 2 the order of calculation is ^{131}I, ^{132}I, ^{133}I. In CHRIS 3 it is ^{135}I, ^{133}I, ^{132}I.

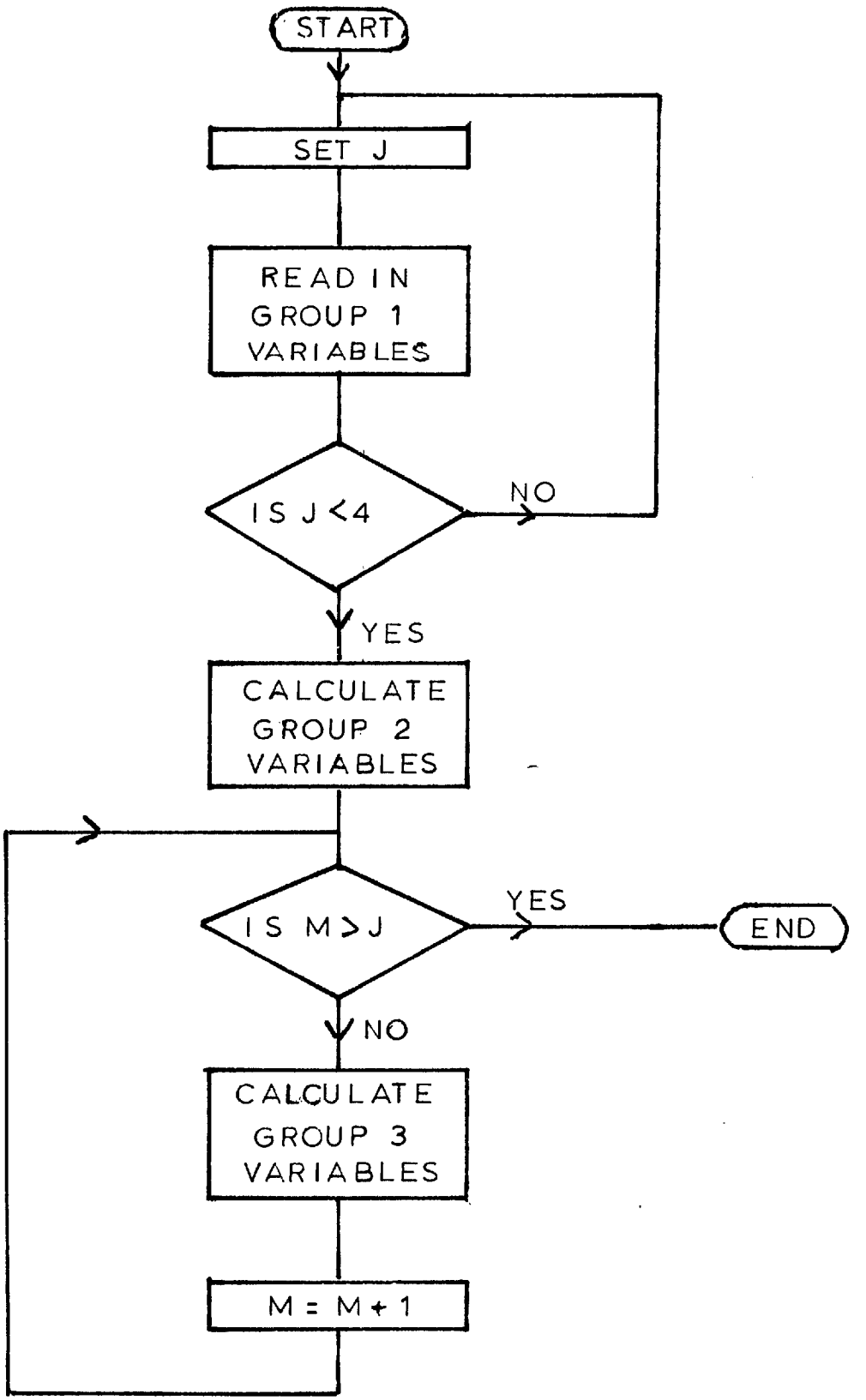
The following pages illustrate how the programs were employed. Typical results, obtained from the analysis of one sample, were used as the input. The redox distribution was found for ^{131}I with CHRIS 2 and for ^{135}I, ^{133}I, ^{132}I with CHRIS 3.

The programs were written in FOCAL (139) for use on a PDP 8 computer. Maximum sensitivity was used and this

required printing all ten decimal places for each value in the output. However, only the first two or three decimal places have any significance.

Fig A1.1

FLOW DIAGRAM FOR CHRIS 1



CHRIS 2: PROGRAM

```
Ø1.1Ø A ?J ?  !; I (FITR(J)-J) 1.15,1.13,1.15
Ø1.13 I (J-4) 1.17
Ø1.15 T "INTEGERS 1-3 ONLY PLEASE.",!!; G 1.1
Ø1.17 I (J) 1.15,1.15
Ø1.4Ø A ?E1 EA E2 EB EN ? !!

Ø2.4Ø A ?X1 X2 X3 ? !!

Ø3.4Ø A ?X A1 AA A2 AB T U T2 T3 ? !!

Ø4.5Ø F M=1,1,J; D 8.Ø

Ø5.1Ø S IN(1)=.82; S IN(2)=.9; S IN(3)=.37
Ø5.2Ø S Y(1)=2.9E-2; S Y(2)=6.5E-2; S Y(3)=5.9E-2
Ø5.3Ø S TH(1)=193.2; S TH(2)=2Ø.3; S TH(3)=6.68
Ø5.4Ø S C0=X*.25314E22; T %, ?C0?; D 9; T 3.5793996E17,!
Ø5.6Ø S R1=(A1/E1+A2/E2)*(FEXP(.15Ø43E-4*T))/2;T ?R1?
Ø5.63 S J1=(AA*AA/A1/A1+EA*EA/E1/E1)*A1*A1/E1/E1
Ø5.64 S J2=(AB*AB/A2/A2+EB*EB/E2/E2)*A2*A2/E2/E2
Ø5.65 S RA=FSQT(J1+J2)*FEXP(.15Ø43E-4*T)/2; D 9; T RA,!
Ø5.71 S PH=R1*.898322E27/C0; T ?PH?
Ø5.73 S P6=FSQT(RA*RA/R1/R1+1.28121E35/C0/C0)*PH; D 9; T P6,!
Ø5.8Ø S KF=PH*EN*U*1.24581; T ?KF?
Ø5.82 S K6=FSQT(P6*P6/PH/PH+.Ø1)*KF; D 9; T K6,!!!
Ø5.85 S C=.Ø129*X1;T ?C ?; D 9; T C*.Ø3,!
Ø5.87 S C1=X2/2Ø-C; T ?C1?; D 9; S CA=FSQT(2.25E-6*X2*X2+9E-4*C*C); T CA,!
Ø5.89 S D=(C+C1)*.592998; T ?D ?; D 9; S DZ=FSQT(9E-4*C*C+CA*CA)*.592998
Ø5.9Ø T DZ,!!!

Ø6.4Ø F M=1,1,J; D 7
Ø6.6Ø T !!!!!!!!!!!!!!!!!; Q

Ø7.Ø5 T "ISOTOPE I 13"
Ø7.1Ø I (M-2)7.12,7.13,7.14
Ø7.12 T "1"; G 7.15
Ø7.13 T "3"; G 7.15
Ø7.14 T "5"
Ø7.15 T !!
```

CHRIS 2 : PROGRAM (CONT.)

```
Ø7.19 S TA(M)=Y(M)*KF*(1-FEXP(-1.38629/TH(M)))
Ø7.2Ø T %1.Ø,"TA(",M,") ",%,TA(M); D 9; T K6*TA(M)/KF,!
Ø7.21 S R2(M)=A3(M)*FEXP(T2*.693147/TH(M))/E3(M)/IN(M)
Ø7.22 T %1.Ø,"R2(",M,") ",%,R2(M); S J3=3.6E-3+EC(M)*EC(M)/E3(M)/E3(M)
Ø7.23 S RB(M)=R2(M)*FSQT(AC(M)*AC(M)/A3(M)/A3(M)+J3); D 9; T RB(M),!
Ø7.24 S R3(M)=(A4(M)*FEXP(T3*.693147/TH(M))/E3(M)/IN(M))
Ø7.25 S R3(M)=R3(M)*(X3*1.Ø7488E-2/C1+.16676); T %1.Ø,"R3(",M,") ",%,R3(M)
Ø7.27 S RC(M)=R3(M)*FSQT(J3+2.25E-6+AD(M)*AD(M)/A4(M)/A4(M)+CA*CA/C1/C1)
Ø7.29 D 9; T %, RC(M),!
Ø7.3Ø S R4(M)=R3(M)*C/C1; T %1.Ø,"R4(",M,") ",%,R4(M)
Ø7.31 S RD(M)=R4(M)*FSQT(RC(M)*RC(M)/R3(M)/R3(M)+9E-4+CA*CA/C1/C1)
Ø7.32 D 9; T RD(M),!; S R5(M)=R4(M)+R3(M); T %1.Ø,"R5(",M,") ",%,R5(M)
Ø7.33 S RE(M)=FSQT(RC(M)*RC(M)+RD(M)*RD(M)); D 9; T RE(M),!
Ø7.34 S R6(M)=R2(M)-R4(M); T %1.Ø,"R6(",M,") ",%,R6(M)
Ø7.35 S RF(M)=FSQT(RB(M)*RB(M)+RD(M)*RD(M)); D 9; T RF(M),!
Ø7.36 S SI(M)=R6(M)*26.1624/X1; T %1.Ø,"SI(",M,") ",%,SI(M)
Ø7.37 S SJ(M)=FSQT(RF(M)*RF(M)/R6(M)/R6(M)+2.25E-6)*SI(M); D 9; T SJ(M),!
Ø7.39 S S0(M)=R5(M)/D; T %1.Ø,"S0(",M,") ",%,S0(M)
Ø7.4Ø S SP(M)=FSQT(RE(M)*RE(M)/R5(M)/R5(M)+DZ*DZ/D/D)*S0(M); D 9; T SP(M)
Ø7.41 S B1(M)=R6(M)/TA(M); T %1.Ø,"B1(",M,") ",%,B1(M)
Ø7.42 S BA(M)=FSQT(RF(M)*RF(M)/R6(M)/R6(M)+K6*K6/KF/KF)*B1(M)
Ø7.43 D 9; T BA(M),!; S B2(M)=R5(M)/TA(M); T %1.Ø,"B2(",M,") ",%,B2(M)
Ø7.44 S BB(M)=FSQT(RE(M)*RE(M)/R5(M)/R5(M)+K6*K6/KF/KF)*B2(M)
Ø7.45 D 9; T BB(M),!; S SB(M)=B1(M)+B2(M); T %1.Ø,"SB(",M,") ",%,SB(M)
Ø7.46 S S2(M)=FSQT(BA(M)*BA(M)+BB(M)*BB(M)); D 9;T S2(M),!
Ø7.47 T %1.Ø,"P (",M,") ",%,B1(M)/SB(M); D 9
Ø7.48 T FSQT(BA(M)*BA(M)/B1(M)/B1(M)+S2(M)*S2(M)/SB(M)/SB(M))*B1(M)/SB(M)
Ø7.49 T %1.Ø,"Q (",M,") ",%,B2(M)/SB(M); D 9
Ø7.5Ø T FSQT(BB(M)*BB(M)/B2(M)/B2(M)+S2(M)*S2(M)/SB(M)/SB(M))*B2(M)/SB(M)
Ø7.51 T !!!

Ø8.2Ø T %1.Ø, "E3(",M,") "; A E3(M); T "EC(",M,") "; A EC(M)!!
Ø8.25 T %1.Ø, "A3(",M,") "; A A3(M); T "AC(",M,") "; A AC(M)!
Ø8.3Ø T %1.Ø, "A4(",M,") "; A A4(M); T "AD(",M,") "; A AD(M)!!

Ø9.1Ø T "          "
```

CHRIS 2:OUTPUT (^{131}I only)

```
 G
J :1

E1 :.8297E-3
EA :.0053E-3
E2 :.7457E-3
EB :.0047E-3
EN :.8


X1 :.13612
X2 :.11154
X3 :.32202


X :4.6E-3
A1 :22.186
AA :.25
A2 :19.414
AB :.22
T :16.3167
U :200E-6
T2 :50.4
T3 :50.55


E3(= 1) :.3361E-2
EC(= 1) :.002E-2


A3(= 1) :5.166
AC(= 1) :.1394

A4(= 1) :.562
AD(= 1) :.052
```

continued from first column

```
C0= 0.1164444000E+20          = 0.3579399598E+18
R1= 0.2639366950E+05          = 0.2418916485E+03
PH= 0.2036166099E+13          = 0.6531260593E+11
KF= 0.4058681741E+09          = 0.4262366976E+08


C = 0.1755948000E-02          = 0.5267843999E-04
C1= 0.3821051999E-02          = 0.1754071096E-03
D = 0.3307149844E-02          = 0.1086055595E-03


ISOTOPE I 131

TA(= 1) = 0.8415363582E+05          = 0.8837689209E+04
R2(= 1) = 0.2245957841E+04          = 0.1483616726E+03
R3(= 1) = 0.2622177624E+03          = 0.3136343510E+02
R4(= 1) = 0.1205010441E+03          = 0.1585560631E+02
R5(= 1) = 0.3827188064E+03          = 0.3514349602E+02
R6(= 1) = 0.2125456797E+04          = 0.1492065218E+03
SI(= 1) = 0.4085149198E+06          = 0.2868418854E+05
S0(= 1) = 0.1157246646E+06          = 0.1128563844E+05
B1(= 1) = 0.2525686235E-01          = 0.3190461690E-02
B2(= 1) = 0.4547858243E-02          = 0.6344365170E-03
SB(= 1) = 0.2980472059E-01          = 0.3252930292E-02
P (= 1) = 0.8474114787E+00          = 0.1414663199E+00
Q (= 1) = 0.1525885213E+00          = 0.2702701394E-01
```

CHRIS 3: PROGRAM

```
Ø1.1Ø A ?J ?  !; I (FITR(J)-J) 1.15,1.13,1.15
Ø1.13 I (J-4) 1.17
Ø1.15 T "INTEGERS 1-3 ØNLY PLEASE.",!!; G 1.1
Ø1.17 I (J) 1.15,1.15

Ø2.4Ø A ?X1 X2 X3 ? !!

Ø3.4Ø A ?KF K6 T2 T3 T4 T5 T6 ? !!

Ø4.5Ø F M=1,1,J; D 8.Ø

Ø5.1Ø S IN(1)=.37; S IN(2)=.9; S IN(3)=.89
Ø5.2Ø S Y(1)=5.9E-2; S Y(2)=6.5E-2; S Y(3)=4.4E-2
Ø5.3Ø S TH(1)=6.68; S TH(2)=2Ø.3; S TH(3)=77.7
Ø5.85 S C=.Ø129*X1;T %, ?C ?; D 9; T C*.Ø3,!
Ø5.87 S C1=X2/2Ø-C; T ?C1?; D 9; S CA=FSQT(2.25E-6*X2*X2+9E-4*C*C); T CA,!
Ø5.89 S D=(C+C1)*.592998; T ?D ?; D 9; S DZ=FSQT(9E-4*C*C+CA*CA)*.592998
Ø5.9Ø T DZ,!!!

Ø6.4Ø F M=1,1,J; D 7
Ø6.6Ø T !!!!!!!!!!!!!!!!!; Q

Ø7.Ø5 T "ISOTØPE I 13"
Ø7.1Ø I (M-2)7.12,7.13,7.14
Ø7.12 T "5"; G 7.15
Ø7.13 T "3"; G 7.15
Ø7.14 T "2"; S T2=T4; S T3=T5
Ø7.15 T !!
Ø7.16 S H=.97Ø9/(FEXP(-.ØØ89*T6)-FEXP(-.3Ø67*T6))
Ø7.19 S TA(M)=Y(M)*KF*(1-FEXP(-1.38629/TH(M)))
Ø7.2Ø T %1.Ø,"TA(",M,") ",%,TA(M); D 9; T K6*TA(M)/KF,!
```

CHRIS 3: PROGRAM (CONT.)

```
07.21 S R2(M)=A3(M)*FEXP(T2*.693147/TH(M))/E3(M)/IN(M)
07.22 T %1.0,"R2(",M,") ",%,R2(M); S J3=3.6E-3+EC(M)*EC(M)/E3(M)/E3(M)
07.23 S RB(M)=R2(M)*FSQT(AC(M)*AC(M)/A3(M)/A3(M)+J3); D 9; T RB(M),!
07.24 S R3(M)=(A4(M)*FEXP(T3*.693147/TH(M))/E3(M)/IN(M))
07.25 S R3(M)=R3(M)*(X3*1.07488E-2/C1+.16676); T %1.0,"R3(",M,") ",%,R3(M)
07.27 S RC(M)=R3(M)*FSQT(J3+2.25E-6+AD(M)*AD(M)/A4(M)/A4(M)+CA*CA/C1/C1)
07.28 D 9; T %, RC(M),!; I (M-2)7.30,7.30,7.29
07.29 S R2(M)=R2(M)*H; S R3(M)=R3(M)*H
07.30 S R4(M)=R3(M)*C/C1; T %1.0,"R4(",M,") ",%,R4(M)
07.31 S RD(M)=R4(M)*FSQT(RC(M)*RC(M)/R3(M)/R3(M)+9E-4+CA*CA/C1/C1)
07.32 D 9; T RD(M),!; S R5(M)=R4(M)+R3(M); T %1.0,"R5(",M,") ",%,R5(M)
07.33 S RE(M)=FSQT(RC(M)*RC(M)+RD(M)*RD(M)); D 9; T RE(M),!
07.34 S R6(M)=R2(M)-R4(M); T %1.0,"R6(",M,") ",%,R6(M)
07.35 S RF(M)=FSQT(RB(M)*RB(M)+RD(M)*RD(M)); D 9; T RF(M),!
07.36 S SI(M)=R6(M)*26.1624/X1; T %1.0,"SI(",M,") ",%,SI(M)
07.37 S SJ(M)=FSQT(RF(M)*RF(M)/R6(M)/R6(M)+2.25E-6)*SI(M); D 9; T SJ(M),!
07.39 S S0(M)=R5(M)/D; T %1.0,"S0(",M,") ",%,S0(M)
07.40 S SP(M)=FSQT(RE(M)*RE(M)/R5(M)/R5(M)+DZ*DZ/D/D)*S0(M); D 9; T SP(M)!
07.41 S B1(M)=R6(M)/TA(M); T %1.0,"B1(",M,") ",%,B1(M)
07.42 S BA(M)=FSQT(RF(M)*RF(M)/R6(M)/R6(M)+K6*K6/KF/KF)*B1(M)
07.43 D 9; T BA(M),!; S B2(M)=R5(M)/TA(M); T %1.0,"B2(",M,") ",%,B2(M)
07.44 S BB(M)=FSQT(RE(M)*RE(M)/R5(M)/R5(M)+K6*K6/KF/KF)*B2(M)
07.45 D 9; T BB(M),!; S SB(M)=B1(M)+B2(M); T %1.0,"SB(",M,") ",%,SB(M)
07.46 S S2(M)=FSQT(BA(M)*BA(M)+BB(M)*BB(M)); D 9;T S2(M),!
07.47 T %1.0,"P (",M,") ",%,B1(M)/SB(M); D 9
07.48 T FSQT(BA(M)*BA(M)/B1(M)/B1(M)+S2(M)*S2(M)/SB(M)/SB(M))*B1(M)/SB(M)!
07.49 T %1.0,"Q (",M,") ",%,B2(M)/SB(M); D 9
07.50 T FSQT(BB(M)*BB(M)/B2(M)/B2(M)+S2(M)*S2(M)/SB(M)/SB(M))*B2(M)/SB(M)
07.51 T !!!

08.20 T %1.0, "E3(",M,") "; A E3(M); T "EC(",M,") "; A EC(M)!!
08.25 T %1.0, "A3(",M,") "; A A3(M); T "AC(",M,") "; A AC(M)!
08.30 T %1.0, "A4(",M,") "; A A4(M); T "AD(",M,") "; A AD(M)!!

09.10 T "          "
```

CHRIS 3:OUTPUT

```
 G
J :3

X1 :.13612
X2 :.11154
X3 :.32202


KF :.4059E9
K6 :.4262E8
T2 :50.4
T3 :50.55
T4 :.4667
T5 :.6167
T6 :49.9333


E3(= 1) :.858E-3
EC(= 1) :.005E-3


A3(= 1) :.574
AC(= 1) :.05

A4(= 1) :.076
AD(= 1) :.024


E3(= 2) :.2188E-2
EC(= 2) :.0018E-2


A3(= 2) :33.93
AC(= 2) :.31

A4(= 2) :3.618
AD(= 2) :.106


E3(= 3) :.1375E-2
EC(= 3) :.001E-2


A3(= 3) :9.416
AC(= 3) :.15

A4(= 3) :1.375
AD(= 3) :.056
```

CHRIS 3:OUTPUT (CONT.)

```
C  = 0.1755948000E-02          = 0.5267843999E-04
C1 = 0.3821051999E-02          = 0.1754071096E-03
D  = 0.3307149844E-02          = 0.1086055595E-03

ISOTOPE I 135

TA(= 1) = 0.4488111316E+07          = 0.4712572166E+06
R2(= 1) = 0.3376497272E+06          = 0.3576819345E+05
R3(= 1) = 0.4870489739E+05          = 0.1581721157E+05
R4(= 1) = 0.2238212596E+05          = 0.7371634721E+04
R5(= 1) = 0.7108702335E+05          = 0.1745064986E+05
R6(= 1) = 0.3152676012E+06          = 0.3651992142E+05
SI(= 1) = 0.6059474794E+08          = 0.7019753846E+07
S0(= 1) = 0.2149495084E+08          = 0.5323649033E+07
B1(= 1) = 0.7024504943E-01          = 0.1098244145E-01
B2(= 1) = 0.1583896173E-01          = 0.4228947053E-02
SB(= 1) = 0.8608401114E-01          = 0.1176851789E-01
P (= 1) = 0.8160057656E+00          = 0.1694724416E+00
Q (= 1) = 0.1839942344E+00          = 0.5519111207E-01

ISOTOPE I 133

TA(= 2) = 0.1741590052E+07          = 0.1828691008E+06
R2(= 2) = 0.9631160736E+05          = 0.5898764222E+04
R3(= 2) = 0.1107216548E+05          = 0.9019302601E+03
R4(= 2) = 0.5088165989E+04          = 0.4996495885E+03
R5(= 2) = 0.1616033146E+05          = 0.1031080940E+04
R6(= 2) = 0.9122344138E+05          = 0.5919887588E+04
SI(= 2) = 0.1753323658E+08          = 0.1138112222E+07
S0(= 2) = 0.4886482991E+07          = 0.3506469478E+06
B1(= 2) = 0.5237939963E-01          = 0.6465523008E-02
B2(= 2) = 0.9279067390E-02          = 0.1140083921E-02
SB(= 2) = 0.6165846702E-01          = 0.6565270680E-02
P (= 2) = 0.8495086265E+00          = 0.1384832048E+00
Q (= 2) = 0.1504913735E+00          = 0.2446754340E-01

ISOTOPE I 132

TA(= 3) = 0.3158176660E+06          = 0.3316124396E+05
R2(= 3) = 0.7726483153E+04          = 0.4829310349E+03
R3(= 3) = 0.1211836765E+04          = 0.1043951029E+03
R4(= 3) = 0.8432391424E+03          = 0.6663250075E+02
R5(= 3) = 0.2678179933E+04          = 0.1238475986E+03
R6(= 3) = 0.1085605858E+05          = 0.4875061791E+03
SI(= 3) = 0.2086545306E+07          = 0.9375143248E+05
S0(= 3) = 0.8098151151E+06          = 0.4593068366E+05
B1(= 3) = 0.3437445004E-01          = 0.3925592402E-02
B2(= 3) = 0.8480146047E-02          = 0.9729537248E-03
SB(= 3) = 0.4285459608E-01          = 0.4044368263E-02
P (= 3) = 0.8021181665E+00          = 0.1188335573E+00
Q (= 3) = 0.1978818335E+00          = 0.2939739712E-01
```

APPENDIX 2

OH^- CALCULATIONS

The following is an attempt to give some qualitative assessment of the chemical activity of the hydroxyl ion in solid KCl under different conditions.

a) Excess alkali

Potassium chloride was made according to the following reaction

$$KCl + H_2O \rightleftharpoons KOH + HCl \qquad A\ 2.1$$

Neutralisation was exceeded slightly with 1 ml 1.03 N KOH in a total volume of 42.9 ml of solution.

The solution was evaporated to dryness.

The resulting crystals contained 2.41×10^{-2} moles $litre^{-1}$ KOH.

If a typical tablet is of weight 0.3 g and of volume 0.1906 cm^3, then in 0.1906 cm^3 KCl there are 4.0237×10^{-3} moles

$\therefore$ in 1,000 cm^3 KCl there are 21.1108 moles

$\therefore$ concentration of KCl is 21.1108 moles/litre

Thus, mole % concentration of OH^- ions in KCl = 1.1416×10^{-1} %.

b) Excess acid

The crystals were made as in (a) but, this time, neutralisation was exceeded slightly, with 1 ml 1.03 N HCl in a total volume of 40.9 ml of solution.

The resulting crystals contained 2.53×10^{-2} moles $litre^{-1}$ HCl.

The equilibrium constant for reaction A 2.1 is given as

$$K = \frac{[a_{KOH}]\ [a_{HCl}]}{[a_{KCl}]\ [a_{H_2O}]} \qquad A\ 2.2$$

a_i is the activity of the ith component

$$a_i = \gamma_i x_i$$

where γ_i is the activity coefficient and x_i is the mole

fraction for the i th component in solution.

For very dilute solutions when $x_i \longrightarrow 0$ or 1, ideal behaviour is approached and $\gamma_i \longrightarrow 1$.

Then
$$K = \frac{[KOH]\ [HCl]}{[KCl]\ [H_2O]} \qquad \text{A 2.3}$$

where square brackets denote molar concentrations.

Assuming complete ionisation in very dilute solutions

$$K = K_W = \frac{[OH^-]\ [H^+]}{[H_2O]}$$

$$= 10^{-14} \text{ at } 25^\circ C$$

Since $H_2O \longrightarrow 1$

$$OH^- = \frac{10^{-14}}{2.53 \times 10^{-2}}$$

$$= 3.96 \times 10^{-13} \text{ g ions litre}^{-1}$$

From (a), the concentration of KCl is 21. 1108 moles litre^{-1}.

$\therefore$ mole % concentration of OH^- ions in KCl = 1.8739×10^{-12} %.

c) Neutral tablet

The following thermodynamical values were used in order to evaluate the equilibrium constant K for the reaction A 2.1.

	ΔH°	ΔS°
	kJ mole^{-1}	J mole^{-1}
KCl (aq)	- 481.39	92.09
H_2O (aq)	- 167.52	55.13
KOH (aq)	- 418.85	157.81
HCl (aq)	- 285.99	69.99

$$\Delta F = \Delta H - T\Delta S$$

$$= 79.93$$

$$\text{But } \Delta F = - RT \ln K$$

$$\ln K = - 32.25$$

$$K = 9.856 \times 10^{-15}$$

$$\therefore \quad \frac{[HCl]\ [KOH]}{[KCl]\ [H_2O]} = 9.856 \times 10^{-15} \qquad \text{A 2.4}$$

From (a) the concentration of KCl is 21.1108 moles litre^{-1}.

$$[HCl]\ [KOH] = 9.856 \times 10^{-15} \times 21.1108$$

$$\therefore \quad [KOH] = 4.5614 \times 10^{-7} \text{ mole/litre}$$

$$\text{mole \% KOH} = 2.161 \times 10^{-6}$$

d) 5λ H_2O added to tablet

In this case $[KCl] \longrightarrow 1$ in equation A 2.4 above. It is assumed that the water diffuses uniformly through the volume of the table (0.09531 cm^3)

$\therefore$ concentration of water $= 2.914 \times 10^{-3}$ mole/litre

$$[HCl]\ [KOH] = 9.856 \times 10^{-15} \times 2.914 \times 10^{-3}$$

$$[KOH] = 5.3591 \times 10^{-9}$$

$$\therefore \quad \text{mole \% KOH} = 2.539 \times 10^{-8}$$

e) Tablet over moisture

Henry's law was applied to this problem. In this case, the solute is water and the solvent is KCl(s).

$$P_B = KX_B$$

where P_B is the partial pressure due to the solute

X_B is the fractional molar concentration of solute

K is Henry's law constant

K was not known accurately but was taken as 8×10^4, since a value of $\sim 10^4$ was given for gases absorbed by liquids. P_B was taken as 23.756 mm Hg, which is the vapour pressure of water at 25°C (137).

$$\therefore \quad X_B = 3.909 \times 10^{-7}$$

Now, if y is the molar concentration of solvent

n_B is the molar concentration of solute

then $$X_B = \frac{n_B}{n_B + y}$$

From problem (a), $y = 21.1108$

$\therefore$ $n_B = 8.2516 \times 10^{-6}$

From problem (d) $[KCl \longrightarrow 1$

$\therefore$ $[HCl]\ [KOH] = 9.856 \times 10^{-15} \times 8.2516 \times 10^{-6}$

$[KOH] = 2.852 \times 10^{-10}$

mole % KOH $= 1.3509 \times 10^{-9}$

f) Tablet over silica gel

Henry's Law was used, as in problem (e).

Fresh silica gel has 2×10^{-3} mm pressure residual water (138).

$\therefore$ $X_B = 3.289 \times 10^{-11}$

and $n_B = 6.944 \times 10^{-10}$

$[KOH] = 2.6162 \times 10^{-12}$

mole % KOH $= 1.239 \times 10^{-11}$

ERRATA

Page No.

29 Line 2: "orbit" instead of "atom"

47 "Equation 1.28" instead of "Section 1.3.3"

53 Insert after Equation 1.31
' $A = M_2/M_1$
where M_1 is mass of incident atom
M_2 is mass of target atom'

89 "Section 5.2.2" instead of "Section 4.2.3"

126 Line 19: "exponential" instead of "experimental"
Line 27: Insert "α" before "phase"

131 Heading: "Annealing techniques" instead of "Annealing behaviour"

132 Line 21: "69" instead of "92"

135 Line 17: Second "orthophosphates" should read "orthophosphites"

136 Line 9: "$^{32}P_H$ =" instead of "^{32}P ="

144 Line 19: "fraction" instead of "formation"

168 Equation 4.1
"$3(UO_2SO_4.3\frac{1}{2}H_2O)$" instead of "$3(UOSO_4.3\frac{1}{2}H_2O)$"

180 Line 6: "Table 4.8" instead of "Table 4.1"

195 Line 9: "$Z_{103.5}$" instead of "$Z_{102.5}$"

207 Line 6: "Figure 4.8" instead of "Figure 4.4"

217 Last line: "iodide" instead of "iodate"

228 Line 18: "Section 4.3.4(c)" instead of "Section 4.3.3(c)"

232 Line 22: $\Delta B \simeq K\sqrt{B}$
Line 25: $\Delta B \simeq \frac{(s-3)}{2}\sqrt{B}$
Line 28: "s=5" instead of "s=10" for ^{131}I

234 Last line: insert "please turn to P.236"

235 Last line: insert "please turn to P.237"

236 Last line: insert "please turn to P.235"

238 Line 11: "Section 3.4" instead of "Section 3.3"

240 Table 5.6 heading "$\Delta H_f°$" instead of "$H_f°$"

246 Line 15: "$a_5 = a_5'/a_o$" instead of "$a = a_5'/a_o$"

247 Line 21: "slope - $r x_1°$" instead of "slope - $r x_1$"

250 Line 20:"Equation 5.17"instead of "Equation 12"
Lines 22, 26: "Equation 5.14" instead of "Equation 9"
Line 24: "Equation 5.16" instead of "Equation 11"

255 Line 12: "Section 5.21" instead of "Section 4.2.2"

259 Line 23: "1.21×10^{21} ions K^+, Cl^-" instead of
"1.21×10^{29} ions K^+, Cl^-"

271 Line 9: "Cl_2^- ions" instead of "Cl^- ions"